Detecting and monitoring subglacial lakes beneath the Greenland Ice Sheet

Jade S. Bowling, BSc (Hons), MRes
Lancaster Environment Centre
Lancaster University

A thesis submitted for the degree of
Doctor of Philosophy

November, 2022

Declaration

I declare that the work presented in this thesis is, to the best of my knowledge and belief, original and my own work. The material has not been submitted, either in whole or in part, for a degree at this, or any other university. This thesis does not exceed the maximum permitted word length of 80,000 words including appendices and footnotes, but excluding the bibliography. A rough estimate of the word count is: 48957

Jade S. Bowling

Detecting and monitoring subglacial lakes beneath the Greenland Ice Sheet

Jade S. Bowling, BSc (Hons), MRes.
Lancaster Environment Centre, Lancaster University

A thesis submitted for the degree of *Doctor of Philosophy*. November, 2022

Abstract

In this thesis I develop novel methods and datasets, using airborne radio-echo sounding and high-resolution satellite-derived digital elevation models, to improve the understanding of subglacial lake distribution and activity beneath the Greenland Ice Sheet.

First, I use 23 years of airborne radio-echo sounding data, totalling over 500,000 km, to conduct the first systematic ice sheet-wide survey of subglacial lakes beneath the Greenland Ice Sheet. Following classification of basal reflector properties, I detect over 50 new stable subglacial lakes beneath the Greenland Ice Sheet. Surface elevation data also revealed 2 previously unidentified collapsed ice-surface basins indicative of subglacial lake activity. The results indicate that subglacial lakes are more common than previously thought and differ from those found beneath the Antarctic Ice Sheet both in their size and spatial distribution.

Next, I develop a new automated technique using statistical analysis of high-resolution, satellite-derived surface elevation data to detect localised elevation changes which are characteristic of subglacial lake drainage events. I then apply this framework to the Greenland Ice Sheet within 50 km of the ice margin to classify 7 potential active subglacial lakes which could be used as candidates for future geophysical surveys and further monitoring to understand to understand the role they play within the subglacial hydrological system.

Finally, using the results from the previous chapter, I utilise a variety of satellite datasets to analyse a unique active subglacial lake in Northern Greenland. From the observational record, the subglacial lake appears to have drained twice in the past 36 years, in 1990 and 2014, but each event with differing drainage characteristics. In particular, observations of downstream ice surface fracturing and excavation of ice blocks 20 m tall in 2014, suggests that drainage event caused a subglacial outburst flood which propagated to the ice surface. This is the first observation of supraglacial emergence of subglacial flood water in Greenland, indicating more varied drainage mechanisms that are currently not accounted for in numerical ice sheet models.

Publications

The candidate confirms that the work submitted is their own, except where work which has formed part of jointly authored publications has been included. The contribution of the candidate and the other authors to this work has been explicitly indicated below. The candidate confirms that appropriate credit has been given within the thesis where reference has been made to the work of others.

The research described in Chapter 3 has been published as: J. S. Bowling et al. "Distribution and dynamics of Greenland subglacial lakes", Nature Communications, 10, 2810 (2019). https://doi.org/10.1038/s41467-019-10821-w. J. S. Bowling led the study supervised by S. J. Livingstone and A. J. Sole. W. Chu provided code to analyse bed reflectivity. All authors commented on the manuscript. A. A. Leeson provided helpful discussions. This research is an extension of work carried out during my Masters degree at the University of Sheffield (Bowling, 2017).

The research described in Chapter 4 is prepared as a manuscript to be submitted as: "A new approach for detecting subglacial lake using high resolution digital elevation models on an icesheet scale". J. S. Bowling led the study, supervised by M. McMillan, A. A. Leeson, S. J. Livingstone, A. J. Sole. All authors commented on the manuscript.

The research described in Chapter 5 is in review as: J. S. Bowling et al. (2022) "Surface outburst of a subglacial flood from the Greenland Ice Sheet". J. S. Bowling led the study, supervised by A. A. Leeson and M. McMillan. B. P. Y. Noël, M. R. van de Broeke, T. Slater, L. Sandberg Sørensen, S. B. Simonsen, L. I. Melling, J. Mouginot and L. Taylor helped with data processing. All authors commented on the manuscript.

Acknowledgements

This work was funded by ENVISION UK Natural Environment Research Council (NERC) and hosted at Lancaster University. I would like to express my gratitude for the financial support and opportunities ENVISION have given me during my project. I am also thankful for receiving additional funding for conference travel costs from the Faculty of Science and Technology.

Thank you to my supervisors Amber Leeson and Malcolm McMillan at Lancaster University for your endless advice, patience and encouragement throughout. It has been an absolute pleasure to work together over the last four years, and I am very grateful for all your support and for providing me the opportunity to develop my research skills and ideas. I would also like to thank my external supervisors at Sheffield University, Stephen Livingstone and Andrew Sole, for your boundless enthusiasm about this work, valuable support, discussions and insight throughout the course of my PhD.

I am also grateful for the support of Winnie Chu, Peter Nienow, Brice Noël, Michiel van den Broeke, Thomas Slater, Louise Sandberg Sørensen, Sebastian B. Simonsen, Jérémie Mouginot, Laura Melling, and Liam Taylor who have not just supplied me with various datasets, but also provided advice, insights and valuable conversations as co-authors on my papers. I have gained valuable experiences from these collaborations.

Thank you to my examiners Martin Siegert and Alan Blackburn for their time and effort in reading and examining my thesis.

Thank you to the wonderful friends I have met at Lancaster University, in particular Matt for not only going above and beyond as a housemate, but also for helping me with coding, I'm glad I got to go through the highs and lows of this PhD journey with you; Juliane and Lorna for the tea breaks and climbing adventures and; Martin and Alex for being great housemates and friends, I appreciate you all so much! Thank you to the glaciology group for sharing icy knowledge, particularly Diarmuid and Jez. Thank you, of course, to John for your endless patience, support and encouragement, this thesis would never have been finished without you.

Mum, Dad, Scott - Thank you for showing me the world and encouraging my love for geography. I appreciate all you have done to get me here and your unwavering support.

Abbreviations and acronyms

ATM Airborne Topographic Mapper

ASTER Advanced Spaceborne Thermal Emission and Reflection Radiometer

CReSIS Center for Remote Sensing of Ice Sheets

CMIP Coupled Model Intercomparison Project

DEM Digital Elevation Model

DSM Digital Surface Model

ELA Equilibrium Line Altitude

ERS-2 European Remote Sensing

ESA European Space Agency

GCM General circulation model

GCPs Ground Control Points

GIMP Greenland Ice Mapping Project

GIS Geographical Information System

GLAS Geoscience Laser Altimeter

GPS Global Positioning System

GrIS Greenland Ice Sheet

ICESat Ice, Cloud and land Elevation Satellite

ICORDS Improved Coherent Radar Depth Sounder

inSAR Interferometric Synthetic Aperture Radar

LiDAR Light Detection and Ranging

MCoRDS Multi-Channel Coherent Radar Depth Sounder

MCRDS Multi-Channel Radar Depth Sounder

NAO North Atlantic Oscillation

NASA National Aeronautics and Space Administration

NEGIS North East Greenland Ice Stream

NSF National Science Foundation

OIB Operation IceBridge

PGC Polar Geospatial Center

RACMO Regional Atmospheric Climate Model

RDS Radar depth sounding

REMA Reference Elevation Model of Antarctica

RES Radio-echo sounding

SAR Synthetic Aperture Radar

SETSM Surface Extraction with TIN-based Search-space Minimization

SMB Surface Mass Balance

SSP Shared socioeconomic pathway

TanDEM-X TerraSAR-X add-on for Digital Elevation Measurement

TOA Top-of-atmosphere

USGS United States Geological Survey

Contents

1 Introduction and background **1**

1.1 The Greenland Ice Sheet . . . 1
1.1.1 Mass balance and climate . . . 2
1.1.2 Past ice sheet evolution . . . 5
1.1.3 Contemporary ice sheet changes . . . 7
1.2 Greenland bed topography . . . 8
1.3 The Greenland Ice Sheet hydrology . . . 10
1.3.1 Supraglacial hydrology . . . 11
1.3.1.1 Supraglacial channels . . . 13
1.3.1.2 Supraglacial lakes . . . 13
1.3.2 Englacial hydrological system . . . 17
1.3.2.1 Crevasses . . . 17
1.3.2.2 Moulins . . . 18
1.3.3 Subglacial hydrology . . . 21
1.3.3.1 Subglacial drainage system morphology . . . 23
1.3.3.2 Spatial and temporal evolution of the subglacial hydrological system and ice dynamics . . . 27
1.3.3.3 Erosion and transfer of subglacial sediment downstream 30
1.4 Subglacial lakes . . . 34
1.4.1 History of subglacial lake exploration . . . 35
1.4.2 Distribution and dynamics of subglacial lakes . . . 39
1.4.2.1 Antarctic subglacial lakes . . . 39
1.4.2.2 Predicted Antarctic subglacial lakes . . . 42
1.4.2.3 Greenlandic subglacial lakes . . . 43
1.4.2.4 Icelandic subglacial lakes . . . 46
1.4.2.5 Subglacial lakes beneath other ice masses . . . 49
1.4.3 Importance of subglacial lakes . . . 51
1.4.3.1 Ice dynamics . . . 51
1.4.3.2 Subglacial ecosystems . . . 53
1.4.3.3 Geomorphology, palaeoclimate and palaeoglaciology . . 54

2 Geophysical techniques used to detect and monitor subglacial lakes 57
2.0.1 Seismic reflection surveys . . . 58
2.0.2 Radio-echo sounding . . . 59
2.0.3 Satellite altimetry . . . 64
2.0.4 Digital Elevation Models . . . 67
2.0.5 Principal challenges with current remote sensing techniques . . . 69
2.1 Thesis aims and objectives . . . 70
2.2 Thesis structure . . . 70

3 Distribution and dynamics of Greenland subglacial lakes 72
3.1 Abstract . . . 73
3.2 Introduction . . . 73
3.3 Methods . . . 75
3.3.1 Subglacial lake identification from radio-echo sounding . . . 75
3.3.2 Surface collapse basin identification . . . 76
3.3.3 Surface elevation change measurements using Operation IceBridge ATM . . . 76
3.3.4 Hydraulic potential analysis . . . 77
3.4 Results . . . 77
3.4.1 Radar evidence for subglacial lakes . . . 77
3.4.2 Ice surface collapse basins . . . 79
3.4.3 Distribution of identified subglacial lakes . . . 81
3.5 Discussion . . . 83

4 Detecting active subglacial lakes beneath the Greenland Ice Sheet using high-resolution digital elevation models 91
4.1 Abstract . . . 92
4.2 Introduction . . . 92
4.3 Datasets and Methods . . . 95
4.3.1 ArcticDEM . . . 96
4.3.1.1 Georeferencing . . . 97
4.3.1.2 Filtering algorithm . . . 99
4.3.1.3 Time stacking . . . 99
4.3.1.4 Classification . . . 100
4.3.2 Landsat . . . 102
4.3.3 Radio-echo sounding . . . 102
4.4 Results & Discussion . . . 102
4.4.1 Mapping temporal variance in ice sheet elevation . . . 102
4.4.2 Potential active subglacial lake detection . . . 104
4.4.3 Detection of new active subglacial lakes - demonstration of concept 105

4.4.3.1 Brikkerne Glacier . . . 105
4.4.3.2 Marie Sophie Gletscher . . . 108
4.4.3.3 Knud Rasmussen Glacier . . . 111
4.4.4 Detection of new active subglacial lakes - based upon their statistical characteristics . . . 113
4.4.4.1 Upernavik Isstrøm . . . 114
4.4.4.2 Sermeq . . . 118
4.4.4.3 Sermeq Kujalleq . . . 119
4.5 Conclusion . . . 121
4.6 Data availability . . . 122

5 Surface outburst of a subglacial flood from the Greenland Ice Sheet 123
5.1 Abstract . . . 125
5.2 Main . . . 125

6 Synthesis 135
6.1 Summary of principal findings . . . 136
6.1.1 A revised inventory of subglacial lakes beneath the Greenland Ice Sheet . . . 136
6.1.2 A new method for mapping localised surface elevation changes . 137
6.1.3 A detailed, regional study of an active subglacial lake in Northern Greenland . . . 138
6.2 Synthesis of principal findings . . . 139
6.3 Key limitations of the research . . . 141
6.4 Recommendations for future work . . . 144
6.4.1 Automatic detection of subglacial lakes in airborne ice penetrating radar . . . 144
6.4.2 Exploration of subglacial lakes . . . 146
6.4.3 Diagnosing other sources of localised surface elevation changes . 147
6.4.4 Extension of method to other ice masses . . . 154
6.4.5 Potential impact of subglacial lake drainage activity on ice dynamics . . . 155
6.5 Concluding remarks . . . 155

Appendix A Supplementary material for Chapter 2: Distribution and dynamics of Greenland subglacial lakes 157
A.1 Supplementary Information for Chapter 2 . . . 157
A.2 Radar evidence for identified Greenland subglacial lakes . . . 157

Appendix B Supplementary material for Chapter 3: Detecting active subglacial lakes beneath the Greenland Ice Sheet using high-resolution digital elevation models **175**
B.1 ArcticDEM processing 176
B.1.1 DSM filtering: Calibration 176
B.1.1.1 Flade Isblink Ice Cap 179
B.1.1.2 Inugpait Quat 181
B.1.1.3 Sioqqap Sermia 182
B.1.1.4 Isunguata Sermia 185
B.1.1.5 Validation 187
B.1.2 Classification framework 187

Appendix C Appendix **193**

References **195**

List of Figures

1.1 Greenland Ice Sheet topography and average ice velocity 2
1.2 Sources and rates of basal melt beneath the Greenland Ice Sheet 4
1.3 Greenland Ice Sheet ice mass change (12,500 ka - 2100 AD) 6
1.4 Spatial patterns of elevation change over the Greenland Ice Sheet (1992-2017) 7
1.5 Geological map of Greenland 9
1.6 Greenland Ice Sheet hydrological system 11
1.7 Images of supraglacial rivers on the Greenland Ice Sheet 14
1.8 Satellite image of supraglacial lakes on the Greenland Ice Sheet 15
1.9 Image of crevassing on the Greenland Ice Sheet 17
1.10 Modes of fracturing 18
1.11 Water-driven fracture propagation 19
1.12 Field images of moulins in Greenland 20
1.13 Types of subglacial drainage morphology 24
1.14 Field images of subglacial channels beneath Svalbard glaciers 25
1.15 Linked cavity systems 26
1.16 Evolution of the hydrological system 29
1.17 Conceptual diagram of Greenland fjord circulations 32
1.18 Images of plumes at the Greenland Ice Sheet margin 33
1.19 Formation of a subglacial lake 35
1.20 Early records of Subglacial Lake Vostok 38
1.21 Distribution of subglacial lakes beneath the Antarctic Ice Sheet 41
1.22 Radio-echo sounding evidence of two Greenland subglacial lakes 44
1.23 Surface signature of an active subglacial lake in southwest Greenland . 45
1.24 Active subglacial lake at Flade Isblink ice cap, Greenland 47
1.25 Geomorphological change in the proglacial environment in response to subglacial lake drainage events in Greenland 48
1.26 Active subglacial lake in Iceland 50
1.27 Exponentially and linearly rising hydrographs 51

2.1 Seismic data of an Antarctic subglacial lake 60
2.2 Radar data of an Antarctic subglacial lake 61
2.3 Satellite altimetry showing surface signature of an active subglacial lake in Antarctica 66
2.4 Comparison of altimetry techniques for detecting active subglacial lakes 67

3.1 Example RES profiles for 13 subglacial lakes identified beneath the Greenland Ice Sheet in this study and the surrounding bed topography 78
3.2 Surface elevation change and evolution of active subglacial lakes in southwest Greenland 80
3.3 Spatial distribution of subglacial lakes identified in the radar echo sounding data 82
3.4 Frequency-distribution histograms of subglacial lakes identified in this study 83
3.5 Comparison between location of identified subglacial lakes and predicted lakes, geothermal heat flux, basal thermal state and bed roughness . . . 84
3.6 Conceptual model of Greenland ice sheet hydrological system, illustrating supraglacial and subglacial features 90

4.1 Spatial and temporal coverage of ArcticDEM Strip DSMs 98
4.2 Methodological approach for detecting new active sublacial lakes 99
4.3 Classification of temporal standard deviation of elevation within 50 km of the ice sheet margin 103
4.4 Distribution of active subglacial lake candidates 106
4.5 Active subglacial lake candidate at Brikkerne Glacier, Northern Greenland 107
4.6 Active subglacial lake candidate at Marie Sophie Gletscher, Northeastern Greenland 109
4.7 Active subglacial lake candidate at Knud Rasmussen Glacier, Northwestern Greenland 112
4.8 Statistical characteristics of active subglacial lake candidates 114
4.9 Active subglacial lake candidate detected using our temporal variance method near Upernavik-2, northwestern Greenland 115
4.10 Active subglacial lake candidate detected using our temporal variance method near Sermeq, southwestern Greenland 117
4.11 Active subglacial lake candidate detected using our temporal variance method near Ussingbraer, central western Greenland 120

5.1 Three-dimensional shaded relief of collapse basin 129
5.2 Surface elevation profiles across collapse basin 130
5.3 Climatological conditions and supraglacial lake volume (188-2021) . . . 132

6.1 Machine learning approach to detecting subglacial lakes in Antarctica . 145
6.2 Testing the temporal variance method over supraglacial lakes in southwestern Greenland . . . 148
6.3 Testing the temporal variance method at a tidewater glacier in northeastern Greenland . . . 150
6.4 Temporal evolution of an ice-marginal lake tongues . . . 151
6.5 Temporal evolution of two small floating ice tongues . . . 152
6.6 Testing the temporal variance method grounding lines at a glacier in northern Greeland . . . 153
6.7 Spatial coverage of Digital Surface Models produced for the REMA project . . . 154

A.1 Radar evidence for L7 and L8 . . . 158
A.2 Radar evidence for L9 . . . 158
A.3 Radar evidence for L10 . . . 159
A.4 Radar evidence for L11 and L12 . . . 159
A.5 Radar evidence for L13 and L14 . . . 160
A.6 Radar evidence for L15 . . . 160
A.7 Radar evidence for L16 and L17 . . . 161
A.8 Radar evidence for L18 and L19 . . . 161
A.9 Radar evidence for L20 . . . 162
A.10 Radar evidence for L21 . . . 162
A.11 Radar evidence for L22 and L23 . . . 163
A.12 Radar evidence for L24 and L25 . . . 163
A.13 Radar evidence for L26 and L27 . . . 164
A.14 Radar evidence for L28 . . . 164
A.15 Radar evidence for L29 . . . 165
A.16 Radar evidence for L30 and L31 . . . 165
A.17 Radar evidence for L32, L33 and L34 . . . 166
A.18 Radar evidence for L35 and L36 . . . 166
A.19 Radar evidence for L37 . . . 167
A.20 Radar evidence for L38 . . . 167
A.21 Radar evidence for L39 . . . 168
A.22 Radar evidence for L40, L41 and L42 . . . 168
A.23 Radar evidence for L43 . . . 169
A.24 Radar evidence for L44 . . . 169
A.25 Radar evidence for L45 . . . 170
A.26 Radar evidence for L46 . . . 170
A.27 Radar evidence for L47 . . . 171
A.28 Radar evidence for L48 . . . 171

A.29 Radar evidence for L49 and L50 172
A.30 Radar evidence for L51, L52 and L53 172
A.31 Radar evidence for L54 and L54 173
A.32 Radar evidence for L56 and L57 173
A.33 Radar evidence for L58 174
A.34 Radar evidence for L59 and L60 174

B.1 Method for filtering ArcticDEM Strip DSMs with reference to ArcticDEM Mosaic 178
B.2 Testing the impact of various filtering threshold values at Flade Isblink active subglacial lake 180
B.3 Testing the impact of various filtering threshold values at Inugpait Quat active subglacial lake 183
B.4 Testing the impact of various filtering threshold values at Sioqqap Sermia (northern) active subglacial lake 184
B.5 Testing the impact of various filtering threshold values at Sioqqap Sermia (southern) active subglacial lake 186
B.6 Testing the impact of various filtering threshold values at Isunguata Sermia L1 active subglacial lake 188
B.7 Testing the impact of various filtering threshold values at Isunguata Sermia L2 active subglacial lake 189
B.8 Testing the impact of various filtering threshold values at Isunguata Sermia L2 active subglacial lake 190
B.9 Number of georeferenced DSMs within 50 km of the margin, and percentage of those removed using different filtering thresholds 191
B.10 Classification at each of the seven known active subglacial lakes 192

C.1 Dynamic temporal variance signal from a large supraglacial channel, Hobbs Gletscher 194

List of Tables

4.1 Number of features identified within different bands of temporal standard deviation, and their associated statistics 101

B.1 Known active subglacial lakes in Greenland and their key characteristics. 177

Chapter 1

Introduction and background

In this chapter, I introduce the Greenland Ice Sheet and the importance of understanding its complex hydrological system for predicting future mass balance and contribution to sea level rise. I then review the production, pathways, storage and discharge of meltwater as it flows throughout the complex system, and its importance for ice dynamics and marine ecosystems and environments. I then explore the history of subglacial lake identification and monitoring, examine the types of subglacial lakes, their distribution and relationship with ice masses, as well as their importance for understanding ice dynamics, microbial communities, landscape evolution, and past environments and climates.

1.1 The Greenland Ice Sheet

The present-day Greenland Ice Sheet has a volume of ∼2.6 million km^3, making it the largest reservoir of frozen freshwater in the Northern Hemisphere. The ice is up to 3.2 km thick in the interior, where the bedrock beneath is relatively flat and close to sea level (Morlighem et al., 2017) (Figure 1.1a). Coastal mountains surround most of the periphery, through which outlet glaciers and ice streams drain the interior (Figure 1.1b). The largest, fastest-flowing glaciers with velocities of about 10^2 - 10^4 m a^{-1}, such as Jakobshavn Isbræ in western Greenland and Helheim Glacier in southeastern Greenland, terminate in marine settings, whereas, land-terminating glaciers, such as Russell Glacier in southwestern Greenland, have typical velocities

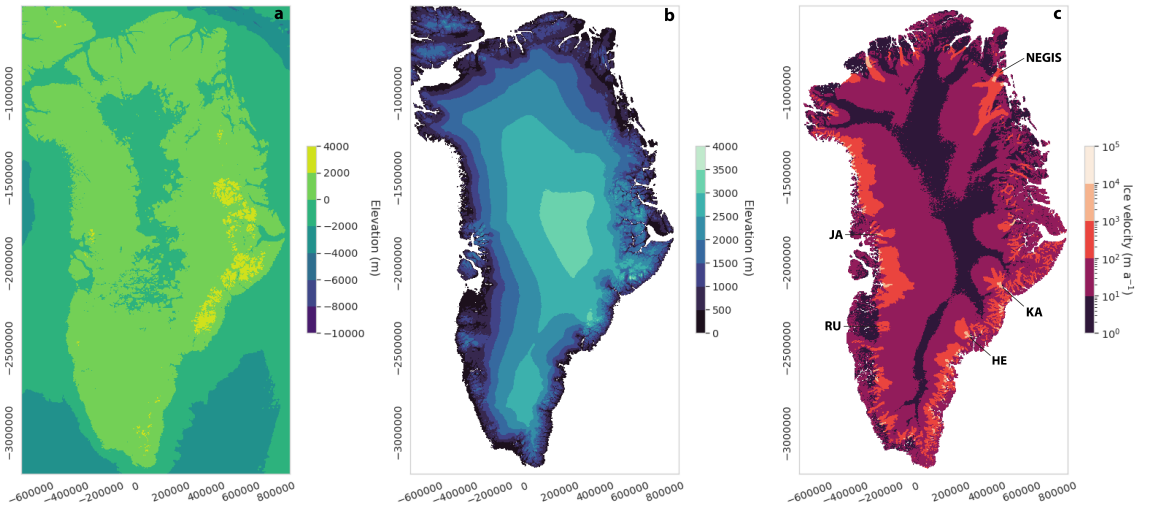

Figure 1.1: (a) Bed topography and (b) surface topography of the Greenland Ice Sheet (Morlighem et al., 2017). (c) MEaSUREs Annual ice sheet velocity from 2018 (Joughin et al., 2017) with key glaciers labelled (NEGIS - North East Greenland Ice Stream; JA - Jakobshavns Isbræ; RU - Russell Glacier; KA - Kangerlussuaq; HE - Helheim Glacier.

of $\sim 10^1$ m a^{-1} (Joughin et al., 2017) (Figure 1.1c). The >600 km long North East Greenland Ice Stream (NEGIS) drains a large portion of the ice sheet (>20%; Rignot and Kanagaratnam, 2006), reaching velocities of about 500 m a^{-1} at the terminus (Joughin et al., 2001), and 20 m a^{-1} less than 150 km from the ice divide (Joughin et al., 2010).

1.1.1 Mass balance and climate

Ice mass in Greenland is constantly changing due to exchanges at its boundary. At the surface, due to interactions with the atmosphere, snow and ice is either lost through ablation processes, including surface melt, surface meltwater runoff and sublimation (change of solid ice to vapour), or accumulated due to precipitation (mainly snowfall), wind-blown snow and avalanching. The net difference between accumulation and ablation is known as surface mass balance (SMB). At the ice base, basal melting (B) is driven by frictional heat produced by ice sliding over the bed, geothermal heat flux from the interior of the Earth, and heat generated by turbulent surface meltwater input into the subglacial system, with each of these contributing factors vary spatially (Karlsson et al., 2021) (Figure 1.2). In the interior of the ice sheet, basal

melt is negligible as basal ice temperatures are likely below the pressure melting point (MacGregor et al., 2016) and there are is a lack of surface meltwater input to the bed. On the other hand, basal melt rates on the order of 10^{-1} m a^{-1} are typically found beneath fast-flowing ice, for example the NEGIS (Fahnestock et al., 2001; Karlsson et al., 2021). Basal melt production in Greenland is estimated to be $\sim$21 $\pm$ 4 Gt a^{-1} between 2000 and 2010, with frictional melt making up about half of this volume (Karlsson et al., 2021). At the lateral margins where the ice sheet meets the ocean, ice is lost through the calving of icebergs and submarine melting, together referred to as solid ice discharge (D).

The total mass balance of the Greenland Ice Sheet can be determined by several methods: satellite and airborne altimetry in order to measure surface elevation changes to estimate ice volumetric change (e.g., Sandberg Sørensen et al., 2011; McMillan et al., 2016; Smith et al., 2020b; Simonsen et al., 2021), gravimetry to estimate ice mass changes (e.g., Barletta et al., 2013; Velicogna et al., 2014; Groh et al., 2019; Velicogna et al., 2020), or the Input-Output method (e.g., Rignot et al., 2008; Colgan et al., 2019; Mouginot et al., 2019) which uses the calculation below to determine the rate of mass change (M):

$$M = SMB - D \tag{1.1}$$

Inter-annual climate variability influences the rate of mass change, both in terms of air temperature and precipitation (Box, 2005; Hanna et al., 2006, 2008; Tedesco et al., 2008; Noël et al., 2014), which in turn influences global sea-level and ocean thermohaline circulation changes. Much of this variability has been attributed to changes in large-scale atmospheric circulation patterns, namely the North Atlantic Oscillation (NAO), which modulates moisture and heat transport to the ice sheet. The negative phase of the NAO reflects a weakening and southward migration of the jet stream (Hall et al., 2015; Lim et al., 2016), enabling anomalously high pressure (Fettweis et al., 2013b) and atmomospheric blocking (Hanna et al., 2016) over the Greenland Ice Sheet (defined as a persistent (>5 days) anticyclonic high pressure system that deflects migratory cyclones (Rex, 1950)). The positive phase of the NAO has the opposite effect, corresponding to colder winters over Greenland. In the early

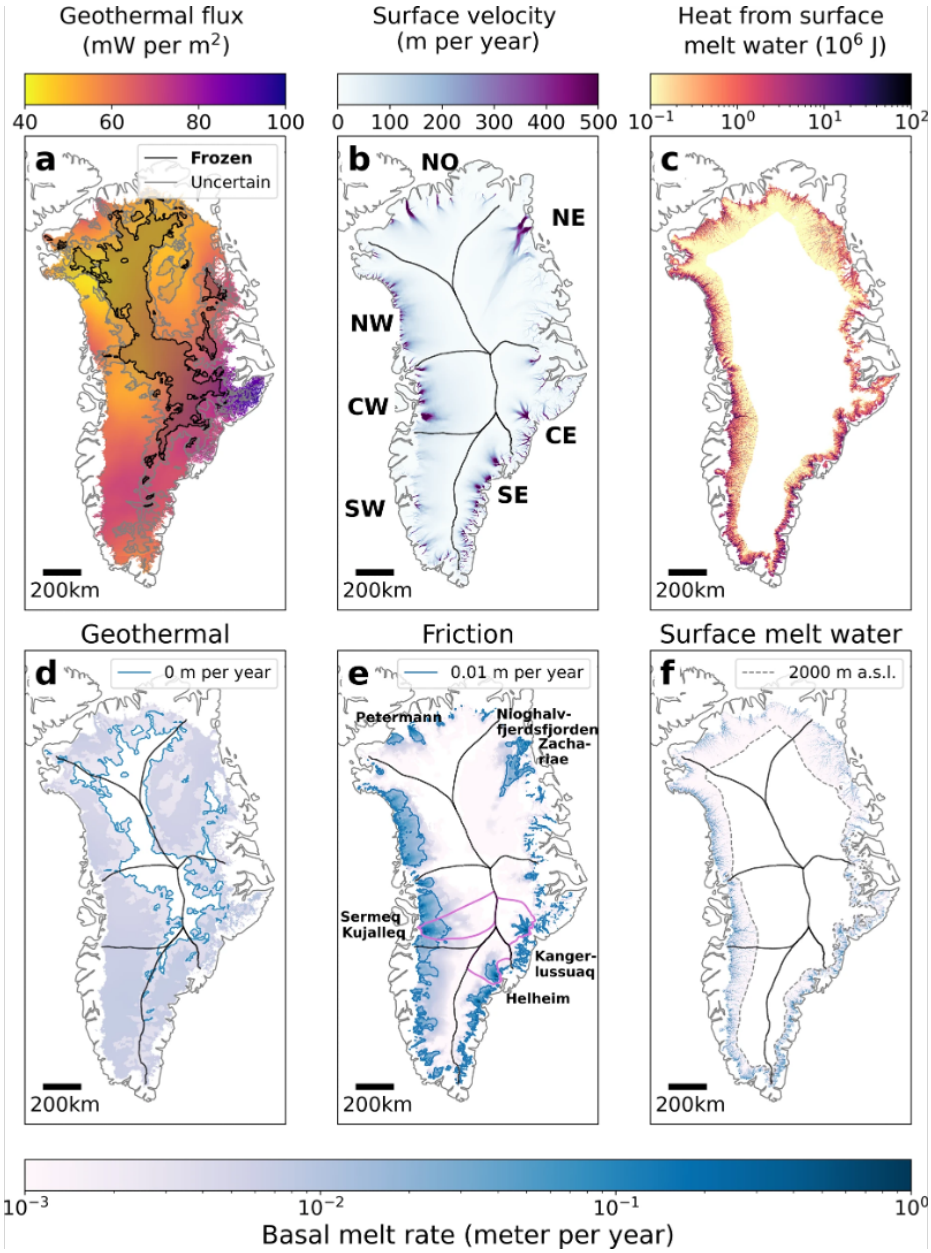

Figure 1.2: Sources and rates of basal melt beneath the Greenland Ice Sheet (Karlsson et al., 2021). (a) Average geothermal heat flux (GHF) derived from 3 GHF models (Shapiro and Ritzwoller, 2004; Fox Maule et al., 2009; Martos et al., 2018). (b) Satellite-derived ice surface velocity from MEaSURES (Joughin et al., 2008). (c) Heat produced from surface meltwater as it enters the subglacial system. (d) Basal melt rates generated by geothermal heat. (e) Basal melt rates generated by frictional heat. (f) Basal melt rates generated by surface meltwater entering the subglacial system.

2000s, the NAO shifted to a negative phase (Angelen et al., 2014), which has been associated with increased annual mass losses through three main processes: (1) reduced summer snowfall leading to increased bare ice exposure, (2) increased solar radiation (Hofer et al., 2017) which enhances surface melting, and (3) an increased transport of warm air, particularly along the west coast of the Greenland Ice Sheet, which augments surface sensible heat fluxes (Tedesco et al., 2016). These impacts are particularly apparent in western Greenland as warm southerly air masses are advected along the western coast (Fettweis et al., 2013a).

Large volcanic eruptions can indirectly impact Greenland Ice Sheet mass balance by causing perturbations in air and surface ocean temperature and precipitation (Abdalati and Steffen, 1997; Evan et al., 2009; Otterå et al., 2010; Booth et al., 2012b; Seo et al., 2015). Sulfate aerosols produced during explosive volcanic eruptions scatter a significant amount of incoming solar radiation, causing a reduction in radiative forcing at the top-of-atmosphere (TOA) and global cooling at the surface (Robock, 2000; Kremser et al., 2016). For example, the 1992 Mount Pinatubo eruption in the Philippines has been associated with significant cooling over Greenland (Box et al., 2009). Whilst climate variability lasts about 2-3 years, it is thought that strong volcanic cooling could intensify vertical mixing processes in the upper ocean, causing changes to the North Atlantic ocean circulation that may persist for decades (Stenchikov et al., 2009; Otterå et al., 2010; Mignot et al., 2011; Zanchettin et al., 2013; Swingedouw et al., 2015). Volcanic eruptions are also a source of light-absorbing impurities, impacting the radiative properties of ice masses around the globe by lowering the albedo, and therefore enhancing meltwater runoff (Dumont et al., 2014; Gabrielli et al., 2014; Möller et al., 2014; Young et al., 2014).

1.1.2 Past ice sheet evolution

The Greenland Ice Sheet has undergone major advances and recessions throughout history. Palaeoglaciological studies and records reveal that the ice sheet was much more extensive, an estimated ∼65% more area than present (Funder et al., 2011), during the Last Glacial Maximum (LGM) between 26.5 and 19 ka BP (Clark et al., 2009). Large portions of the surrounding continental shelves were glaciated (Funder

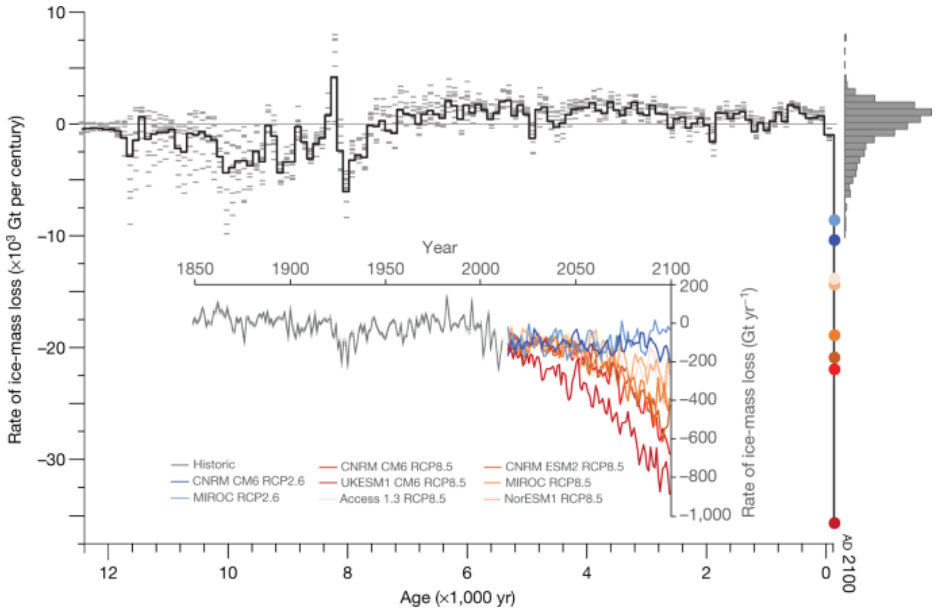

Figure 1.3: Centennial average rate of Greenland ice mass change between 12,500 ka and 2100 AD (solid black line), with simulated outputs shown by grey bars. General climate warming has occurred since the Little Ice Age (1290 - 1850 AD), with a short cool period, subsequently followed by Arctic warming in the 19th century. Inset shows modelled rate of ice mass change between 1850 and 2100, with coloured lines representing predictions under various Representative Concentration Pathway (RCP) scenarios corresponding to low to high greenhouse gas projections. Histogram on the right shows all Holocene rates of ice mass change (n=1,125). Source: Briner et al., 2020.

and Hansen, 1996; Bennike and Björck, 2002; Weidick et al., 2004), likely due to low accumulation and climatic cooling, similar to present-day Antarctic conditions (Cuffey and Clow, 1997). The ice sheet experienced considerable recession, further inland than the present day extent, during the Holocene Thermal Maximum (9-5 ka) when temperatures were about 3 ± 1°C warmer than the pre-industrial period (Briner et al., 2016; Lecavalier et al., 2017; McKay et al., 2018; Pendleton et al., 2019). A decline in orbitally-induced summer insolation eventually led to a general cooling trend (albeit with oscillations) and regrowth and advance of the ice sheet during the Neoglacial period (∼4 ka - present day) (Figure 1.3), with the coldest temperatures and maximum ice extent occurring during the Little Ice Age (1290 - 1850 AD) (Dahl-Jensen et al., 1998).

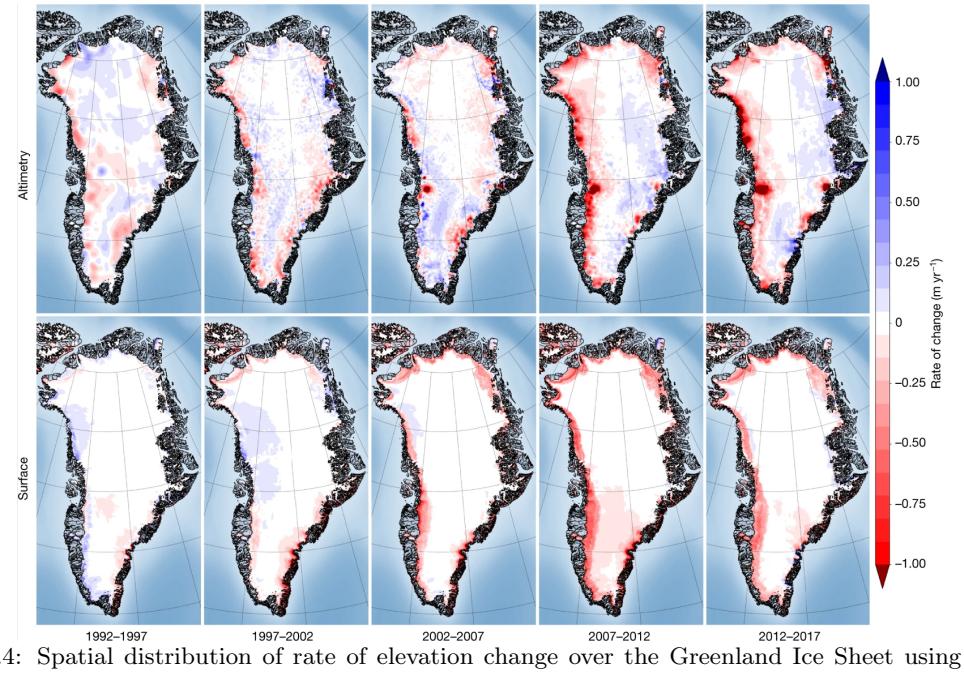

Figure 1.4: Spatial distribution of rate of elevation change over the Greenland Ice Sheet using satellite measurements (top row) and SMB from a regional climate model (bottom row). Negative trends, particularly along the western and northern margins have intensified in the last decade. Source: Shepherd et al., 2020.

1.1.3 Contemporary ice sheet changes

Since the culmination of the Little Ice Age there was a short-lived cooling period, followed by the onset of industrial-era Arctic warming in the mid-nineteenth century (Abram et al., 2016). Greenland Ice Sheet mass balance was positive between 1972 and 1980 (Colgan et al., 2015; Mouginot et al., 2019), and stayed in quasi-equilibrium in early 1990s (Hanna et al., 2013; Khan et al., 2015) (Figure 1.3). However, nearly 5,000 Gt of ice has been lost between 1992 and 2018, mostly concentrated along the western and southeastern margins (Figure 1.4), contributing a total of ∼14 mm to global sea level rise (Shepherd et al., 2020). Several extreme annual mass losses (>460 Gt a^{-1}) have occurred in the last two decades, for example in 2010, 2012 and 2019 (Nghiem et al., 2012; Tedesco et al., 2013; Keegan et al., 2014; Khan et al., 2015; Sasgen et al., 2020; Shepherd et al., 2020; Velicogna et al., 2020). The substantial increase in rate of ice mass loss in the past two decades (Shepherd et al., 2020) is unprecedented, and a recent switch in the dominant driver of these ice mass losses has become apparent (Mouginot et al., 2019; Goelzer et al., 2020; Payne et al., 2020; Shepherd et al., 2020), with relative contribution of SMB increasing from ∼42% between 2000-2005 to ∼68%

between 2009-2012 (Enderlin et al., 2014). These processes are likely to be exacerbated with predicted increases in Arctic warming throughout the 21st Century (Barnes and Polvani, 2015; Dai et al., 2019). General circulation model (GCM) outputs from the Coupled Model Intercomparison Project (CMIP) Phase 5 and 6 suggest that the Greenland Ice Sheet could contribute between 79-167 mm to sea level by 2100 under representative concentration pathways (RCP) 8.5 (intermediate emissions scenario) and shared socioeconomic pathways (SSP) 585 (extreme emissions scenario) (Choi et al., 2021). However, whilst progress has been made to improve Greenland Ice Sheet mass change models, there is still large uncertainty due to the complexity and contentiousness of the physical processes that govern mass balance, moreover our future human behaviour and climate policy remains a large unknown (Stearns and Van der Veen, 2018; Minchew et al., 2019; Sutherland et al., 2019).

1.2 Greenland bed topography

About 20% of Greenland is ice-free, which is predominantly composed of crystalline rocks (mostly gneiss and granite) of the Precambrian shield (Figure 1.5), which formed during several large-scale tectonic events and were welded together (Escher and Watt, 1976). The highest peak is 3,733 m, with rocks as old as 3.9 billion years in the Isua region in southwestern Greenland (Escher and Watt, 1976). The Precambrian shield acted as a stable, coherent base for younger sediments (deposits from the break up of Columbia) to accumulate in eastern Greenland, and has persisted due to its resistance to glacial erosion, unlike sedimentary deposits thought to underlie much of Antarctica (Drewry, 1976; Studinger et al., 2001).

The remaining 80% of Greenland's bed topography is concealed beneath the vast ice sheet and is inaccessible. We largely rely on ice-penetrating radar (see Section 2.0.2) and remote-sensing techniques to characterise and map the landscape beneath the ice mass (e.g., Bamber et al., 2013a; Morlighem et al., 2017, 2020). Albeit challenging to elaborate the bed elevation, particularly at the margins where the ice is temperate and crevasses at the surface which causes signal scattering in the radar and attenuation can prevent the signal from reaching the true bed. Furthermore, the deep entrenched valleys may create signal echoes from adjacent valley sides. Several studies have

Figure 1.5: Geological map of Greenland. Inset map shows geological correlations with Canada. Source: Dawes, 2009.

mapped the bed topography beneath the entire ice sheet at various resolutions e.g., 5 km gridded maps of ice thickness and bed elevation (Bamber et al., 2001) which was then updated with different data sources to create a 1 km grid (Bamber et al., 2013a). Morlighem et al., 2017 later produced a 150 m resolution map of the bed topography including bathymetry of the ice margins to provide data for the ice-ocean interface. Detailed knowledge of the bed elevation is important because it is required in ice sheet numerical models to predict the evolution of the ice sheet in response to a changing climate. Furthermore, it allows subglacial hydrological pathways and drainage basins (area of ice drained by a single outlet glacier, which can be aggregated to form sectors) to be delineated and modelled (e.g., Livingstone et al., 2013).

Models of the subglacial terrain beneath the Greenland Ice Sheet reveal that the landscape is relatively flat and >500 m below sea level in the ice sheet interior, corresponding to ice approximately 3 km thick. Here, the ice is largely frozen to the bed (MacGregor et al., 2016). Towards the periphery, the bed terrain becomes more complex, gradually rising to become becomes rougher and steeper, with deep troughs and peaks beneath the ice (Morlighem et al., 2017). Prior to glaciation, river erosion is thought to have played an important part of the early formation of valleys in which glaciers lie today, and other subglacial structures e.g., large channels (Cooper et al., 2016; Livingstone et al., 2017) and the "mega canyon" (Bamber et al., 2013b). These channels provide drainage for meltwater at the base, and as such the bed topography can influence the dynamics of ice flow (Werder et al., 2013), as well as have implications for grounding line migration and calving dynamics in marine-terminating glaciers.

1.3 The Greenland Ice Sheet hydrology

Each melt season, temperatures rise above zero over a proportion of the Greenland Ice Sheet surface, causing melting of the snow, firn and ice. Meltwater can flow over the ice surface (supraglacially), through the ice (englacially), along or within the bed (subglacially), or though a combination of these flow paths (Figure 1.6). Water can also be retained supraglacially, englacially or beneath the ice sheet as a liquid or as ice following refreezing (Jansson et al., 2003). The production, storage and transport of water influences ice sheet and glacier behaviour, therefore it is crucial to understand

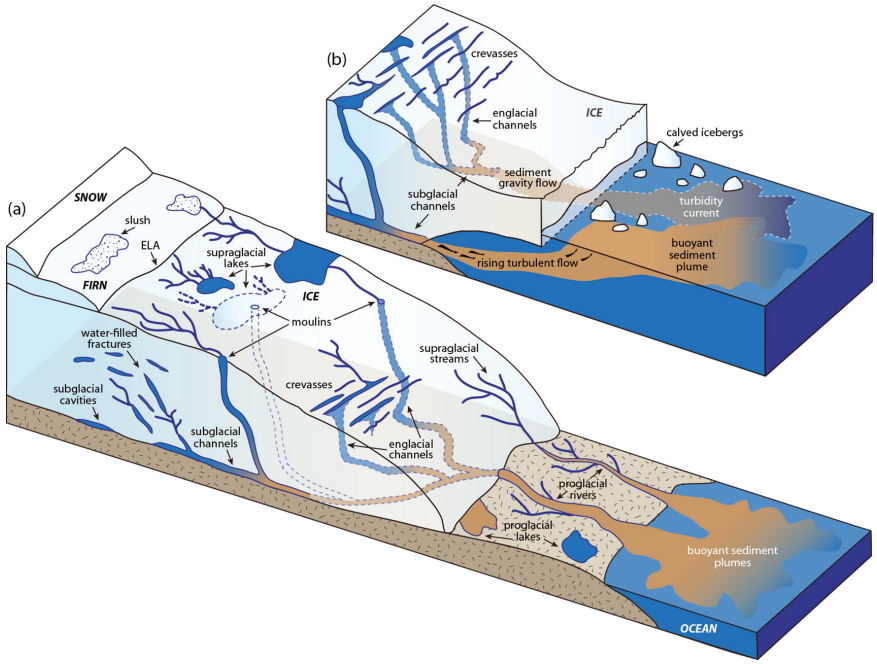

Figure 1.6: Illustration showing the primary supraglacial, englacial and subglacial meltwater pathways and storage for typical (a) land-terminating and (b) marine-terminating sectors of the Greenland Ice Sheet (Chu, 2014).

its flow throughout the entire hydrological system, and how its behaviour might evolve under a warming climate.

1.3.1 Supraglacial hydrology

The Greenland Ice Sheet is generally divided into the accumulation zone and the ablation zone. The accumulation zone is characterised by three main regions: (1) the dry snow zone in the interior of the ice sheet, where neglible melting occurs and therefore there is no supraglacial drainage, (2) the percolation zone, where limited surface meltwater infiltrates into snow and firn (partially compacted snow from previous years) in the melt season, and (3) the wet snow zone, where accumulation since the previous melt season is fully saturated (Benson, 1960). The equilibrium line altitude (ELA) is found at the lower limit of the wet snow zone. The ablation zone is where the previous years accumulation completely melts during summer, resulting in exposed bare ice.

At the beginning of the melt season, solar radiation warms the ice/ snow surface and produces meltwater. In the upper percolation zone, surface meltwater may percolate downwards into the porous snow and firn (permeabilites in the range 10^{-9} - 10^{-10} m^2; (Albert and Perron Jr, 2000)), through preferential flow paths (Marsh and Woo, 1984; Pfeffer and Humphrey, 1998; Williams et al., 2010; Humphrey et al., 2012). Meltwater infiltrating the firn layer, which can be up to 80 m thick (Herron and Langway, 1980), can be retained as liquid by capillary forces (Colbeck, 1974; Humphrey et al., 2012), stored in perennial firn aquifers (Forster et al., 2014), or refreeze at depth (Pfeffer et al., 1991; Braithwaite et al., 1994; Harper et al., 2012). Where melting is moderate, refreezing may form ice slabs (several metres thick), layers (0.1-1 m thick) or lenses (<0.1 m thick) (de la Peña et al., 2015; Machguth et al., 2016; MacFerrin et al., 2019; Culberg et al., 2021). As the melt season progresses, inefficient surface drainage occurs due to low flow rates (<3 mm h^{-1}) (Fountain and Walder, 1998), and ultimately becomes a slush flow (Onesti and Hestnes, 1989). Metamorphic processes transform firn into ice which is impermeable to water flow, thus initiating surface runoff.

The proportion of surface meltwater that subsequently refreezes within the snow and firn, which is governed by pore space, cold content (the energy required to bring firn to melting temperature), and hydraulic permeability (Verjans et al., 2019; Vandecrux et al., 2020), can influence Greenland ice dynamics and mass balance. If deep, heterogenous infiltration and localised refreezing dominate (Brown et al., 2011; Humphrey et al., 2012), then critical saturation must be reached for runoff to begin. This temporary storage can delay the onset of surface melting and the start of runoff (Harper et al., 2012). Widespread perennial firn aquifers (covering 20-90,000 km^2 between 1200-2000 m elevation; Forster et al., 2014; Miége et al., 2016; Steger et al., 2017) can store water year-round and persist over multiple years (Forster et al., 2014; Munneke et al., 2014; Miége et al., 2016), postponing the delivery of meltwater to the terminus, and consequently impacting the contribution to sea level rise (Harper et al., 2012). On the other hand, ice horizons can prevent meltwater from reaching greater depths, inducing lateral surface water runoff more rapidly (Pfeffer et al., 1991; Machguth et al., 2016; Mikkelsen et al., 2016; MacFerrin et al., 2019) and lowering the surface albedo (Charalampidis et al., 2015). Models indicate that projected Arctic warming could cause increased firn temperature, density and near-surace ice layers

throughout the percolation zone (Angelen et al., 2013; de la Peña et al., 2015; Machguth et al., 2016; Noël et al., 2017; MacFerrin et al., 2019). This could have a knock-on effect by reduction the capacity of meltwater storage, and potentially drive a change from meltwater retention to surface runoff, and thus increased contribution to sea-level rise. As melt migrates further inland, areas at higher elevations that were previously unaffected by melt may experience meltwater infiltration and ice layer development.

1.3.1.1 Supraglacial channels

Streams form on the ice surface if the channel incision rate exceeds the melt rate (Marston, 1983; Nolin and Payne, 2007). An arborescent network of supraglacial channels (collective term for both supraglacial streams and rivers) convey meltwater across the ice surface, similar in drainage pattern to terrestrial river systems (Ferguson, 1973) (Figure 1.7). Water routing is controlled by surface topography, therefore the position of larger supraglacial streams is relatively constant between melt seasons (Hagen et al., 1991). Supraglacial streams can flow for many kilometres, before entering englacial connections (Section 1.3.2), supraglacial lakes (Section 1.3.1.2) or can drain directly off the ice into terrestrial hydrological systems or the ocean (Poinar et al., 2015; Yang and Smith, 2016). The extent, density and discharge of a supraglacial stream network depends on surface melt rates and catchment area (which is controlled by surface topography and distribution of crevasses and moulins).

1.3.1.2 Supraglacial lakes

Supraglacial meltwater ponds in undulations in the ice surface, forming supraglacial lakes within regions with high ablation rates, such as western Greenland (Echelmeyer et al., 1991; Box and Ski, 2007; McMillan et al., 2007; Sneed and Hamilton, 2007; Sundal et al., 2009; Lampkin and van der Berg, 2011; Selmes et al., 2011; Tedesco and Steiner, 2011; Howat et al., 2013) (Figure 1.8). Their location is determined by bedrock topography, therefore they reform in the same locations in successive years (Echelmeyer et al., 1991; Box and Ski, 2007; Selmes et al., 2011), with lake coverage and frequency progressing from near the margin to further inland over the melt season (McMillan et al., 2007; Sneed and Hamilton, 2007; Sundal et al., 2009; Liang et al.,

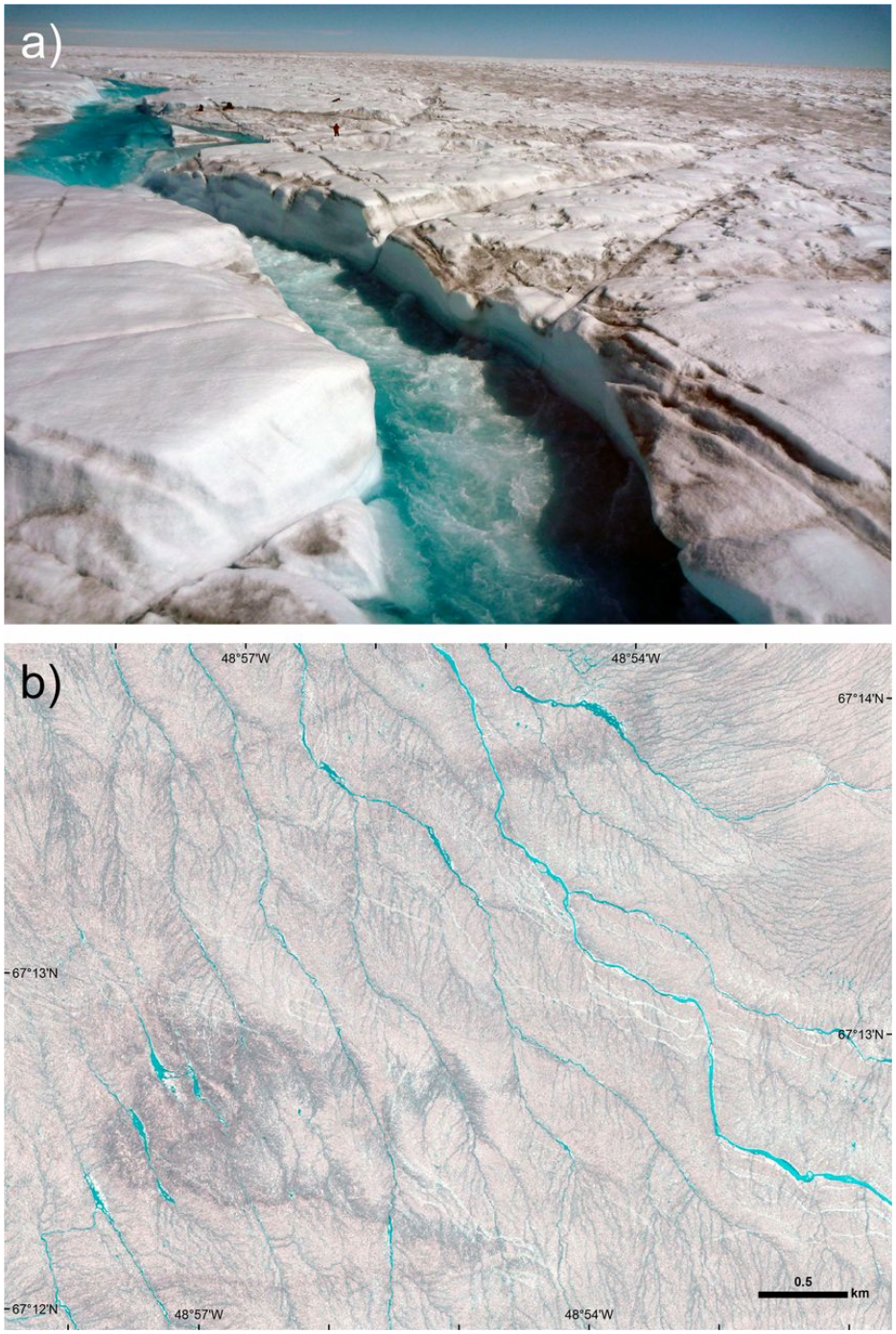

Figure 1.7: (a) Field photo taken on 23rd July 2012 of supraglacial river with human for scale (b) Optical image from WorldView-2 satellite taken on 23rd July 2012. Both images taken about 55 km inland from Kangerlussuaq, southwest Greenland. Source: Smith et al., 2015.

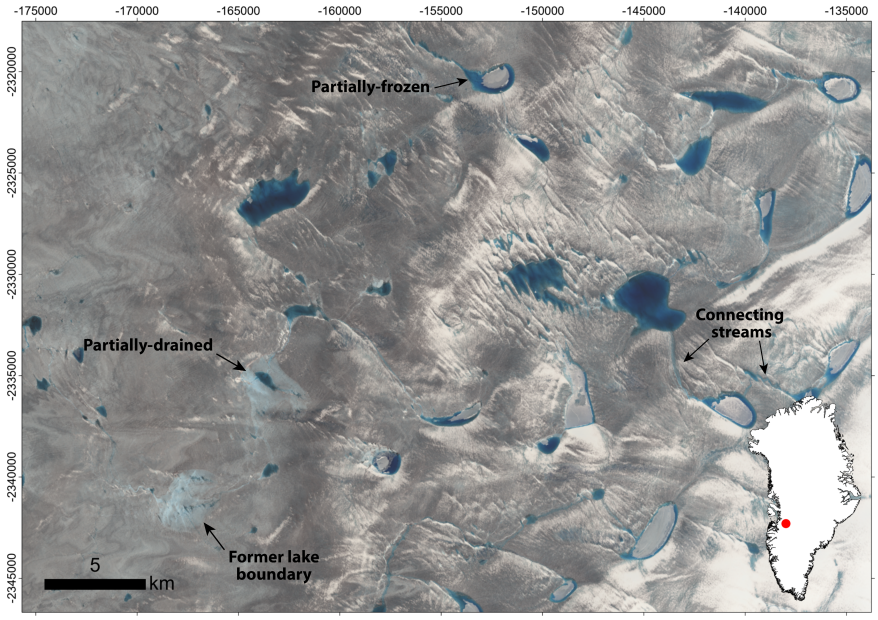

Figure 1.8: Landsat 8 optical image acquired on 31st July 2021 showing supraglacial lakes near Nordenskiold glacier, southwestern Greenland

.

2012; Johansson et al., 2013). Supraglacial lakes vary in size and depth, with remote sensing observations of lakes growing up to 17 km^2 in area (Selmes et al., 2011) and 12 m in depth (Box et al., 2012).

Supraglacial lakes drain either slowly, by incision of a channel at the basin edge and overtopping their banks into crevasses and moulins further downstream (Hoffman et al., 2011; Tedesco et al., 2013), or rapidly, in hours to days (Box and Ski, 2007; Das et al., 2008; Doyle et al., 2013; Tedesco et al., 2013; Stevens et al., 2015; Chudley et al., 2019), for example, Chudley et al., 2019 observed a 0.05 km^3 lake drainage in 5 hours. Rapid drainage occurs when water reopens an existing, or creates a new, connection to the bed, via hydrofracture (Das et al., 2008; Banwell et al., 2012; Doyle et al., 2013; Tedesco et al., 2013; Stevens et al., 2015; Chudley et al., 2019). This connection can remain open for the duration of remaining the melt season. In western Greenland, between 28 and 45% of supraglacial lakes drain rapidly (Fitzpatrick et al., 2014; Cooley and Christoffersen, 2017). Supraglacial lakes can drain in clusters (Fitzpatrick et al., 2014), suggesting that one drainage event can trigger other supraglacial lake drainages within a local vicinity (Christoffersen et al., 2018; Hoffman et al., 2018). This cascading

effect is due to increases in tensile stresses caused by meltwater reaching the bed of nearby supraglacial lakes (Stevens et al., 2015; Christoffersen et al., 2018; Hoffman et al., 2018).

Supraglacial lakes can influence ice dynamics in several ways. Firstly, the lower albedo of the supraglacial lake water (compared to the surrounding ice) enhances melt through increased absorption of shortwave radiation, by 100 to 170% (Lüthje et al., 2006; Tedesco et al., 2012). Secondly, rapid drainage events inject large volumes of meltwater to the bed beneath the ice sheet, having the potential to overwhelm the subglacial drainage system, decreasing effective pressure, facilitating ice-bed decoupling and basal sliding, and consequently short-term (hourly-weekly timescales) increases in ice slow, up to 220% of background winter velocities (Das et al., 2008; Bartholomew et al., 2010, 2012; Banwell et al., 2013; Doyle et al., 2013; Tedesco et al., 2013; Banwell et al., 2016). Once the surface-to-bed connection is initiated, meltwater can be delivered to the base of the ice sheet throughout the remaining melt season, with the potential to have long-lasting impacts on the subglacial drainage system and sustain these ice speed ups (Joughin et al., 2008; Shepherd et al., 2009; Tedstone et al., 2014; Banwell et al., 2016; Koziol et al., 2017; Williamson et al., 2018).

Not all supraglacial lakes drain each melt season, they can be maintained throughout the winter season as subsurface or buried lakes beneath an ice and snow lid (Koenig et al., 2015). Koenig et al., 2014 estimate approximately 1.5 Gt of water is accumulated in subsurface lakes, which is a small fraction of the 140 Gt thought to be stored in firn aquifers (Forster et al., 2014). However, subsurace lakes can persist for several seasons (Lampkin et al., 2020) and are generally distributed at higher elevations than supraglacial lakes (up to 1,900 m a.s.l) (Miles et al., 2017). Subsurface lakes have potential implications for ice rheology, by warming the underlying ice via latent heat transfer in winter (Phillips et al., 2010, 2013), and are an enduring source of meltwater in the hydrological system, with potential impacts for subsequent melt seasons (Koenig et al., 2015; Law et al., 2020).

Figure 1.9: Crevassing near the coast of Melville Bay, West Greenland taken during Operation IceBridge airborne campaign in May 2015. Photo credit: NASA/ John Sonntag

1.3.2 Englacial hydrological system

Supraglacial meltwater can enter the Greenland Ice Sheet and flow englacially upon encountering a permeable pathway. Crevasses and moulins provide such pathways, and are discussed in the following sections.

1.3.2.1 Crevasses

Crevasses are brittle fractures in the ice that are prevalent in the lower ablation zone of the ice sheet (Clason et al., 2015; Koziol et al., 2017) (Figure 1.9). They range from millimetre-scale cracks to fractures measuring 10s of metres wide (Holdsworth, 1969). The pattern of crevasses will depend on the direction of the principal stresses within the ice, which depends on a number of factors, including temperature, water content, density and structure (van der Veen, 1998, 1999). There are three modes of fracture growth: (1) Mode 1 (tensile opening), where a fracture forms from a culmination of tensile stresses stretching the crack apart, (2) Mode II (sliding) where a fracture lengthens due to an increase in parallel shear stresses, and (3) Mode III (tearing) which also forms as a result of shear stresses but the fracture grows normal to the direction of shear (Figure 1.10). Crevasses typically open via Mode I due to a glaciers longitudinal stress field (van der Veen, 1998; Colgan et al., 2011), however, crevasses

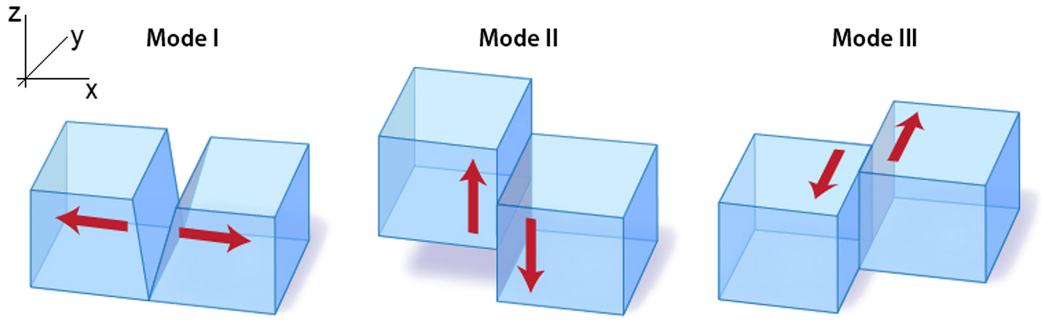

Figure 1.10: Illustration showing three primary modes of fracture: Mode I (tensile opening), Mode II (sliding) and Mode III (tearing). Source: Colgan et al., 2016.

can experience multiple modes, referred to as mixed-mode fracture (van der Veen, 1999). The movement of ice as it flows towards the terminus can rotate and bend crevasses according to velocity gradients, e.g., crevasse fields at Jakobshavn Isbræ rotated about 45% between 1985 and 2009 (Colgan et al., 2011).

Crevasses are typically confined to the upper surface layer due to tensile stresses being outweighed by compressive stresses from the weight of the overlying ice, which increase steeply with depth, forcing the crevasse closed. In the melt season, surface meltwater can flow into crevasses. If ponding occurs within the crevasse, it can cause the downwards propagation of the fracture via a process termed "hydrofracture" (van der Veen, 2007). In order for a fracture to form and propagation to occur, the local tensile stress must exceed the critical stress intensity (Alley et al., 2005) (Figure 1.11). If sufficient water is available, the fracture can propagate to the bed, delivering meltwater to the subglacial system. Once formed, frictional heat generated by turbulent meltwater flow will maintain this connection as long as melt rate exceeds the rate of creep closure (Fountain and Walder, 1998; Krawczynski et al., 2009).

1.3.2.2 Moulins

Moulins are mostly vertical channels in the ice, formed when fast-flowing supraglacial meltwater water intersects crevasses (Figure 1.12). Although water-filled crevasses close as they are advected downstream with glacier flow, frictional heat dissipation of the turbulent meltwater can keep the pathway open and enlarge it (Holmlund, 1988). Moulins range in size from centimetres to 10s of metres in diameter. In contrast

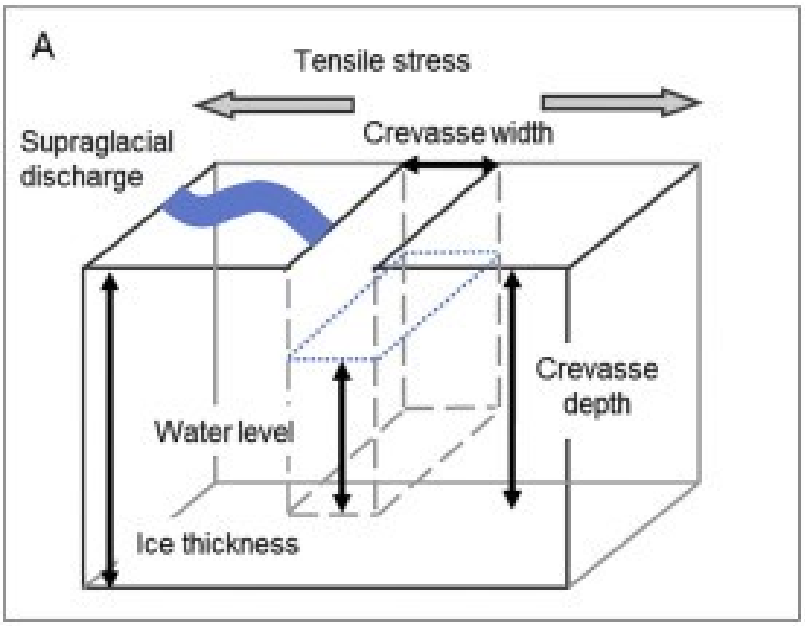

Figure 1.11: Process of water-driven fracture propagation (hydrofracture). Far field tensile stresses perpendicular to the plane of the crevasse allow the opening of a crevasse. If sufficient water accumulates within a crack, hydrostatic pressure exceeds the ice overburden pressure and tensile strength of the ice, allowing the fracture to propagate to the bed, thus delivering meltwater to the subglacial system. Source: (Greenwood et al., 2016).

to crevasses, moulins can deliver rapid pulses of meltwater from larger upstream catchments into the englacial and subglacial systems (Colgan et al., 2011; McGrath et al., 2011).

A significant percentage of surface meltwater is transported to the bed of the Greenland Ice Sheet via crevasses or moulins, before entering the ocean through subglacial channels (Das et al., 2008; Andrews et al., 2014; Clason et al., 2015; Koziol et al., 2017). In West Greenland, Koziol et al., 2017 find that crevasses and moulins drain 86% of surface meltwater combined. Crevasse zones have increased in spatial extent by over 10% between 1985 and 2009 in western Greenland, due to ice thinning (Colgan et al., 2011), potentially enhancing water delivery to the basal system. This can have implications for ice flow dynamics (discussed in detail in Section 1.3.3.2). Water discharge from firn aquifers has recently been found to enter crevasses and reach the bed in winter in southeast Greenland (Poinar et al., 2017), with the potential to export ∼140 Gt of water to the ice margin (Koenig et al., 2014). Water retention in the snow and firn layer is predicted to decrease (Angelen et al., 2013), which has

Figure 1.12: (a) Field photo of a moulin near Russell Glacier, southwest Greenland with research for scale. (b) Researchers inside a moulin in southwest Greenland (c) Photo of climber in Phobos moulin, southwest Greenland, showing the sub-horizontal morphology with a plunge pool near the bottom centre of the image. Photo credit for all images: Jason Gulley

the potential to make an unaccounted contribution to sea-level rise, with unknown impacts on ice flow.

1.3.3 Subglacial hydrology

Due to a lack of direct access to the bed and logistical fieldwork challenges, much of our knowledge of the Greenland Ice Sheet subglacial drainage system has been developed from alpine glacier configurations from indirect observations, such as hydrological flow tracing (e.g., Nienow et al., 1998), physical and chemical properties of glacial runoff and outburst floods (e.g., Tranter et al., 1993; Anderson et al., 1999), and borehole sampling (e.g., Hubbard et al., 1995), as well as direct observations from deglaciated regions (e.g., Walder and Hallet, 1979). Our current understanding is that if meltwater is not stored or refreezes at the bed, water flows beneath the ice (either within subglacial sediment or at the interface between the ice and underlying substrate), following the hydraulic potential gradient (ϕ) (Shreve, 1972). Water may also be driven into regional groundwater flow fields beneath subglacial till due to the loading of thick ice. Groundwater flow has the potential to add or evacuate water at the ice bed as it flows towards the ice terminus, and hence play a role in modulating ice flow (Gooch et al., 2016; Siegert et al., 2018). Furthermore, if groundwater is discharged into marine settings, it may influence biogeochemical cycles, ocean circulation and ice-ocean interactions (Liljedahl et al., 2021). Groundwater may also alter the advection of geothermal heat flux (Gooch et al., 2016), yet the groundwater component of the hydrological cycle is often neglected in ice dynamic modelling for both Antarctica and Greenland.

Unlike at the surface, where water flow is controlled by gravity and surface slope, beneath the ice, meltwater is under immense pressure, therefore ϕ is determined by the vertical and horizontal gradients in water pressure, as well as the bed topography:

$$\phi = \rho_w g z_b + \rho_i g(z_s - z_b) - N \tag{1.2}$$

where ρ_w is the density of water (1,000 km m^{-3}), g is the acceleration due to gravity, z_b and z_s are bed and surface topography, and ρ_i is density of ice (917 kg m$^-3$),

respectively. N is effective pressure which can be calculated as the difference between water pressure ρ_w and the pressure in the surrounding ice, ρ_i (Iken and Bindschadler, 1986; Fowler, 1987; Schoof, 2010):

$$N = \rho_i - \rho_w \tag{1.3}$$

Depending on the thickness of the ice, at a local scale subglacial water can ignore gravity and flow uphill or parallel to the slope. Although, generally water flows downhill as the bed topography slopes towards the terminus and ice becomes thinner. Basal water pressure is regulated by four variables: (1) glacier thickness; thinner ice produces lower basal water pressure, (2) rate of water supply; a large influx of meltwater can increase the basal water pressure, (3) rate of meltwater discharge; a distributed drainage system (see Section 1.3.3.1) may increase basal water pressure, and (4) underlying geology; more permeable rock will reduce the basal water pressure. Valley glacier hydrology theory suggests that increased basal water pressure reduces the effective pressure at the bed, resulting in reduced frictional strength (Lliboutry, 1968; Bindschadler, 1983). If water cannot drain away freely, pore-water pressures develop and can support part of the weight of the glacier resulting in 'hydraulic jacking' of the overlying ice (Iken, 1981). Where sediment underlies the ice, tension forces disappear, increasing sediment deformation, and therefore causing a speed up of ice flow (Engelhardt et al., 1978; Hodge, 1979; Iken and Bindschadler, 1986; Fowler, 1987; Iverson et al., 1999; Bingham et al., 2008).

Basal water flow is sensitive to changes in the ice sheet surface. The surface topography governs the hydraulic potential of the ice sheet, which has been shown to be a larger influence (approximately 11 times) on basal flow paths than basal topography (Shreve, 1972). Even subtle changes in surface elevation between 5-15 m have been shown to correlate with the rerouting of subglacial water flow beneath the East Antarctic Ice Sheet (Wright et al., 2008). In Greenland, large-scale shifts in surface elevation over centuries or less at the NEGIS can change subglacial water pathways (Karlsson and Dahl-Jensen, 2015). Subglacial water competition between adjacent glacier catchments (termed 'water piracy') is thought to trigger the onset or shutdown of ice flow in Antarctica (Anandakrishnan and Alley, 1997; Vaughan et al.,

2008; Carter et al., 2013). In Greenland, the piracy of water can influence the speed in which ice flows by changing the pattern of regional water pressure and reorganising meltwater at the surface (Lindbäck et al., 2015).

1.3.3.1 Subglacial drainage system morphology

Subglacial drainage systems can be categorised into two main configurations: (1) channelised (efficient) systems, where water is confined to conduits, and (2) distributed (inefficient) systems which spread across large portions of the bed, or a combination of both (Figure 1.13). Channelised systems are generally hydraulically efficient, allowing water to be routed quickly through well-connected networks; Röthlisberger or Hooke channels incised up into ice (Röthlisberger, 1972), Nye channels incised into the bed (Nye, 1976) or a combination of both configurations (Figure 1.13). On the other hand, distributed systems are less efficient, with slow routing of water through subglacial films or sheets of water (Weertman, 1962, 1972; Creyts and Schoof, 2009), linked cavities formed on the lee-side of bedrock bumps (Walder, 1986; Kamb, 1987), and porous (or Darcian) flow through sediments (Boulton and Jones, 1979) (Figure 1.13). In general, when meltwater discharge is low, a distributed system is expected, whereas a channelised system is expected during high discharge. However the subglacial drainage system is not binary; both systems can be present and interact with one another beneath the same glacier (Hubbard et al., 1995; Alley, 1996).

Röthlisberger channels (or R-channels) are ice-walled conduits (Figure 1.13) which are formed and maintained by heat dissipation from flowing water, which outweighs the rate of creep closure from the overlying ice (Figure 1.14). R-channels were first described by (Röthlisberger, 1972), which originally theorised that water flows through semi-circular conduits under steady state conditions, where discharge is inversely proportional to the pressure gradient that drives flow. Because such channels operate at low water pressure (or high effective pressure), this would lead to the formation of an arterial drainage system, where few large channels are fed by a network of smaller tributaries (Röthlisberger, 1972; Shreve, 1972).

However, this assumption has since been challenged, as in reality, flow is unlikely to be steady since discharge can vary with the rate of melt at the ice surface, which

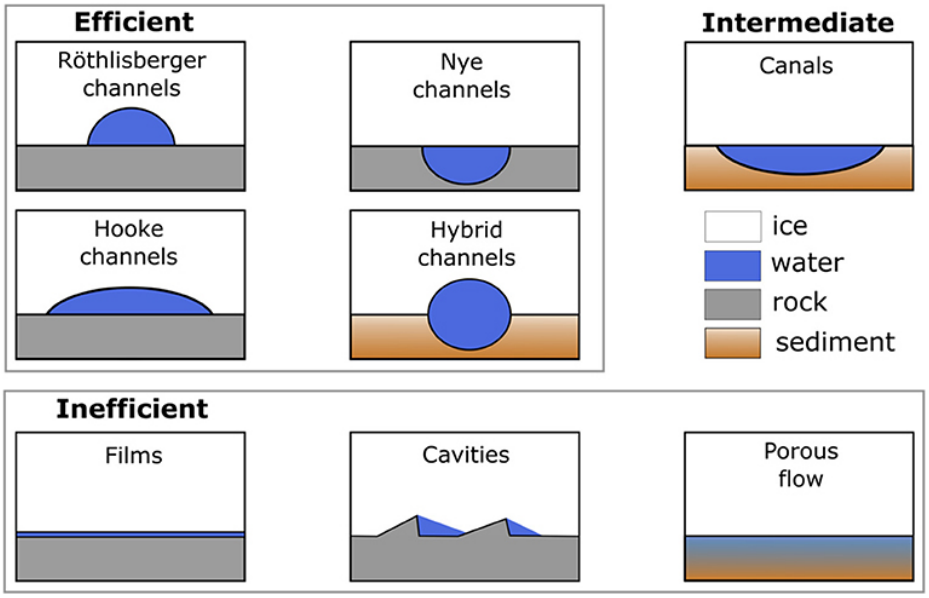

Figure 1.13: Illustration showing efficient, inefficient and intermediate subglacial drainage morphologies. Source: Davison et al., 2019.

fluctuates diurnally and in response to atmospheric conditions. Therefore, channels may be unsaturated at low flows (Lliboutry, 1983; Hooke, 1984), and during peak discharge, water pressures may exceed the local ice overburden pressure (Hubbard et al., 1995). Hooke et al., 1990 and Hock and Hooke, 1993 argued that subglacial channels are more likely to have broader, lower cross-sectional geometries due to ice melt being concentrated at the channel margins during low discharge, and inward creep rates being high at the ceiling when channels are partially full. These channels are named Hooke channels (or H-channels).

Nye channels (or N-channels) are incised into the underlying bedrock (Nye, 1976) as a result of meltwater erosion (Figure 1.13 & 1.14). Hybrid channels can occur when water-filled N-channels partially melt the overlying ice to form an N-R channel hybrid (Figure 1.13).

Sheets or films of water (millimetre thick) can form between the ice sheet and its bed (Figure 1.13). Extensive meltwater films were first proposed as part of the theory of regelation, where water is produced due to high pressure on the up-glacier side of obstacles and undulations in the bed, which lowers the pressure melting point (Weertman, 1962, 1972). On the down-glacier side of the obstacle, the contact pressures

Figure 1.14: Efficient subglacial channels beneath Svalbard glaciers. Left: Nye channel incised in till beneath Rieperbreen glacier which formed during the melt season, glaciologists from the University Centre in Svalbard for scale. Credit: Jason D. Gulley. Right: An upward-incised channel beneath Hansbreen glacier, with glaciologists for scale. Credit: Jason D. Gulley

are low, and the pressure melting point is raised, thus refreezing occurs (Hubbard and Sharp, 1993). Water films were originally thought to be the main method for water transport (Weertman, 1972), however their role in transporting subglacial water is likely to be limited because theory suggests that thick water films are innately unstable (Walder, 1982; Weertman and Birchfield, 1983). As the water film thickness increases (>several millimetres), water flux would eventually melt the overlying ice (via viscous dissipation), enhancing local melt rates and rapidly forming a network of efficient channels (Nye, 1976; Walder, 1982; Weertman and Birchfield, 1983) or a linked cavity system. The exception to this is when bedrock protrusions bridge the water film, partially supporting the overlying ice, which results in the rate of ice roof closure exceeding water film expansion, thus enabling thin films to develop (Creyts and Schoof, 2009).

Water-filled cavities open up on the down-glacier side of obstacles or bumps (decimetre scale) at the bed where basal water pressure exceeds the local ice pressure at the ice-bed interface (Lliboutry, 1979; Walder, 1986; Fowler, 1987). Cavities are typically either stepped, with an abrupt step on the lee side of the bedrock obstacle, or waved, where the bed is smooth (Kamb, 1987). A network of these cavities of various sizes and frequency can develop, interconnected by orifices, forming a linked-cavity system (Lliboutry, 1968; Lliboutry, 1979; Walder, 1986; Fowler, 1987; Kamb, 1987)

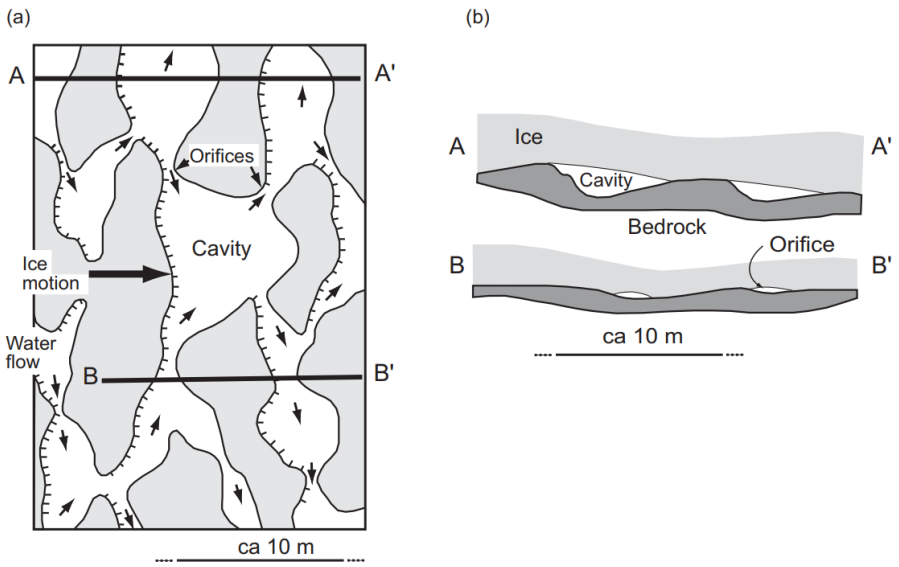

Figure 1.15: Schematic diagrams of a linked cavity system. (a) Plan view. (b) Cross-sections through cavities (A-A') and orifces (B-B'). Source: Hooke, 2005, after Kamb, 1987.

(Figure 1.15). The size of the cavity varies depending on ice velocity, ice viscosity, subglacial discharge and effective pressure; larger cavities are attributed to lower effective pressure, fast ice flow, high ice viscosity and high discharge (Walder, 1986; Kamb, 1987).

The bed beneath the Greenland Ice Sheet is comprised of both 'hard' bedrock (e.g., Harper et al., 2017) and areas of sediment (e.g., Booth et al., 2012a; Dow et al., 2013; Walter et al., 2014; Kulessa et al., 2017). Porous flow refers to meltwater flow within subglacial sediments (unlike the previously described configurations which are related to hard bedrock) (Figure 1.13). Subglacial sediments are typically permeable, therefore deform easily when saturated and subjected to ice overburden pressures. The precise mechanism for meltwater flow through porous sediment remains unclear, however several theories have been suggested, such as: Darcian flow where water flows along the hydraulic potential gradient through pores within the subglacial sediment layer (Boulton and Jones, 1979; Walder and Fowler, 1994); advection of water within the sediment layer; through pipes and small channels within the subglacial sediment; or as a thin film of meltwater at the top of the sediment.

Where ice flows over till, incision into the saturated, deformable basal sediments can

create channels that exhibit canal-like characteristics (Walder and Fowler, 1994; Ng, 2000). Canals are sustained by the competition between creep closure and sediment erosion and meltwater flux (Walder and Fowler, 1994; Ng, 2000). This drainage element is categorised as intermediate drainage as canals can evacuate water efficiently (Ng, 2000), but may also be inefficient.

Bartholomew et al., 2010 suggest that valley glacier hydrological processes can be up-scaled and applied to ice sheet scenarios, however there are considerable geometric differences between valley glaciers and ice sheets, particularly further inland, low surface melt input and shallow bed topography restrict the development of the subglacial drainage system (Meierbachtol et al., 2013; Rennermalm et al., 2013; Dow et al., 2014; Doyle et al., 2014). Furthermore, ice is generally much thicker in Greenland and faster flowing compared to valley glaciers. Greenland field data, such as borehole measurements, are limited to the lower ablation zone of the ice sheet of land-terminating glaciers due to complex terrain and accessibility (e.g., Bhatia et al., 2011; Smeets et al., 2012; Chandler et al., 2013; Meierbachtol et al., 2013; Andrews et al., 2014; Doyle et al., 2015; van de Wal et al., 2015). Tidewater glaciers are notoriously difficult to study due to their heavily crevassed terrain and subglacial outflow exits at the base of the calving front, hundreds of metres below the fjord surface. As such, tidewater glacier subglacial hydrology is typically studied using modelling (e.g., de Fleurian et al., 2016; Cook et al., 2020). The precise structure of the subglacial drainage system beneath the Greenland Ice Sheet remains unclear, however it is unlikely that the distributed and efficient systems are independent units, rather they are more likely to be hydraulically connected, and both configurations are thought to even exist beneath the same glacier (Hubbard et al., 1995; Andrews et al., 2014).

1.3.3.2 Spatial and temporal evolution of the subglacial hydrological system and ice dynamics

The nature of the drainage system will likely vary from glacier to glacier due to the vast array of spatially and temporally varying factors which influence subglacial water pressure, such as bed topography and characteristics, ice thickness, basal ice temperature, ice sliding speed, and the rate and distribution of water supply to the bed (Fountain and Walder, 1998). Early in the melt season, inefficient distributed

drainage system is thought to dominate since minimal runoff reaches the bed and creep closure rates exceed wall melt rates (Figure 1.16). As the melt season develops, surface melting rapidly increases and runoff inundates the bed, disturbing and overwhelming the inefficient drainage system (Andrews et al., 2014; Wright et al., 2016) (Figure 1.16). An initial acceleration in ice flow, referred to as a 'spring event', occurs due to the increased water pressure (Bartholomew et al., 2010; Sundal et al., 2011; Fitzpatrick et al., 2013; Moon et al., 2014; Vijay et al., 2019) (Figure 1.16). The spring event typically begins in early May and lasts a few days to a week, with ice velocity increases up to 300-400% of pre-melt season levels (Sole et al., 2013). As the melt season progresses, an efficient channelised system consequently evolves as wall melt rates exceed creep closure allowing channels to expand (Kamb, 1987; Bingham et al., 2005; Schoof, 2010) and triggering a lowering of basal water pressure (Figure 1.16). This subsequently leads to a deceleration in ice flow (Bartholomew et al., 2010, 2012; Sole et al., 2013) (Figure 1.16). Brief increases in ice velocity (by >100%) can occur during this period, in response to sudden injection of large volumes of meltwater, for example during abnormaly warm intervals or periods of heavy rainfall (Tedesco et al., 2013; Doyle et al., 2015) or rapid supraglacial lake drainage events (Das et al., 2008; Shepherd et al., 2009; Hoffman et al., 2011; Doyle et al., 2013; Tedesco et al., 2013) (Figure 1.16). A slow-down in ice flow usually follows the initial spike in ice velocity following rapid supraglacial lake drainage (Andrews et al., 2018) (Figure 1.16). Towards the end of summer, surface melt and supply to the bed is reduced, causing the gradual closure of channels as creep closure outweighs wall melt rates. During winter, when runoff has come to an end, the weakly-connected, inefficient drainage system is re-established, and subglacial water pressure subsequently increases, thereby slowly restoring ice velocity rates to pre-melt season speeds (Joughin et al., 2008; Colgan et al., 2012).

The inland limit of efficient subglacial drainage beneath the Greenland Ice Sheet is contested within the glaciological community. Theory suggests that in the interior of the ice sheet where the surface slopes are shallower, meltwater production is lower and the ice is thicker, the development of efficient subglacial drainage is hindered due to rapid creep-closure (Röthlisberger, 1972) and reduced hydropotential gradients. Borehole water pressure observations indicate channel formation beneath ice up to

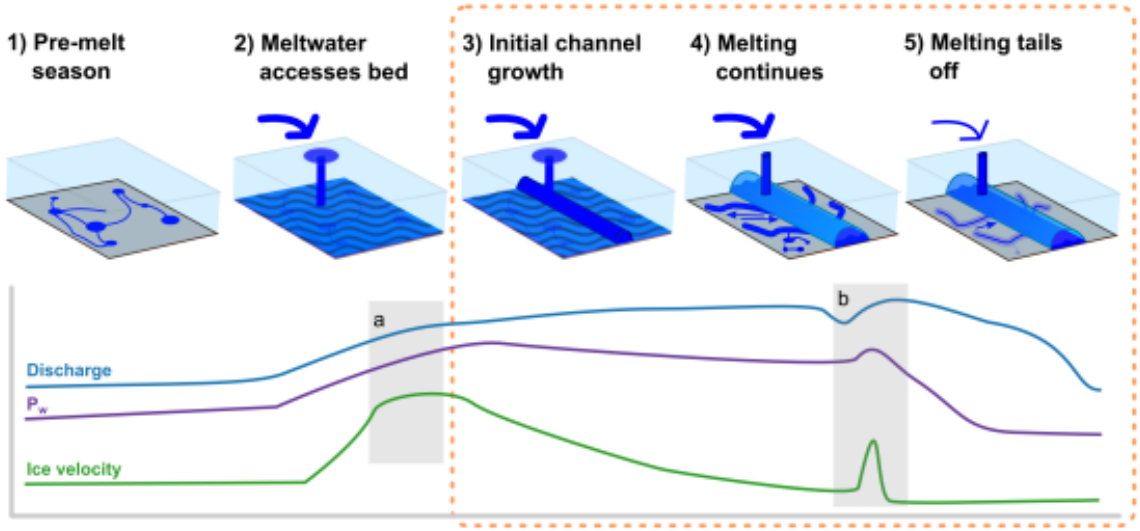

Figure 1.16: Conceptual diagram illustrating the evolution of the hydrological system at a typical land-terminating glacier in Greenland throughout the melt season. Box (a) refers to a 'spring event', and (b) refers to a transient increase in rate of meltwater supply, for example from a supraglacial lake drainage. Source: Tedstone, 2015.

~600 m thick (Andrews et al., 2014; van de Wal et al., 2015). Water tracer transit times indicate that efficient channels form rapidly (Cowton et al., 2013), and can reach at least ~40 km inland (Chandler et al., 2013). Modelling studies suggest that efficient channels can form up to ~50 km from the margin, beneath thick ~900 m ice (de Fleurian et al., 2016; Koziol and Arnold, 2018), but not at about 70 km inland beneath 1,200 m thick ice (Dow et al., 2014). This infers a transition to an inefficient drainage system towards the interior of the ice sheet. There is, however, high uncertainty in these numerical models due to sparse observational data. The spatial distribution of moulins is also thought to influence spatial variations in subglacial hydrology. High density of moulins has been linked to widespread and rapid channelisation beneath ~800 m thick ice (Banwell et al., 2016). Water from supraglacial lakes can also change the seasonal efficiency of the subglacial drainage system (Sundal et al., 2009; Hoffman et al., 2011; Andrews et al., 2018) and create new routes to the bed, thereby adding meltwater to the basal system throughout the season (Catania and Neumann, 2010; Hoffman et al., 2018).

1.3.3.3 Erosion and transfer of subglacial sediment downstream

Glaciers erode their underlying bedrock or sediment by three main processes: (1) abrasion, the process whereby particles contained within the basal ice are dragged across the underlying bed, producing fine-grained material (2) glacial quarrying (or plucking), where the glacier removes and entrains large fragments of the bed by fracturing or crushing bedrock, and (3) glacial meltwater erosion, which is the result of either mechanical (i.e. fluvial abrasion by the transport of suspended sediment and bedload within meltwater at the base of the ice) or chemical (i.e., the removal of rock and debris in solution) processes (Anderson and Anderson, 2010; Blomdin and Harbor, 2017). Erosion rates of 5 mm a^{-1} have been estimated for the margins of the Greenland Ice Sheet (Cowton et al., 2012), however, sediment fluxes are influenced by a number of factors including glacier hydrology, bedrock lithology, glacier size and subglacial sediment stores (Hallet et al., 1996).

A complex relationship exists between the hydrological system and bedrock erosion, and hence sediment fluxes. The development, duration and spatial extent of the subglacial drainage system is dependent upon spatio-temporal variations in meltwater supply, therefore high evacuation rates often correlate with high surface melt rates during summer. Efficient channelised drainage systems have higher capacity for sediment yields, compared with inefficient distributed systems (Alley et al., 1997; Swift et al., 2002; Cowton et al., 2012). Thick and fast-flowing ice also allow for high sediment yields (Hasholt et al., 2013). Glacial quarrying is influenced by fluctuations in effective pressure at the bed (Cohen et al., 2006; Iverson, 2012), which is an important modulator of basal sliding. It is important to understand the relationship between hydrology and sediment discharge, as it influences various processes such as fjord circulation and tidewater glacier dynamics, nutrient fluxes into the ocean, biogeochemical interactions downstream, and landscape evolution. I will discuss each of these impacts in turn.

The majority of glacial discharge enters the ocean through fjord systems which surround much of the periphery of the ice sheet, connecting to the open ocean downstream (Straneo and Cenedese, 2015). Each fjord system has unique geometry, tides, freshwater runoff and other external forcings, but in general, in deep fjords,

warm salty Atlantic water is typically found at depths greater than 200 m with cold, fresher Polar water above, and during summer, a thin layer (∼50 m or less) of relatively warm near-surface water (Straneo et al., 2012; Ohashi et al., 2020) (Figure 1.17). The release of freshwater from subglacial conduits into fjord environments (Xu et al., 2012; Chauche et al., 2014; Carroll et al., 2015; Carroll et al., 2016; Mankoff et al., 2016; Stevens et al., 2016; Slater et al., 2018a), as well as iceberg melt (Enderlin et al., 2016; Moon et al., 2018) and terminus melt (Slater et al., 2015), can alter fjord circulation. The majority of sediment-laden freshwater enters the dense, saline seawater at depth from englacial and subglacial conduits, which then rises up the glacier front as a turbulent buoyant plume, entraining and mixing nutrient-rich fjord waters to create 'glacially modified waters', before reaching neutral buoyancy (or the fjord surface) and flowing towards the ocean (Hudson et al., 2014; Carroll et al., 2015; Straneo and Cenedese, 2015; Meire et al., 2016b; Jackson et al., 2017) (Figure 1.17). The surfacing and turbulent nature of these plumes (Figure 1.18) transfers ocean heat to the ice, enhancing submarine melt (Sciascia et al., 2013; Xu et al., 2013; Kimura et al., 2014; Slater et al., 2015, 2018a) and undercutting, thus accelerating calving rate (O'Leary and Christoffersen, 2013; Luckman et al., 2015; Andrés et al., 2018; Schild et al., 2018; Vallot et al., 2018; How et al., 2019). Plume characteristics are primarily driven by the intensity of subglacial discharge; buoyancy forces are dominant during low discharge, meaning that water rises to the surface rapidly as a forced plume, whereas at higher subglacial discharges, momentum forces dominate and thus plumes are carried horizontally before rising (Powell, 1990).

Glacial discharge also has complex implications for marine biological processes by providing a source of organic matter and mineral nutrients, including nitrogen, phosphorus, iron and silica throughout the melt season (Bhatia et al., 2013; Hawkings et al., 2015; Wadham et al., 2016; Beaird et al., 2018). The upwelling of the nutrient-rich subglacial meltwater can encourage plankton blooms in the summer (Meire et al., 2015; Kanna et al., 2018) which is important for marine life such as fish and Arctic seabirds (Arimitsu et al., 2012; Naito et al., 2019; Matsuno et al., 2020) and as a consequence, the fishing industry in Greenland (Meire et al., 2017). However, with projected future climatic warming, this impact is predicted to diminish as glaciers retreat on land (Meire et al., 2017; Hopwood et al., 2018). The addition of material to

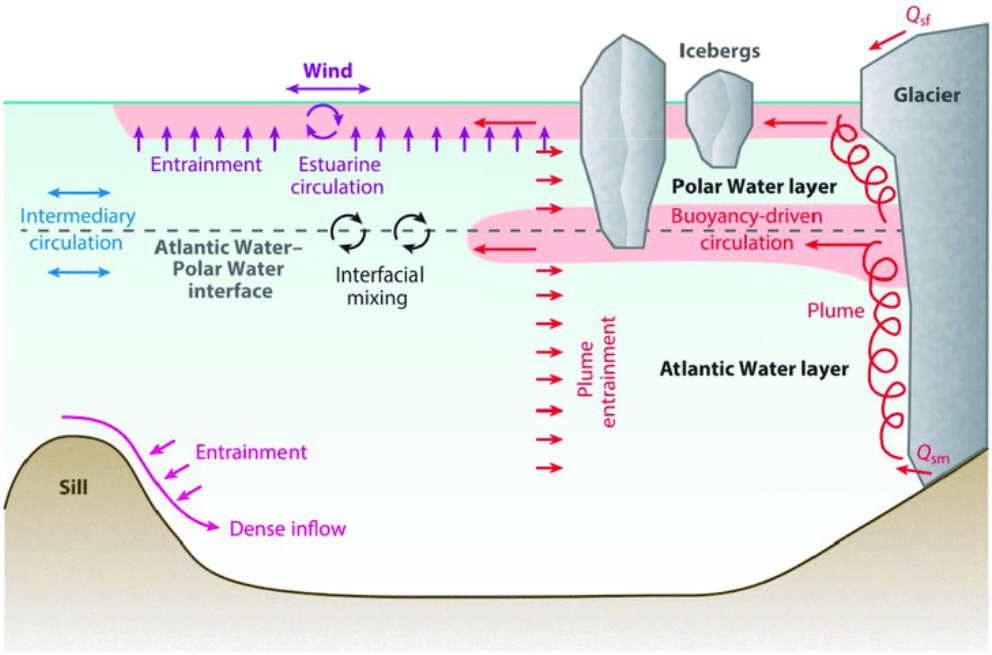

Figure 1.17: Conceptual diagram illustrating different circulations within a typical Greenland fjord. Buoyancy-driven circulation from submarine melting, subglacial discharge and surface runoff are shown in red. Intermediary baroclinic circulation is show in blue. Estuarine circulation from surface runoff only is shown in purple. The circulation as a result of dense inflow over sill is shown in pink. Source: Straneo and Cenedese, 2015.

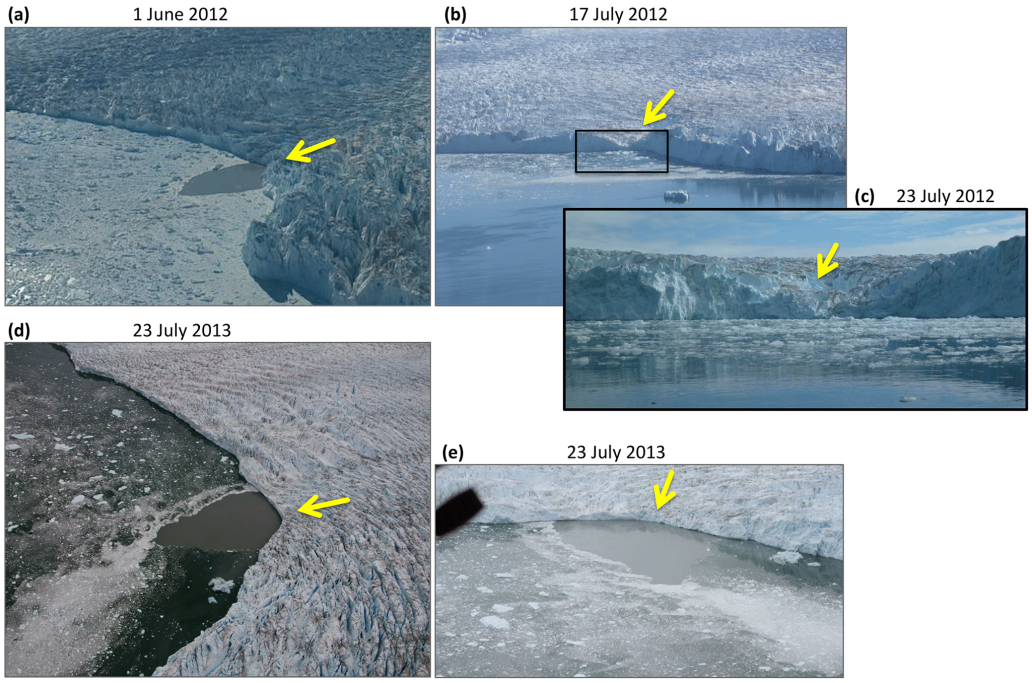

Figure 1.18: Aerial images of a plume at the ice front of Saqqarliup–Saqqarleq, western Greenland on (a) 1st June 2012 (b) 17th July 2012 (c-e) 23rd July 2012 but taken from the boat in (c). Yellow arrows indicate approximate direction of ice flow and origin of plume. Source: De Andrés et al., 2020.

the fjord via subglacial discharge has also been linked to diminished phytoplankton productivity by increasing turbidity which causes stress to benthic ecosystems (Korsun and Hald, 2000), and limiting light attenuation and photosynthesis (Murray et al., 2015; Holinde and Zielinski, 2016; Burgers et al., 2017).

Meltwater routed via distributed drainage networks is slow-moving and therefore exposed to highly geochemically reactive sediments. These environments are suitable for colonies of microbes, and allows several redox reactions, for example, dentrification (Wadham et al., 2016) and methanogenesis (Boyd et al., 2010). The release of microbial methane, generated during erosion of the underlying bedrock, has been recently detected in subglacial runoff from several Greenland outlet glaciers (Dieser et al., 2014; Christiansen and Jørgensen, 2018; Lamarche-Gagnon et al., 2019; Christiansen et al., 2021; Pain et al., 2021). Efficient subglacial drainage networks allow methane to be transported to the ice margin rapidly before being oxidised to carbon dioxide and emitted to the atmosphere. This source of CO_2 has been largely understudied until recently and could amplify climate warming, particularly with increased ice sheet melting rates. However, the extent of the impact remains uncertain (Wadham et al., 2008, 2019; Christiansen et al., 2021).

1.4 Subglacial lakes

In most physical models and conceptual frameworks, water beneath the Greenland Ice Sheet is thought to flow relatively unhindered to the coast. However, in recent years the discovery of subglacial lakes in Greenland has shown that meltwater - originating from either the surface or the base - can be stored at the bed for longer periods to time. Currently, however, the distribution and dynamics of subglacial lakes beneath the Greenland Ice Sheet is poorly understood, and much of our knowledge is based on Antarctic and Icelandic studies.

Subglacial lakes are bodies of liquid water which form when meltwater accumulates in topographic depressions in the bed or regions of hydraulic convergence (Figure 1.19). A subglacial lake is sustained by a combination of the insulation and pressure provided by the overlying ice sheet, frictional heat and geothermal heat flux (Robin et al., 1970;

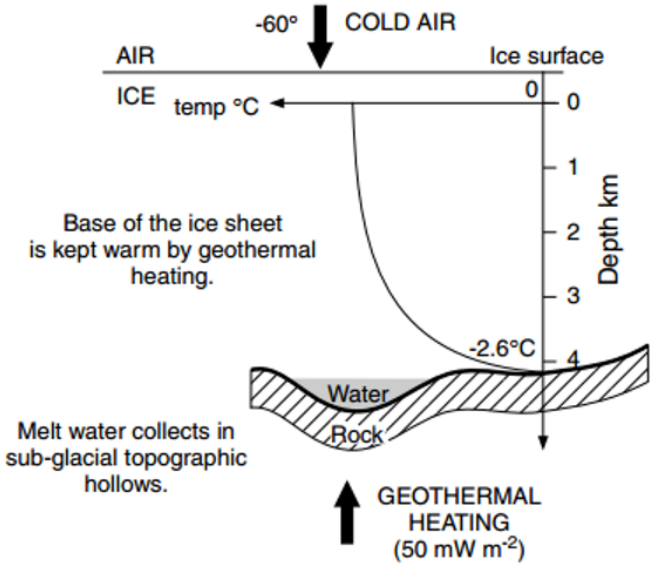

Figure 1.19: Formation of a subglacial lake beneath the Antarctic Ice Sheet: meltwater forms in a topographic hollow in the bed and is sustained due to goethermal heating. The ice-overburden pressure causes the melting point of water to be below 0°C. Source: Siegert et al., 2003.

Siegert, 2000a; Pattyn, 2010) (Figure 1.19). Subglacial lakes are categorised into 'stable' lakes which are persistent, relatively closed environments with long residence times, and are typically identified using Radio-Echo Sounding (RES) or seismic techniques, and 'active' subglacial lakes which episodically fill and drain, suddenly discharging water and are typically detected by monitoring surface elevation changes. In this section, I describe the history and development of subglacial lake knowledge, the distribution and dynamics of subglacial lakes beneath ice sheets and ice caps across the globe, and the wider importance of their presence and behaviour.

1.4.1 History of subglacial lake exploration

Subglacial lakes were first, inadvertently, discovered in 1961 by R.V. Robinson, a Russian pilot who used notably flat features on the Antarctic Ice Sheet surface for flight navigation, describing these geomorphological features as "lakes" with "gentle shores" (Robinson, 1961). It was later revealed that flat and smooth ice surfaces are characteristic of the existence of a subglacial lake beneath the ice, due to low friction between the overlying ice and the subglacial lake surface. This is mostly typical for

larger subglacial lakes, as smaller lakes (<4 km wide) do not tend to have this surface expression as the overlying ice may not be in hydrostatic equilibrium (Siegert and Ridley, 1998).

In the early 1960s, seismic surveys (Section 2.0.1 describes the seismic survey techniques in detail) were refined and carried out by Russian scientists, including Andrey Kapitsa, to measure the thickness of ice over what is now known to be Subglacial Lake Vostok (Kapitsa, 1960). The seismic data recorded an ice thickness of ∼3,700 m, with two reflections near the ice base, which were interpreted as the lower boundary of ice and the lower boundary of a frozen sedimentary layer (Kapitsa, 1968). The team were unaware of the subglacial lake, which was then interpreted some 30 years later.

In the 1970s, airborne radar sounding surveys of the Antarctic Ice Sheet were performed by a joint UK, USA and Danish team, led by Gordon Robin, to map the subglacial topography and ice thickness. As the equipment is mounted to an aircraft, this technique allowed greater, more systematic and efficient surveys compared to seismic studies. Subglacial lakes are easily distinguished in radar data by their bright, flat and specular reflectors, relative to the surrounding bedrock (see Section 2.0.2 for in-depth details). This technique led to the detection of 17 small subglacial lakes (≤15 km wide) in Eastern Antarctica, mostly south of Vostok Russian Station (Oswald and Robin, 1973). A few years later, a large lake reflector was identified near Vostok Russian Station and Subglacial Lake Vostok was identified (Robin et al., 1977).

The launch of the European Space Agency (ESA) European Remote Sensing satellite (ERS-1) enabled accurate measurements of the Earth's surface, including the polar ice sheets (see Section 2.0.3 for more details on altimetry techniques). Ridley et al., 1993 utilised these elevation data to map the abnormally flat region above Subglacial Lake Vostok (Figure 1.20a), which corresponded with lake margins detected in radar data. These studies and observations led to the re-examination of the seismic and radar data collected in the 1960s and 70s at a conference in 1994. The subsequent international, collaborative study (Kapitsa et al., 1996) reinterpreted the two seismic reflectors as an ice-water interface and lake bottom reflector, representing the 230 km long, 50 km wide, at least 500 m deep Subglacial Lake Vostok (Figure 1.20b).

The pivotal study showing the geometric scale of Subglacial Lake Vostok sparked significant scientific interest in subglacial lakes and the basal hydrological system, particularly from the microbial community which speculated that the subglacial lakes could support life (e.g., Ellis-Evans and Wynn-Williams, 1996). The first inventory of Antarctic subglacial lakes was produced in 1996 showing the location and characteristics of 77 subglacial lakes beneath the ice sheet (Siegert et al., 1996). Further radar surveys in the late 1990s and early 2000s from numerous scientific teams, increased this number to 145 (Siegert et al., 2005). Until this juncture, subglacial lakes were typically regarded as stable, persistent, relatively closed environments, with long residence times and slow circulations (Kapitsa et al., 1996; Siegert et al., 2001; Bell et al., 2002).

Analysis of timeseries of surface elevation changes from European Remote Sensing (ERS-2) satellite altimeter challenged this perception, revealing a localised region of surface lowering by about 4 m between 1997 and 1999 in central East Antarctica (Wingham et al., 2006b). Over the same period, three regions of the ice sheet over 290 km away at the mouth of the Adventure Trench, a major subglacial valley, rose by over 1 m. These observations were interpreted as evidence of the rapid drainage of a $\sim$1.8 km^3 subglacial lake, which transferred water to at least two other downstream subglacial lakes (Wingham et al., 2006b). This demonstrated a highly active basal hydrological system in Antarctica, with connected subglacial lakes, which was previously unknown (Siegert et al., 2007). Other vertical ice displacements with similar timing and magnitude were discovered in West Antarctica, also linked to rapid subglacial lake drainage events (Gray et al., 2005; Fricker et al., 2007). Surface lowering of $\sim$9 m was detected beneath the Whillans Ice Stream, near the grounding line, associated with an estimated 1.2 km^3 outburst flood, with a discharge of 40 m^3 s^{-1} over an 18-month period (Fricker et al., 2007). Repeat interferometric synthetic aperture radar (inSAR) was utilised to detect localised subsidence and surface uplift, inferred to correspond with the transport of $\sim$20 $\times 10^6$ m^3 and $\sim$10 $\times 10^6$ m^3 water beneath the Kamb and Bindschadler Ice Streams, respectively (Gray et al., 2005). These findings led to the first comprehensive inventory of 'active' subglacial lakes (i.e. lakes which episodically fill and drain, and are hydraulically connected) using satellite altimetry, detecting 124 such subglacial lakes and assessing their connectivity (Smith et al., 2009).

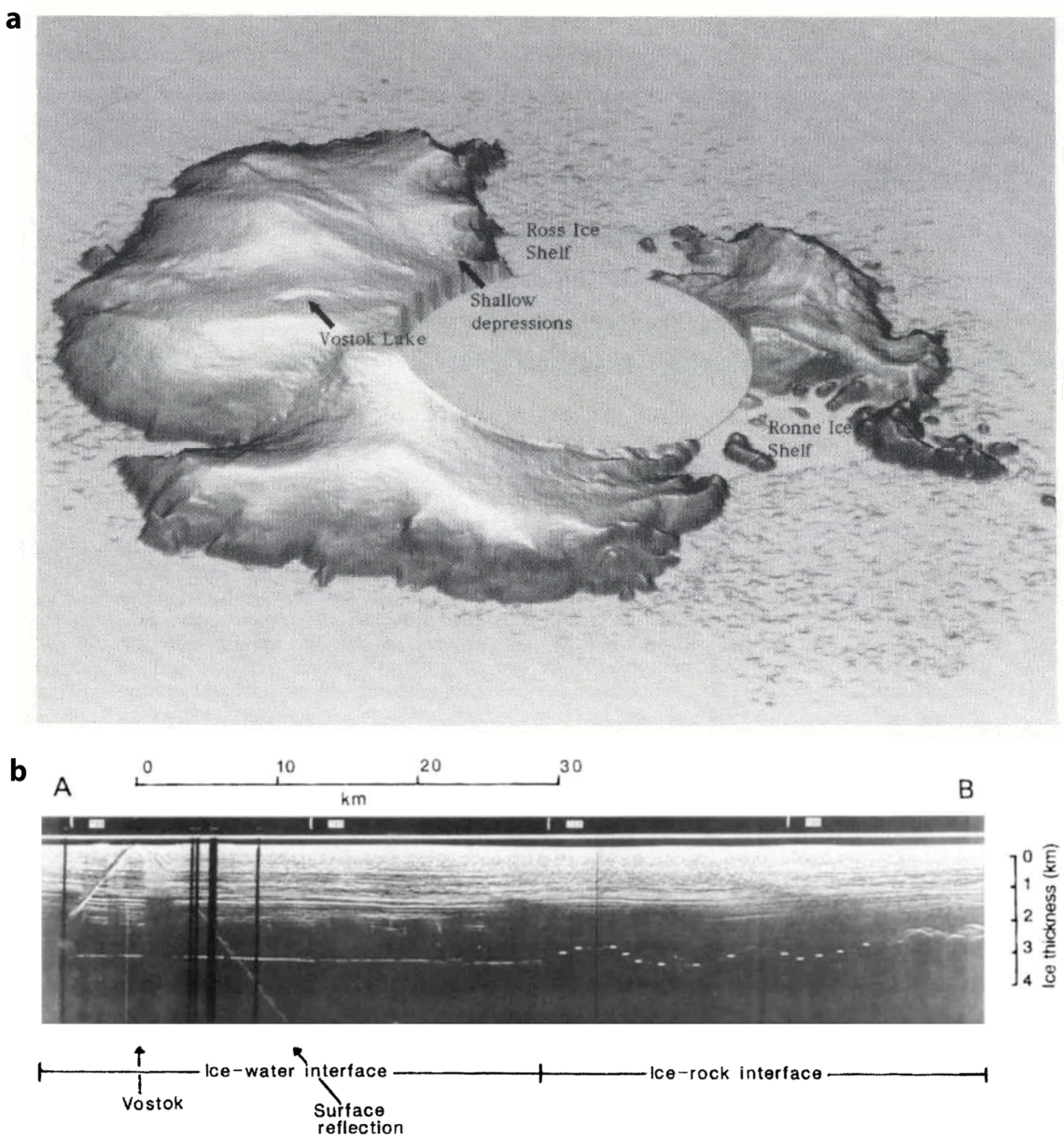

Figure 1.20: Early records of Subglacial Lake Vostok (a) 3D surface topography of Antarctica derived from ERS-1 radar altimetry, showing location of Subglacial Lake Vostok. Source: Ridley et al., 1993. (b) Radio-echo sounding profile across the subglacial lake showing a 30 km long ice-water reflection on the left, which turns to weaker echoes from the ice-bedrock interface Source: Kapitsa et al., 1996.

The latest inventory of subglacial lakes combines both stable RES-detected lakes and these active lakes, bringing the total number of subglacial lakes beneath Antarctica to 379 (Wright and Siegert, 2012), although hundreds of subglacial lakes have since been discovered including ∼70 across Dome C and the Aurora Subglacial Basin (Wright et al., 2012; Young et al., 2017), over 100 stable lakes in the Gamburtsev Subglacial Mountains, beneath Dome A (Wolovick et al., 2013), 3 lakes near Byrd Glacier (Wright et al., 2014), 1 beneath the Institute Ice Stream and Minnesota Glacier ice divide (Rivera et al., 2015), ∼30 stable lakes in Dronning Maud Land (Goeller et al., 2016), a large subglacial lake inferred by the flat ice surface in Princess Elizabeth Land (PEL), and later confirmed by RES data (Jamieson et al., 2016), 33 RES-detected lakes in the Ellsworth Subglacial Highlands (Napoleoni et al., 2020), 4 large active lakes beneath Thwaites Glacier (Smith et al., 2017a; Hoffman et al., 2020; Malczyk et al., 2020), and 2 small active lakes near the grounding line of Kamb Ice Stream (Kim et al., 2016; Siegfried and Fricker, 2018).

1.4.2 Distribution and dynamics of subglacial lakes

Subglacial lakes have been detected beneath the Antarctic and Greenland Ice Sheets, ice caps in Iceland and Canada and a few subglacial lakes beneath valley glaciers in the European Alps.

1.4.2.1 Antarctic subglacial lakes

In Antarctica, the majority of stable subglacial lakes are situated in the continental interior in close proximity to major ice divides, with 73% of RES-detected lakes in the latest inventory being located within 300 km of the flow divide (Wright and Siegert, 2011) (Figure 1.21). The ice in the interior is slow-moving and ∼3-4 km thick. The ice surface is nearly flat (Morlighem et al., 2020), whilst several large, deep, likely sedimentary basins with low relief exist beneath the ice, separated by mountainous ridges (Morlighem et al., 2020). These conditions promote basal melting; under thick ice, the temperature at the bed can reach pressure melting point, subglacial water produced by local geothermal heat will flow along hydraulic potential gradients to pool in hydraulic minima (Shreve, 1972). As a result, many small ($<$20 km^2, with the exception of 800 km^2 Subglacial Lake Concordia; Tikku et al., 2005), shallow

subglacial lakes are concentrated in the deep Aurora, Vincennes and Wilkes basins (Tabacco et al., 2003, 2006; Wright and Siegert, 2011). Towards the margins of these subglacial basins, but still near major ice divides, significant topographic depressions are found in the bedrock. Large, elongated, deep subglacial lakes such as Vostok, 90°E, Sovetskaya and possibly Princess Elizabeth Land (PEL) occupy these types of depressions, thought to be controlled by extensional tectonics (Meybeck, 1995; Bell et al., 2006; Tabacco et al., 2006; Jamieson et al., 2016), which trap substantial basal water (Dowdeswell and Siegert, 1999). Subglacial lakes in the interior can also be situated on the flanks of subglacial highlands at the edges of these basins, such as the Belgica and Gamburtsev Mountains in East Antarctica (Dowdeswell and Siegert, 2003). These lakes are small (<10 km in length) and constrained by steep local topography, and exist due to anonymously high localised geothermal heat flux (Dowdeswell and Siegert, 2003).

About a third of subglacial lakes in Antarctica are classified as hydraulically active (Wright and Siegert, 2012). Active subglacial lakes in Antarctica do not appear to have a strong relationship with distance to the ice divide. Indeed, only 13% of active subglacial lakes are situated within 300 km of the flow divide, with a modal distance of 750 km (Wright and Siegert, 2011). Active subglacial lakes are predominantly detected closer to the ice margin within 200 km of major outlet glaciers and ice streams, such as Academy and Recovery Glaciers, and Mercer, Whillans and MacAyeal Ice Streams (Fricker and Scambos, 2009; Smith et al., 2009; Fricker et al., 2010; Siegfried and Fricker, 2018). At the onset of enhanced ice flow and beneath the tributaries feeding ice streams, high frictional melt at the bed (Bentley et al., 1998; Studinger et al., 2001) is thought to produce a constant supply of meltwater to feed and replenish active subglacial lakes (Smith et al., 2009). At the head of Recovery Ice Stream, several large active subglacial lakes have been detected which have a large upstream catchment area (Bell et al., 2007a). These lakes have similar characteristics with large stable lakes in the ice sheet interior, exhibiting signs of tectonic origin (Bell et al., 2007a). However, it should be noted that not all fast-flowing outlets are associated with subglacial lake activity.

The volume of water stored in active subglacial lakes varies temporally, with fill-

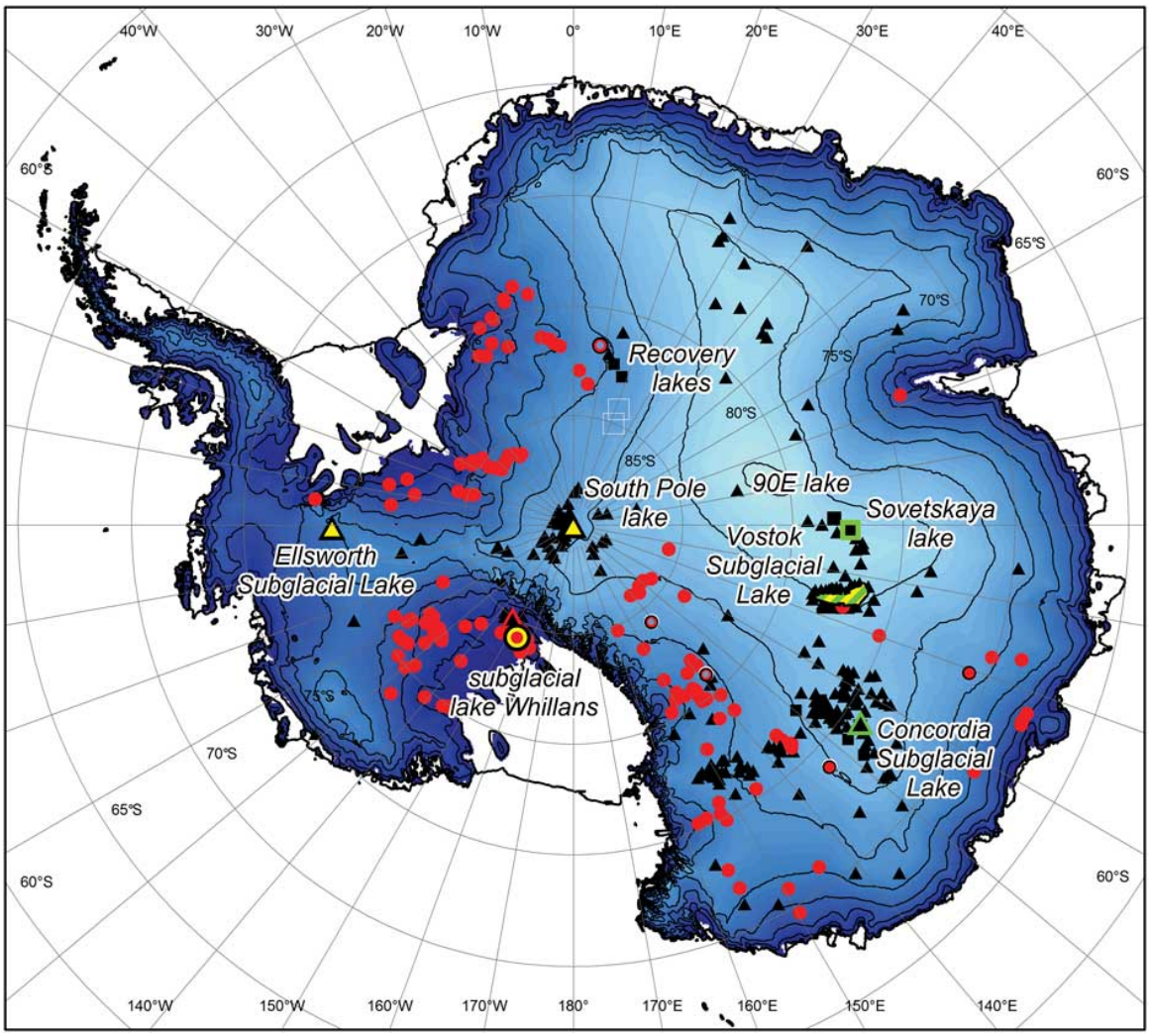

Figure 1.21: Distribution of Antarctic subglacial lakes from the latest inventory. Black/triangles are lakes detected using radio-echo sounding, yellow symbols are identified using seismic sounding, green symbols using gravitational field mapping, red/circle are detected by surface elevation change measurements, square symbols represent lake identified from a flat ice surface. The outline of Subglacial Lake Vostok is shown. Source: Wright and Siegert, 2012.

drain recurrence typically lasting years, but some drainage events take over a decade to evolve, for example Cook_{E2} (McMillan et al., 2013) and subglacial lakes beneath Thwaites (Smith et al., 2017a) and Slessor ice streams (Siegfried and Fricker, 2018). A subglacial lake can drain due to a break in the hydropotential seal (Fowler, 1999) or high water flux (Dow et al., 2016). These factors cause substantial changes in pressure which results in the episodic release of water into the downstream subglacial system. Subglacial lake connectivity can alter the timescale of drainage, with the release of upstream subglacial lake water filling and interrupting the cycle of a downstream lake (Smith et al., 2017a). Ice thinning has also been proposed as a triggering mechanism of subglacial lake drainage. Changes in the ice surface of Crane Glacier, Antarctic Peninsula, namely steepened surface slope during glacier retreat, is thought to have tilted the subglacial lake surface, increasing the water (and stress) level at the downstream edge of the lake, until it breached and drained downstream (Scambos et al., 2011).

1.4.2.2 Predicted Antarctic subglacial lakes

Livingstone et al., 2013 used hydraulic potential calculations to predict subglacial lake locations beneath the ice sheets, estimating that subglacial lakes cover $\sim 4\%$ of the ice-bed interface, although when applying a mask to cold-bedded regions, this was reduced to 2.7% coverage (350,000 km^2). This is an order of magnitude greater than that predicted in Dowdeswell and Siegert, 1999. Goeller et al., 2016 also predicted subglacial lake locations using hydraulic potential and a grid resolution of 5 km, estimating 5% coverage of the ice-bed interface, which was then scaled down to 0.6% or 77,000 $\pm$ 18,000 km^2 based on the number of predicted lakes that were not confirmed by radar data. Both of these studies used Bedmap2 for bed topography (Fretwell et al., 2013) where interpolation produces an unrealistically smooth bed, with high uncertainty (up to 1 km) along with artefacts. MacKie et al., 2020 used a probabilistic metric for subglacial lake locations and integrated surface area to overcome these disadvantages. Using different roughness scenarios, MacKie et al., 2020 estimate between $\sim$5-15,000 km^2 coverage at the bed.

1.4.2.3 Greenlandic subglacial lakes

Subglacial lakes have only been discovered beneath the Greenland Ice Sheet in the last decennial (Palmer et al., 2013; Howat et al., 2015; Palmer et al., 2015; Willis et al., 2015; Livingstone et al., 2019). Palmer et al., 2013 detected the first subglacial lakes in northwestern Greenland using RES, finding two small (<2.5 km in length) stable lakes, within 20 km of the nearest ice divide (Figure 1.22). The ice above these lakes is relatively cold and thin (approximately 800 m thick). Further radar and seismic investigations have since confirmed the presence of water in one of the lakes, with a depth of approximately 15 m, and volume of 0.15 km^3 (Maguire et al., 2020). Several hypotheses have been proposed to explain the presence of these lakes: (1) ancient marine water in a closed system similar to hypersaline lakes in Antarctica (Hubbard et al., 2004; Lyons et al., 2005; Mikucki et al., 2009; Lyons et al., 2019) and the Devon Ice Cap, Canadian Arctic (Rutishauser et al., 2018) (see Section 1.4.2.5), however the northwest Greenland subglacial lake is over 500 m above sea level, therefore it is unlikely to be trapped seawater, and although an ancient evaporite deposit is possible (Rutishauser et al., 2018), the geology of this region does not suggest this (Dawes, 2004); (2) unlike Antarctica which has scarce surface meltwater, the Greenland Ice Sheet has abundant meltwater at the surface which can be transported to the subglacial system. Surface meltwater input, for example from a supraglacial lake drainage, could recharge the subglacial lake beneath (Palmer et al., 2013) or; (3) elevated geothermal heat flux enabling basal melting, which are estimated at 50-60 mW m^{-2} in this region (Rogozhina et al., 2016; Martos et al., 2018; Artemieva, 2019). Maguire et al., 2020 suggest that geothermal heat flux or hypersalinity due to local ancient evaporite are most likely clauses for subglacial lakes to be present here.

In 2015, two active subglacial lakes were identified using digital elevation models to map changes in the ice surface (Howat et al., 2015; Palmer et al., 2015). The first is located about 50 km from the southwest margin of the Greenland Ice Sheet, where a $\sim$1.5 km^2, 70 m deep depression with slopes of 10-15° formed in 2011 as a result of an estimated 2.5 $\times 10^{-2}$ km^3 subglacial lake suddenly draining (Howat et al., 2015; Palmer et al., 2015) (Figure 1.23). Supraglacial lakes and moulins in the vicinity are likely to have provided a pathway to the bed, allowing the subglacial lake beneath to fill until surpassing the hydraulic potential 'dam', and the subglacial lake drainage

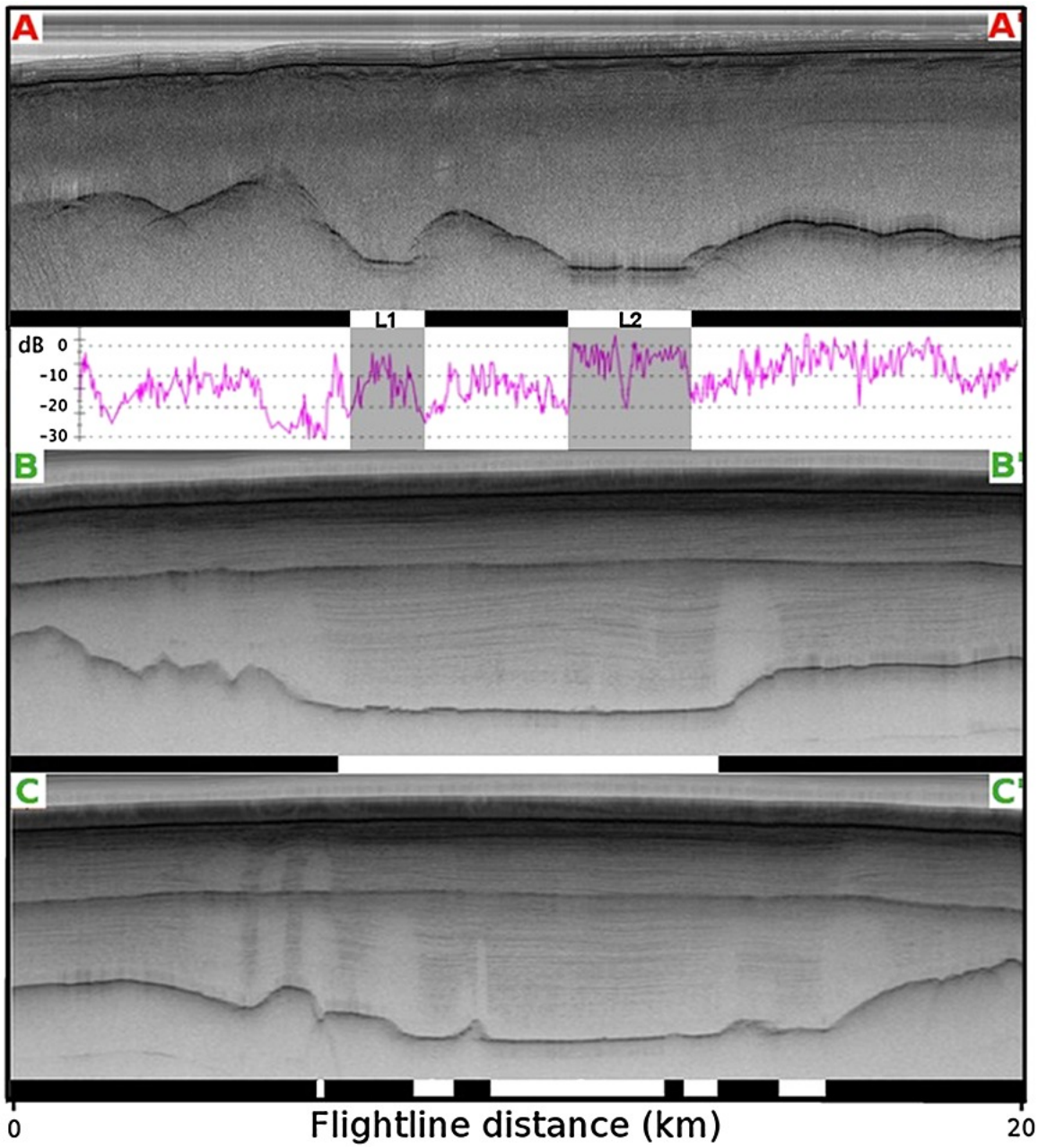

Figure 1.22: (a) Radio-echo sounding evidence for two subglacial lakes (L1 and L2) beneath the Greenland Ice Sheet, with bed reflectivity shown below. (b-c) RES data from May 2012 showing a smooth and relatively flat bed which could represent saturated sediment and therefore a previous subglacial lake extent. Source: Palmer et al., 2013.

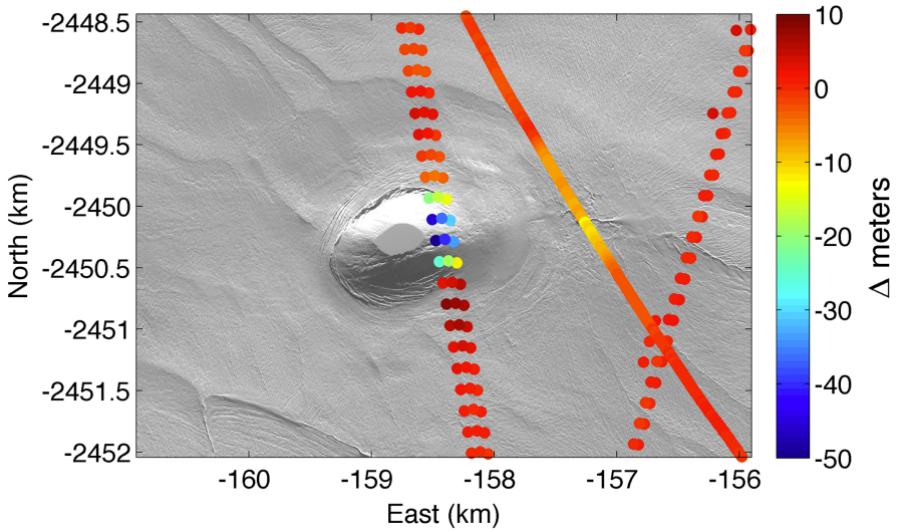

Figure 1.23: WorldView-1 panchromatic satellite image acquired on 28th October 2011, with elevation difference between WorldView-1 Digital Elevation Model (derived in 2011) and airborne topographic mapper LiDAR (derived in 1993) overlaid. Crevassing around the edge of the collapse basin is evident. The centre of the basin is flat due to ponding of meltwater. Source: Howat et al., 2015.

would melt and enlarge a subglacial channel through viscous heat dissipation, leading to continued drainage, despite reduced water pressures (Howat et al., 2015; Palmer et al., 2015). It is thought that the subglacial outburst flood (∼30 m^3 s^{-1} over a 14-day period) was efficiently routed to the ice margin (Palmer et al., 2015). These results provided the first evidence that, like in Antarctica, subglacial lakes can actively drain beneath the Greenland Ice Sheet and may modify the hydrological system.

The second active subglacial lake to be detected in Greenland is located in northeast Greenland, beneath the Flade Isblink ice cap, which is isolated from the main ice sheet (Willis et al., 2015) (Figure 1.23). A 8.4 km^2, 70 m deep surface depression (or collapse basin) with crevasses around the outer edges formed near the southern summit of the ice cap in autumn 2011 where the ice is about 500 m thick (Willis et al., 2012). The feature has two sub-basins, separated by a shallow saddle, and has a mitten-like shape. The formation of this collapse basin is interpreted to be a consequence of a ∼0.4 km^3 subglacial lake suddenly draining (Willis et al., 2015). It is estimated that the subglacial lake drained at a rate of 215 m^3 s^{-1} over a 21 day period, and the subglacial outburst flood was routed to a marine-terminating grounded outlet glacier to the north of the ice cap (Willis et al., 2015). Supraglacial streams intersect

the crevasses around the edge of this feature, allowing refilling of the subglacial lake beneath, as seen by uplift of the floor of the basin (up to 38 m over 2 years) for several years after the drainage event.

Several years later, three quasi-circular features (<1 km^2) were identified within 2 km of the lateral margin of Isunguata Sermia, West Greenland, through a technique called Digital Elevation Model (DEM) differencing (see section 2.0.4) (Livingstone et al., 2019). The drainage and refilling of three subglacial lakes are interpreted as causing vertical displacements at the ice surface. Due to their location in the lower ablation zone, these lakes are presumed to be recharged by upstream surface meltwater inputs, however despite their close proximity to each other, their drainage patterns do not suggest that they are connected like some Antarctic subglacial lakes (Livingstone et al., 2019). The outburst flood of the 2015 drainage event reached the proglacial foreland, depositing approximately 7.5 $\times 10^6$ m^3 of sediment aggradation near the ice margion (Livingstone et al., 2019) (Figure 1.25).

1.4.2.4 Icelandic subglacial lakes

In Iceland, active and dormant central volcanic systems exist beneath the four largest ice caps, with the most active volcanoes beneath Mýrdalsjökull and Vatnajökull (Gudmundsson and Högnadóttir, 2007). Volcanic and geothermal activity continuously melts the ice at the glacier bed, creating persistent depressions at the ice surface (Björnsson, 1974). A pressure sink is created at the ice bed due to relatively low ice overburden pressure beneath the depression, causing basal meltwater from surrounding areas to accumulate and form a subglacial lake, whilst high ice overburden pressure at the rim around the surface depression seals the lake. The three largest subglacial lakes are found beneath Vatnajökull; Grímsvötn and eastern and western Skaftá lakes, which have surface cauldrons several kilometres wide and hundreds of metres deep (Figure 1.26) (Björnsson, 1974; Einarsson et al., 2017; Magnússon et al., 2021). Large-scale melting from volcanic eruptions can cause these subglacial lakes to rapidly increase in volume and suddenly drain, leading to jökulhlaups - glacial outburst floods - which can be a hazardous for human populations near these ice caps (Björnsson, 2010). Grímsvötn subglacial lake drains approximately every 1-10 years (Björnsson, 2003), whilst Skaftá subglacial lakes drain at 2- to 3-year intervals.

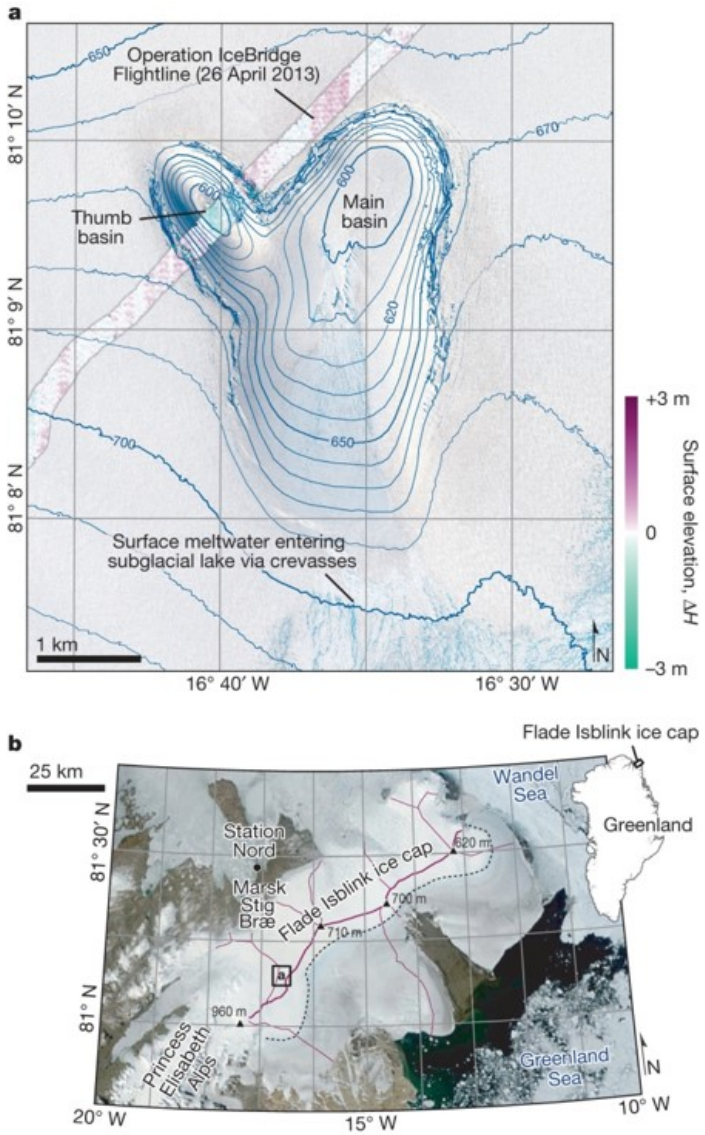

Figure 1.24: (a) RGB composite image acquired on 14th August 2012 from WorldView-2 of the mitten-shaped collapse basin, showing supraglacial meltwater flowing into the crevasses on the edge of the basin. Surface elevation difference between LiDAR (acquired on 26th April 2013 from NASA IceBridge airborne laser altimeter) and WorldView-1 satellite digital elevation model acquired on 17th May 2012 are shown by the green to purple colours. (b) Location of collapse basin on the Flade Isblink ice cap, with ice divides shown in purple. Source: Willis et al., 2015.

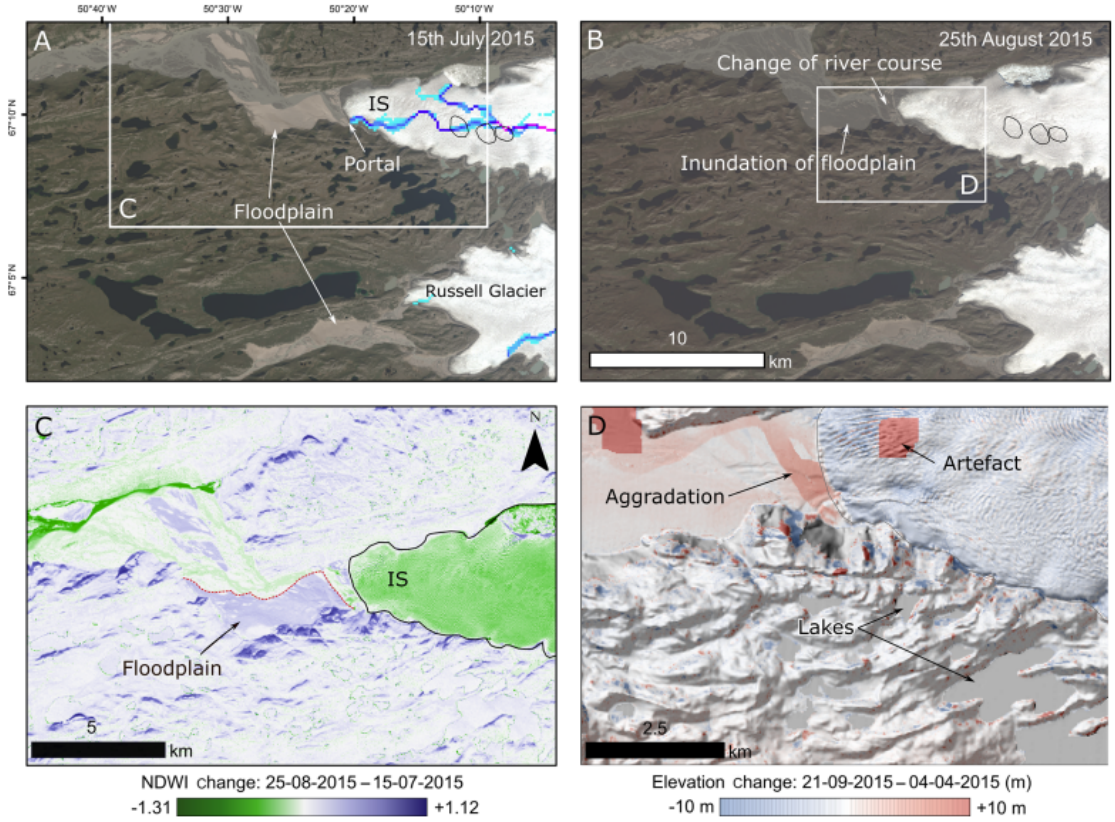

Figure 1.25: Evidence of geomorphological change in the proglacial environment following drainage of a subglacial lake in 2015. (a-b) RGB composite images acquired on 15th July 2015 (before drainage event) and 25th August 2015 (after drainage event). Location of three subglacial lakes are outlined in black. (c) Difference in normalised difference water index (NDWI) between 7th July 2015 and 15th August 2015. (d) Difference in elevation between two ArcticDEM digital elevation models acquired on 4th April 2015 and 21st September 2015. Source: Willis et al., 2015.

Icelandic subglacial lakes are characterised by slow filling, with either exponentially rising discharge and a more rapid drainage, or linearly rising discharge (discharge increases linearly at a significantly greater rate than exponential) until peak, before more gradual drainage (Figure 1.27). Smaller floods (peak discharge $<3 \times 10^3$ m^3 s^{-1}) tend to exhibit exponentially rising drainage styles, reaching their peak discharge in 2-3 weeks, and terminating about 1 week later. This pattern can be explained by the expansion of a single ice tunnel, due to frictional melting generated by water flow (Nye, 1976; Spring and Hutter, 1981; Clarke, 2003). Less commonly, larger subglacial floods can occur (peak discharge up to 4×10^4 m^3 s^{-1}), with linearly rising discharge patterns, where rapid filling of a subglacial lake causes flotation of the ice dam, and discharge increases faster than can be accomodated by ice tunnels, resulting in a flood wave with sheet-like flow (Björnsson, 1992; Johannesson, 2002; Flowers et al., 2004; Einarsson et al., 2017). An outburst flood of this type occurred in 1996, when the Gjálp volcanic eruption injected ∼2.7 km^3 of meltwater to the already ∼0.5 km^3 Grímsvötn subglacial lake. A subglacial sheet flood (peak discharge of 45-53 m^3 sec^{-1}) was forced up to the glacier surface through crevasses near the ice margin, and dislodged large ice blocks (Roberts et al., 2000; Russell et al., 2006), all within a period of 40 hours.

1.4.2.5 Subglacial lakes beneath other ice masses

Two subglacial lakes (approximately 5 and 8.3 km^2) were identified beneath the Devon Ice Cap, one of the largest ice caps in the Canadian Arctic (Rutishauser et al., 2018). The subglacial lakes were located using radio-echo sounding and are located within 5 km of a major ice divide, beneath 500-700 m thick ice (Rutishauser et al., 2018). These lakes are thought to consist of hypersaline water derived from dissolution of the surrounding evaporite-rich geology, since they do not receive surface meltwater input and exist at temperatures well below the pressure-melting point (Rutishauser et al., 2018). In the European Alps and Cascade mountain range, small outburst floods have been attributed to the sudden rupturing of subglacial water-filled cavities beneath some valley glaciers (Haeberli, 1983; Driedger and Fountain, 1989). The stepped bed topography at Mount Rainier is thought to support the development of such subglacial cavities, which can recurringly enlarge and drain causing cyclical outburst floods (Haeberli, 1983).

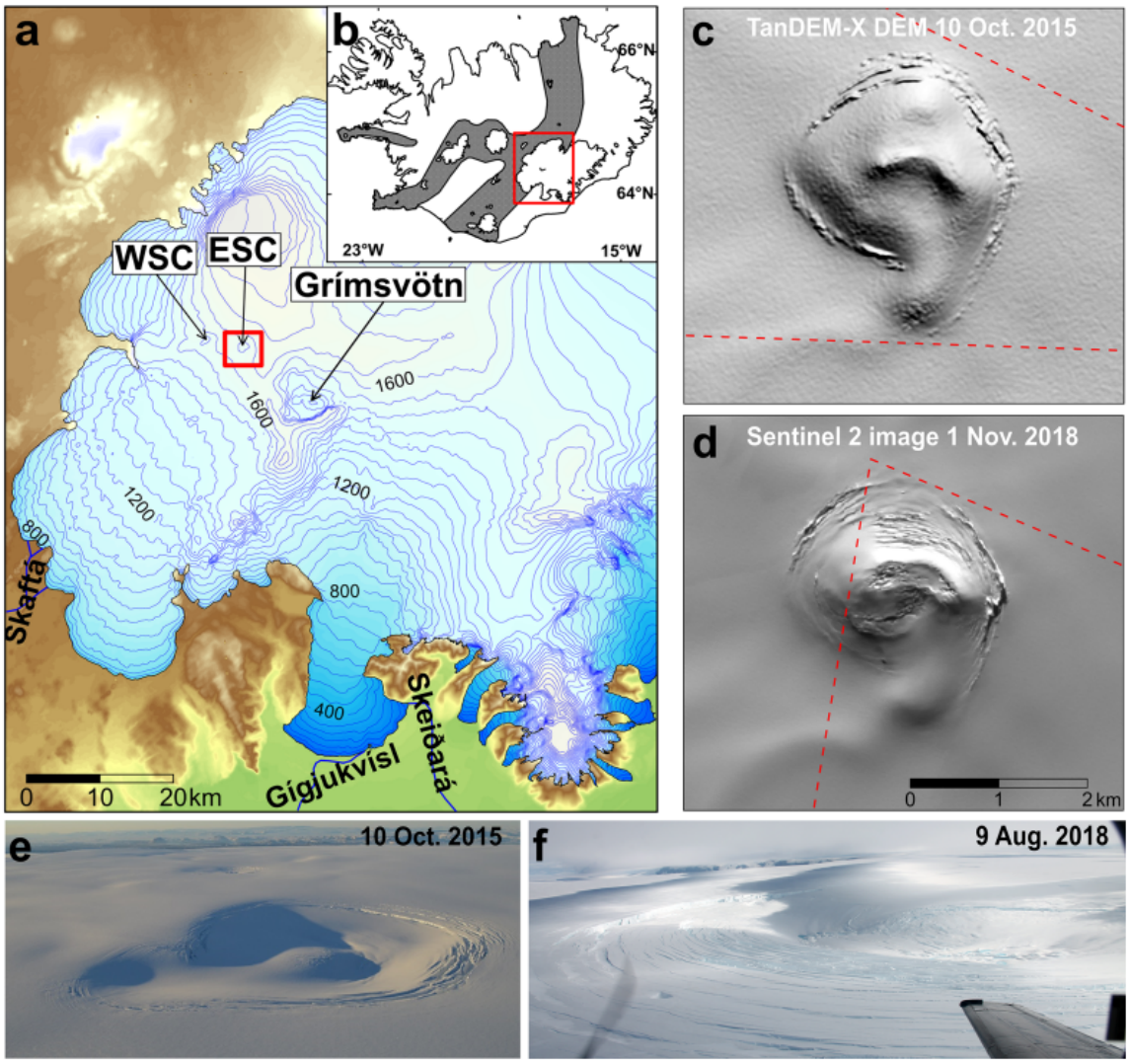

Figure 1.26: Skaftá cauldrons at Vatnajökull ice cap. (a-b) Map showing location of western Skaftá cauldron (WSC) and eastern Skaftá cauldron (ESC), near Grímsvötn subglacial lake. (c) TanDEM-X shaded relief of the ESC acquired on 10th October 2015, a week after the 2015 jökulhlaup. Location represented by red box in panel a. (d) Sentinel-2 optical image of the ESC acquired on 1st November 2018, approximately 3 months after the 2018 jökulhlaup. (e) Aerial photograph of ESC taken on 10th October 2015, about a week after the 2015 jökulhlaup (credit: Benedikt Ófeigsson). (f) Aerial photograph of ESC taken on 9th August 2018 about a week after the 2018 jökulhlaup (credit: Magnús T. Guðmundsson). Viewing angles for these photographs are represented in panels c and d. Note crevassing around the edges of the cauldron. Source: Magnússon et al., 2021.

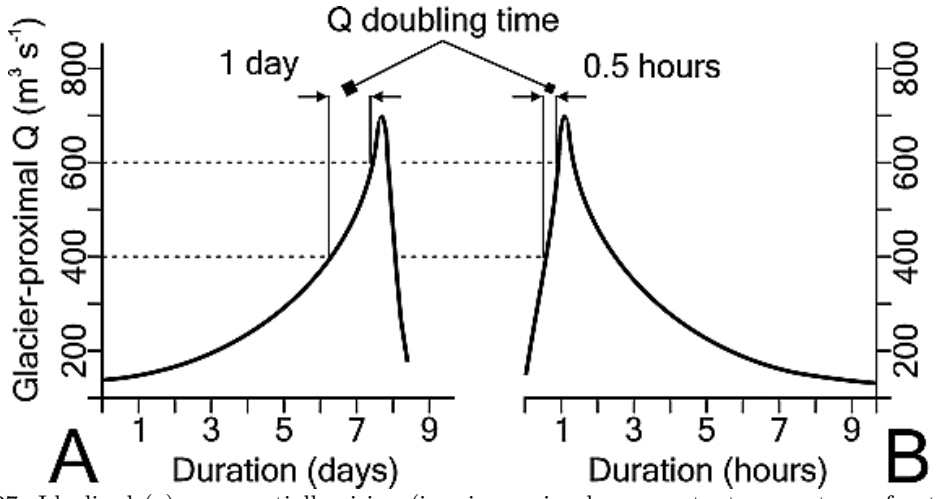

Figure 1.27: Idealised (a) exponentially rising (i.e., increasing by a constant percentage of net discharge per unit time) and (b) linearly rising (i.e., increasing by a constant amount per unit time) glacier-proximal hydrographs showing different jökulhlaup drainage styles. Source: Roberts, 2005.

1.4.3 Importance of subglacial lakes

Subglacial lakes are thought have several impacts on ice dynamics, are viable habitats for microbial life adapted to extreme environmental conditions and hold important historical information within their sediments. Our understanding of the wider impact of subglacial lakes is still in its infancy and is limited by the lack of direct observations and knowledge of subglacial hydrology being largely based on theory. Furthermore, much of our understanding is based on Antarctic and Icelandic subglacial lake studies, with relatively little investigation into constraining the importance of subglacial lakes in Greenland, since Greenland subglacial lakes are anticipated to be a less crucial component of the hydrological system.

1.4.3.1 Ice dynamics

Our understanding of the ice dynamical impact of subglacial lakes is still in its infancy, and is limited by data availability. As such, much of our knowledge comes from numerical modelling studies (e.g., Pattyn, 2008). Both stable and active subglacial lakes can interact with the overlying ice through lake circulation and subglacial lake discharge.

Due to hydrostatic equilibrium, subglacial lakes have an inverse sloping surface of

approximately 11 times the ice surface gradient. The pressure melting point along the ice-water interface varies depending on ice thickness, for example at Subglacial Lake Vostok, the pressure melting point is estimated to be about 0.3°C lower in the south where the ice is ∼3,800 m compared to the north where the ice is thickest (∼4,200 m). Several numerical modelling studies suggest that this temperature difference leads to density-driven vertical convection of lake water, whereby cold, dense meltwater sinks and warm water (by geothermal heat) rises, even within smaller subglacial lakes (Wüest and Carmack, 2000; Williams, 2001; Thoma et al., 2007, 2009, 2011; Pattyn et al., 2016). Some Antarctic subglacial lakes contain salinity (e.g., (Tulaczyk et al., 2014)), which also influences the lake circulation. These physical processes can influence the distribution of melting and accretion at the ice-lake interface, which is important as this accreted ice has a different rheology, which can modify basal flow (Pattyn et al., 2016). Furthermore, lake circulation can redistribute nutrients released in the overlying ice, which is important for microorganisms which may inhabit the lake (see Section 1.4.3.2).

As discussed in Section 1.3.3, the presence of subglacial water lubricates the ice base and reduces basal friction (Pattyn, 2010; Bell et al., 2011; Pattyn et al., 2016). Ice flow velocity is therefore expected to increase over subglacial lakes (Bell et al., 2007b; Pattyn, 2010; Bell et al., 2011; Pattyn et al., 2016). Active subglacial lake drainage events have been correlated with transient accelerations in local ice flow in outlet glaciers and ice streams due to the injection of subglacial water (e.g., Bell et al., 2007a; Stearns et al., 2008; Scambos et al., 2011; Siegfried et al., 2016). For example, GPS data on Whillans and Mercer ice streams, West Antarctica, captured three episodic ice flow accelerations of up to 4% over a 2 year period, associated with cascading subglacial lake drainages (Siegfried et al., 2016). In East Antarctica, the drainage of two subglacial lakes beneath Byrd Glacier (mean discharge 70 m^3 s^{-1}) lead to an acceleration in ice flow by up to 10% between 2005 and 2007 (Stearns et al., 2008).

The impact on ice flow greatly depends on the characteristics of the downstream subglacial system. For example, if the outburst flood enters an efficient system, the ice flow response will likely be neglible (Walder and Costa, 1996). In regions with

high surface meltwater inputs, e.g., Greenland, where observed subglacial lakes are smaller and surface melt is high, lake drainage events are expected to have limited impact on ice dynamics. Whilst subglacial lake drainage events elicit short-term peaks in local ice velocity, their overall long-term impact is likely to be minimal, as ice flow acceleration will likely be succeeded by a deceleration. This is likely due to a reduction in water pressure within the main channel and high pressure water draining from other regions of the bed. For example, Livingstone et al., 2019 found a short-term slowdown by ∼25% following a subglacial lake outburst at Isunguata Sermia, West Greenland.

1.4.3.2 Subglacial ecosystems

Microbial communities were first detected in the accreted ice layer over Subglacial Lake Vostok in the late 1990s (Jouzel et al., 1999; Karl et al., 1999). Geothermal mixing of nutrient- and oxygen-enriched meltwater from the overlying ice (Couston and Siegert, 2021) and/ or the sediments and bedrock beneath (Smith et al., 2018) are thought to enable viable communities to persist in these remote, isolated and extreme environments, otherwise anoxic conditions would occur. Complex microbial communities in large, deep subglacial lakes in the continental interior are relatively understudied, due to failed drilling missions and logistical challenges, but they are likely to have been isolated from surficial inputs and environments for tens of millions of years (Duxbury et al., 2001), and are therefore important to study to improve our understanding of microbial evolution and function in extreme (no light, high pressures and sub-zero temperatures) conditions (Achberger et al., 2016; Vick-Majors et al., 2016; Campen et al., 2019; Priscu et al., 2020), as well as understanding extraterrestrial environments, such as subsurface waters on Jupiter's (Pappalardo et al., 2013) and Saturn's moons (McKay et al., 2008).

Two dynamically active subglacial lakes have been directly sampled in West Antarctica; Subglacial Lake Whillans and Subglacial Lake Mercer, revealing a high diversity of microorganisms in both the water column and underlying sediments (Christner et al., 2014; Tulaczyk et al., 2014; Achberger et al., 2016; Hodson et al., 2016; Mikucki et al., 2016; Priscu et al., 2020). As basal meltwater, produced by high geothermal heat fluxes and frictional heating (Fisher et al., 2015), flows along the

base of the Antarctic Ice Sheet, it entrains subglacial sediment containing minerals and organic matter (Tranter et al., 2005). These basal waters feed and connect active subglacial lakes, releasing ice-entrained solutes, particulate matter and atmospheric gases, enabling diverse heterotrophic and autotrophic communities to exist (Christner et al., 2014; Purcell et al., 2014; Achberger et al., 2016; Vick-Majors et al., 2016; Michaud et al., 2017). Metabolically active microbial ecosystems are capable of cycling important greenhouse gases, such as methane (CH_4), which could be transferred to the Southern Ocean during large subglacial floods or deglaciation, and subsequently released into the atmosphere (Wadham et al., 2012, 2013; Dieser et al., 2014). Rapid subglacial lake drainage events could also release nutrients, for example iron, nitrogen and silicon, into the iron-limited ocean and could have a fundamental impact on Southern Ocean marine primary productivity, and thus carbon sequestration (Sigman and Boyle, 2000).

In contrast to Antarctic subglacial lakes, it is not expected that Greenland subglacial lakes, at least around the margin, will harbour ecosystems that have been isolated for an extended period of time. Greenlandic active subglacial lakes are thought to be recharged by surface meltwater inputs (Willis et al., 2015), delivering oxygen and organic matter to the subglacial drainage system. This seasonal influx of oxygen-rich water could create regions of anoxia if unable to reach deeper parts of the lake. Lamarche-Gagnon et al., 2019 found several tonnes of microbial methane released from beneath the Greenland Ice Sheet, and suggest that Arctic warming projections and melt rates could increase subglacial methane being released into the atmosphere in the future. Subglacial floods produced by active lake drainages in Greenland have the potential to contribute to this process, however, the extent of this impact is highly uncertain due to a current lack of knowledge.

1.4.3.3 Geomorphology, palaeoclimate and palaeoglaciology

Large subglacial lake outburst floods can be a source of sediment transportation, erosion (Russell et al., 2006) and deposition (Maizels, 1997; Russell and Knudsen, 1999) several kilometres downstream. Such events can erode bedrock and redistribute sediment, causing modification of the proglacial landscape. Large palaeo outburst floods have even left behind characteristic landforms which can persist for millennia. Landforms

such as metre-kilometre scale eskers (sinuous ridges of glaciofluvial sediments that preserve former meltwater drainage networks) and outwash plains (Burke et al., 2008) and macro-scale megaripple dune fields and bedrock channels (e.g., Denton and Sugden, 2005; Alley et al., 2006; Domack et al., 2006; Lewis et al., 2006; Jordan et al., 2010; Kuhn et al., 2017; Kirkham et al., 2019; Larter et al., 2019) can be mapped and analysed to infer subglacial flood paths and peak discharge. A 5 km long system of channels in Wright Valley, Antarctica has been attributed to repeated subglacial lake outburst floods with estimated peak discharge of 1.6-22 $\times 10^6$ m^3 s^{-1} during the Miocen epoch (23-5.3 Ma) (Denton and Sugden, 2005; Lewis et al., 2006). The sudden input of sediment-laden freshwater from mega-scale subglacial outburst floods into the ocean have been hypothesised to alter global ocean circulation and climate (Shaw, 1989; Jordan et al., 2010).

Contemporary active subglacial lakes beneath the Antarctic Ice Sheet have fill and drain cycles of months to years (Dow et al., 2016) and typically release relatively low volumes of water with typical discharge rates in the order of tens of cubic metres per second. The largest observed subglacial lake drainage event in Antarctica is estimated to be 5 $\pm$ 1.5 km^3 over a 2 year period (Flament et al., 2014). As such, active subglacial lake drainage events in Antarctica are unlikely to have significant geomorphic impact, compared to palaeo-drainages. On the other hand, rapidly rising subglacial lake outburst floods in Iceland can significantly alter the proglacial landscape (Maizels, 1997). For example, the 1996 jökulhlaup from Subglacial Lake Griímsvötn beneath Vatnajökull, Iceland, with a peak discharge of 4 $\times 10^4$ m^3 s^{-1}, not only caused destruction to infrastructure, but removed vast quantities of sediment from the outwash plain (Snorrason et al., 2002; Björnsson, 2003; Russell et al., 2006). In Greenland, an outburst flood from a small active subglacial lake beneath Isunguata Serma, western Greenland, caused geomorphic change by aggrading the proglacial channel by up to 8 m in 2015 (Livingstone et al., 2019).

Some stable subglacial lakes, particularly in the interior of the Antarctic ice sheet, have remained undisturbed for millennia. The stratified sediments beneath stable subglacial lakes could hold important insights for understanding palaeo-ice sheet dynamics, -environments, -hydrology and -climate (Tulaczyk et al., 2014; Hodson et al.,

2016; Smith et al., 2018). The structure and mechanical properties of subglacial lake bed sediments are strongly influenced by the overlying ice dynamics (Post et al., 2014), therefore sedimentary sequences can reveal changes in the conditions at the base of the ice sheet in response to the succession of glacial-interglacial cycles. Some lake beds may contain non-glacial sediments, e.g., marine sediments deposited during periods of major ice sheet retreat or collapse. Furthermore, biomarkers and fossils in subglacial lake sediments could provide information about past climates and environments, which is important for predicting future ice sheet-climate interactions. However, few subglacial lakes have been directly sampled and analysis of bed sediments has been limited.

Chapter 2

Geophysical techniques used to detect and monitor subglacial lakes

As eluded to in Section 1.4.1, there are several geophysical techniques methods for detecting and characterising stable and active subglacial lakes beneath thick ice masses. Field-based seismic and airborne ice-penetrating radar surveys were initially used to discover the first stable subglacial lakes beneath the Antarctic Ice Sheet, which rely on identifying contrasts in electromagnetic properties between ice and water (acoustic properties in seismic methods, and dielectric properties in radar methods). A pivotal collaborative study in 1996 which combined seismic, radar and satellite-derived surface elevation, to map the geometry of Subglacial Lake Vostok (Kapitsa et al., 1996), led to the first inventory of stable Antarctic subglacial lakes. Since, advancements in satellite technology and polar missions have provided improved spatial and temporal coverage for monitoring elevation changes associated with the active subglacial lake filling and drainage events, as well as volumetric change measurements. A combination of geophysical methods enables direct access, measurement and sampling of lake water and sediment e.g., via hot water drilling. In the following chapter I will review each geophysical technique in turn. Based upon this review, I summarise the key knowledge gaps relating to Greenland subglacial lakes, and use this to frame the aims and objectives of my thesis.

2.0.1 Seismic reflection surveys

Ground-based seismic reflection surveys involve generating seismic energy from a source, such as detonating high explosives buried in deep holes, or striking an impact plate on the ice surface with a sledgehammer. Seismic waves from each shot travel through the ice column to the ice bed, where it is reflected and recorded by a receiver (e.g, by geophones spaced at certain intervals along the ice surface from the source), and the seismic data processed to produce a visual representation of the bed topography (Figure 2.1). Different interfaces within and at the base of the ice reflect the seismic energy back according to their acoustic impedance (product of seismic velocity and density). Two-way travel-time difference between reflectors from the ice-surface and the ice-bed interfaces can be utilised to calculate the ice thickness and bed topography. Moreover, unlike radar waves, seismic p-waves are unimpeded by water, therefore the depth of water within subglacial lakes, and lake bed morphology can also be established (Kapitsa et al., 1996; Peters et al., 2007; Peters et al., 2008; Woodward et al., 2010; Horgan et al., 2012; Popov et al., 2012; Smith et al., 2018). Seismic studies have revealed lake depths in Antarctica from ∼10 m at Subglacial Lake Whillans (Horgan et al., 2012) to 1.1 km at Subglacial Lake Vostok (Filina et al., 2008), and lake depth of 10-15 m at a subglacial lake in northwest Greenland (Maguire et al., 2020). These dimensions enable improved estimates of the magnitude of water storage in subglacial lakes beneath ice sheets, and therefore predictions of the potential consequences of such release of meltwater (e.g., Dowdeswell and Siegert, 1999).

The acoustic impedance and seismic reflection strengths of the water-sediment interface can provide information about the lake bed and the surrounding subglacial material (Filina et al., 2007; Peters et al., 2008; Horgan et al., 2012), for example, if the lake bed contains soft, wet sediments or impermeable bedrock. The structure and properties of the underlying sedimentary material is important for determining whether a subglacial lake is a closed (i.e. no water flows in and out of the subglacial lake) or open (water can flow in and out of the lake across the shoreline, through a permeable sediment bed, or by ice-water interface processes) hydrological system, identifying likely sources of water and the subglacial lake catchment. All of these subglacial characteristics are important for modelling subglacial lake circulation and ice-water interactions.

Seismic surveys can also be used estimate sediment thickness and speculate on sediment age. Sediments beneath Subglacial Lake Ellsworth are estimated to be about 6 m thick and at least 150 ka (Smith et al., 2018). Combined ground-based and airborne geophysical data have revealed a Late Palaeozoic to Mesozoic rift system in East Antarctica, comprising Subglacial Lake Vostok and many other subglacial lakes (Ferraccioli et al., 2011).

2.0.2 Radio-echo sounding

Ground-based ice-penetrating radar surveys were originally performed with radio-echo sounding (RES) devices mounted to snow sledges or vehicles, or even by foot in heavily crevassed regions. To allow for greater spatial coverage, advancements in RES instruments were made and subsequently mounted to aircrafts, for example, National Aeronautics and Space Administration NASA's Operation IceBridge (OIB) was the largest scientific airborne survey of the polar ice (2009-2021) enabling ice sheet-wide, and in some regions repeated, coverage of RES data (MacGregor et al., 2021) (used in Chapter 3). A RES system typically consists of a transmitter, a receiver, and a pair of antennae. Electromagnetic waves, at frequencies between 1 and 1000 MHz, are transmitted through the ice where they are either reflected or absorbed (Figure 2.2). High-frequency (high-resolution) radar systems (e.g., >800 MHz) are often used to study the shallow snow layer, mid-frequency radars (e.g., ∼200 MHz) have been implemented in the studies of the firn layer (e.g., Arcone et al., 2005) or crevasse formation in Antarctica (Nath and Vaughan, 2003), and low-frequency radars (<25 MHz) are typically used to resolve deep solid ice and the ice-bed interfaces (e.g., Robin et al., 1977; Gogineni et al., 2001).

The propagation and reflection of electromagnetic waves is controlled by two main properties: (1) dielectric permittivity and (2) electric conductivity. The permittivity (or dielectric constant) of glacier ice is $\varepsilon = 3.15$ (or 5% of that of freshwater) (Bohleber et al., 2012), whilst the electrical conductivity is negligibly small (∼0.01 mS m^{-1}, or 2% of that of freshwater) (Hubbard and Glasser, 2005). The dielectric constant of ice is sensitive to the presence of water, impurities and material properties e.g., crystal orientation. The conductivity of ice varies with temperature and pressure, and is

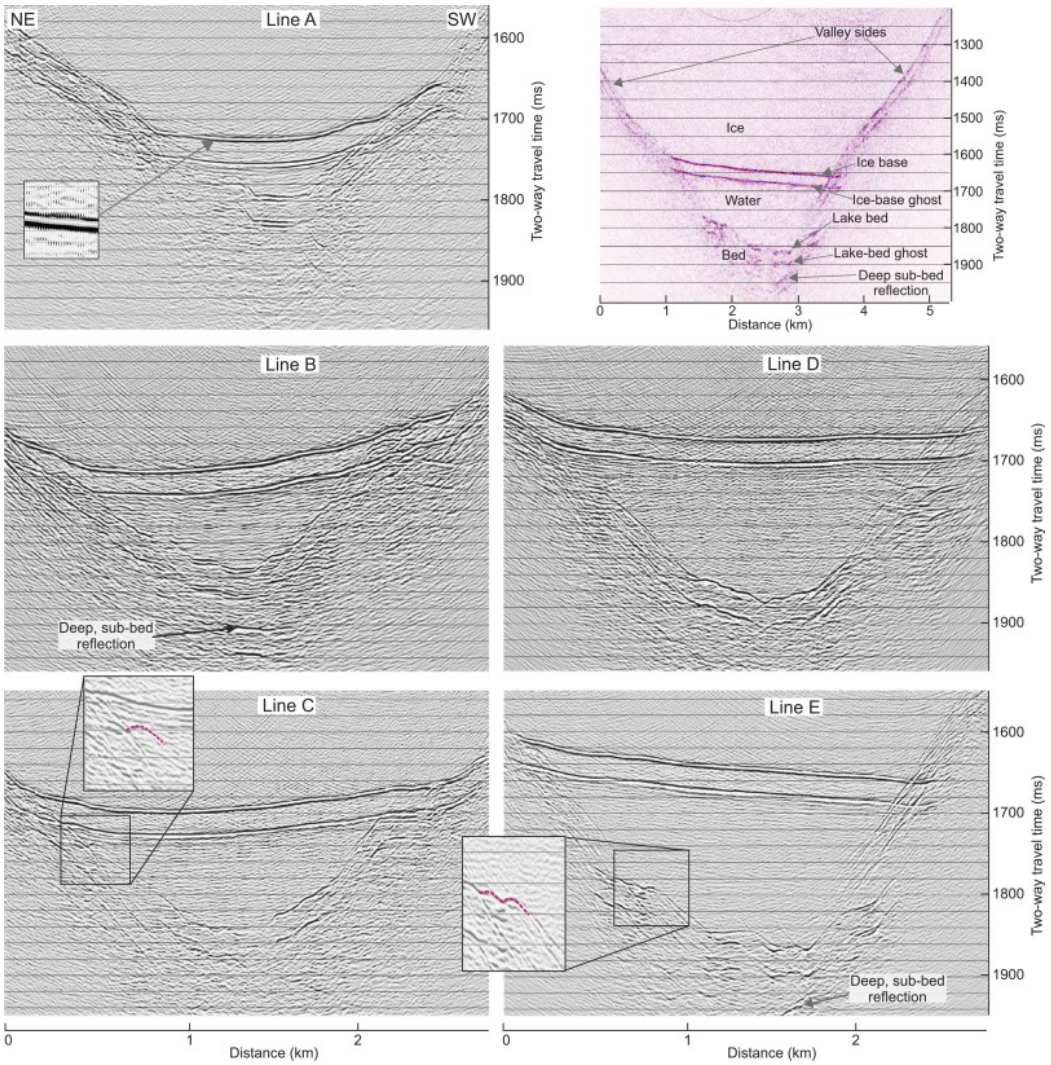

Figure 2.1: Processed seismic reflections over Subglacial Lake Ellsworth, West Antarctica, showing different reflectors for the lake bed, water-ice interface and valley sides. Source: Smith et al., 2018.

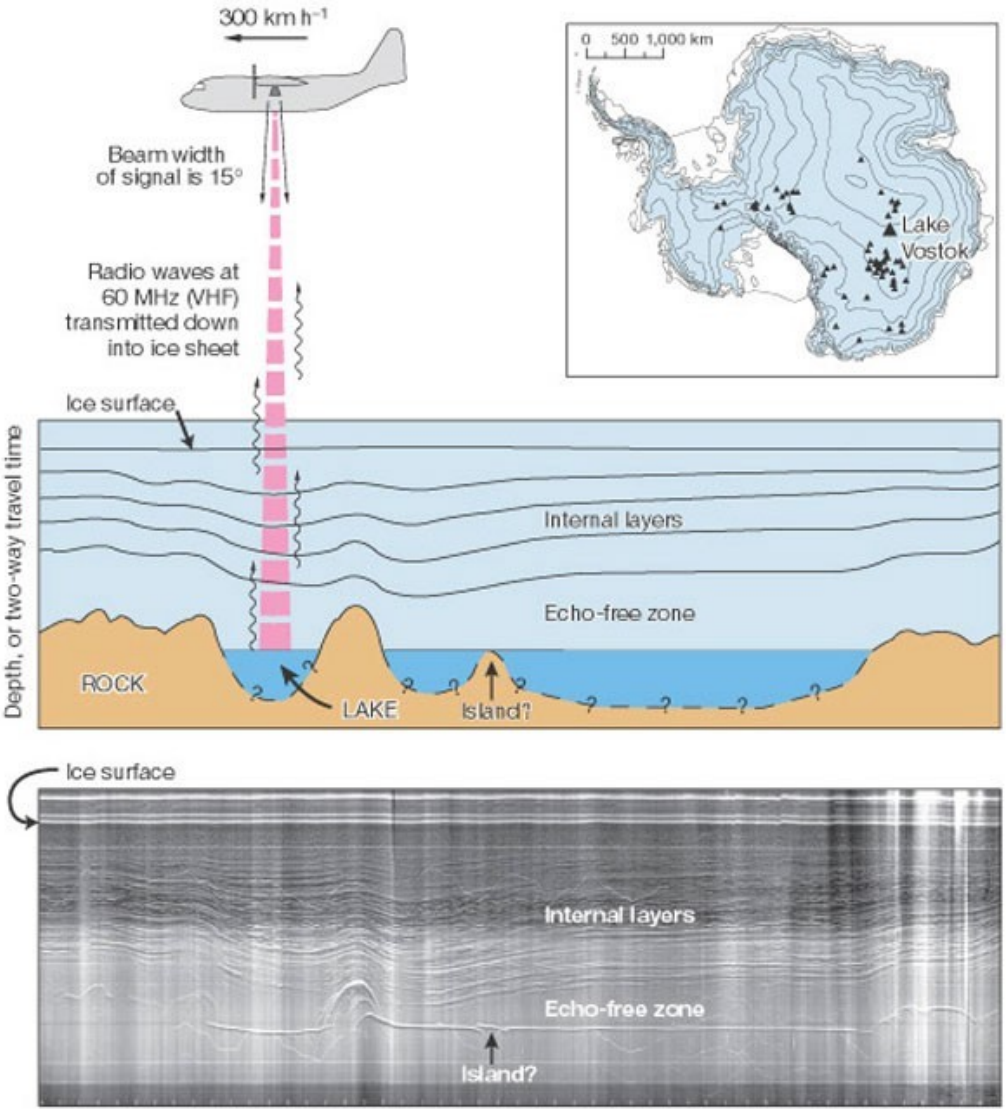

Figure 2.2: Airborne radio-echo sounding method: a radar transmitter and receiver, mounted to an aircraft, records radio waves that are reflected off different interfaces in the ice. RES records (bottom image) can be used to identify lakes beneath the ice due to their uniformly strong and flat appearance. Inset map shows known subglacial lake locations as triangle, including the largest Subglacial Lake Vostok. Source: Siegert et al., 2001.

principally controlled by the impurity concentration (Glen and Paren, 1975; Johari and Charette, 1975; Moore and Fujita, 1993; Stillman et al., 2013; Pettinelli et al., 2015). Different interfaces have different dielectric constants e.g., the bed and surface interfaces, englacial layers, ice cavities and subglacial water (Evans, 1963; Robin et al., 1970). Electromagnetic waves are therefore partially reflected at these boundaries at different speeds of wave propagation.

The receiver records these reflections and signals which are processed to produce radargrams (Figure 2.2). Like seismic surveys, the two-way travel time of the electromagnetic wave between transmitter and receiver can be calculated and converted into ice thickness. This active remote-sensing approach has revealed deep troughs, high plateaus and complex valleys beneath both Antarctic and Greenland Ice Sheets, and therefore can be used to produce medium- and low-resolution DEMs of subglacial topography (e.g., Bamber et al., 2009; Morlighem et al., 2017). Such DEMs are useful to support numerical modelling of ice sheet dynamics, estimate ice sheet thickness and volume changes (e.g., Howat et al., 2008; Motyka et al., 2010), and map subglacial hydrological networks (e.g., Livingstone et al., 2013).

The returned bed-echo power (P) depends on basal reflectivity R of the target interface and can be extracted by correcting for geometric spreading (G), radar system performance S (such as transmission power and system gain), englacial attenuation (due to dielectric absorption of radiowaves in ice) (L) and birefringence (caused by ice fabric anisotrophy) loss (B) (Matsuoka et al., 2010). The bed returned power is commonly converted to logarithmic decibel scale ($[x]_{dB} = 10 \log_{10} x$) (Matsuoka et al., 2010):

$$[P]_{dB} = [S]_{dB} - [G]_{dB} + [R]_{dB} - [L]_{dB} - [B]_{dB} \tag{2.1}$$

Geometric spreading losses from the transmission through the air-ice interface (Grima et al., 2014; Schroeder et al., 2016a) can be corrected by:

$$[G]_{dB} = 2[h + H/\sqrt{\varepsilon}]_{dB} \tag{2.2}$$

where h is the height of the radar system above the surface, H is the thickness of ice and $\varepsilon = 3.15$ is the relative dielectric permittivity of ice, to give the geometrically

corrected bed-echo power (Schroeder et al., 2016a):

$$[P^c]_{dB} = [P]_{dB} + [G]_{dB} = [S]_{dB} + [R]_{dB} - [L]_{dB} - [B]_{dB} \tag{2.3}$$

It is typically assumed that the effects of S and B losses are negligible (Fujita et al., 2006; MacGregor et al., 2007; Matsuoka et al., 2009, 2012), for example the probability that B varies more than 10 dB is 3% (Fujita et al., 2006), thus equation 2.3 can be reduced to:

$$[P^c]_{dB} = [R]_{dB} - [L]_{dB} \tag{2.4}$$

Isolating the power loss to the bed due to englacial attenuation L is challenging due to high uncertainties. There are two approaches to estimate englacial attenuation rates: forward modelling and empirical techniques. Forward modelling uses estimates of attenuation as a function of englacial temperature (e.g., MacGregor et al., 2007; Matsuoka et al., 2012; Chu et al., 2016). This approach requires accurate temperature and ice chemistry values, which can be constrained by thermomechanical ice-flow models (e.g., Hindmarsh et al., 2009), laboratory experiments and ice core data (MacGregor et al., 2007), however on an ice-sheet scale, the uncertainty in these values can prohibit calibration of R (Matsuoka, 2011), a simpler empirical method for deriving englacial attenuation can be applied using the linear regression of bed-echo power and ice thickness (e.g., Jacobel et al., 2009; Schroeder et al., 2016b). Englacial radar attenuation varies spatially across an ice sheet due to different temperatures of the ice, for example, attenuation rates of $\sim$6 dB km^{-1} have been estimated in the colder northern interior of the Greenland Ice Sheet compared to $\sim$30 dB km^{-1} towards the warmer south-western margins (Jordan et al., 2016).

Following these corrections, the returned bed-echo power can be used to characterise variations in Antarctic and Greenland Ice Sheet basal thermal state (i.e. frozen or thawed) (e.g., MacGregor et al., 2016; Chu et al., 2018), the distribution or storage of subglacial water (e.g., Peters et al., 2005; Chu et al., 2016; Chu et al., 2018; Jordan et al., 2018; Lindzey et al., 2020), basal roughness (MacGregor et al., 2013; Christianson et al., 2016; Jordan et al., 2017) and bed lithology (Siegert et al., 2016b). As such, RES investigations have been used to detect hundreds of subglacial lakes

beneath ice masses through analysis of their distinct characteristics:

1. Due to the strong dielectric contrast between water and ice, subglacial water gives a strong and bright bed reflector, with relatively high returned bed-echo power, typically about 10-20 dB greater compared to the surrounding rock echoes, (Oswald and Robin, 1973; Siegert, 2000b; Peters et al., 2005; Wright and Siegert, 2012)

2. Smooth basal interfaces (due to pressure equalisation; (Siegert et al., 2005)) compared to the rough bedrock surface which scatters the electromagnetic wave energy, decreasing its reflection strength,

3. Near horizontal reflections (due to lack of shear stresses), typically ∼10 times, and the opposite direction to, the ice surface (Oswald and Robin, 1973) (Figure 2.2).

Carter et al., 2007 acknowledge that subglacial lake reflectors may not meet all of the criteria, and thus proposed a classification system which ranks lakes as 'definite', 'dim', 'fuzzy' or 'indistinct', based on the extent they fulfil the three criteria, to compensate for these ambiguities. Unlike seismic surveys, subglacial lake depth can not be determined by RES surveys as the majority of electromagnetic radiation are reflected at the subglacial lake surface, and the transmitted waves are quickly absorbed, therefore not yielding enough energy to be recorded at the ice surface.

2.0.3 Satellite altimetry

Elevation measurements from satellite radar interferometry (InSAR) and satellite radar and laser altimetry have been widely used to derive and monitor changes in polar ice sheet surface elevation since the launch of Earth Remote Sensing Satellite-1 (ERS-1) in 1991 (e.g., Wingham et al., 1998; Bamber et al., 2009; Pritchard et al., 2009; McMillan et al., 2016; Sandberg Sørensen et al., 2018; Slater et al., 2018b; Schröder et al., 2019; Shepherd et al., 2019; Simonsen et al., 2021). Radar altimetry measures the time taken for pulses of electromagnetic radiation to travel from the satellite to the ice sheet surface and back, as well as the magnitude and shape of the backscattered echo

(waveform). Laser altimetry operates in a similar manner but uses light pulses (at a typical rate of 10-30 Hz) instead of electromagnetic radiation. Repeated measurements over consecutive orbits allow elevation changes to be calculated over various timescales. These measurements can be used to map features and localised variations in the ice sheet surface associated with the storage and motion of meltwater at the bed. Abrupt drainage of subglacial lakes can cause draw down of the ice surface above, whereas filling of subglacial lakes can cause uplift of the ice surface. Whilst this technique is typically used to show the ice surface expression of active subglacial lakes, if stable lakes are large enough, smooth flat surfaces, which indicate that the ice is floating in hydrostatic equilibrium (Ridley et al., 1993), can also be detected.

The National Aeronautics and Space Administration (NASA) launched the Ice Cloud and Land Elevation Satellite (ICESat) satellite in 2003, which carried the Geoscience Laser Altimeter (GLAS) instrument with three independent lasers able to determine interannual elevation changes over the ice sheets (Zwally et al., 2002b; Luthcke et al., 2005). The mission ended in 2010 (Schutz et al., 2005), but proved to be an effective method for mapping subglacial lake activity in Antarctica due to its small footprint (60-70 m), dense along-track spacing ($\sim$170 m) and high vertical accuracy (Fricker et al., 2007; Fricker and Scambos, 2009; Smith et al., 2009; Fricker et al., 2010). Smith et al., 2009 carried out the first systematic, continent-wide satellite assessment of active subglacial lakes in Antarctica, detecting 124 previously undiscovered subglacial lakes and estimated their volumetric changes. Previous to this study, only a few active subglacial lakes had been detected in the Kamb and Whillans Ice Stream catchments (Gray et al., 2005) and in East Antarctica (Wingham et al., 2006a) using RADARSAT and ERS-2 satellite data, respectively, with only one drainage event captured. Using ICESat elevation data, Smith et al., 2009 discovered that many of newly detected lakes were filling and draining on timescales of months to years, in volumes on the order of 0.1-1 km^3. Interestingly, the median size of the active subglacial lakes was about 13 km, which is approximately the same as the ICESat track spacing at $\sim$80°S, thus Smith et al., 2009 suggested that smaller lakes may be unidentified.

More recent radar altimeters, such as the ESA's Cryosat-2 radar altimeter (launched 2010) with its SARin mode provides surface height measurements at greater spatial

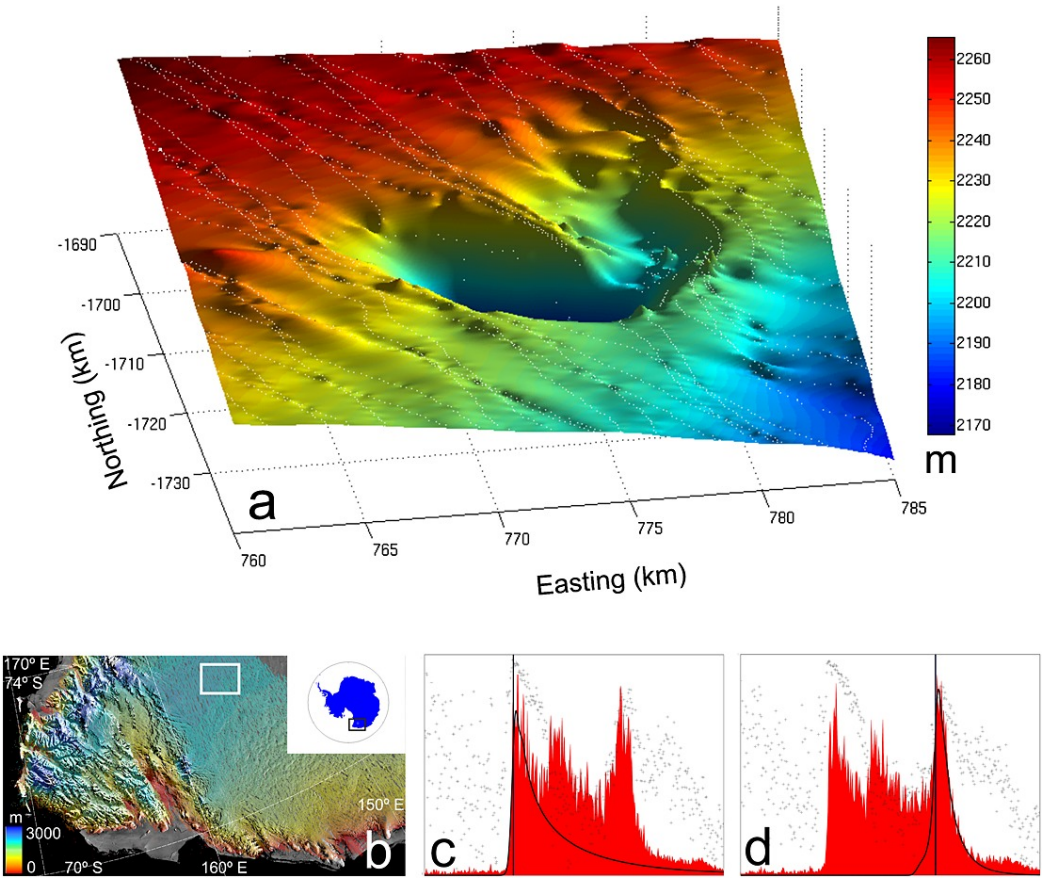

Figure 2.3: (a) Three-dimensional map of the ice surface above CookE2 subglacial lake as it drained, using CryoSat-2 interferometric mode data between January and November 2011. (b) Location of subglcial lake in Antarctica. (c, d) Power and coherence (red and black dots, respectively) of two consecutive SARin mode echoes across the surface depression. Source: McMillan et al., 2013.

coverage compared to ICESat (Siegfried et al., 2014, 2016; Siegfried and Fricker, 2018). However the SARin mode only operates around the margin, with the low resolution mode for shallow sloping interior part of the ice sheets. Furthermore, CryoSat-2 radar altimeters are insensitve to cloud coverage, unlike laser altimeters. Cryosat-2 has successfully been utilised to identify new, large subglacial lake drainage events (Siegfried et al., 2014; Kim et al., 2016; Smith et al., 2017a), and extend the ICESat timeseries at Cook E2 subglacial lake in East Antarctica (McMillan et al., 2013) (Figure 2.3) and in the Lower Mercer and Whillans Ice Streams in West Antarctica (Siegfried et al., 2014).

NASA's ICESat-2 laser altimeter (Markus et al., 2017) was recently launched

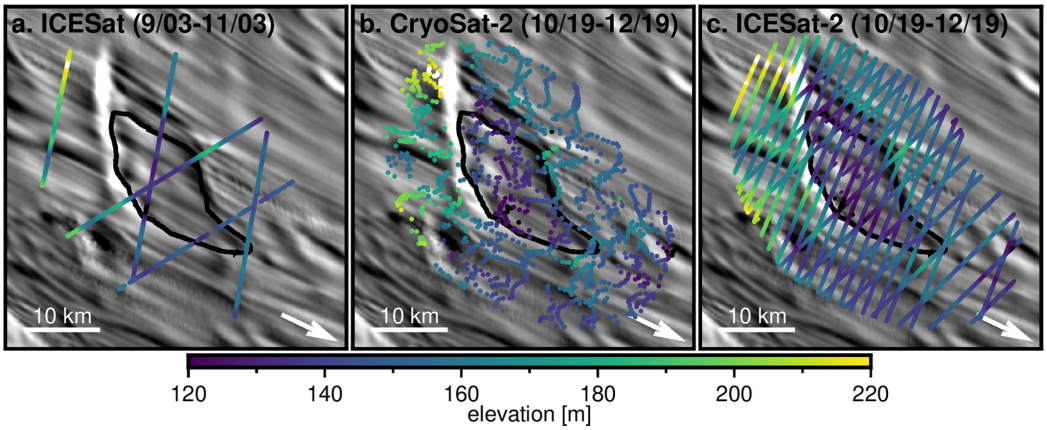

Figure 2.4: Comparison of altimetry techniques. Source: Siegfried and Fricker, 2021.

in 2018, and introduces new opportunities to detect explore active subglacial lake processes, such as drainage outlet development and lakeshore migration (Siegfried and Fricker, 2021), that previous altimeters could not resolve, as well as detect new lake candidates due to the high along-track spatial resolution (40 m), high precision (Brunt et al., 2019), dense cross-track spacing due to the six-beam Advanced Topographic Laser Altimeter System (ATLAS) instrument with a 91-day repeat cycle (Smith et al., 2020a).

McMillan et al., 2019 demonstrate the capabilities of Sentinel-3 Delay-Doppler (SAR mode) altimetry in resolving subglacial lake activity signals in Antarctica. The Sentinel-3 satellites have 27-day sampling with centimetre accuracy (Markus et al., 2017), enabling further detection of subglacial lakes and improved estimations of extents and interconnectivity. The Copernicus Polar Ice and Snow Topography Altimeter (CRISTAL) mission, proposed to launch in 2027 and designed to carry a dual-frequency high-resolution radar altimeter and last over a decade in orbit (Kern et al., 2020), will enable continued development of cryosphere monitoring in the future, with the potential for use in subglacial lake studies.

2.0.4 Digital Elevation Models

A Digital Elevation Model (DEM) is a gridded representation of Earth's surface with each pixel value corresponding to a surface height, and is produced from ground-based, airborne or satellite surveys, as well as by digitising maps. Remote sensing

techniques to generate DEMs include stereo-photogrammetry, which uses at least two images taken from different vantage points to obtain depth and perspective where the images overlap, airborne and spaceborne inSAR which uses multiple radar images from antennas captured at a similar time to generate a DEM, and Light Detection and Ranging (LiDAR) which measures reflected light from the Earth's surface to determine elevation.

DEMs have become an integral part of a vast array of scientific applications and are particularly useful in glaciology to produce important inputs for ocean and ice sheet numerical models. DEMs of bed topography such as BedMachine (Morlighem et al., 2017, 2020) and Bedmap2 (Fretwell et al., 2013), which use mass conservation methods to estimate what lies between the RES tracks, allow detailed information on ice thickness and ice flow motion and are useful for generating hydraulic potential surfaces to map subglacial routing and identify hydraulic minima (e.g., Carter et al., 2011; Livingstone et al., 2013. DEMs have also been applied to identify and map features on the ice surface which are associated with subglacial lakes. For example, DEMs derived from satellite altimetry have revealed elongated, flat regions of the ice surface which have been associated with large subglacial lakes such as Subglacial Lake Vostok (Ridley et al., 1993) and a 1250 km^2 lake in Princess Elizabeth Land (PEL) (Kim et al., 2016), following ground truthing from radar surveys. DEMs are frequently used as a reference to find elevation anomalies in order to specify the boundaries and spatial and temporal variations in active subglacial lakes (e.g., Scambos et al., 2011; Kim et al., 2016; Siegfried and Fricker, 2021).

The recent release of high-resolution ($<$20 m) Digital Surface Models (DSMs) (e.g. ArcticDEM (Porter et al., 2018), Reference Elevation Model of Antarctica (REMA) (Howat et al., 2019), Advanced Spaceborne Thermal Emission and Reflection Radiometer (ASTER) DSM (Hirano et al., 2003), and TerraSAR-X add-on for Digital Elevation Measurement (TanDEM-X) (Moreira et al., 2004)), generated from optical photogrammetry, radar altimetry, or SARin, have demonstrated the potential for monitoring active subglacial lake behaviour to be detected with high vertical precision. This is particularly useful in Greenland where the subglacial lakes are much smaller and harder to resolve using satellite altimetry (Howat et al., 2010; Palmer et al., 2015;

Willis et al., 2015; Livingstone et al., 2019).

2.0.5 Principal challenges with current remote sensing techniques

All geophysical approaches for detecting and monitoring stable and active subglacial lakes beneath ice masses have inherent strengths and weakness. Field-based radar and seismic surveys can provide detailed knowledge of subglacial lake extent, depth and bed characteristics, but it is difficult to know where to search for new subglacial lakes, and it is impossible to get continental-scale coverage. Improved RES technologies and large-scale mapping through airborne radar missions, such as Operation IceBridge, offer much larger spatial coverage than ground-based methods and the ability to conduct finer-grid measurements than satellite-based methods. Such campaigns offer relatively easy and rapid acquisition of bed data compared with seismic methods, with the ability to collect multi-temporal data if the same flight paths are taken year on year. Large-scale mapping through airborne radar missions have enabled hundreds of subglacial lakes to be detected beneath the Antarctic Ice Sheet (Siegert et al., 1996; Siegert et al., 2005; Wright and Siegert, 2012), however, detection of subglacial lakes in airborne RES is largely based on time-consuming visual interpretation of radar echograms, and inaccurate estimations of englacial attenuation can cause false identification of water at the ice-bed interface (Matsuoka, 2011). Seismic technologies may prove to be a more effective method in regions where there is substantial englacial water.

Satellite altimetry provides the best coverage in both space and time, but radar altimeters are typically quite low resolution. Laser altimeters offer moderate resolution, but are limited in their temporal coverage and sampling. These are particular issues for the Greenland Ice Sheet, where subglacial lakes are small and potentially more dynamic; no studies have used altimetry to study subglacial lakes in Greenland, thus far. DEMs had previously been limited to spatial resolutions of >500 m in Antarctica, which is compatible for ocean and ice sheet numerical models. More recent DEMs now achieve the required spatial resolution to resolve smaller subglacial lake activity.

2.1 Thesis aims and objectives

Subglacial lakes are a widely documented phenomenon in Antarctica with both stable and active lakes being prevalent. Subglacial lakes can have implications for ice dynamics, landscape evolution and evidence suggests that microorganisms inhabit these extreme environments. Yet relatively few subglacial lakes have been detected beneath the Greenland Ice Sheet, despite widespread basal water being acknowledged as important. Ice-sheet-scale surveys are essential to capture these basal features, in order to understand their distribution and potential behaviour. This thesis aims to develop methods to detect and monitor subglacial lakes beneath the Greenland Ice Sheet, to improve our understanding of the basal hydrological system.

The following list of objectives have been defined in order to address the aim of this thesis:

1. A comprehensive ice sheet-wide assessment of subglacial lakes beneath the Greenland Ice Sheet, primarily using airborne radar data (**Chapter 3**)

2. Examine the spatial distribution and glaciological setting of the subglacial lakes identified in objective 1 (**Chapter 3**).

3. Develop and evaluate a method for identifying potential active subglacial lakes at the ice sheet scale, using satellite-derived digital surface models (**Chapter 4**).

4. Utilise the output from objective 3 to perform a detailed study of the evolution of an individual active Greenland subglacial lake (**Chapter 5**).

2.2 Thesis structure

The remainder of this thesis is structured as follows: in Chapter 3, I systematically analyse all Operation IceBridge airborne radio-echo sounding data acquired over the Greenland Ice Sheet for the period 1993-2016, to create the first continent-wide inventory of subglacial lakes in Greenland. I also investigate the factors controlling their spatial distribution and characteristics, particularly in comparison to Antarctic subglacial lakes. In Chapter 4, I develop a new automated method for detecting active

subglacial lake candidates on an ice sheet scale, using satellite-derived high-resolution ArcticDEM digital elevation models. In Chapter 5, I undertake a detailed glaciological study of one of the new active subglacial lake candidates identified in Chapter 4. Finally, in Chapter 6, I synthesise the thesis findings, explore these results within a wider context and discuss potential avenues for future research.

Chapter 3

Distribution and dynamics of Greenland subglacial lakes

Jade S. Bowling[1,2], Stephen J. Livingstone[2], Andrew J. Sole[2], Winnie Chu[3].

[1]Lancaster Environment Centre, Lancaster University, Lancaster, UK
[2]Department of Geography, University of Sheffield, Sheffield, UK
[3]Department of Geophysics, Stanford University, Stanford, USA

Correspondence:
Jade Bowling (j.bowling@lancaster.ac.uk)

The following work represents an expanded version of what was published in *Nature Communications* on 26th June 2019. The published supplementary material can be found in Appendix A. The published supplementary table can be found here: Table 1.

3.1 Abstract

Few subglacial lakes have been identified beneath the Greenland Ice Sheet (GrIS) despite extensive documentation in Antarctica, where periodic release of water can impact ice flow. Here we present an ice-sheet-wide survey of Greenland subglacial lakes, identifying 54 candidates from airborne radio-echo sounding, and 2 lakes from ice-surface elevation changes. These range from 0.2–5.9 km in length, and are mostly distributed away from ice divides, beneath relatively slow-moving ice. Based on our results and previous observations, we suggest three zones of formation: stable lakes in northern and eastern regions above the Equilibrium Line Altitude (ELA) but away from the interior; hydrologically-active lakes near the ELA recharged by surface meltwater and; small, seasonally-active lakes below the ELA, which form over winter and drain during the melt season. These observations provide important constraints on the GrIS's basal thermal regime and help refine our understanding of the subglacial hydrological system.

3.2 Introduction

Only four subglacial lakes have been discovered beneath the Greenland Ice Sheet (GrIS), despite evidence suggesting a significant proportion of the bed is thawed (MacGregor et al., 2016; Jordan et al., 2018) and that some of this basal water forms metre-scale diameter ponds over ∼3 cm deep (Oswald and Gogineni, 2008). Two small (>10 km^2) lakes, separated by a bedrock island, were detected beneath the Bowdoin Glacier, northwest Greenland, from airborne radio-echo sounding (RES) (Palmer et al., 2013). The presence of ice-surface collapse basins in ice-marginal settings provided evidence for two further active subglacial lakes, recharged by surface meltwater penetrating to the bed (Howat et al., 2015; Palmer et al., 2015; Willis et al., 2015). The scarcity of subglacial lakes identified in Greenland has been associated with steeper ice-surface slopes, and therefore a stronger hydraulic gradient, compared to Antarctica (Pattyn, 2008; Livingstone et al., 2013). However, hydrological potential calculations predict that subglacial lakes could cover ∼1.2% of the GrIS bed (Livingstone et al., 2013), and may constitute a significant component of the subglacial drainage system in regions conducive to their formation, such as high subglacial relief regions in the eastern

sector of the ice sheet, or beneath fast-flowing outlet glaciers, such as the North East Greenland Ice Stream (NEGIS).

In contrast, over 400 subglacial lakes have been detected beneath the Antarctic Ice Sheet using a combination of ice-penetrating radar, ground-based seismic surveys and satellite surface altimetry (Wright and Siegert, 2012). Antarctic subglacial lakes range in size from water bodies less than 1 km in length (Wright and Siegert, 2011) to the largest, subglacial Lake Vostok, which is ∼250 km long (Popov and Chernoglazov, 2011). Hydrologically active lakes which fill and drain over decadal or shorter timescales causing uplift and subsidence of the ice surface, are typically identified from ice-surface elevation changes and commonly form close to the ice margin beneath fast-flowing outlet glaciers and ice streams (Gray et al., 2005; Smith et al., 2009; Fricker et al., 2016). Conversely, larger subglacial lakes, predominantly detected from RES surveys (showing bright, hydraulically flat, specular bed reflections, typically 10–20 dB stronger than surrounding bedrock), are located within 200 km of ice divides and tend to be stable over >103 years (Wright and Siegert, 2012). Antarctic subglacial lakes have been implicated in initiating ice stream flow (Bell et al., 2007a; Langley et al., 2011) and causing transient ice accelerations driven by periodic drainage events (Stearns et al., 2008; Scambos et al., 2011; Siegfried et al., 2016), highlighting their important role in ice sheet mass balance, and consequently sea-level rise (Stearns et al., 2008). Furthermore, direct sampling of subglacial lake environments has revealed complex microorganisms adapted to isolated and extreme conditions (Achberger et al., 2016; Vick-Majors et al., 2016).

In this paper, we conduct the first comprehensive survey of subglacial lakes beneath the GrIS using National Aeronautics and Space Administration (NASA's) Operation IceBridge (OIB) airborne RES database (1993-2016), in addition to OIB Airborne Topographic Mapper (ATM) L2 surface elevation data, and 5 m ArcticDEM composite and 2 m multi-temporal swaths to detect collapsed ice-surface basins and monitor changes in ice-surface elevation. Our results reveal a different distribution of subglacial lakes compared to their Antarctic counterparts, with a dominance of small subglacial lakes that act as a stable storage of water above the Equilibrium Line Altitude (ELA).

3.3 Methods

3.3.1 Subglacial lake identification from radio-echo sounding

We analysed OIB airborne RES profiles collected between 1993 and 2016 and obtained from the Center for Remote Sensing of Ice Sheets (CReSIS) archive (http://data.cresis.ku.edu) (Gogineni et al., 2001). A number of RES instruments (Improved Coherent Radar Depth Sounder (ICORDS), Multi-Channel Radar Depth Sounder (MCRDS), and Multi-Channel Coherent Radar Depth Sounder (MCoRDS) on board various NASA aircraft were used, which have a frequency range of 140-230 MHz and a transmit power of 200-2000 W. We used the L1B synthetic aperture radar (SAR) products for our analysis, which were processed by CReSIS. The basic processing steps included pulse compression with time and frequency windowing, followed by compensation for aircraft motions. The data were then stacked coherently before application of focused SAR processing. The depth range resolution in ice after the final processing was ∼4.3 m with a final product along-track resolution of ∼25 m. Bed depths were defined by the returned bed echoes identified by CReSIS with automatic detectors and manual pickers.

We interrogated over 574,000 km of radar echograms for subglacial lakes based on two metrics: first, qualitative visual inspections for hydraulically flat and smooth bed reflectors (Siegert et al., 1996; Siegert et al., 2005; Carter et al., 2007), second, quantitative analysis of bed reflectivity (Matsuoka et al., 2012). Relative basal reflectivity, determined from the bed returned power, is a well-established method for detecting subglacial water and basal conditions beneath both the Antarctic Ice Sheet (Carter et al., 2009; Jacobel et al., 2009; Fujita et al., 2012; Matsuoka et al., 2012; Wolovick et al., 2013; MacGregor et al., 2016; Schroeder et al., 2016a) and the GrIS (Oswald and Gogineni, 2008; Chu et al., 2016; Livingstone et al., 2017). Studies typically suggest anomalies of 10–20 dB constitute a suitable threshold for distinguishing wet and dry beds, however, this threshold is sensitive to basal roughness; high reflectivity anomalies can also be associated with a smooth, flat bed and saturated sediment (Jordan et al., 2017). We therefore use relative basal reflectivity thresholds based on the statistics of the bed returned power within a 10 km radius around the identified lake (1σ, 2σ and 3σ from the mean), together with hydraulically flat

reflectors at the ice-bed interface, to delineate subglacial lakes. Following the qualitative identification of subglacial lakes in the RES data, lakes were classified based on the coincidence of horizontal reflectors and high relative basal reflectivity. Confidence levels range from low confidence (a flat reflector but low relative reflectivity) to very high confidence (a flat reflector which is three standard deviations above the mean).

3.3.2 Surface collapse basin identification

In addition to RES analysis, we applied a simple technique to identify potential collapse basins in the surface of the ice sheet, which are indicative of subglacial lake drainage and recharge events (Palmer et al., 2015; Willis et al., 2015). We removed the sinks in the high resolution (5 m) ArcticDEM (v2.0) from the Polar Geospatial Center (Porter et al., 2018) and then subtracted this from the original Digital Elevation Model (DEM) to identify topographic surface depressions. These ice-surface depressions were then classified based on the similarity of their depth-to-area ratios to existing collapse basins (21.07 m to 0.55 km^2). Multi-temporal ArcticDEM strip files (2012-2016) at 2 m resolution enabled elevation change detection, providing additional information about potential subglacial lake drainage events.

3.3.3 Surface elevation change measurements using Operation IceBridge ATM

OIB Airborne Topographic Mapper (ATM) Level-2 Icessn Elevation, Slope and Roughness version 2 dataset, provided and processed by National Snow and Ice Data Center (NSIDC) (Studinger et al., 2003), were used to assess the activity of subglacial lakes detected in the RES data. This laser altimeter system provides swath surface elevation measurements at a sampling frequency of 5 kHz, cross-track width of $\sim$400 m, and a footprint diameter of $\sim$1 m. Co-located measurements are repeated annually (2009–2017), providing a surface elevation time series for each identified subglacial lake.

3.3.4 Hydraulic potential analysis

To calculate hydraulic potential gradients, we apply the Shreve (Shreve, 1972) hydraulic potential equation using BedMachine v3 (Morlighem et al., 2017) (150 m resolution) bed elevation and ice thickness data, following methods outlined in a previous study (Livingstone et al., 2013). Minima in the hydraulic potential surface were identified using TopoToolbox (Schwanghart and Scherler, 2014), a Matlab-based software. Hydraulic potential surfaces were calculated for a range of flotation fraction values from 0.8 to 1.11 to test the sensitivity of lake locations to changes in water pressure.

3.4 Results

3.4.1 Radar evidence for subglacial lakes

Inspection of OIB airborne RES data reveals 54 previously uncharted subglacial lake candidates beneath the GrIS, accounting for 0.025% of the ∼574,000 km of flight lines analysed (Supplementary Figs. 1–34). These are identified based on two methods: first, qualitative visual inspection for the presence of hydraulically flat and specular bed reflectors, analogous to subglacial lakes identified in Antarctic surveys (Siegert et al., 1996; Siegert et al., 2005); second, quantitative relative basal reflectivity analysis where subglacial lakes are identified by basal reflectivity exceeding 1σ, 2σ or 3σ above the mean reflectivity within a 10 km radius surrounding region (Oswald and Gogineni, 2008) (Figure 3.1). We categorise our results using four confidence levels. Low confidence where the potential lake reflector is hydraulically flat, but relative basal reflectivity anomalies are not found (Figure 3.1a), or the reflector is not hydraulically flat, but exhibits reflectivity anomalies over 1σ above the mean of the surrounding region. Medium/high/very high confidence where the hydraulically flat reflector coincides with relative basal reflectivity exceeding 1σ /2σ /3σ above the mean of the surrounding region (Figure 3.1b–h). Our results classify only 7% of subglacial lakes as low confidence, while 44% of the lakes identified in this study are ranked as either high or very high confidence (Supplementary Table 1). For the more uncertain lake candidates (i.e., low and medium confidence) that do not have an obvious flat reflector or with a relative basal reflectivity $<2\sigma$, we acknowledge that our approach

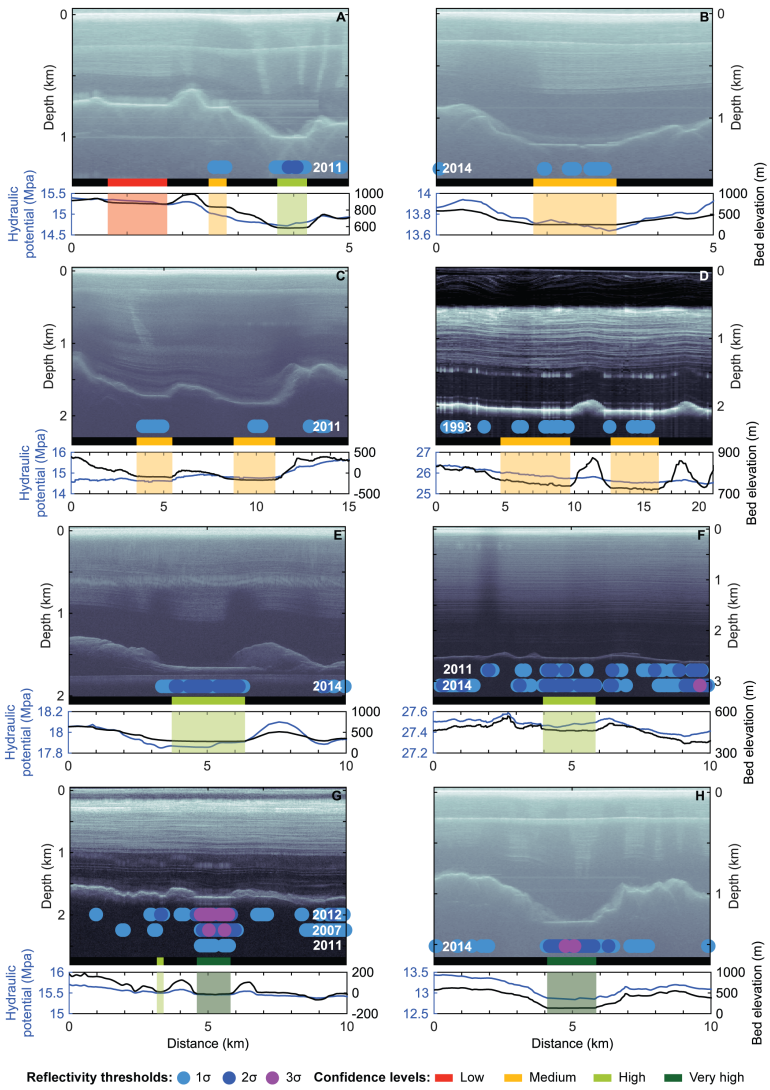

Figure 3.1: Example RES profiles for 13 subglacial lakes identified beneath the Greenland Ice Sheet in this study and the surrounding bed topography. Relative basal reflectivity values (1–3σ) are indicated by the blue-purple circles. Lakes are depicted by a bar colour-coded according to the confidence level (see Figure 3.3). The bedrock elevation (black) and hydraulic potential (blue) are shown in the graphs below. a Lakes 32–34 along flight line 20120516_01_059, b lake 39 along flight line 20120503_03_037, c lakes 24–25 along flight line 20110329_01_019, d lakes 56–57 along flight line 19930702_01_012, e lake 29 along flight line 20140313_08_001, f lake 45 along flight line 20140424_01_033, with reflectivity values for years 2011 and 2014, g lakes 18–19 along flight line 20020530_01_007, with reflectivity values for years 2002, 2007 and 2011, h lakes 30–31 along flight line 20140313_08_002

cannot clearly differentiate very shallow lakes from flat areas of saturated sediment (akin to the fuzzy Antarctic lakes (Carter et al., 2007)).

Of the lake candidates identified using RES, 35% were surveyed multiple times between 1993 and 2016, allowing us to investigate their minimum persistence (Supplementary Table 1). Significantly, all of these subglacial lakes were detected quantitatively by high relative reflectivity indicative of basal water in each of the years surveyed, suggesting that they persisted through the period of data availability. This includes 8 lakes with RES data covering 2–5 years, 8 lakes with 13–16 years of RES data and 3 lakes that have RES data across 20 years (Supplementary Table 1). The absence of any surface elevation changes indicative of drainage or filling in both the multi-temporal OIB IceBridge L2 Airborne Topographic Mapper (ATM) data (2009–2017), covering 48% of RES lakes, and timestamped ArcticDEM data (2012–2016), across all RES lakes, provides further support that these lakes are stable and therefore persistent features. Together, these data provide evidence that all RES identified lakes are stable over multiple years, with 20 persisting for at least 10 consecutive years (Supplementary Table 1).

3.4.2 Ice surface collapse basins

Analysis of surface depressions with depth-to-area ratios equivalent to collapse basins previously linked to subglacial lake drainages (see methods) (Palmer et al., 2015), revealed two new surface depressions situated about 35 km apart, between Sermeq and Sioqqap Sermia glaciers in southwest Greenland (Figure 3.2). The depressions measured ∼0.18 and ∼0.64 km^2 in 2012 and are approximately 15.4 and 18.1 m deep, respectively (using the ArcticDEM 2 m resolution swath data). Surface elevation change, measured from multi-temporal ArcticDEM swaths, revealed ∼11 ± 0.2 m uplift of the northern basin (Figure 3.2a) and ∼14 ± 0.2 m uplift of the southern basin between 2012 and 2015 (Figure 3.2b). Landsat 4, 5, 7 and 8 imagery shows evolution from surface depressions to dome-like features through continued uplift (Figure 3.2c–j). We interpret these as collapse basins that are slowly filling following subglacial lake drainage events (Palmer et al., 2015). Based on the timestamped ArcticDEM data and Landsat imagery, although equivocal, recharge at the northern

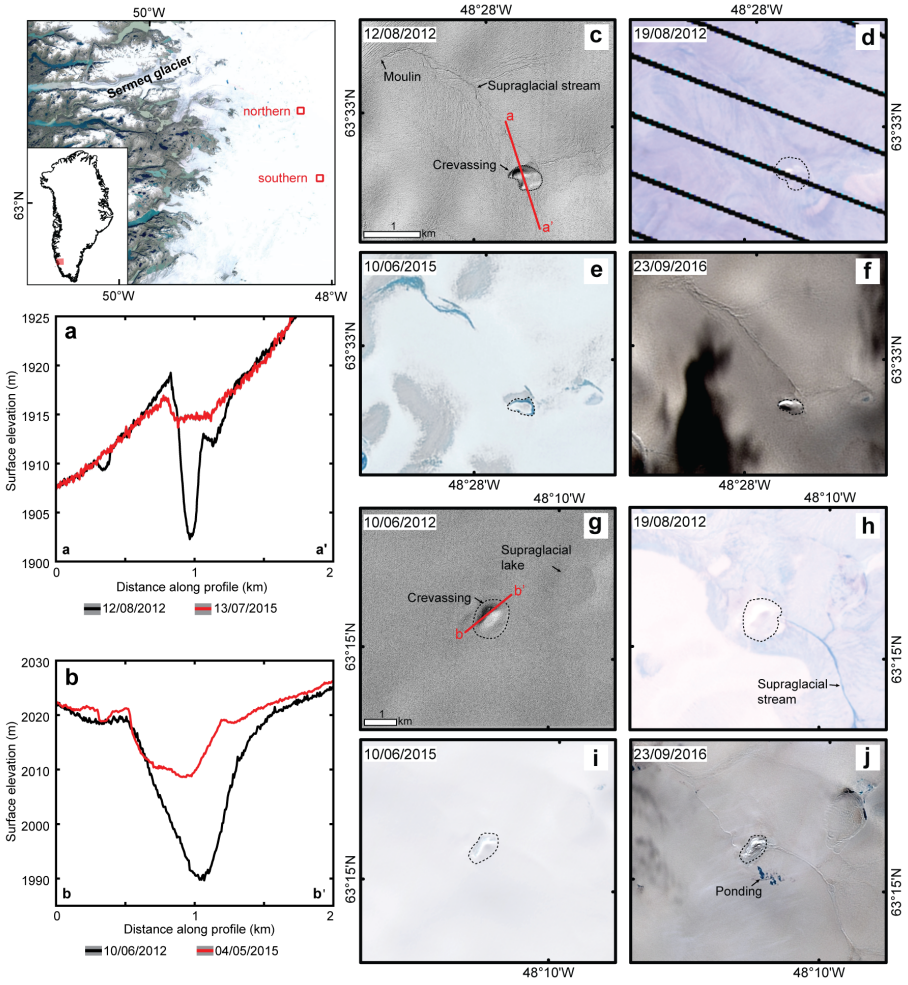

Figure 3.2: Surface elevation change and evolution of active subglacial lakes in southwest Greenland. Inset map shows location of collapse basins near Sermeq glacier. a Surface elevation profile across flow at northern collapse basin, measured using the ArcticDEM 2 m resolution strip files. ±0.2 m error bars are shown. b Surface elevation change along flow at southern collapse basin. Hillshades of the ArcticDEM and Landsat 4, 5, 6, 7 imagery showing evolution of collapse basins from depression to dome-like features through continued uplift between 2012 and 2016 for north basin (c–h) and south basin (g–j), indicating subglacial lake drainage events.

collapse basin is estimated to have been occurring for >5 years, though the subglacial lake drainage event was not identified (Figure 3.2a). For the southern collapse basin, a major depression appears in the Landsat imagery around 2001 and repeat imagery indicates that the depression has since shrunk in area (Figure 3.2h–j), suggesting that the subglacial lake beneath has been refilling for a period of 17 years (2001–2018) so far. Observations of surface meltwater ponding, moulins (Figure 3.2c) and sudden supraglacial lake drainage in this region may indicate at least partial recharge of the subglacial lake by meltwater draining to the bed (Willis et al., 2015). No RES flight lines run directly through these lakes, therefore we cannot determine whether, like Antarctica, the radar records for these active lakes show an absence of lake reflectors (Siegert et al., 2014).

3.4.3 Distribution of identified subglacial lakes

The spatial distribution of subglacial lakes beneath the GrIS is illustrated in Figure 3.3. We observe three main clusters of subglacial lakes in north-western, northern and central-eastern Greenland, which coincide with recent observations of ponded water from radar signal characteristics (Oswald et al., 2018). The minimum length of lake reflectors ranges from 0.2 to 5.9 km, with a mean of 1.4 km (Figure 3.4a). The largest lakes (>3 km length) are located in the central-eastern sector of the ice sheet, while the smallest lakes (<0.5 km length) are predominantly situated in northwest Greenland (Figure 3.3). The thickness of the ice overlying the identified subglacial lakes ranges from ∼300 to 3200 m, with an average of 1647 m (Figure 3.4b). Few subglacial lakes (22%) are located within 50 km of the margin, and lakes are generally absent beneath major ice divides (Figure 3.4c) and fast-flowing outlet glaciers (Figure 3.3). Most lakes (74%) are found beneath relatively slow-moving ice (<15 m a^{-1}). Subglacial lakes appear in a variety of topographic settings; a third of lakes occur in regions of low relief confined by small bedrock bumps (≤10% bedrock gradient), while nearly a quarter of subglacial lakes are surrounded by steep bedrock hills (>30% gradient).

The spatial distribution of simulated subglacial lakes beneath the GrIS, following hydraulic potential analysis methods (Livingstone et al., 2013), updated for BedMachine v3 (Morlighem et al., 2017) (150 m resolution) is shown in Figure

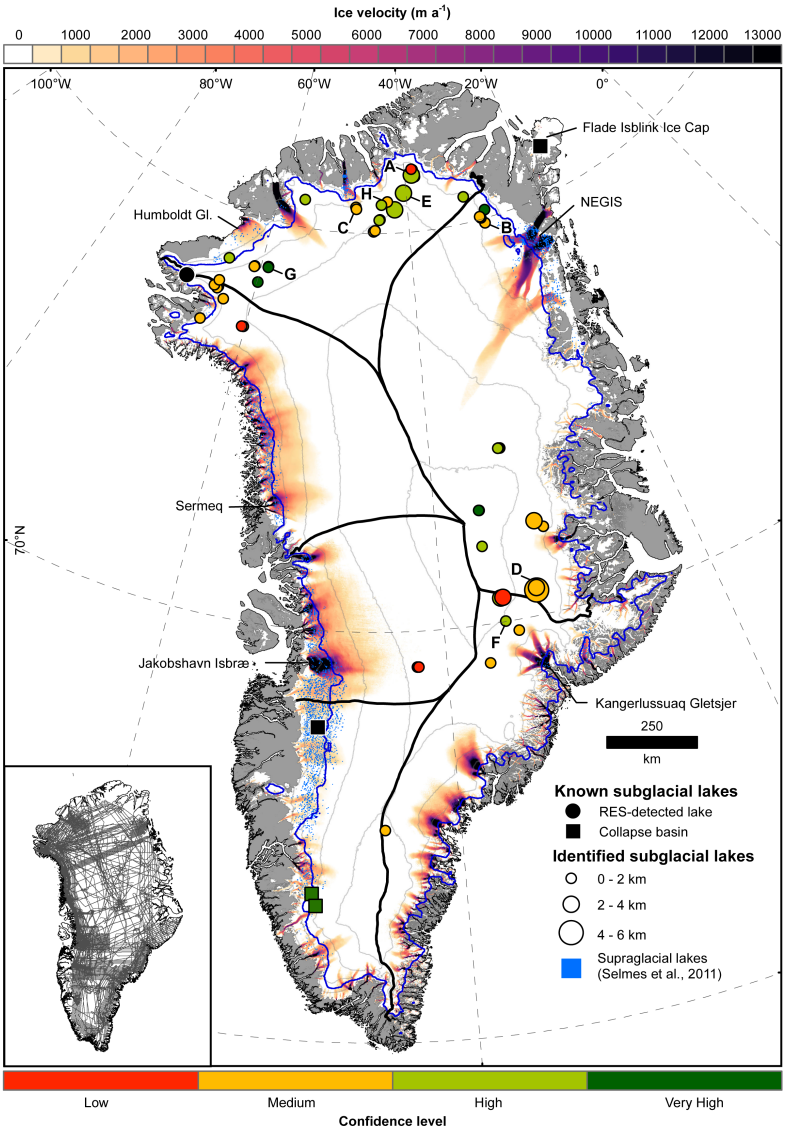

Figure 3.3: Spatial distribution of subglacial lakes identified in the radar echo sounding data. Lakes are colour-coded according to confidence level and proportionate in size to the length of the lake reflector. Black circles represent known subglacial lakes, squares depict collapse basins (black = in existing literature, green = this study). Ice-surface elevation contours at 500 m intervals are shown in grey (Morlighem et al., 2017), with the equilibrium line altitude in blue (for the period 2000–2009) using MAR 3.5 forced by ERA-Interim (Fettweis et al., 2013a) and ice divides depicted by the thick black lines (Rignot and Mouginot, 2012). Supraglacial lake data derived from MODIS between 2005–2009 is also displayed(Selmes et al., 2011). Background map shows MEaSUREs Greenland Ice Sheet velocity map derived from InSAR(Joughin et al., 2017). Inset map displays OIB radar flight lines (1993–2016) used in this study.

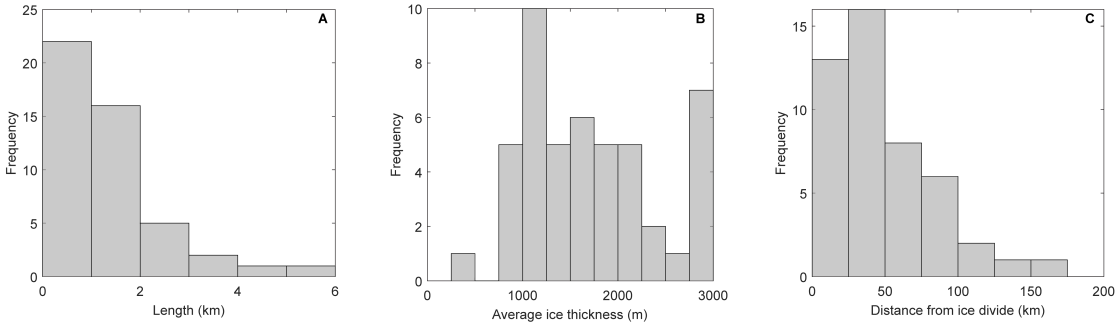

Figure 3.4: Frequency-distribution histograms of subglacial lakes identified in this study. a Minimum length of lake reflector identified in RES data, calculated by measuring the horizontal extent of the lake reflection. b Average ice thickness (Morlighem et al., 2017) within 5 km^2 area overlying the subglacial lake c Geodesic distance from major ice divides (Rignot and Mouginot, 2012) depicted in Figure 3.3.

3.5a. Only 32% of our identified subglacial lakes are located within 1 km of estimated hydraulic minima (f=0.9). This is reduced to 9% when a flotation fraction of f=1 is applied. The majority of subglacial lakes coincide with regions of estimated geothermal heat flux (Martos et al., 2018) between 50 and 61 mW m^{-2} (Figure 3.5b), while central-eastern lakes mostly appear in the zone of elevated geothermal heat flux (>66 mW m^{-2}). Figure 5c displays locations of identified subglacial lakes in relation to basal thermal state predictions, estimated using thermomechanical ice flow modelling, radiostratigraphy, surface ice velocity and borehole observations1. 20% of subglacial lakes identified in the RES data are situated in the likely frozen region, all of which are found in central-eastern Greenland, a quarter of lakes are located in the likely thawed region, predominantly in north-western Greenland, and the remaining 55% are detected in regions where the predicted basal thermal state is uncertain (Figure 3.5c). The majority (63%) of subglacial lakes in this study are found in regions of relatively high (dimensionless) bed roughness (>1.29), towards the margins (Figure 3.5d).

3.5 Discussion

Subglacial lakes are discrete bodies of water beneath ice masses which can vary on a spectrum from ephemeral ponding of water, for example in the lee side of bedrock bumps (e.g., Gray et al., 2005), to large, deep (>100 km long) lakes such as Subglacial Lake Vostok (Siegert et al., 2001). Shallow pockets of water can also exist, being connected by saturated sediments. The subglacial lake candidates identified in this

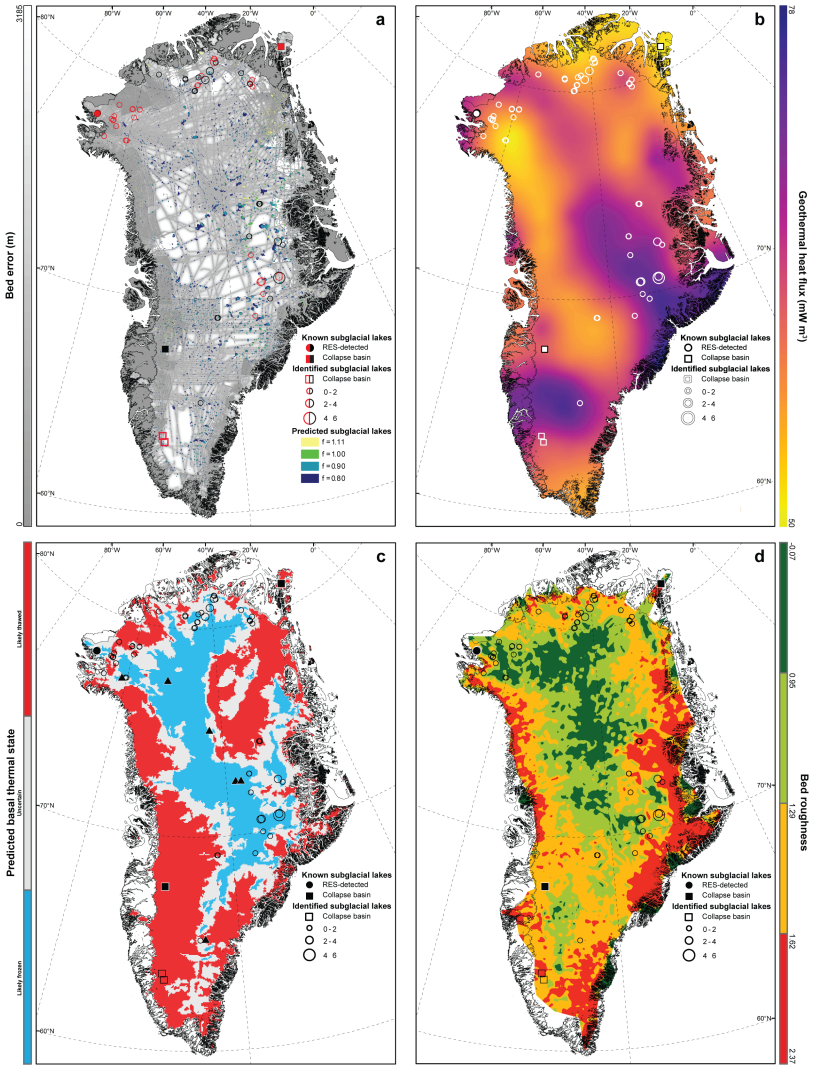

Figure 3.5: Comparison between location of identified subglacial lakes and predicted lakes, geothermal heat flux, basal thermal state and bed roughness. a Predicted subglacial lake locations, using Shreve hydraulic potential equation and varying flotation fractions (f) overlain on the BedMachine DEM error map (Morlighem et al., 2017). Lakes in black coincide with hydraulic minima (using f = 0.9), whilst those in red were not successfully predicted. b Estimated geothermal heat flux derived from magnetic data (Martos et al., 2018). c Predicted basal thermal state1 (blue = likely frozen, white = uncertain, red = likely thawed). d Dimensionless bed roughness beneath the GrIS (Rippin, 2013), measured using the fast Fourier transform approach which converts bed topography (derived from radar echo sounding) into the frequency domain. Known subglacial lakes in existing literature are shown by black circles (RES-detected) and squares (detected through elevation changes). Deep ice core locations are depicted by black triangles. Lakes identified in this study are shown by circles, and the size of the circle is proportional to the minimum length of the lake reflector.

study differ from those observed in Antarctica, both in terms of topographic setting and size. Antarctic subglacial lakes detected by RES typically occur in close proximity to ice divides under thick (>4000 m), warm-based ice (Pattyn, 2010), with the largest subglacial lakes occupying tectonically controlled topographic depressions (Studinger et al., 2003; Tabacco et al., 2006). In contrast, Greenland subglacial lakes are typically absent beneath the isostatically depressed, smooth interior basin along the main N–S ice divide, and are instead concentrated toward the ice margin. In the centre of the GrIS, ice is largely frozen to its bed (MacGregor et al., 2016), with water becoming more prevalent towards the margin where ice surface speeds are typically higher (Jordan et al., 2018) and surface-to-bed hydraulic connectivity more likely. This is in contrast, however, to a recent analysis of radar signal characteristics which suggests extensive ponded water around the North GRIP drill site at the onset of the NEGIS (Oswald et al., 2018). The largest GrIS subglacial lakes are constrained by steep bedrock relief in the East Greenland subglacial mountain chain, whereas the smaller lakes (<2 km) tend to be prevalent in regions associated with low subglacial roughness, such as northwest Greenland (Rippin, 2013). On average, GrIS subglacial lakes are nearly eight times shorter than their Antarctic counterparts (1.4 km compared to 11 km on average in Antarctica, excluding Lake Vostok (Dowdeswell and Siegert, 2003), reflecting the steeper average ice-surface (and thus subglacial hydraulic) gradient and different bed topographic settings controlling the locations of subglacial lakes. In particular, Greenland bed topography is relatively flat and well-organised with respect to ice flow (Morlighem et al., 2017), whereas the topography beneath Antarctica is more complex (Fretwell et al., 2013), and therefore offers sites where large volumes of basal water can be stored e.g., Subglacial Lake Vostok, Concordia and Ellsworth. Subglacial lakes in Greenland tend to occupy the middle of the spectrum in terms of size. Whilst the known subglacial lakes are mostly stable, there are some larger unstable bodies of water which exhibit cyclic drainage and refilling.

About 40% of identified subglacial lakes in Antarctica are active (i.e., evidence of drainage/filling from ice-surface elevation changes), and these are mostly found beneath ice streams in West Antarctica (Siegert et al., 2016a). In contrast, we observe only two further examples of active subglacial lakes in Greenland (4 in total; 6.7% of all discovered lakes), and a general absence of subglacial lakes beneath fast-flowing

outlet glaciers. This could be due to the reliance on altimetry methods rather than RES techniques to resolve active lakes (Siegert et al., 2016a). However, as well as assessing surface elevation changes above RES-detected lakes using both timestamped ArcticDEM and OIB IceBridge ATM2 datasets, we also carried out an ice-sheet wide survey for ice surface collapsed basins using the 5 m resolution ArcticDEM v2.0 mosaic (Porter et al., 2018) (see methods), finding just two collapsed ice basins consistent with lake drainage events (Figure 2).

There is a general paucity of lakes in fast-flowing western and southern sectors of the GrIS, and beneath the NEGIS (Figure 3.3), despite hydraulic potential (Livingstone et al., 2013) and bed reflectivity analysis (Oswald and Gogineni, 2008; Jordan et al., 2018) predicting widespread basal water in these regions. The southern and western sectors of the GrIS have extensive ablation areas where large volumes of surface meltwater are generated each summer (Noël et al., 2015; Smith et al., 2015). Lakes in the ablation area may be more difficult to detect from airborne radar because the ice is thin, and the ice-surface is rougher and steeper than further inland. In addition, we hypothesise that the drainage of this meltwater to the bed inhibits subglacial lake formation on annual or longer timescales, due to the seasonal evolution of efficient subglacial drainage systems able to connect and drain stored water to the ice margin (Lindbäck et al., 2015). Evidence of seasonal subglacial water storage from RES data supports this; water is stored on bedrock plateaus during the winter and flushed out during summer when efficient subglacial drainage develops (Chu et al., 2016). These small, seasonally active subglacial lakes are difficult to resolve from monitoring ice-surface elevation alone due to large seasonal mass changes in the ablation zone, including the drainage and filling of supraglacial lakes, which can coincide with subglacial lake locations (Sergienko, 2013). Over longer time-scales, focused erosion by subglacial water cutting channels into the bed beneath fast-flowing southern and western sectors (e.g., due to the perennial drainage of supraglacial lakes) and the NEGIS (e.g., due to geothermal and frictional basal melting) may lead to the removal of hydraulic minima (Livingstone et al., 2012, 2017). This may explain why the few active subglacial lakes large and stable enough to be detected under the GrIS are found in close proximity to the ELA, where there is less surface melting and where the formation of efficient subglacial drainage is inhibited by thicker ice and low

surface slopes (Schoof, 2007; Meierbachtol et al., 2013). More persistent, RES-detected subglacial lakes, are associated with regions of low melt input variability; the majority of subglacial water recharging these lakes is generated from elevated geothermal heat flux rather than surface melt (the region of surface lakes only coincides with one RES detected subglacial lake–Figure 3.3) (Martos et al., 2018). Finally, the lack of subglacial lakes detected beneath the fast-flowing southern and western sectors of the GrIS and the NEGIS may represent a limitation of our approach. In particular, we consistently struggle to discriminate lakes in uniformly thawed regions (MacGregor et al., 2016) (Figure 3.5c), where they are predicted to be prevalent (Livingstone et al., 2013), likely because extensive water/saturated sediment results in a higher mean reflectivity and thus reduced relative contrast of the lake compared to background bed conditions. This may partially explain the discrepancy with previous studies which find extensive ponded water at the onset of and beneath the NEGIS (Oswald et al., 2018).

The recall of just 32% of the identified subglacial lakes by hydraulic potential analysis using a flotation fraction of f=0.9 (Figure 3.5a) contrasts with similar analyses in Antarctica that successfully recall >50% of the known subglacial lakes (Livingstone et al., 2013; Goeller et al., 2016). We suggest three reasons why hydraulic potential analysis is less useful at predicting subglacial lakes in Greenland, even under steady state basal conditions. Firstly, there is a clear size bias, with larger lakes being generally easier to recall (Livingstone et al., 2013). As Greenland lakes are on average 8 times shorter than those in Antarctica, they are typically more difficult to discern from the hydraulic potential analysis. However, recall of subglacial lakes is still low even in regions of the ice sheet characterised by high data coverage and low bed error, such as northwest Greenland (Figure 3.5a), where we would expect smaller hydraulic minima to be more accurately constrained. We therefore posit that low bed roughness in areas such as northwest Greenland (Rippin, 2013; Jordan et al., 2017) (Figure 3.5d), makes it more difficult to accurately pick out hydraulic minima because there is a small difference in elevation between the lake surface and basin lip (0% recall in northwest Greenland using a flotation fraction of f=0.9). In contrast, regions with higher bed roughness, such as north-eastern Greenland (Rippin, 2013) have correspondingly higher recall rates (44%), and indeed, like Antarctica, lakes that

form in deep topographic depressions also tend to be larger. Finally, only 25% of low and 31% of medium confidence lake candidates fall within 1 km of hydropotential lows, compared to 50% for very high confidence lakes, supporting the inference that these lower confidence lakes may actually comprise regions of swampy saturated sediment rather than well-defined lake basins (Carter et al., 2007).

We have shown that subglacial lakes are more prevalent in Greenland than previously assumed. These subglacial lake candidates are repeatedly identified in RES data, suggesting that they could act as long-term meltwater reservoirs; active drainage of lakes towards the ice sheet margin is restricted or difficult to detect. The majority of subglacial lakes are concentrated in the uncertain regions of predicted basal thermal state1 where ice sheet models and ice-penetrating radar do not agree on whether the bed is frozen or thawed. As our method is based on relative bed echo strength, it is likely to pick out lakes surrounded by colder, less reflective bed material more easily, compared to lakes surrounded by warm-bedded regions (e.g., beneath the NEGIS). Thus, our results may indicate that this uncertain region is heterogeneous (a mosaic of cold and warm basal conditions) on length scales that enable us to detect multiple water pockets from RES, but which ice-sheet models running at coarser resolution would have difficulty resolving. The lack of alignment between RES-detected lakes and hydraulic potential analyses may therefore occur because subglacial water is spatially constrained by the prevalence of frozen bed conditions rather than topography (Livingstone et al., 2012). The presence of subglacial lakes scattered within these uncertain regions consequently helps to further constrain the thermal state of the bed.

Similar to previous investigations (Palmer et al., 2013; Howat et al., 2015; Palmer et al., 2015; Willis et al., 2015) we suggest that the actively draining lakes in southwest Greenland are recharged by seasonal surface meltwater transferred to the bed due to the association of these locations with surface meltwater ponding and drainage. Although further study is required to assess the net influence of subglacial lakes on GrIS dynamics, it is likely to be limited due to the paucity of active lakes large enough to induce dynamic surface height changes, their proximity to the margin, and the strong control of surface meltwater in determining the character of subglacial

drainage and its influence on ice-sheet dynamics. However, this inventory of Greenland subglacial lakes could be utilised to locate candidates for direct sampling. Seasonal surface meltwater transporting microbial life, minerals, organic matter and pollutants into the hydraulically connected subglacial system may have important implications for basal biogeochemistry, while their sedimentary deposits contain an archive of ice sheet evolution (Hodgson et al., 2016) and palaeoenvironmental change (Bentley et al., 2011).

There is little doubt that our inventory, although representing a significant augmentation of the number of identified lakes, is incomplete and further subglacial lakes remain to be discovered with continued expansion and repetition of OIB flights, in addition to the launch of NASA's IceSat-2 satellite enabling improved active subglacial lake identification. However, the distribution (Figure 3.3), size (Figure 3.4a) and activity (Supplementary Table 1) of identified subglacial lakes allows us to propose a conceptual model of GrIS subglacial water storage and dynamics (Figure 3.6). Beneath the ice sheet interior there is limited detectable water storage due to the frozen and flat bed. Where the bed is inferred to comprise a heterogeneous patchwork of frozen and warm-bedded conditions, isolated subglacial lakes persist from year to year. Regions characterised by high relief basal topography and geothermal heat flux sustain the largest lakes (e.g., large parts of East Greenland). We identify a range of lake detection confidence levels, with some lakes clearly distinguishable, whereas others are less distinct and may represent shallow water lenses or even patches of saturated sediment. Around the ELA, there is some evidence of hydrologically active lakes recharged seasonally by inputs of surface water (Palmer et al., 2015). However, relatively numerous small subglacial lakes that drain on seasonal timescales when efficient subglacial networks develop during the melt season, likely exist in the ablation zone (Chu et al., 2016). These lakes are difficult to detect from monitoring surface elevation due to their small size and the large seasonal surface mass changes in the ablation zone. Although we do not identify many subglacial lakes beneath fast-flowing warm-based regions of the ice-sheet, we do not rule out significant additional water storage here given the potential limitations of our approach for effectively identifying lakes where the mean reflectivity is high. Long-term basal meltwater storage beneath the region beyond the ELA could be activated in the future as the ablation area

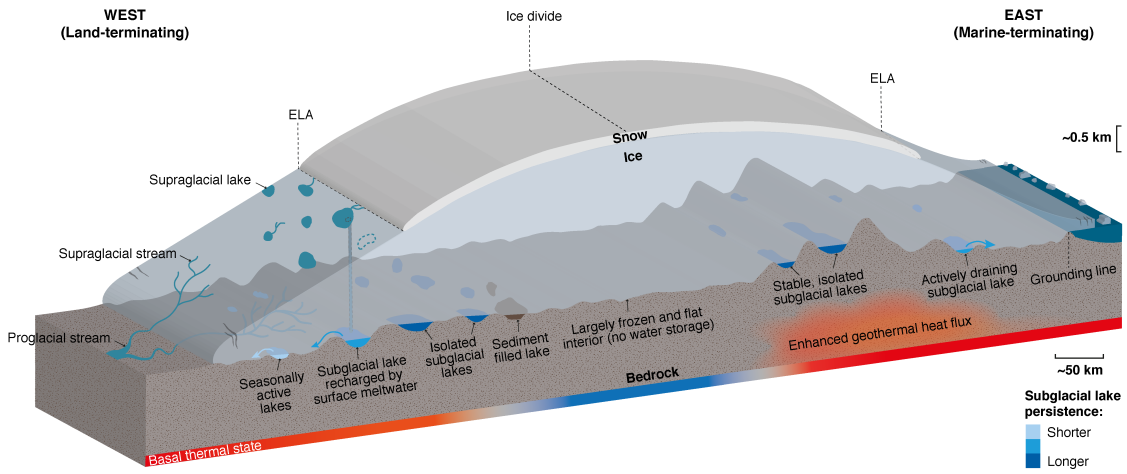

Figure 3.6: Conceptual model of Greenland ice sheet hydrological system, illustrating supraglacial and subglacial features. Subglacial lakes are colour-coded according to lake persistence, those that are less distinct and could represent shallow water lenses or patches of saturated sediment are coloured brown. Estimated basal thermal state is represented by the red to blue colour bar, with red being likely thawed, white being uncertain regions, and blue being likely frozen (MacGregor et al., 2016). In the ice sheet interior, the ice is mostly frozen to the bed and the basal topography is flat, prohibiting water storage and subglacial lake formation. Above the equilibrium line altitude (ELA) but away from ice divides, where the bed is predicted to comprise a heterogeneous patchwork of frozen and warm-bedded conditions, subglacial lakes are relatively common but stable features. Around the ELA, subglacial lakes are hydrologically active and recharged seasonally by inputs of surface water. Finally, relatively numerous small subglacial lakes that drain on seasonal timescales when efficient subglacial networks develop during the melt season likely exist in the ablation zone.

migrates inland (Leeson et al., 2015). The resulting increased input of meltwater to the bed at higher elevations could open new subglacial drainage pathways through enhanced sliding and potentially connect this dormant storage to the ice sheet margin.

Chapter 4

Detecting active subglacial lakes beneath the Greenland Ice Sheet using high-resolution digital elevation models

Jade S. Bowling[1], Malcolm McMillan[2], Amber Leeson[1], Stephen J. Livingstone[2], Andrew J. Sole[2].

[1]Lancaster Environment Centre, Lancaster University, Lancaster, UK
[2]Centre for Excellence in Environmental Data Science, Lancaster University, Lancaster, UK
[2]Department of Geography, University of Sheffield, Sheffield, UK

Correspondence:
Jade Bowling (j.bowling@lancaster.ac.uk)

The following work will soon be submitted to *The Cryosphere*.

4.1 Abstract

As Earth's climate warms, surface meltwater production and runoff is expected to increase on the Greenland Ice Sheet, delivering increased volumes of freshwater into the ocean and contributing to global sea level rise. Understanding and monitoring the routing of water on the surface, through and ultimately beneath the ice sheet is important, because it can influence ice flow. It is therefore crucial that physical models that project ice sheet evolution accurately represent how the ice sheet responds to changing hydrology. A relatively understudied component of the subglacial hydrological system in Greenland is the storage and discharge of meltwater in active subglacial lakes. Subglacial outburst floods flushing high sediment and freshwater flux to the ice margin could have important implications for ice flow, ocean circulation, ice-ocean interactions and marine biodiversity. However, currently little is known about their distribution and dynamics at the ice sheet scale. Here we present an ice sheet-wide framework for identifying subglacial hydrological activity, using ∼26,000 high spatial resolution (2 m) ArcticDEM digital surface models (DSMs). This new dataset provides unprecedented detail of localised surface elevation changes around the entire margin of the Greenland Ice Sheet (∼700,000 km^2), and allows us to identify previously unknown signals of subglacial lake drainage events. To evaluate our new method, we analyse 7 signals of local elevation change, and demonstrate that they represent subglacial drainage activity between 2008 and 2019. These findings represent an important first step towards understanding the distribution and dynamics of subglacial lake activity beneath the Greenland Ice Sheet, and hence the short- and long-term evolution of the ice sheet's subglacial hydrological system.

4.2 Introduction

Over recent decades, pronounced increases in atmospheric (Fettweis et al., 2017) and oceanic temperatures (Straneo and Heimbach, 2013), and variability in cloud cover (Hofer et al., 2017) have caused marked Greenland Ice Sheet mass losses of ∼4,000 Gt between 1992-2018 (Shepherd et al., 2020). Fluctuations in mass loss are caused by complex variations in surface mass balance (SMB) (van den Broeke et al., 2009; Fettweis et al., 2017) and ice dynamical processes (Enderlin et al., 2014; Mouginot

et al., 2019). The proportion of mass loss due to these processes has varied throughout both time and spatially, with SMB becoming the dominant driver in the last two decades (Mouginot et al., 2019).

Each summer, meltwater generated at the surface of the Greenland Ice Sheet is routed through supraglacial channels (Smith et al., 2015; Pitcher and Smith, 2019). The majority of this meltwater is directed to the bed via moulins (englacial conduits) (Catania et al., 2008; Lampkin and van der Berg, 2014; Smith et al., 2015; Yang and Smith, 2016; Koziol and Arnold, 2018), forming a dynamic subglacial drainage system that transports most meltwater to the coast. Spatio-temporal variability in meltwater fluxes to the basal environment and characteristics of the subglacial system can alter local basal water pressure and modulate ice velocity (Zwally et al., 2002a; Joughin et al., 2004; Bartholomaus et al., 2008; Das et al., 2008; van de Wal et al., 2008; Shepherd et al., 2009; Bartholomew et al., 2010; Schoof, 2010; Bartholomew et al., 2011; Kulessa et al., 2017). The delivery of freshwater, entrained with sediment and associated mironutrients, to the fjords and the nearby ocean can alter fjord dynamics, such as the physical structure of the water column (Mortensen et al., 2013; Kjeldsen et al., 2014), as well have potential implications on local ice dynamics through submarine melting and undercutting, promoting calving (Straneo et al., 2011; Bartholomaus et al., 2013; Motyka et al., 2013; O'Leary and Christoffersen, 2013; Inall et al., 2014; Rignot et al., 2015). Increased freshwater discharge can also impact marine ecosystems by altering light availability and thus primary productivity, or by enhancing phytoplankton blooms (Bhatia et al., 2013; Sanders et al., 2014; Hawkings et al., 2015; Murray et al., 2015; Meire et al., 2016a; Halbach et al., 2019). It is therefore important to be able to measure these meltwater fluxes to understand how the ice sheet might respond to further warming.

If not refrozen or exported to the ice margin, subglacial meltwater can be stored in subglacial lakes. In Antarctica ∼35% of known subglacial lakes are defined as 'active', those which have been observed to fill and drain episodically, whilst the remainder are deemed 'stable', i.e. relatively closed systems (Wright and Siegert, 2012). Active subglacial lakes in Antarctica, predominantly sourced from geothermal heat and pressure melting due to a scarcity of surface melting, can discharge water on short

timescales (months-years) (Fricker et al., 2007, 2014), and in some cases connect with other subglacial lakes several kilometres downstream (Wingham et al., 2006b; Fricker and Scambos, 2009; Smith et al., 2009; Fricker et al., 2014; Smith et al., 2017a). Such water flow can temporarily alter Antarctic mass balance by regulating the amount and distribution of subglacial water beneath fast-flowing ice streams and outlet glaciers (Bell et al., 2007a; Siegfried and Fricker, 2018). Transient accelerations in ice flow have coincided with subglacial lake drainage events at Byrd Glacier (Stearns et al., 2008), Crane Glacier (Scambos et al., 2011), Mercer and Whillans ice streams (Siegfried et al., 2016) and Thwaites Glacier (Smith et al., 2017a). Furthermore, large subglacial lake outburst floods transport large fluxes of water and sediment downstream, which can alter ice-ocean interactions (Le Brocq et al., 2013; Alley et al., 2016; Marsh et al., 2016; Li et al., 2021) if they surpass the grounding line into sub-ice shelf cavities, and modify ocean circulation (Evatt et al., 2006).

In contrast to the well-studied and well-documented network of Antarctic subglacial lakes, very little is known about the extent of subglacial lake activity beneath the Greenland Ice Sheet. To date, only 7 active subglacial lakes have been identified based on local studies (Howat et al., 2015; Palmer et al., 2015; Willis et al., 2015; Bowling et al., 2019), however, a systematic continental-scale assessment is yet to be carried out in Greenland. Active subglacial lakes in Greenland could have several important implications, which differ from their Antarctic counterparts due to the input of supraglacial meltwater. Firstly, such lakes have the capacity to store meltwater generated over multiple seasons, the release of which may provide a large volume of subglacial water flux into the system, that would be greater than simply from supraglacial input. Secondly, crevasses formed during deformation of the ice surface following subglacial lake drainage events create a new direct pathway for surface meltwater to reach the bed, enabling subglacial lakes to refill (e.g., Willis et al., 2015), as well as warm and soften the basal ice through heat released by trapped meltwater (Thoma et al., 2012). Furthermore, this input of seasonal surface meltwater carrying microbes, minerals and pollutants to the subglacial system may have implications for basal biogeochemistry. Thirdly, if active subglacial lakes are situated close to the calving front of marine glaciers in Greenland, they have the potential to drive higher rates of melting at the front when they drain e.g., through entraining ocean heat.

Episodic changes in subglacial lake volume, can cause the overlying ice sheet surface to deform; these localised surface elevation changes can be detected and monitored using high-precision repeat satellite altimetry and radar interferometry missions (e.g. Gray et al., 2005; Fricker and Scambos, 2009; Smith et al., 2009; McMillan et al., 2013; Siegfried et al., 2014; Siegfried and Fricker, 2018). Satellite altimetry instruments are, however, limited by their relatively large ground footprint (typically several 10's - 100 m for laser altimetry, and several 100 - 1000 m for radar altimetry) and sparse ground tracks (e.g. Schutz et al., 2005; Wingham et al., 2006a. Whilst this is adequate for detecting many active subglacial lakes beneath the Antarctic Ice Sheet, which are typically >100 km^2 (Wright and Siegert, 2012), this technique is less suited for Greenlandic active subglacial lakes which are smaller (<10 km^2) (Howat et al., 2015; Palmer et al., 2015; Willis et al., 2015; Bowling et al., 2019). High-resolution (metre-scale), high-coverage Digital Surface Models (DSMs) offer the potential to address some of the shortcomings of altimetry, namely enabling comprehensive measurements of both ice sheet and peripheral glacier topography, without the need to interpolate between tracks. In this paper, we develop a method to detect potential subglacial lake activity using timeseries of DSMs. We utilise ∼26,000 2 m resolution ArcticDEM DSMs within 50 km of the ice margin to identify ∼130 localised surface elevation changes that may be indicative of subglacial lake activity. We use the 7 known active Greenlandic subglacial lakes to test the viability of this method for detecting active subglacial lakes, and present evidence of 7 new active subglacial lakes in a variety of settings.

4.3 Datasets and Methods

The methodological framework presented in this chapter enables the detection of localised surface elevation changes associated with subglacial lake activity from time-varying ArcticDEM data. Here, we summarise the datasets and processing workflow used in this study, with the full details are discussed in Supplementary Information B.

4.3.1 ArcticDEM

ArcticDEM (https://www.pgc.umn.edu/data/arcticdem/) is an initiative to provide open-source DSMs of the Arctic north of 60° (Porter et al., 2018). The public-private partnership between the US National Geospatial-Intelligence Agency (NGA) and a team led by the US National Science Foundation (NSF) funded Polar Geospatial Center (PGC) enabled these high-resolution elevation models to be generated. Using petascale computing, a Surface Extraction with Triangulated Irregular Network-based Search-space Minimization (SETSM) automatic photogrammetric algorithm (Noh and Howat, 2015) is applied to overlapping optical stereo-image pairs from Digital Globe's GeoEye-1 and WorldView-1, -2, and -3 satellite sensors. The outcome is two products: (i) the 2 m resolution ArcticDEM Mosaic, compiled from statistically-determined, high-quality Strip DSMs, which have been merged and feathered to provide a seamless DSM with reduced artefacts and voids, covering an area of ∼23 million km^2 (Porter et al., 2018), and (ii) 2 m resolution ArcticDEM Strips which consists of ∼260,000 individual time-stamped DSMs (2008-2019) that were used to assemble the Mosaic product (Porter et al., 2018). The dimensions of the ArcticDEM Strips vary depending on the sensor used, however the average size is ∼700 km^2.

ArcticDEM covers a vast geographical area with multi-temporal coverage and very high spatial resolution, enabling inter-annual and seasonal elevation change measurements in various remote sensing studies, for example, in the analysis of debris-covered glaciers in the Russian Arctic (Barr et al., 2018), estimating river surface heights in Alaska (Dai et al., 2018), and quantifying lava flows from volcanic eruptions in Russia (Dai and Howat, 2017). ArcticDEM has a much higher resolution than other large-scale Digital Elevation Models (DEMs), such as Advanced Spaceborne Thermal Emission and Reflection Radiometer-Global DEM (ASTER GDEM) (15 m) (Tachikawa et al., 2011), TerraSynthetic Aperture Radar-X add-on for Digital Elevation Measurement (TanDEM-X) (90 m) (Krieger et al., 2007), or Multi-Error-Removed Improved-Terrain (MERIT) (90 m) (Yamazaki et al., 2017) DEMs. Additionally, ArcticDEM offers time-varying elevation data which is advantageous compared to both global DEMs and Greenland-specific data, such as the Greenland Ice Mapping Project (GIMP) which has a resolution of 30 m (Howat et al., 2014).

In this study, we retrieved all available ArcticDEM Strips over the Greenland Ice Sheet from Release 7 within 50 km of the ice margin, as active subglacial lakes are unlikely to be located in the interior of the ice sheet where the ice is frozen to the bed (MacGregor et al., 2016). This region is ∼700,000 km^2, covering approximately 39% of the ice sheet (Figure 4.1a). In total, over 26,000 ArcticDEM Strips (2008-2019) were acquired within the region of interest (Figure 4.1a-c), totalling more than 30 TB of data. The highest density of ArcticDEM strips are found along the western margin and around well-studied glaciers, such as Petermann and Humboldt glaciers in northern Greenland (Figure 4.1). The majority of scenes were acquired between April and July (Figure 4.1d), with an average size of 744 km^2 (Figure 4.1e).

4.3.1.1 Georeferencing

Whilst the ArcticDEM products offer continuous coverage and high resolution elevation models, few studies have carried out assessments to quantify their accuracy (e.g., Noh and Howat, 2015; Glennie, 2018), which is fundamental for elevation change analysis. Glennie, 2018 suggests ArcticDEM Strips provide vertical accuracy of 2-4 m (1 σ) in flat, open terrain, but this worsens to about 7-12 m standard deviations in regions of vegetation cover. In glaciated regions, vertical and horizontal errors of 3-5 m have been recorded, which is reduced to 0.2 m in the vertical if high-accuracy airborne Light Detection and Ranging (LiDAR) data is used for co-registration (Noh and Howat, 2015). However, airborne LiDAR data may not be available in the Arctic, particularly over large regions. Instead, we georeference each ArcticDEM Strip using the dx, dy and dz offsets provided by the ArcticDEM team, to improve their vertical accuracy and geolocation (see Supplementary Information B.1 for more detail). These translation values are calculated based on seasonally subsetted National Aeronautics and Space Administration (NASA) Ice, Cloud, and land Elevation Satellite (ICESat) altimetry data, which have been filtered to exclude hydrographic features and regions with high relief, and where applicable LiDAR or surveyed Global Positioning System (GPS) points (Porter et al., 2018).

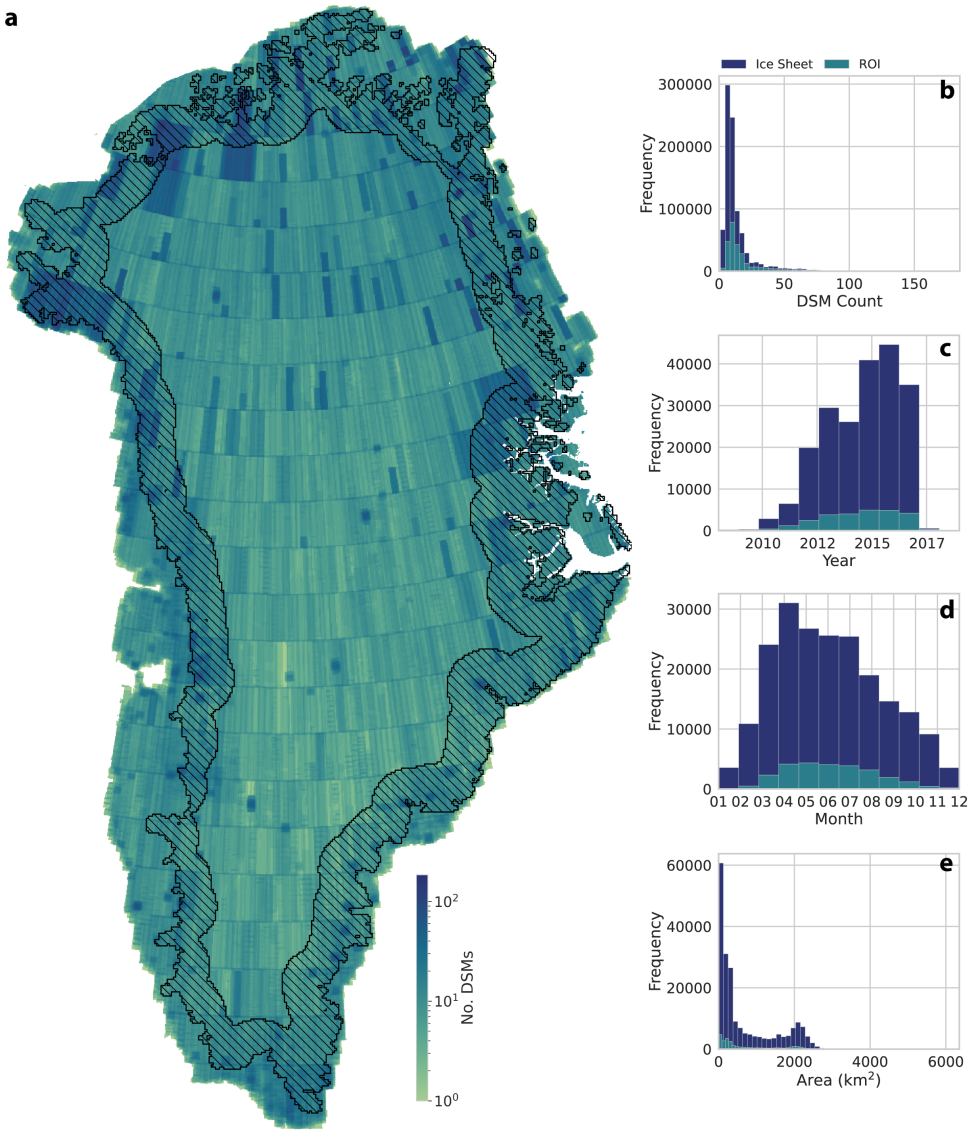

Figure 4.1: Spatial and temporal coverage of ArcticDEM Strip DSMs. (a) Spatial distribution of DSMs as count of ArcticDEM Strips across the Greenland Ice Sheet, with region of interest (within 50 km of ice margin) shown by black hashed polygon. (b) Histogram showing DSM count for the Greenland Ice Sheet (dark blue) and region of interest (green). (c) Yearly distribution of the DSM count as a histogram from 2008 to 2019 for the ice sheet (dark blue) and region of interest (green). (d) Monthly distribution of the DSM count as a histogram for the ice sheet (dark blue) and region of interest (green). (e) Histogram of area of ArcticDEM Strip footprint for the ice sheet (dark blue) and the region of interest (green).

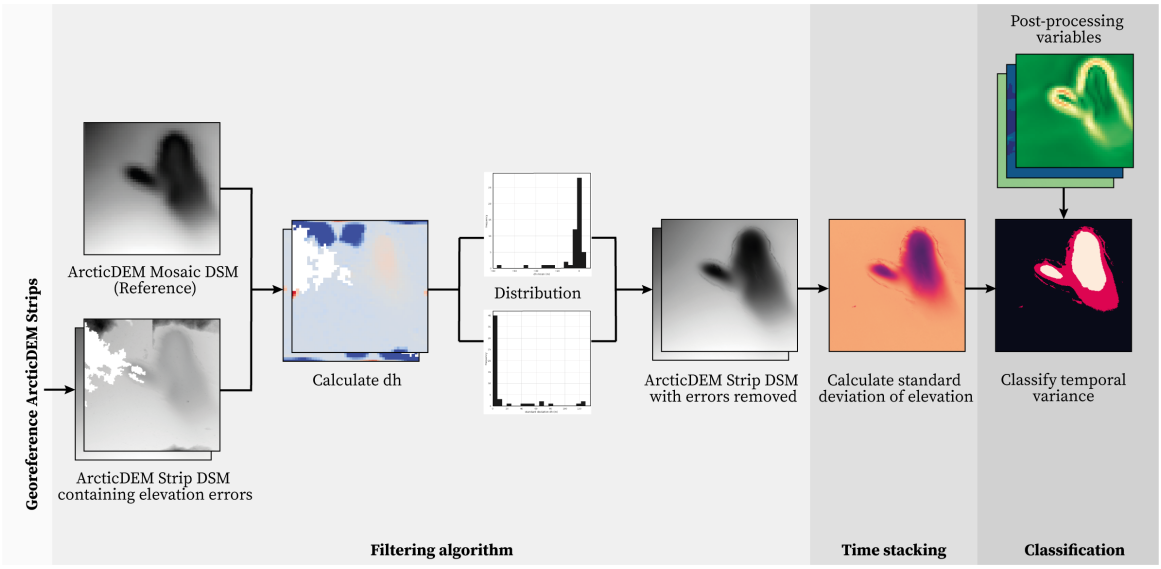

Figure 4.2: Flow diagram of the methodology describing the processing steps from georeferencing ArcticDEM Strip DSMs to classifying potential active subglacial lake candidates. Processing steps in bold correspond to sections in Methods.

4.3.1.2 Filtering algorithm

Because ArcticDEM products are generated from optical imagery, voids can occur due to the presence of clouds, fog, shadows or dust (Porter et al., 2018). Furthermore, height errors, artefacts and noise may be caused by errors in SETSM autocorrelation due to issues such as homogeneous terrain (e.g., covered by snow), areas of open water, or poor edge matching (Porter et al., 2018). Following georeferencing, we therefore excluded all ArcticDEM Strips for which the standard deviation of the elevation difference *dh* with the 100 m ArcticDEM Mosaic, was larger than 20 m (Figure 4.2). Elevation differences were calculated by re-sampling the Strips using cubic interpolation to match the Mosaic 100 m spatial resolution. Further details on the validation and calibration of this threshold are available in Supplementary Information B.1.1.

4.3.1.3 Time stacking

Using all remaining Strip DSMs, we created three-dimensional arrays (time t, space x and y) of elevation h(t, x, y), divided into 139,889 tiles of 5 x 5 km within the region of interest to decrease computing time. Surface elevations below sea level and

elevations >3,200 m are removed to further mitigate the effect of outliers which are outside reasonanle elevations found on the ice sheet. Then we calculated the standard deviation (σ) of elevation iteratively at each 2 m^2 pixel within the tile, to analyse vertical shifts in the ice surface. At the pixel scale, ice sheet surface elevation undergoes temporal changes (e.g., seasonal, annual, decadal) due to physical processes such as firn densification, accumulation, dynamic thinning and isostatic adjustment (Hawley et al., 2020), with trends that significantly vary spatially (e.g., region, glacier, zone of the ice sheet). As our objective is to detect active subglacial lake drainage events with characteristics that far exceed typical ice sheet surface elevation change e.g., 70 m deep collapse basin at Flade Isblink Ice Cap (Willis et al., 2015), we do not adjust for temporal trends in surface elevation.

4.3.1.4 Classification

The temporal variance in elevation within the region of interest were categorised using natural breaks (Jenks) classification algorithm (Jenks, 1977), which creates class breaks based on natural groupings in the data i.e. similar values, and maximises the variance between classes. We classify the standard deviation of elevation values into six classes: Class 1: $0 < \sigma < 4$ m; Class 2: $4 \leq \sigma < 10$ m; Class 3: $10 \leq \sigma < 19$ m; Class 4: $19 \leq \sigma < 31$ m; Class 5: $31 \leq \sigma < 48$ m; Class 6: $48 \leq \sigma < 100$ m. Using Geographical Information Systems (GIS) tools we convert and dissolve the raster pixels into polygons (or features). Table 4.1 shows the number of features within each Class and their varying sizes with most classified as Class 1. To attribute these changes to active subglacial lake drainage events, we vetted our approach on the seven known active subglacial lakes (see Supplementary Information).

Due to the vast number of features within these classification bands (Class 2: 1,408,282, Class 3: 393,516), we apply some additional post-processing filtering steps (Figure 4.2):

1. Remove features (Class 2: n=1,400,349, Class 3: n=391,815) which are smaller than 0.16 km^2 or have a perimeter larger than 15 km, to remove false positives, e.g., very linear or elongated features which are unlikely to be representative of

Class	Standard deviation of elevation	% of pixels	No. features	Mean area (km^2)	Area range (km^2)
1	>0 & <4 m	56.93	2,689,900	0.127	0.002 - 95,466
2	≥4 & <10 m	29.80	1,408,268	0.032	0.002 - 5,147
3	≥10 & <19 m	8.33	393,516	0.021	0.002 - 1,119
4	≥19 & <31 m	2.95	139,555	0.015	0.002 - 149
5	≥31 & <48 m	1.22	57,692	0.013	0.002 - 28
6	≥48 & <100 m	0.77	36,390	0.012	0.002 - 9

Table 4.1: Number of features identified within different bands of temporal standard deviation, and their associated statistics

active subglacial lakes. The minimum area is based on the minimum area of known active subglacial lakes in Greenland (Table B.1).

2. Removal of features (Class 2: 4,848: , Class 3: n=1,701) located outside a distance of 1 km of the ice margin (using the mask described in Morlighem et al., 2017) and terminus termini of marine-terminating glaciers (Moon and Joughin, 2008) to differentiate between potential subglacial lakes, typically found further inland, and high dynamic change at glacier termini.

3. Removal of features (Class 2: 479, Class 3: n=115) located in areas of very high slope (>30°, derived from the ArcticDEM 100 m Mosaic product; Porter et al., 2018), to remove surface anomalies in close proximity to steep mountainous terrain where erroneous elevations are more common.

4. Remove features (Class 2: 128, Class 3: n=42) derived from <5 Strip DSMs to calculate temporal standard deviation of elevation.

In total, across the ice sheet scale, approximately 6,745 (26%) Strip DSMs are removed in the filtering steps (Section 4.3.1.2. During post-processing, 1,798,725 features were removed to generate 3,059 features across both Class 2 and 3. Following these post-processing steps, features between 0.16 and 0.5 km^2 were categorised as lower confidence active subglacial lake candidates, those in Class 2 and greater than 0.5 km^2 were deemed medium confidence candidates, and those in Class 3 and greater than 0.5 km^2 were classed as high confidence candidates.

4.3.2 Landsat

To assist mapping the temporal evolution of the ice surface in response to potential subglacial lake activity at selected candidates, we produced natural colour composites using cloud-free Level-1 Landsat-5, -7 and -8 imagery (between 1987-2021), collected from the United States Geological Survey (USGS)-Earth Explorer portal (http://earthexplorer.usgs.gov). Landsat satellites provide high coverage (e.g., Landsat-8 captures ∼700 images globally per day over the 16-day orbit repeat cycle) observations of the Earth's surface, with a spatial resolution of 30 m. For each case study we obtain imagery before and after the estimated drainage event to identify evidence of subglacial lake activity, such as crevasses at the ice surface, shadowing to imply a depressed surface or sediment plumes at the terminus, as well as supraglacial hydrological features. Some of the Landsat-7 images are obscure with missing data due to the scan line corrector failure.

4.3.3 Radio-echo sounding

4.4 Results & Discussion

4.4.1 Mapping temporal variance in ice sheet elevation

Using the approach described previously, we derive estimates of the temporal variance in ice sheet surface elevation for every 2 m^2 pixel within the ∼700,000 km^2 region of interest. The pixels are then classified and converted into features (or polygons) using GIS tools (Figure 4.3). The majority (57%) of pixels are categorised into Class 1 ($0 < \sigma < 4$ m; Table 4.1) which captures large regions of the ice sheet (maximum feature size: 95,466 km^2) above the equilibrium line altitude (ELA) (Figure 4.3). Values close to 0 indicate minimal variation, e.g., flatter surface topography towards the ice sheet interior where physical processes such as firn densification, accumulation, dynamic thinning are negligible (Figure 4.3). About 30% of the pixels were categorised as Class 2 ($4 < \sigma < 10$ m; Table 4.1). These signals also cover large areas (maximum feature size: 5,147 km^2) and are typically found in the upper ablation zone where small-scale dynamic changes occur (Figure 4.3a-d). Smaller features, such as supraglacial lakes are also typically categorised as Class 2, which exhibit variability due to their periodic

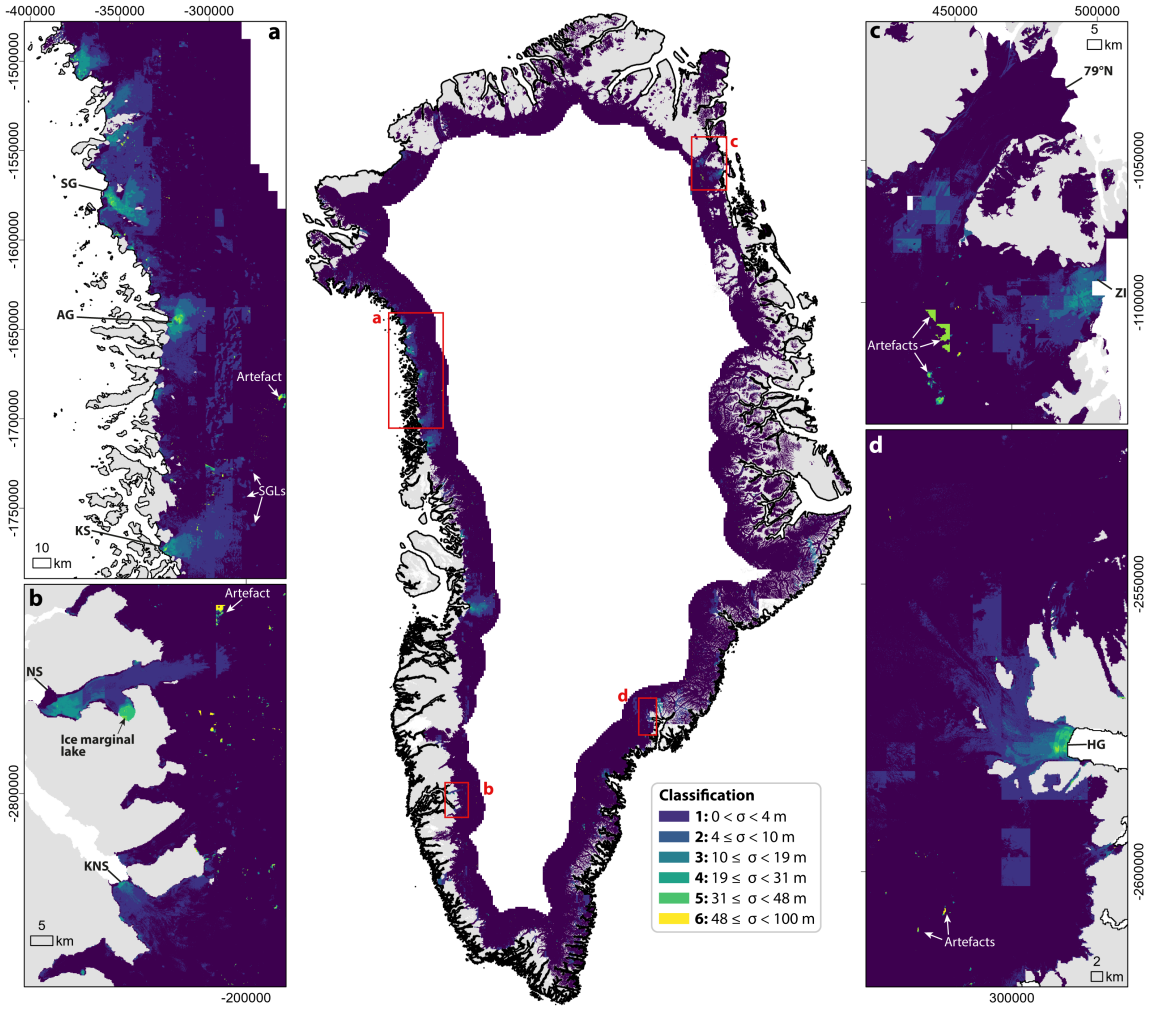

Figure 4.3: Temporal standard deviation of elevation within 50 km of the ice sheet margin, classified using the six classes described in Table 4.1. (a) Northwestern glaciers Steenstrup Glacier (SG), Alison Glacier (AG) and Kavfait Sermia (KS) are classified as Class 3-5 (>10 m standard deviation of elevation) towards the terminus, with higher elevations grouped in Class 1 (<4 m standard deviation of elevation). Supraglacial lakes are typically highlighted as small regions with 4-10 m standard deviation of elevation (Class 2). Some artefacts classified as Class 6 (>48 m standard deviation of elevation) are indicated at high elevations. (b) Southeastern glaciers Narssap Sermia (NS) and Kangiata Nunâta Sermia (KNS) are classified as Class 2-4, with greater temporal variance at the ice terminus. A large ice-marginal lake at NS is categorised as Class 4 (19-31 m standard deviation of elevation). Again some artefacts occur in the upper accumulation zone which are typically classified as Class 6. (c) Northeastern glaciers 79°N Glacier and Zachariae Isstrøm (ZI), where large artefacts classified as Class 5-6 are found at the upper accumulation zone. (d) Helheim Glacier (HG) showing increasing classification class towards the glacier terminus (up to Class 5).

fill-drain cycles (Figure 4.3a). Approximately 9% of features are in Class 3 ($10 < \sigma < 19$ m), which have a mean area of 0.02 km^2 (Table 4.1). These signals are typically distributed in the mid ablation zone of outlet glaciers (Figure 4.3). The most prominent regions of high standard deviation of elevation (Class 4 - 5) correspond to areas of fast-flowing ice (Figure 4.3a-d), particularly along the western margin of the ice sheet, where many marine-terminating glaciers are known to be dynamically thinning (Felikson et al., 2017) (Figure 4.3a-b). Although not visible in the continental scale map, areas of high variance also correspond to small features on the ice sheet surface such as crevasse fields and even supraglacial streams, as well as iceberg calving at the ice terminus. Examples of which are shown in Chapter 5.2. Finally, despite carrying out extensive filtering of Strip DSMs, some artefacts still occur which typically have very high (>48 m) standard deviation of elevation signals (Figure 4.3, although only 0.8% of features are classified as Class 6 (Table 4.1).

4.4.2 Potential active subglacial lake detection

Following post-processing steps described in Section 4.3.1.4, we extracted 3,059 features from both Class 2 and 3 to identify potential active subglacial lake candidates. We further categorised these features into low (<0.5 km km^2), medium (Class 2 & >0.5 km^2) and high (Class 3 & >0.5 km^2) confidence ranking. The majority (80%) of features are categorised as low confidence. These candidates are 0.3 km^2 on average and are typically distributed at low surface elevations (500-800 m), particularly along the western margin (Figure 4.4). 16% of features were categorised as medium confidence, which are again largely distributed along the western margin, at around 1,100-1,400 m elevations and are 0.9 km^2 on average (Figure 4.4). 4% of features were deemed high confidence candidates which are typically situated at elevations of <1,000 m and are 0.9 km^2 on average (Figure 4.4). When compared to predicted subglacial lake sites generated in Chapter 3, only 15% of higher confidence candidates are located within 1 km of hydraulic minima ($f = 0.9$). 7% of high confidence candidates are within 100 m of supraglacial lake extents estimated by Lea and Brough, 2019.

Of the 7 known active Greenland subglacial lakes, 3 fell within standard deviation of elevation Classes 2 and 3. The two largest active subglacial lake signatures, Flade

Isblink and Inugpait Quat, fell within the upper category, whilst Sioqaap Sermia (South) was detected using the lower category. In neither scenario was the Sioqaap Sermia (North) active subglacial lake, (identified in Chapter 2.2), due to it's small size, nor the three subglacial lake signatures at Isunguata Sermia due the homogenous signal across the glacier, which disguised the local signal.

4.4.3 Detection of new active subglacial lakes - demonstration of concept

To evaluate the capability of our method to locate new, and previously unknown active subglacial lakes, we visually identified localised areas of high standard deviation that had a similar visible signature to the known active subglacial lakes (Table B.1). This analysis revealed three initial candidates for future exploration at marine-terminating glaciers in northern Greenland. We describe each in turn.

4.4.3.1 Brikkerne Glacier

Brikkerne Glacier (81.5°N, 44.48°W) is a marine-terminating glacier in northern Greenland, with three frontal lobes that feed into Victoria fjord, and a forth lobe with terminates in an ice-marginal lake (Figure 4.5a). In summer 2015, the main lobe of the glacier had a 1.2 km floating ice tongue and measured approximately 6 km wide at the grounding line (Hill et al., 2017). Between 1968 and 1978 the glacier advanced by 9 km and has been retreating at an average rate of 76 m a^{-1} between 1978 and 2015 (Hill et al., 2017). Based on velocity records, Brikkerne Glacier has been identified as a surge-type glacier (Higgins, 1991).

Based upon the classified temporal variance in elevation (Figure 4.3), we identified a 1.8 km^2 oval-shaped ice surface anomaly approximately 25 km inland from the margin, at the base of a rock outcrop (Figure 4.5b). The ice here is relatively slow-moving ($<$20 m a^{-1} between 2016-2017; Joughin et al., 2018) and $<$100 m thick (Mouginot et al., 2017). This ice surface feature has a standard deviation of elevation of up to 17 m (Figure 4.5b). The surrounding ice has relatively low ($<$5 m) standard deviation of elevation, except at the terminus of Brikkerne and C.H. Ostenfeld glaciers due to the migration of the calving front (Figure 4.5a). An artefact with $>$30 m standard

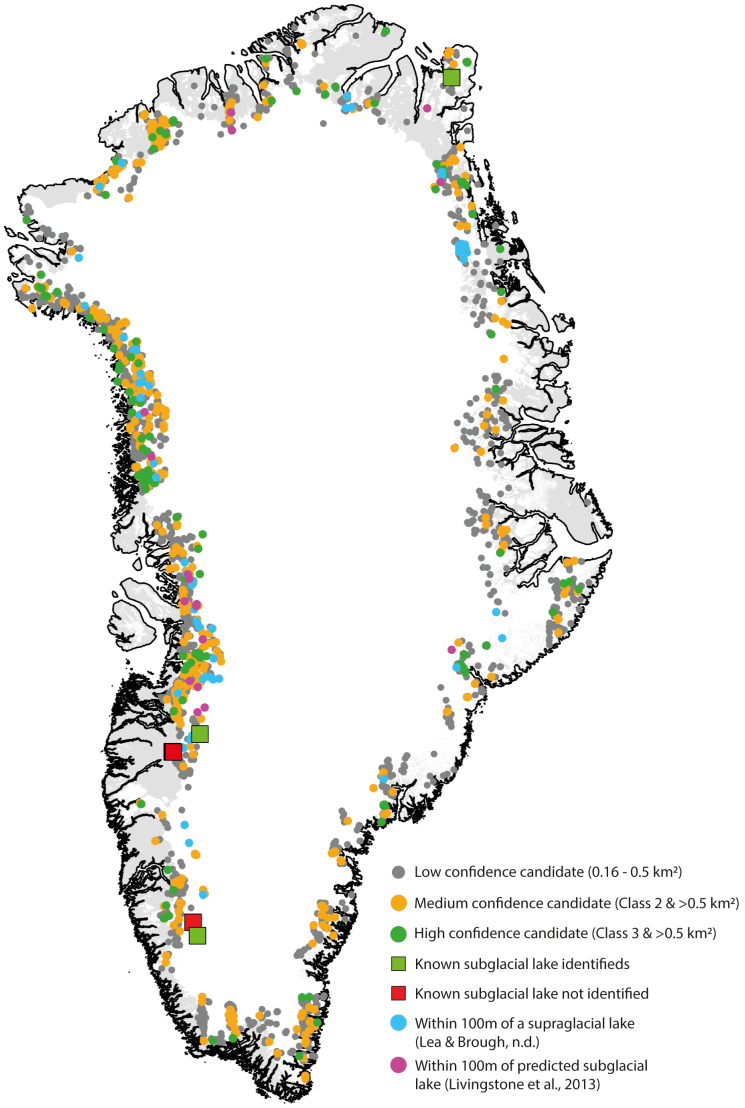

Figure 4.4: Distribution of active subglacial lake candidates. Grey points depict lower confidence active subglacial lake candidates between 0.16 and 0.5 km^2, orange points indicate medium confidence active subglacial lake candidates over 0.5 km^2 and in Class 2 ($\geq$4 & $<$10 m), and green points indicate high confidence active subglacial lake candidates over 0.5 km^2 and in Class 3 ($\geq$10 & $<$109 m). Known active subglacial lake locations are shown by squares (green if our filtered class successfully identifies the known lake, and red if not). Lake candidates within 100 m of supraglacial lakes from Lea and Brough, 2019 are shown in blue, and those within 100 m of hydraulic minima predictions from Bowling et al., 2019 are shown in pink.

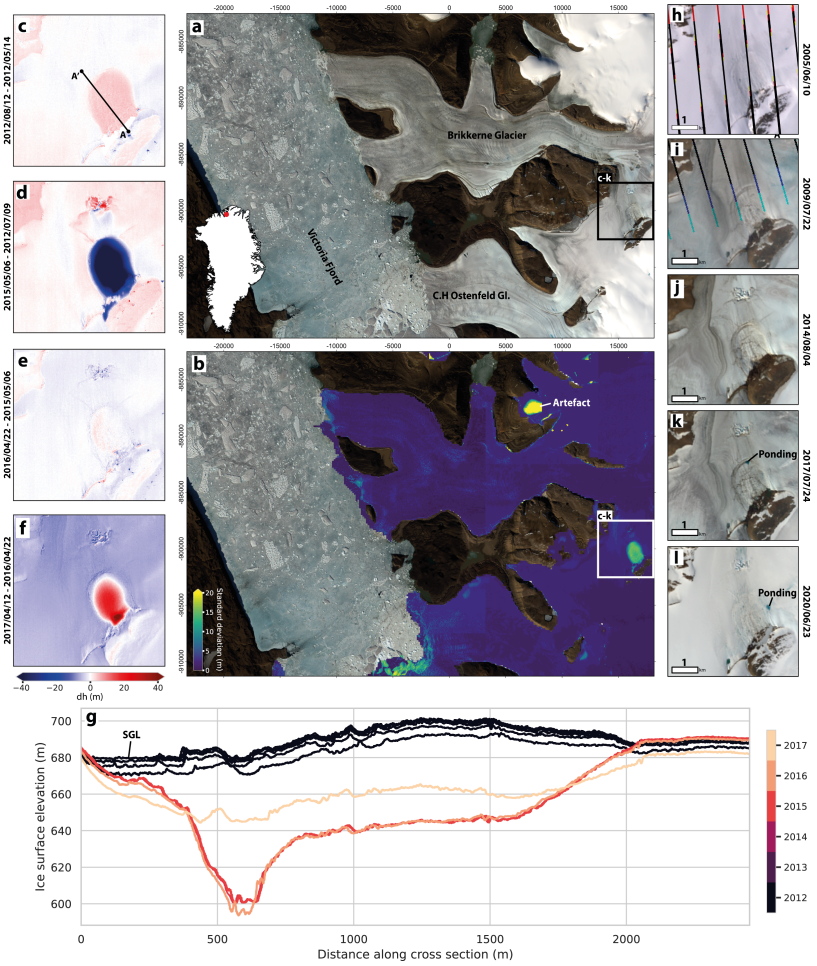

Figure 4.5: (a) Landsat 8 scene taken on 1st August 2014 showing the study area, with the active subglacial lake candidate highlighted by the black box. Inset map shows location of the candidate, in northern Greenland. (b) The standard deviation of elevation overlaid over the same Landsat 8 scene, showing temporal variance in ice sheet elevation. An artefact with high variance is labelled. (c) Difference in elevation between Strip DSMs acquired on 14th May 2012 and 12th August 2012, showing localised region of uplift. (d) Difference in elevation between Strip DSMs acquired on 9th July 2012 and 6th May 2015 show a large drop in elevation o >40 m and a localised region of uplift about 1 km down glacier of the feature. (e) Difference in elevation between Strip DSMs acquired on 6th May 2015 and 22nd April 2016, showing minimal elevation change. (f) Difference in elevation between Strip DSMs acquired on 22nd April 2016 and 12th April 2017, showing uplift of 20-30 m within the feature. (g) Transect along the profile A-A' shown in panel c, showing the evolution of the ice-surface anomaly through time.
(h) Landsat 8 scene taken on 10th June 2005 showing oval shaped feature near a rock outcrop. (i) Landsat 8 scene taken on 22nd July 2009. Surface ponding is shown at the base of the rock outcrop. (j) Landsat 8 scene taken on 4th August 2014 showing depression and localised uplift about 1 km down glacier from the feature. (k) Landsat 8 scene taken on 24th July 2017 showing depression and localised uplift is still present. Ponding is evident at the edge of the feature. (l) Landsat 8 scene taken on 23rd June 2020, ponding is indicated at the edge of the feature.

deviation of elevation that lies about 15 km north of the candidate subglacial lake (Figure 4.5b).

To assess the temporal evolution of the ice surface at this active subglacial lake candidate, we analyse all 10 Strip DSMs available. Between 14th May 2012 and 12th August 2012, the ice surface was slowly increasing in height (0.04 m d^{-1}) (Figure 4.5h). Elevation profiles taken across the candidate in the direction of ice flow indicates that the ice surface is domed in 2012, with a flat profile between 50-300 m along the transect, likely due to a supraglacial lake (Figure 4.5l). Between May 2012 and May 2014, the ice surface had lowered by up to 85 m (-10.95 m a^{-1} on average) (Figure 4.5i), and was no longer domed in shape (Figure 4.5l). Between 2014 and 2017, the ice surface in this localised region rose by 3.7 m a^{-1} (Figure 4.5k), and again was domed in shape (Figure 4.5l).

To determine the persistence of this candidate, we examined Landsat optical imagery dating back to the 1990s. This shows that the oval shape surface feature has existed in the ice surface since 1990, and occasionally meltwater ponds at the edge of the feature (Figure 4.5c-g). We interpret the localised rising and sudden drop in surface elevation as the surface signature of an active subglacial lake drainage and refilling. These observed characteristics (e.g., depth and circular crevassing) have similarities with other active subglacial lakes in both Greenland and Antarctica (see Chapter 5 for detail). Unfortunately there are no RES data over the candidate lake to determine if there is a flat lake reflector, the nearest flight line is about 8 km away.

4.4.3.2 Marie Sophie Gletscher

Marie Sophie Gletscher (76.7°N, 67.8°W) is one of the two main glaciers which feed into Independence Fjord, northern Greenland (Figure 4.6a). The glacier is approximately 75 km long, ∼4 km wide, and ∼130 m thick on average. Small tongues on both sides of the glacier terminate into ice-dammed lakes. Between 1948 and 2015, the glacier retreated by ∼15 m a^{-1}, with an average acceleration in velocity by 1 m a^{-1} between 1995/96 and 2015/16 (Hill et al., 2018). These low magnitude retreat rates have been associated with the shallow seaward-sloping bed topography, which represents a relatively stable configuration (Hill et al., 2018).

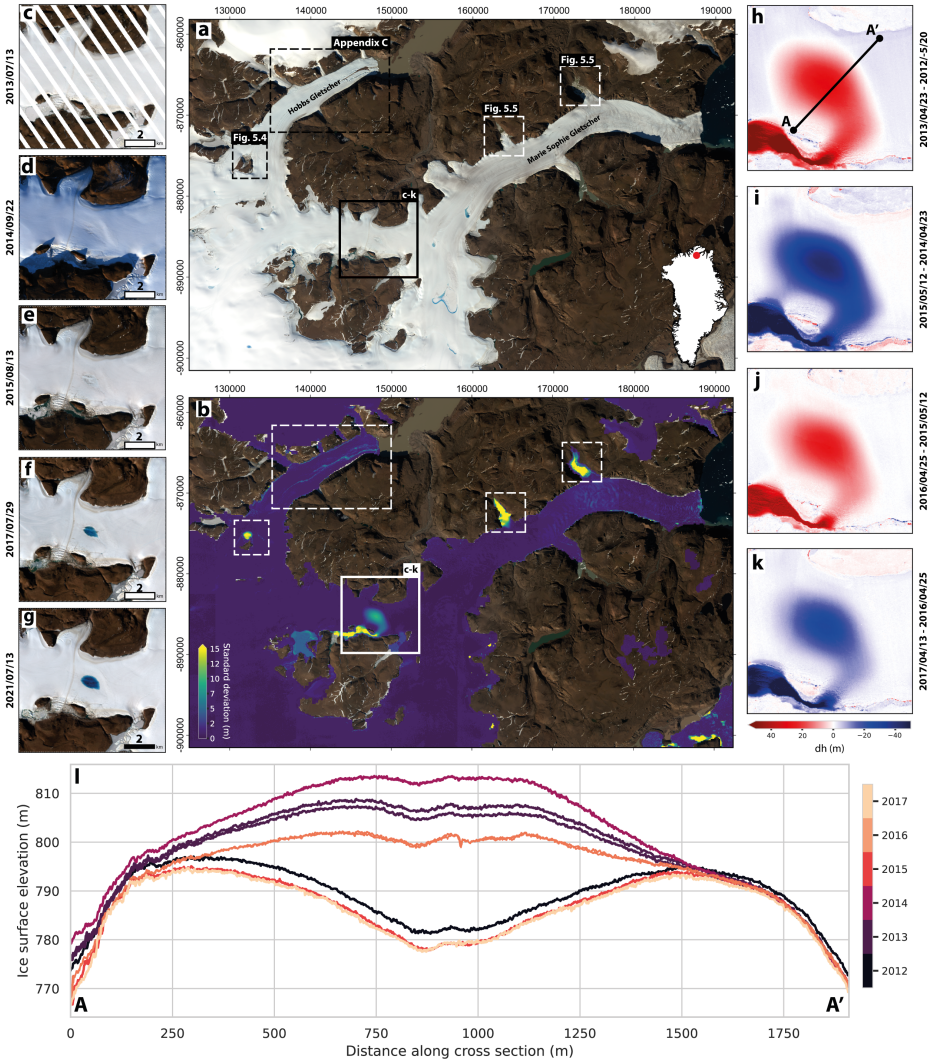

Figure 4.6: (a) Landsat 8 scene taken on 13th August 2015 showing the study area. Dashed boxes refer to Figure 6.5, 6.4 & C.1. (b) Standard deviation output highlighting regions of high variability in the surface elevation, overlaid over the same Landsat scene. (c) Landsat 8 scene taken on 13th July 2013 showing lake candidate in more detail. (d) Landsat 7 scene taken on 22nd September 2014 showing a surface depression. (e) Landsat 8 scene taken on 13th August 2015 showing a surface depression. (f) Landsat 8 scene taken on 29th July 2017 showing a supraglacial lake in the basin. (g) Landsat 8 scene taken on 13th July 2021 present day appearance of the feature, with a supraglacial lake in the centre of the depression. (h) Difference in elevation between Strip DSMs acquired on 20th May 2012 and 23rd April 2013, showing lowering of ice surface and change at the ice margin. (i) Difference in elevation between Strip DSMs acquired on 23rd April 2014 and 12th May 2014, showing surface uplift of ice surface and change at the ice margin. (j) Difference in elevation between Strip DSMs acquired on 12th May 2015 and 25th April 2016, showing lowering of ice surface and change at the ice margin. (k) Difference in elevation between Strip DSMs acquired on 25th April 2016 and 13th April 2017, showing modest uplift of the ice surface and change at the ice margin. (l) Transect along the profile A-A' shown in panel h, showing the temporal evolution of the active subglacial lake candidate.

Using our map of classified temporal variance in elevation (Figure 4.3), we identified a 5.3 km^2 ice surface anomaly approximately 50 km inland from the calving front of Marie Sophie Gletscher, where ice flows between two mountain ranges (Figure 4.6a). The ice here is slow-moving (<10 m a^{-1} between 2016-2017; Joughin et al., 2018) and <100 m thick (Mouginot et al., 2017). The ice-surface anomaly has a standard deviation of elevation of up to 15 m, and appears to be linked to a large marginal lake (∼4 km^2) to the south which ice calves into (Figure 4.5b). Ice-marginal lakes towards the terminus of the glacier, and floating ice tongues are also highlighted with high standard deviation of elevation signals, as well as a large supraglacial channel along Hobbs Gletscher to the west (dashed boxes in Figure 4.6a, C.1).

To assess the temporal evolution of the ice surface at this active subglacial lake candidate, we analyse all 8 Strip DSMs available. In May 2012, an approximately 30 m deep depression, was observed relative to the surrounding ice sheet surface (Figure 4.5h, l). Between May 2012 and April 2014, the localised ice rose on average by 7.3 m a^{-1} creating a domed expression in the ice surface, and coincided with filling of the adjacent ice-marginal lake (Figure 4.5i, l). Between April 2014 and May 2015, the ice surface lowered by average -14.6 m a^{-1} to a similar elevation to that of 2012 (Figure 4.5l), before rising again by average 7.3 m a^{-1} between May 2015 and April 2016 (Figure 4.5k, l). By 2017, the depression was a similar depth to 2012 and 2015. In total there were two and a half cycles of rising and falling ice surface in this localised region, alongside changes at the ice margin.

Throughout the Landsat record (1980s-present), this candidate feature has persisted since at least 1987 where it was infilled with surface meltwater to form a supraglacial lake. Meltwater has also ponded here during the summers of 2017 and 2021 (Figure 4.6f-g). A supraglacial steam often extends from this supraglacial lake towards the ice-marginal lake south of this feature, allowing the supraglacial lake to periodically drain. The Landsat images also indicate calving of the lateral ice into the ice-marginal lake. We interpret the repeated rising and uplift cycles in ice surface elevation as characteristic surface signature of an active subglacial lake drainage and refilling. We suggest that the active subglacial lake is hydrologically connected to the ice-marginal lake, where as the ice surface depresses, the marginal lake surface also lowers and

vice versa when the ice surface rises. Unfortunately there are no RES data over the candidate lakes to confirm if there is a flat lake reflector, the nearest flight line is about 9 km away.

4.4.3.3 Knud Rasmussen Glacier

The 1900 km^2 North Ice Cap is situated in northwest Greenland, independent of the main ice sheet, near Thule Air Base. The ice cap has a maximum elevation of ∼1200 m a.s.l., and has several outlet glaciers, including the ∼15 km long Knud Rasmussen Gletscher which feeds into Wolstenholme Fjord (81.5°N, 33.1°W) (Figure 4.7a). One small glacier (a few kilometres in length) converges with Knud Rasmussen Gletscher, near the terminus, and several marginal lakes exist along the southern lateral margin of the glacier. Knud Rasmussen terminus has retreated by a maximum of 1.5 km between 2000/01 and 2016/17 (Moon and Joughin, 2008).

Using our classified standard deviation of elevation output, we detect a 1.4 km^2 ice surface anomaly approximately 18 km inland, near the head of the glacier where the ice flows around exposed bedrock into a small, thin tributary terminating in a 0.9 km^2 marginal lake (Figure 4.7a). The ice here is approximately 300 m thick (Morlighem et al., 2017), but slow-moving (<10 m a^{-1}; Joughin et al., 2018).To assess the temporal evolution of the ice surface and dynamics at this active subglacial lake candidate, we assess all 29 Strip DSMs available. Between June 2012 and April 2014, substantial lowering of up to 66 m occurred (average -18.3 m a-1), forming a large deep, steep-sided depression (Figure 4.7h, l). Lowering was also observed at the ice-marginal lake and ice margin adjacent to the candidate feature (Figure 4.7h). Since this collapse, the ice surface within the feature has been rising at an average rate of 7.3 m a^{-1} between July 2015 and July 2017, and the marginal lake has been refilling (Figure 4.7i-l).

Analysis of the Landsat record shows no visible abnormality in the ice surface in this region before 2012. At the base of the bedrock outcrop, meltwater accumulates in a small pond, which drains supraglacially over the feature towards the lateral margin and marginal lake via two streams depicted in the cross-section of the feature (Figure 4.7l). Between 15th July 2012 and 3rd September 2012, the ice surface appears to

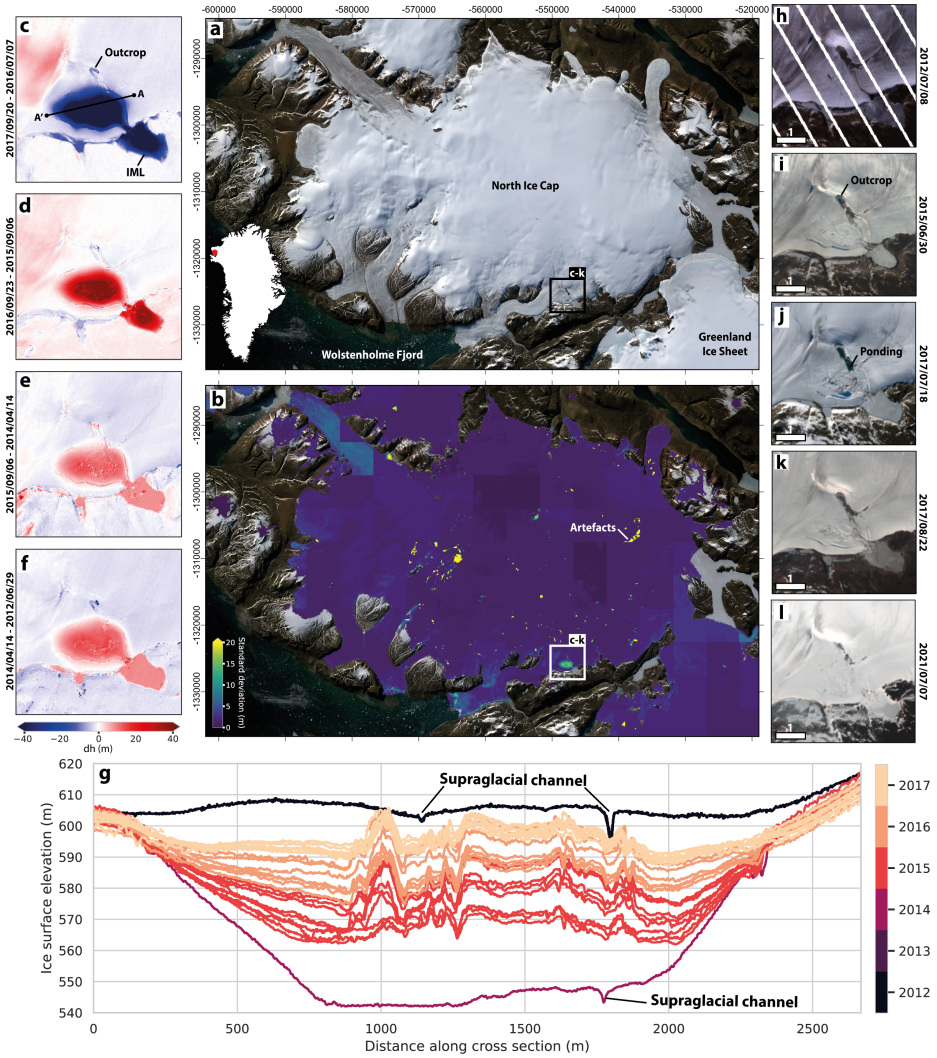

Figure 4.7: (a) Landsat 8 scene taken on 13th August 2015 showing the study area. (b) Landsat 7 scene taken on 13th July 2013 showing lake candidate in more detail. (c) Landsat 7 scene taken on 22nd September 2014 showing a surface depression. (d) Landsat 8 scene taken on 13th August 2015 showing a surface depression. (e) Landsat 8 scene taken on 29th July 2017 showing a supraglacial lake in the basin. (f) Landsat 8 scene taken on 13th July 2021 present day appearance of the feature, with a supraglacial lake in the centre of the depression.

have collapsed, with heavy fracturing around the edge of this feature and the break up of ice next to the marginal lake (Figure 4.7). Due to the depth of this surface depression, surface meltwater accumulates at the base to form a supraglacial lake during the summer of 2013 and a particularly large lake filled the surface depression almost entirely in 2014 (no Strip DSMs were available for 2013 and the acquisition date for the 2014 DSM was 14th April, so the supraglaical lake is not captured in the profiles). Between 2014 and 2017, the ice surface within the basin is undulated due to broken ice and snow, with occasional melt ponds forming.

Based on the optical imagery and Strip DSMs, we hypothesise that the substantial localised collapse in the ice surface was due to the rapid drainage of a subglacial water body beneath the thin ice here (over a maximum of 50 days, but likely to be over a shorter duration). The Greenland Ice Sheet experienced extreme and widespread surface melt during 2012 (Nghiem et al., 2012), and so it is possible that this drainage event could have been linked to the unusual climatic conditions of that year, namely that increased input of surface meltwater could have triggered the subglacial lake to drain. If the subglacial outburst flood reached the ocean, this could have implications, such as ocean circulation and dynamics. The surface of the ice within the collapse basin has been slowly rising since the drainage event. We posit that the 7.3 m a^{-1} uplift between 2015 and 2017 was due to the subglacial lake refilling; the ballooned surface is characteristic of subglacial lake recharge in Greenland (Willis et al., 2015). Unfortunately there are no RES data over the candidate lake to confirm if there is a subglacial lake reflector, the nearest flight line is >1 km away.

4.4.4 Detection of new active subglacial lakes - based upon their statistical characteristics

The previous active subglacial lake candidates were identified using manual inspection. In the following section we use test whether statistics can be utilised instead to give a more objective approach. We calculated the area and mean standard deviation of elevation at each of each active subglacial lake candidate feature (Figure 4.8), and compared with such characteristics with known active subglacial lakes and the three candidates identified during visual analysis of the classified standard deviation of

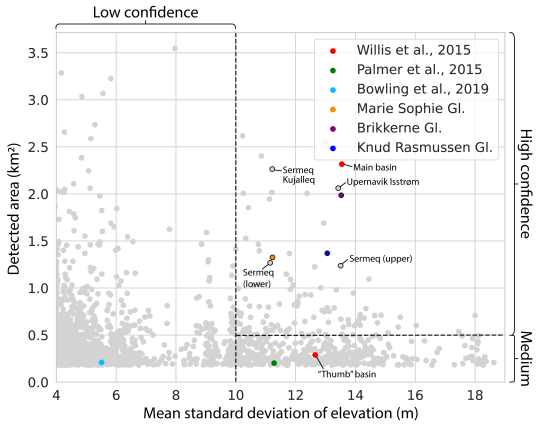

Figure 4.8: Average standard deviation of elevation versus area of each active subglacial lake candidate detected using our approach. The coloured dots represent known active subglacial lakes in Greenland and the three candidates presented in the initial analysis (Section 4.4.3). The four labelled dots are discussed in Section 4.4.4. Those with more than one point are split into multiple polygons using our approach, for example the mitten-shaped collapse basin in Willis et al., 2015 has two polygons, one representing the main basin, and a second representing the 'thumb' of the mitten shape. Dashed lines differentiate high, medium and low confidence candidates based on feature area and the temporal variance in elevation.

elevation output (Section 4.4.3). Based on this analysis we analyse 4 further high confidence active subglacial lake candidates that have a similar area (1.2-2.5 km^2) and temporal variance (11-14 m σ) to the larger Flade Isblink, Brikkerne, Knud Rasmussen, and Marie Sophie Gletscher known and candidate active subglacial lakes (Figure 4.8).

4.4.4.1 Upernavik Isstrøm

Upernavik Isstrøm was a major ice stream in northwestern Greenland, draining approximately 65,000 km^2 of the ice sheet (Haubner et al., 2018). The ice stream is now separated into four different marine-terminating outlet glaciers, named Upernavik 1 to 4 (Figure 4.9a). Radar data shows that in 2013 Upernavik-2 had a floating tongue of approximately 2.5 km in 2013, and was about 250 m (Larsen et al., 2016), and has been accelerating since 2008, increasing by around 300 m a^{-1} until 2013 (Larsen et al., 2016). The standard deviation of elevation highlights these dynamic changes at the margin with high variability at the glacier terminus (Figure 4.9b).

Our method identifies a 1.8 km^2 ice surface anomaly with an average standard deviation of elevation of ~14 m, and a maximum of ~22 m about 35 km from the terminus of Upernavik-2. These are similar variance and area characteristics to the

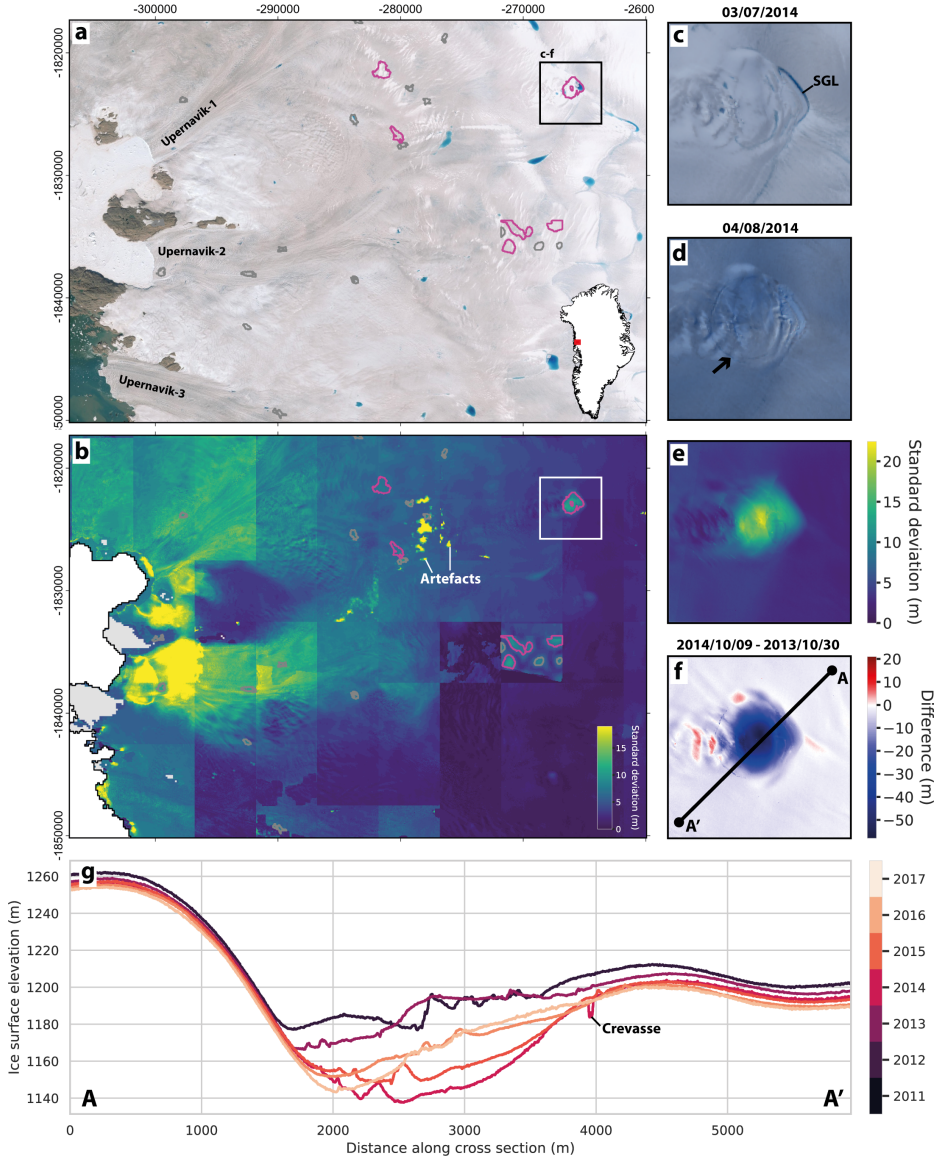

Figure 4.9: Predicted active subglacial lake candidate near Upernavik-2, northwestern Greenland. (a) Optical image of the study area from Earthstar Geographics (TerraColor NextGen) imagery, with predicted subglacial lake outlines in grey (low confidence) and pink (High and medium confidence). Inset map shows location on the Greenland Ice Sheet. (b) Standard deviation of elevation output with predicted subglacial lake outlines in pink and grey. (c) Landsat 8 optical image of candidate lake on 3rd July 2014. (d) Landsat 8 optical image of candidate lake on 4th August 2014. Arrow points to circular crevasses, which suggest subsidence. (e) Zoom in showing the standard deviation of elevation over candidate. (f) Elevation difference between DSMs acquired on 9th October 2014 and 30th October 2013. (g) Elevation profiles throughout time, taken along transect A-A' shown in panel f.

Brikkerne Glacier potential subglacial lake candidate. The ice at this location is relatively fast-moving (∼300 m a^{-1} between 2016-2017; Joughin et al., 2018) and 900-1,000 m thick (Mouginot et al., 2017). Five other higher confidence ice surface anomalies are also delineated in the area, which are mostly due to supraglacial lake or noise signals (Figure 4.9b).

6 Strip DSMs are available at the high confidence active subglacial lake candidate. We analysed these Strips to understand the temporal evolution of this feature. In 2011, a depression (up to 30 m deep) was observed with an undulated surface between 2,700-3,600 m along the transect (Figure 4.9g). In 2013, the surface within this feature is similar, with a ∼10 m drop in elevation between 1,800-2,500 m along the cross section (Figure 4.9g). Localised surface lowering occurred by up to 55 m between 30th October 2013 and 9th October 2014 (Figure 4.9f). Between 2015 and 2016, the surface within this feature has been rising at a rate of 14 m a^{-1}, but in 2017, the elevation remains largely unchanged. The elevation profiles depict the ice within the basin has a surface slope of about 16° (Figure 4.9g).

Landsat optical imagery shows a small (∼0.7 km^2) supraglacial lake adjacent to a the candidate feature (Figure 4.9c). In August 2014, a circular crevasse is present to the west of the supraglacial lake (black arrow; Figure 4.9d, also indicated in Figure 4.9g). We propose that this surface feature was formed by the rapid drainage of a subglacial lake beneath the 900 m thick ice. After the drainage event, the subglacial lake has been slowly refilling, causing the localised surface to rise between 2014 and 2016. The relatively unchanged elevation post 2016 could suggest that a surface to bed connection has been closed by 2017, or that the subglacial drainage system has perhaps been altered. Immediately downstream of the feature, overlapping circular patterns can be seen in the optical imagery (Figure 4.9d), suggesting possible evidence of past drainage events which have since advected downstream. Unfortunately there are no RES data over the candidate lake to confirm if there is a subglacial lake reflector, the nearest flight line is >3 km away.

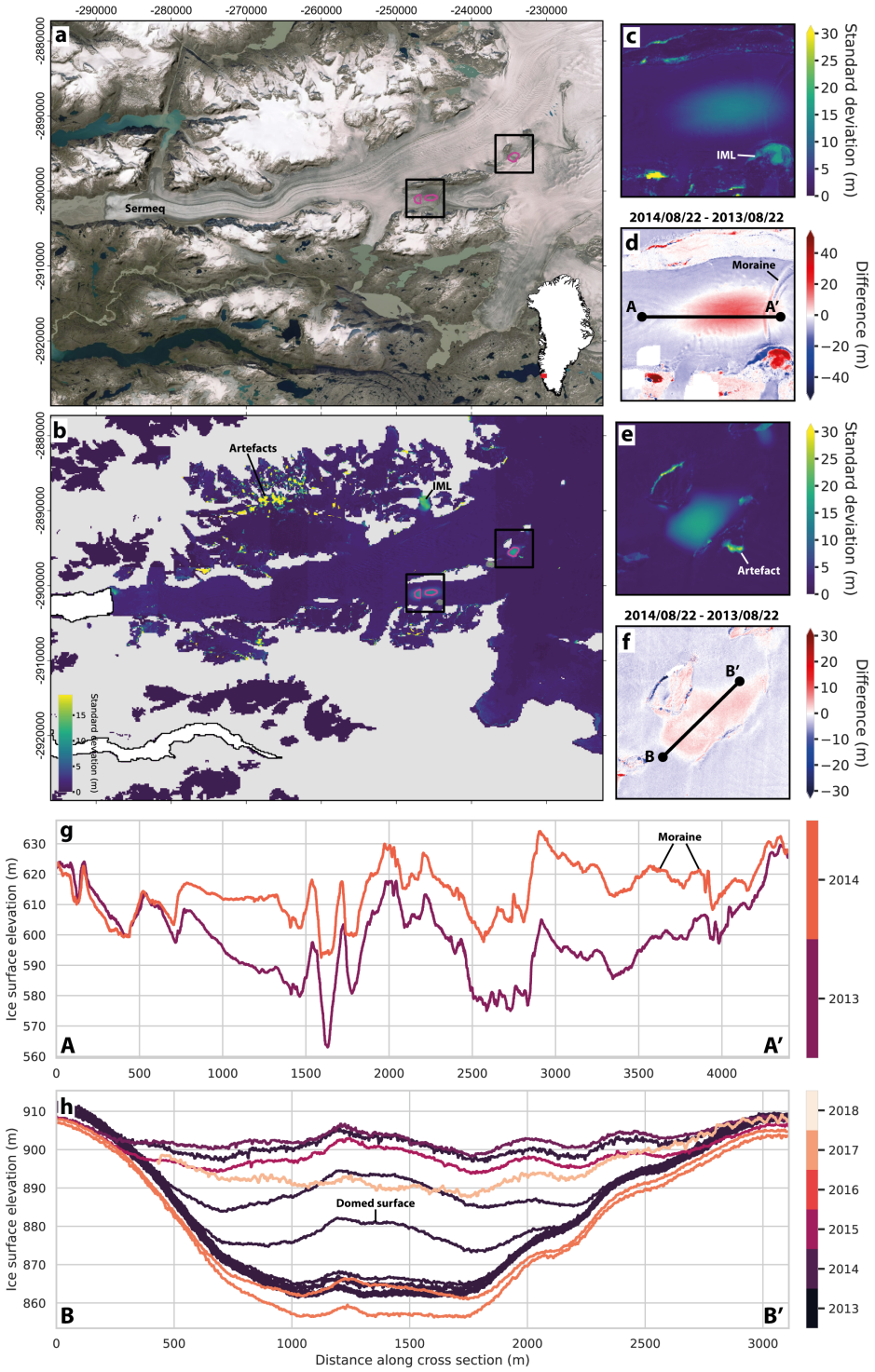

Figure 4.10: Active subglacial lake candidate detected using our temporal variance method near Sermeq, southwestern Greenland. (a) Optical image of the study area from Earthstar Geographics (TerraColor NextGen) imagery, with active subglacial lake candidate outlines in grey (low confidence) and pink (High and medium confidence). Inset map shows location on the Greenland Ice Sheet. (b) Standard deviation of elevation output with predicted subglacial lake candidate outlines again in pink and grey. (c) Zoom in showing the standard deviation of elevation over lower candidate. (d) Elevation difference between DSMs acquired on 22nd August 2014 and 22nd August 2013. (e) Zoom in showing the standard deviation of elevation over upper candidate. (f) Elevation difference between DSMs acquired on 22nd August 2014 and 22nd August 2013. (g) Elevation profiles at lower candidate throughout time, taken along transect A-A' shown in panel d. (h) Elevation profiles at upper candidate taken along transect B-B' shown in panel f.

4.4.4.2 Sermeq

Sermeq is a land-terminating glacier measuring over 100 km in length in southwest Greenland, about 70 km south of Kangiata Nunaata Sermia (Figure 4.10a). The glacier has several smaller tongues which terminate in ice-marginal lakes, and a small glacier converges with Sermeq from the main ice sheet.

Our method outlines three active subglacial lake candidates off the main glacier tongue, in complex terrain (Figure 4.10a-b). We group the lower two candidate outlines as one feature as they cover the same standard deviation signal. These candidates have similar area and mean standard deviation of elevation to Knud Rasmussen and Marie Sophie Gletscher candidates (Figure 4.8). The lower candidate lower feature ($\sim$ 1.3 km^2) is situated where ice flows between two mountain ridges, and two glaciers merge with a lateral moraine dividing the ice (Figure 4.10a). A localised region of surface uplift is observed, mostly on the western side of the moraine (Figure 4.10c-d), where the ice surface rose by a maximum of $\sim$30 m between 2013 and 2014.

The second high confidence active subglacial lake candidate (approximately 1.2 km^2) is found about 3 km northeast of the lower feature between two steep-sided peaks, where three small ice tongues converge (Figure 4.10a-b). The candidate exhibits several cycles of uplift and lowering, with a gradual increase in ice height during 2013 of about 20-30 m (between January and December). Between 2013 and 2015, the ice surface remained at a similar position (although only 1 DSM per year is unrepresentative and changes could have occurred between these acquisition dates). By 2016 the localised region of ice lowered by a maximum of 40 m and then rose by 1.9 m a^{-1} over the following year (Figure 4.10g). This feature mimics the surface uplift at the lower feature but on a smaller scale. This smaller feature domes in the centre with crevassing around the edges.

Whilst a detailed study is required to understand the exact causes for these complex dynamic changes, the synchronous elevation changes between the upper and lower candidates suggest that they may be hydrologically linked. We hypothesise that the movement of subglacial water between lakes beneath the ice may have caused the dynamical signals observed at the ice surface. We posit that a subglacial lake located

at the upper candidate site fills throughout 2013 and 2014, causing the ice surface to rise. Between the summers of 2015 and 2016, the subglacial lake drained into the ice marginal lake downstream. By summer 2016, the downstream subglacial water body fills causing the ice surface to rise substantially. Unfortunately there are no RES data over the candidate lakes to confirm if there is a subglacial lake reflector, the nearest flight line is ∼6 km away.

4.4.4.3 Sermeq Kujalleq

Sermeq Kujalleq glacier is a marine-terminating glacier that feeds into Ussing Isfjord in Northwest Greenland (Figure 4.11a). The catchment is estimated to be 2900 km^2, with an ice flux of 3.86 km^3 a^{-1} (Pope et al., 2019). The glacier has retreated up to 800 m between 2000/01 and 2016/17 (Moon and Joughin, 2008).

Our method identifies a 2.3 km^2 ice surface anomaly about 40 km inland from the ice margin (Figure 4.11a-b). This candidate has similar area to the main basin at Flade Isblink ice cap and similar temporal variance to Marie Sophie Gletscher candidate (Figure 4.8). Several large artefacts are observed in the upper ablation zone with high (>48 m standard deviation of elevation), and some smaller localised regions of <10 m standard deviation of elevation which are likely supraglacial lakes (Figure 4.11b). The large (∼ km2) high confidence candidate has a average standard deviation of elevation of 11.2 m, and a maximum of 20 m (Figure 4.11c), compared to the surrounding ice (<5 m standard deviation of elevation). A second high confidence candidate lake is identified using our method, but this candidate is likely to be an artefact, given it's proximity to the linear anomaly with very high standard deviation of elevation.

Only 2 Strip DSMs were acquired at this candidate lake, showing the surface in this region dropped by up to 30 m between February 2015 and March 2016 (Figure 4.11d-e). The cross section shows a flat surface in 2015, which is typically indicative of water or a refrozen ice lid. The surface depression observed here is much deeper than a typical supraglacial lake (∼6-10 m depth; Box et al., 2012), and is positioned quite far inland meaning that there is unlikely enough melt to create such a large volume supraglacial lake. Whilst it is unclear what this candidate is, it is possible that

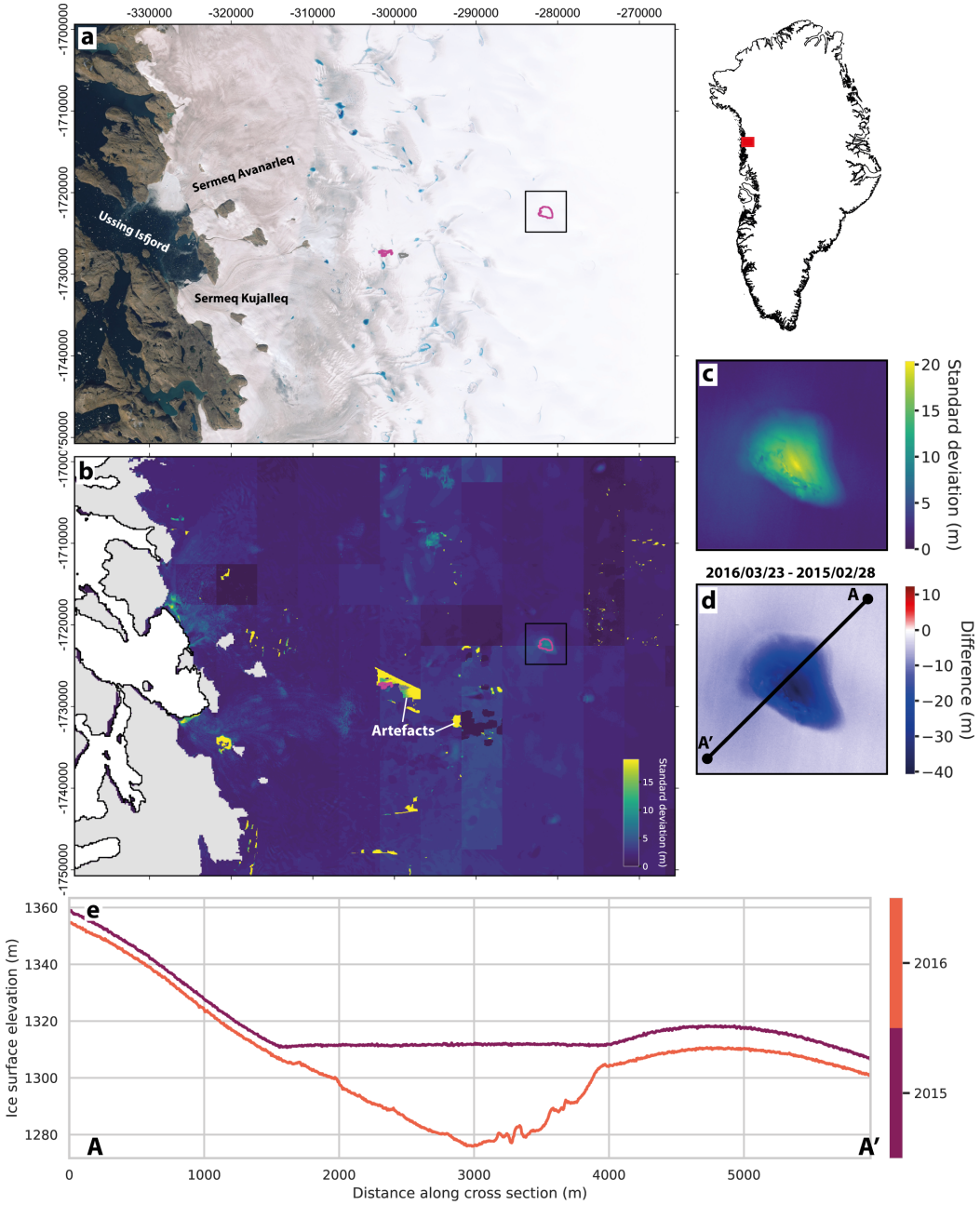

Figure 4.11: Active subglacial lake candidate detected using our temporal variance method near Ussingbraer, central western Greenland. Inset map shows location on the Greenland Ice Sheet. (b) Standard deviation of elevation output with high confidence subglacial lake candidate outlines in pink. (c) Zoom in showing the standard deviation of elevation over the candidate. (d) Elevation difference between DSMs acquired on 23rd March 2016 and 28th February 2015. (e) Elevation profiles throughout time, taken along transect A-A' shown in panel d.

a supraglacial lake has formed over several years, with the lid freezing over in winter but staying liquid below, and then eventually drains. Or the depression could have formed as a result of a subglacial lake drainage event, and a supraglacial lake lies at the surface. Landsat optical imagery shows an undulated and broken surface within this feature over winter 2016, and by summer, supraglacial meltwater has ponded in the depression. Circular crevassing around the edge of the candidate feature are not apparent. Unfortunately there are no RES data over the candidate lake to confirm if there is a subglacial lake reflector, the nearest flight line is ∼4 km away.

4.5 Conclusion

We have developed an automated method for detecting subglacial lake activity based upon calculating temporal variance in ∼26,000 high-resolution ArcticDEM DSMs. Our approach is the first comprehensive and systematic assessment on an ice-sheet scale to detect ice-surface anomalies. 128 high confidence and 500 medium confidence and ∼3,000 low confidence active subglacial lake candidates were identified in our study. Half of the 7 known active subglacial lakes in Greenland were successfully identified, the remainder are generally small and located in complex terrain, and are therefore difficult to separate from the surrounding signals using an automated approach. Using our technique and evaluation of candidate characteristics, we present 7 new potential active subglacial lakes in Greenland, doubling the total record of known subglacial lakes.

Several of these potential active subglacial lakes exhibit repeated filling and draining cycles, which is the first time such activity has been observed in Greenland, previous literature only captures one drainage event and subsequent refilling. Our method is a way to automatically identify at the continental scale candidate lakes, which can then be studied in further detail in dedicated case studies to understand both their dynamics and setting. Chapter 5 gives one example of an in depth case study, but there are many more interesting signals to explore in the future.

The viable candidates outlined in this study provide a valuable insight into the complex basal drainage system beneath the Greenland Ice Sheet. For example, lake

candidates at Sermeq Glacier portray synchronous drainage patterns, implying that they may be interconnected. Although this type of behaviour has been previously observed in Antarctica (Fricker and Scambos, 2009; Smith et al., 2017a), it has not, until now, been observed in Greenland. In this study we also show that subglacial lakes can also be connected to ice marginal lakes and can be found in a variety of settings: both land-terminating glaciers and marine-terminating glaciers; both close to the ice margin, and further inland; and under a range of ice thickness and ice speeds.

In addition to the detection of active subglacial lakes, the methodology we have implemented also captures a variety of other dynamic signals, such as terminus retreat and supraglacial lake drainage events. These observations indicate further glaciological applications for the method that could be explored in the future (see Chapter 6.4). Our results are, of course, limited by the data available from ArcticDEM, which can contain artefacts and relatively infrequent temporal sampling. Additionally, expert judgement is required to interpret the features produced in the framework. However, future releases of ArcticDEM strip DSMs will enable further ice surface anomalies to be detected and monitored, and in conjunction with other altimetry datasets, such as ICESat-2, we will likely see an improved understanding of these features and their potential impact on the broader glaciological environment. Further work is needed to establish whether predicted climatic warming will cause changes to subglacial lake formation and drainage cycles in the future.

4.6 Data availability

Ice thickness is from IceBridge BedMachine Greenland, Version 4 (https://nsidc.org/data/IDBMG4). Ice sheet velocity is obtained from MEaSUREs Greenland Ice Sheet Velocity Map from InSAR Data, Version 2 (https://nsidc.org/data/nsidc-0478). Terminus positions are available from MEaSUREs Annual Greenland Outlet Glacier Terminus Positions from SAR Mosaics (https://nsidc.org/data/NSIDC-0642/versions/1).

Chapter 5

Surface outburst of a subglacial flood from the Greenland Ice Sheet

Jade S. Bowling[1,2], Malcolm McMillan[2,3], Amber A. Leeson[1,4], Stephen J. Livingstone[5], Andrew J. Sole[5], Peter Nienow[6], Brice Noël[7], Michiel R. van den Broeke[7], Thomas Slater[8,2], Louise Sandberg Sørensen[9], Sebastian B. Simonsen[9], Jérémie Mouginot[10,11], Laura Melling[1], Liam Taylor[7,2]

[1]Lancaster Environment Centre, Lancaster University, Lancaster, UK
[2]UK Centre for Polar Observation & Modelling
[3]Centre for Excellence in Environmental Data Science, Lancaster University, Lancaster, UK
[4]Data Science Institute, Lancaster University, Lancaster, UK
[5]Department of Geography, University of Sheffield, Sheffield, UK
[6]University of Edinburgh, School of Geosciences, Edinburgh, UK
[7]Institute for Marine and Atmospheric Research, Utrecht University, Utrecht, the Netherlands
[8]School of Earth and Environment, University of Leeds, Leeds, UK
[9]Geodesy and Earth Observation, DTU Space, Technical University of Denmark, Denmark
[10]Department of Earth System Science, University of California, Irvine, USA
[11]Institut des Géeosciences de l'Environnement, Université Grenoble Alpes, CNRS,

Grenoble, France
[12]School of Geography, University of Leeds, Leeds, UK

Correspondence:
Jade Bowling (j.bowling@lancaster.ac.uk)

The following work was submitted to *Nature Geoscience* on 1st July 2021 and is currently under review.

5.1 Abstract

As Earth's climate warms, surface melting of the Greenland Ice Sheet is projected to intensify, contributing to rising sea levels (Robinson et al., 2012; Koenig et al., 2014; Aschwanden et al., 2019; Golledge et al., 2019). Observations (Das et al., 2008; Chandler et al., 2013; Andrews et al., 2014) and theory (van der Veen, 2007; Clason et al., 2015; Koziol et al., 2017) indicate that meltwater generated at the surface of an ice sheet can drain to its bed via crevasses and moulins, where it flows relatively unhindered to the coast. This understanding of the movement of water within, and beneath, ice sheets, underpins theoretical models which are used to make projections of ice sheet change (Shannon et al., 2013). In this study, we show the first evidence of a disruptive drainage pathway in Greenland, whereby a subglacial flood – triggered by a draining subglacial lake – breaks through the ice sheet surface. This unprecedented outburst of water causes fracturing of the ice sheet, and the formation of 25-metre-high ice blocks. These observations reveal a complex, bidirectional coupling between the surface and basal hydrological systems of an ice sheet, which was previously unknown in Greenland. Analysis of over 30 years of satellite imagery confirms that the subglacial lake has drained at least once previously. However, on that occasion the floodwater failed to breach the ice surface. The two contrasting drainage regimes, coupled with the increased rates of ice melting and thinning that have occurred over the past three decades years, suggest that Arctic climate warming may have facilitated a new, disruptive mode of hydrological drainage on the ice sheet. As such, our observations reveal an emerging and poorly understood phenomenon, which is not currently captured in physical ice sheet models.

5.2 Main

The Greenland Ice Sheet has been losing ice at an average rate of ∼150 billion tonnes per year since 1992, contributing ∼11 mm to global sea level rise (Shepherd et al., 2020). Approximately one half of this ice mass loss has been attributed to surface mass balance (SMB) processes (Mouginot et al., 2019; Shepherd et al., 2020), driven primarily by enhanced melting and run-off from the ice sheet surface. As Arctic warming continues to amplify throughout the 21st century (Barnes and Polvani, 2015;

Dai et al., 2019), both the intensity and areal extent of Greenland surface melting and run-off are projected to increase, leading to even greater ice mass loss (Pattyn et al., 2018). Notably, the past decade has seen two widespread summertime melt episodes across the Greenland Ice Sheet, in 2012 and 2019, and concomitant extreme losses in ice mass (Nghiem et al., 2012; Tedesco et al., 2013; Keegan et al., 2014; Sasgen et al., 2020; Shepherd et al., 2020). The increased frequency of events such as these is likely to drive further positive feedback mechanisms related to changes in bare ice exposure and the capacity of firn to accomodate meltwater refreezing, which may further accelerate the Greenland Ice Sheet's contribution to sea level rise (Noël et al., 2017, 2019; Ryan et al., 2019).

Understanding the passage of meltwater from its origin on the ice sheet to the ocean is critical for understanding the Greenland Ice Sheet's future mass balance, sea-level rise, and indeed the fate of the wider Arctic climate and ecological system. It is well established that surface meltwater penetrates to the bed of the Greenland Ice Sheet via moulins and crevasses (Das et al., 2008; Chandler et al., 2013; Andrews et al., 2014). Observational studies, mainly in south and west Greenland, have shown that the subglacial hydrological system can rapidly evolve in response to seasonal water input, in turn modulating ice dynamics (Das et al., 2008; Joughin et al., 2008; Bartholomew et al., 2010; Andrews et al., 2014; Davison et al., 2020). These studies demonstrate that temporal variability in water flow through the subglacial system is a key control on the dynamic response of the ice. As such, it is critical to determine both the mode (continuous versus episodic) and pathway (whether meltwater drains across the surface, within or beneath the ice sheet) of drainage, together with the extent to which meltwater is stored (englacially or subglacially) whilst in transit. These factors affect the capacity of meltwater to impact a broad range of glaciological and climatological processes, including ice dynamics, thermodynamics, ice-ocean interactions, fjord circulation, primary productivity, and rates of sediment and nutrient transfer to the ocean (Nienow et al., 2017).

Although subglacial lakes were first mapped in Antarctica (Robin et al., 1969; Oswald and Robin, 1973) and Iceland (Björnsson, 1974) over 50 years ago, they have only been identified beneath the Greenland Ice Sheet in the past decade (Palmer

et al., 2013; Bowling et al., 2019). Recently, dynamically active Greenlandic lakes have been discovered, which, unlike their Antarctic counterparts, are primarily fed by seasonal inputs of surface meltwater (Howat et al., 2015; Palmer et al., 2015; Willis et al., 2015; Bowling et al., 2019; Livingstone et al., 2019). Active subglacial lakes have wider importance because they provide a mechanism to force large volumes of water and sediment through the subglacial hydrological system when they drain. In turn, this has the potential to alter the morphology of the subglacial drainage system, and thus impacting both the local dynamics and the characteristics of the overlying ice sheet (Stearns et al., 2008; Smith et al., 2009; Dow et al., 2018), together with its downstream behaviour (Mallalieu et al., 2020). For example, following the 2015 drainage of a subglacial lake in southwest Greenland, a ∼25% reduction in ice flow speed was observed (Livingstone et al., 2019). Given projected increases in Arctic atmospheric temperatures, ice melting and run-off during the 21st century (Hofer et al., 2020; Noël et al., 2021), subglacial lake drainage events may be expected to increase in extent and frequency (Bowling et al., 2019; Livingstone et al., 2022). However, the impact of such extreme forcing upon the Greenland Ice Sheet remains highly uncertain, due to a paucity of observations.

Brikkerne Glacier (81.5°N, 44.48°W) is a marine-terminating glacier draining ice from one of the most northerly sections of the Greenland Ice Sheet into Victoria Fjord (average depth ∼250 m; Morlighem et al., 2017). The glacier has three tidewater outlets, with the main (northernmost) terminus measuring ∼4 km wide, and maintaining a small floating ice tongue (Hill et al., 2017). Between 1968 and 1978, the main glacier outlet advanced by 9 km, before retreating at an average rate of 76 m a^{-1} between 1978 and 2015 (Hill et al., 2018). The glacier exhibits a pronounced seasonal cycle with velocities typically increasing from June, and reaching peak values in late July/ August at about 2 times the annual average (Supplementary Material Figure 1). Air temperatures at the upper part of this glacier have progressively increased over the past half-century, with decadal average air temperatures rising from -14.6°C in the 1960s to -13.2°C in the 2010s (Noël et al., 2019) (Supplementary Material Figure 2a-c). As a result, the percentage of days per year where surface melt exceeds 5 mm w.e. has almost doubled, increasing from 8% to 14% between the 1960s and 2010s (Noël et al., 2019).

In this study, we use 2 m resolution timestamped ArcticDEM (http://arcticdem.org) Digital Surface Models (DSMs) (Porter et al., 2018), Landsat optical and Sentinel-1 radar imagery, and satellite altimetry to monitor the evolution of the ice sheet surface across the Brikkerne Glacier catchment between 2012 and 2019. During this 7-year period, the majority of the glacier surface remained relatively stable. However, during a 10-day interval in the late summer (August) of 2014, a localised region of the ice surface ∼25 km inland from the margin, dropped in elevation by up to 85 m, forming a ∼2 km^2 collapse basin (Figure 5.1). The stresses exerted on the surrounding ice by this rapid, localised subsidence of the surface caused structural failure, leading to the formation of concentric crevassing around the rim of the collapse basin (Figure 5.1). Prior to the collapse, the basin footprint had been rising at an average rate of 46 cm a^{-1} between 2012 and 2013, with the outer edge of the basin domed by ∼10-15 m above the surrounding ice surface (Figure 5.2). We interpret this dynamic feature to be the surface signature of a subglacial lake filling, then rapidly draining, similar to events that have been previously observed in Greenland (Howat et al., 2015; Palmer et al., 2015; Willis et al., 2015; Bowling et al., 2019), Antarctica (McMillan et al., 2013) and Iceland (Björnsson, 2003; Gaidos et al., 2020). Unfortunately, no Operation Icebridge RES tracks cross the collapse basin to determine if there is a subglacial lake (i.e. a flat, bright and specular reflector relative to the surrounding bedrock) or estimate the ice thickness. The nearest flight line is 8 km inland.

Assuming the volume of the feature was equivalent to the volume of water lost during the subglacial lake drainage event, the outburst flood had a total volume of 9 $\times 10^7$ m^3. This equates to a mean rate of water discharge of 101 m^3 s^{-1} during the 10-day period between satellite acquisitions (22nd July - 1st August 2014); albeit the drainage duration may have been much shorter, and the peak discharge higher. Nevertheless, this mean discharge rate is still approximately 2 orders of magnitude greater than that of an Antarctic subglacial lake of the same volume (Livingstone et al., 2022). This newly identified active subglacial lake represents the largest such event recorded beneath the mainland Greenland Ice Sheet, albeit smaller than the 4×10^8 m^3 subglacial lake drainage under the neighbouring Flade Isblink Ice Cap (Willis et al., 2015). What is remarkable, and unprecedented for Greenland, is the observed behaviour of the ice sheet downstream of the subglacial lake.

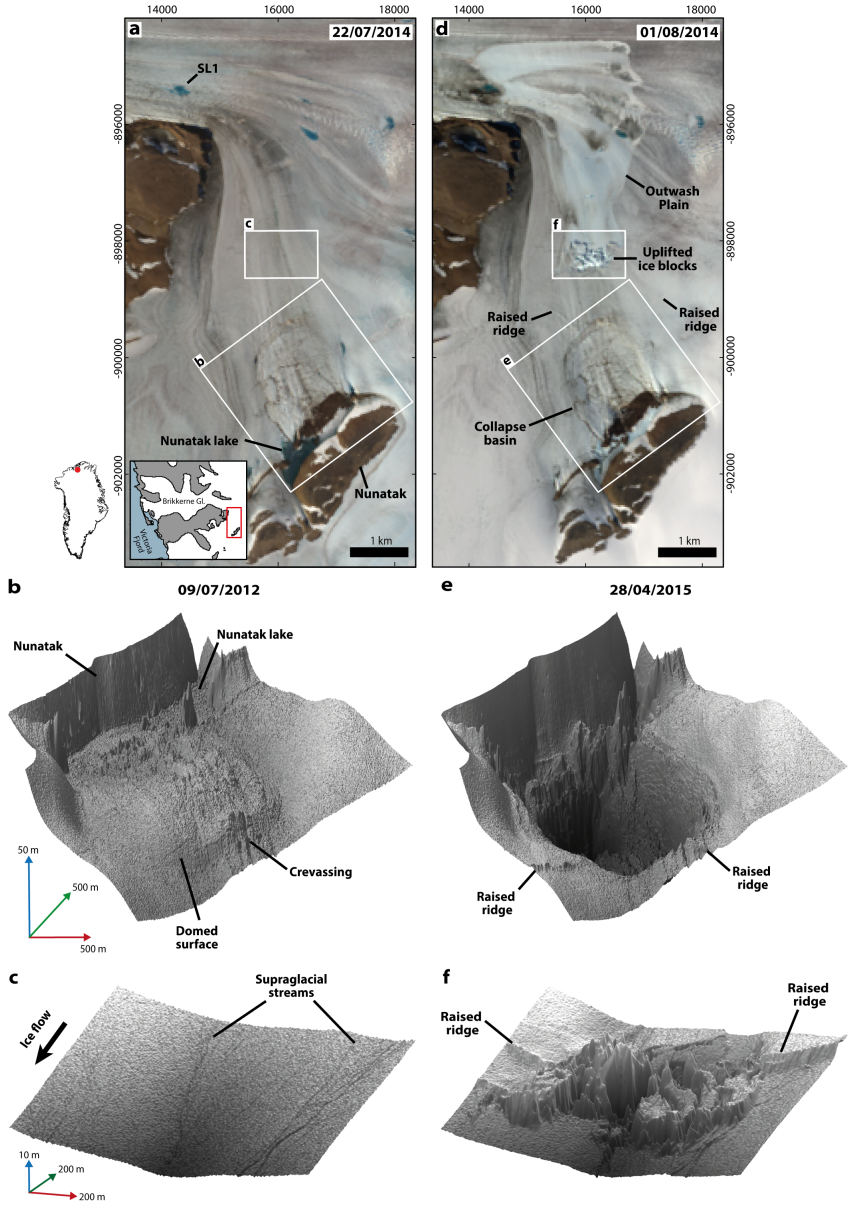

Figure 5.1: (a) True colour composite Landsat 8 scene on 22nd July 2014 before basin collapses (b) Three-dimensional shaded relief of the collapse basin mapped using 2 metre resolution ArcticDEM data acquired on 9th July 2012 (c) Shaded relief of downstream region before collapse (d) True colour composite Landsat 8 scene immediately after the subglacial lake drainage and surface outburst on 1st August 2014 (e) Three-dimensional shaded relief of the collapse basin after the subglacial lake drains on 28th April 2015 (e) Three-dimensional shaded relief of the downstream region after the collapse showing uplifted ice blocks (up to 25 m high), crevassing extends up to 40 m below surface.

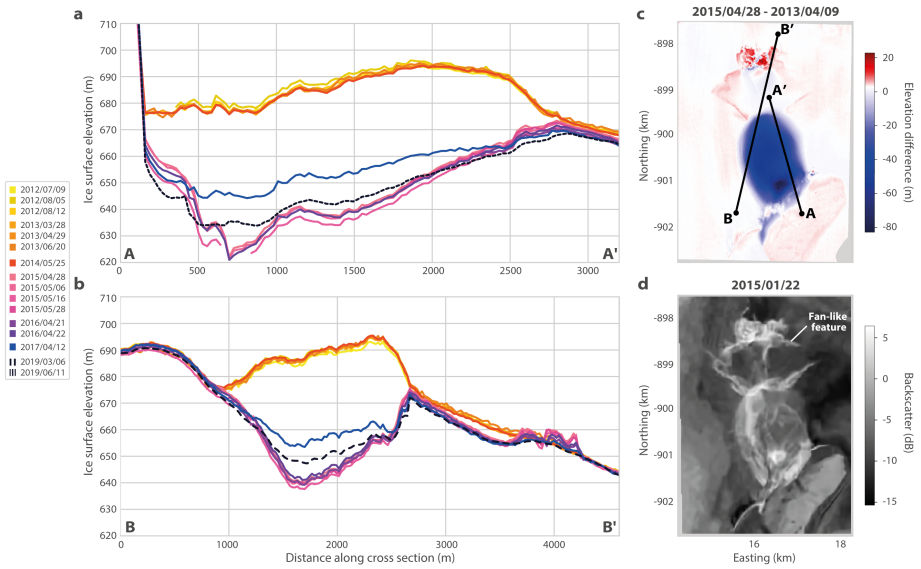

Figure 5.2: Elevation profiles through time. **a** Elevation profile A-A′ (shown in **Figure 5.1i)** following ICESat-2 track 1130 along ice flow. The profiles show a "ballooned" surface towards the northern rim of the basin in 2012. The basin floor drops by 2015, due to the sudden drainage of the subglacial lake in 2014. In 2017, the basin floor rises, likely due to recharge of the subglacial lake, before subsiding again by summer 2019 (ICESat-2 dashed line). Repeat elevation profile B-B′ (shown in **Figure 5.1i**) along ICESat-2 track 1032 show supraglacial ponds at the beginning of the transect which form on the leeside of a moraine ridge. Crevassing from the subsurface outburst flood is evident at ∼4800 m along the transect. **b** Surface elevation change between 9th July 2012 and 28th April 2015 as a result of subglacial lake drainage. Maximum displacement is ∼85 m near the headwall. Subsidence also occurs near the headwall due to the drainage of a supraglacial lake. A fan-like feature is shown beyond the basin, with a raised linear ridge, and a crevasse field caused by subglacial water breaking the ice surface. **c** Sentinel-1 SAR scene post collapse (22nd January 2015).

As the subglacial lake drained suddenly, a ∼1 km wide rupture with crevasses to a depth of at least 40 m and ice blocks up to 25 m in height appeared in the ice surface approximately 1 km downstream of the collapse basin (Figure 5.1f & 5.2). Immediately downslope of these ice blocks, a ∼6 km^2 region of the ice surface became scoured clean. Together, these observations indicate that a substantial volume of water had flooded across the ice surface (Figure 5.1). Similar to subglacial lake jökulhlaups in Iceland characterised by extremely rapid linear rises in lake discharge, we suggest that a turbulent sheet flood, produced by the subglacial lake drainage, propagated to the surface via englacial routeways and hydrofracturing due to basal water pressures greatly in excess of ice overburden pressure (Tómasson, 1996; Kavanaugh and Clarke, 2000; Roberts et al., 2000; Roberts, 2005). Upstream of the ice blocks there is additional disturbance of the ice surface, with a newly formed ∼1.6 km^2 fan-shaped feature bounded by two raised linear ridges extending ∼800 m in length and up to

5 m in height (Figures 5.1 & 5.2). We propose that some water was also forced up through a concentric ring fracture at the rim of the collapse basin (Figure 5.1), and this outburst of water produced a slushflow fan (Nyberg, 1989). Having breached the surface and flooded across the ice, outburst water re-entered the englacial (and presumably subglacial) system through moulins located several kilometres downstream (Supplementary Material Figure 3b-c), where it would have been routed to the glacier's calving front.

This is the first time that such a phenomenon has been observed on the Greenland Ice Sheet, and demonstrates a previously unknown level of complexity and interconnectedness between its surface and basal hydrological systems. In particular, contrary to current understanding of the ice sheet's hydrological system, it provides evidence that water flow is not always unidirectional from the ice sheet surface to its base, but instead can travel from the surface to the bed, and back again, over short spatial and temporal scales. Although this type of behaviour has previously been observed on much smaller, geothermally-active, Icelandic ice caps (Roberts et al., 2000; Roberts, 2005), it has not, until now, been resolved as a mechanism affecting the larger ice masses of Greenland or Antarctica.

In addition to the formation of the collapse basin and the downstream fracturing of the ice surface, several other unusual events occurred during the same 10-day period. In the vicinity of the collapse basin, a supraglacial lake adjacent to the nunatak, which had been growing annually in size since 2004 (Figure 5.3a-c), abruptly drained. At the same time, several changes were observed further downstream and at the glacier terminus, namely (1) a large calving event (the 7th largest event recorded in the past 32 years) occurred at the main glacier terminus, leading to a 500-600 m retreat of the glacier's calving front (Figure 5.3e-g), (2) an ice-marginal lake broke through its lateral moraine dam and emptied in its entirety (Supplementary Material Figure 3c), and (3) two downstream supraglacial lakes on the main glacier drained completely (Supplementary Material Figure 3a). Given the destructive nature of the outburst flood, it is likely that at least some of these events may have been connected, although the 10-day temporal sampling of the optical satellite imagery makes it impossible to determine the chronology of these events precisely.

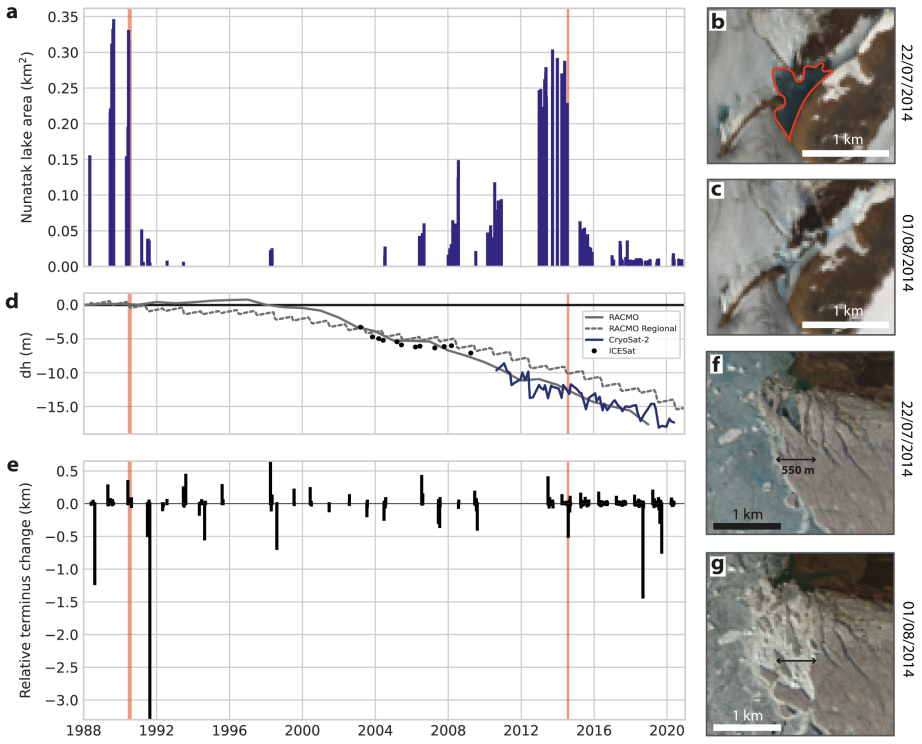

Figure 5.3: Change in area of the supraglacial lake at the base of the nunatak between 1998 and 2020. Red bars indicate the periods when the subglacial lake drained in 1990 and 2014. (b) Nunatak supraglacial lake before the basin collapsed on 22nd July 2014 as indicated by Landsat 8 (c) Drainage of supraglacial lake at base of nunatak on 1st August 2014, coinciding with subglacial lake drainage (d) Change in ice elevation at the location of the collapse basin according to RACMO2.3p2 (Noël et al., 2019) (solid grey line), and averaged for all ice between 500 and 800 m a.s.l in drainage basins 1.2 and 1.3 according to RACMO2.3p2 1 km product (Noël et al., 2019) (dashed grey line) and CryoSat-2 (dark blue line), and ICESat elevation change computed about 30 km south of the collapse basin (black points) (e) Change in terminus of the main northern outlet relative to previous observation, measured using GEEDiT and MaQiT tools (Lea, 2018), negative values indicate glacier retreat, positive values indicate glacier advance (f) Northern outlet of the glacier before drainage event on 22nd July 2014 and (g) after drainage event showing ∼550 m retreat at the terminus.

As the subglacial lake is likely to have been filled by summer supraglacial meltwater input, it is probable that the lake had been gradually filling for some time. As the lake filled, subglacial water pressure would have increased, and we hypothesise that in 2014 the pressure was sufficient to break the seal on the lake, thus initiating the subglacial sheet flood. Indeed, subglacial outburst floods in Iceland which breach the ice surface are typically triggered by a rapid input of meltwater, such as a volcanic eruption rapidly melting the ice (Tómasson, 1996). Here, the coincident drainage of the large adjacent supraglacial lake (Figure 5.3a-c) would have provided an additional rapid injection of water into the system causing a rapid linearly rising discharge event, irrespective of whether it triggered, or was triggered by, the subglacial lake drainage itself. It is also notable that the drainage event occurred at the same time as the largest rainfall event that year (based upon Regional Atmospheric Climate Model (RACMO) 2.3p2 (Noël et al., 2019) simulations; Supplementary Material Figure 2d-f), thereby adding a further source of water to the flood. Future work should seek to carry out radar surveys over the active subglacial lake and surrounding area to better understand the basal properties and ice thickness, and to search for direct evidence of a subglacial lake.

In the years following the drainage event, the ice surface of the collapse basin began to rise rapidly (average rate of 12 m a^{-1} between 2016-2017; Figure 5.2), indicating refilling of the subglacial lake, most likely due to recharge by surface meltwater (Willis et al., 2015). Between 2017 and 2019, the floor of the collapse basin subsided again by $\sim$10 m (Figure 5.2), suggesting continued dynamic behaviour of the underlying lake. To place these observations within a longer-term context, we therefore analysed Landsat imagery from the past 36 years to look for evidence of past similar drainage events. This analysis revealed that the distinctive oval-shaped surface feature above the subglacial lake has existed since at least 1985, and persists to the present day (24th May 2021). To identify past lake drainage, we inspected consecutive Landsat images for evidence of a simultaneous (1) change from doming to a depression in the surface, and (2) formation of tension fractures around the rim of the basin. Using these criteria, we identified a single drainage event prior to 2014, which occurred between 21st June 1990 and 1st August 1990 (Supplementary Material Figure 3d-g). On this occasion however, and in contrast to the behaviour recorded during the 2014 event, no

downstream surface fracturing and outburst of water occurred, suggesting that the flow of water from the lake outburst flood to the ocean occurred entirely at the ice sheet base.

We hypothesise that the contrasting response of the ice sheet to the 1990 and 2014 outburst floods is attributable to the extensive thinning of the ice sheet that has occurred during the intervening period. Specifically, that recent thinning of ice in this region may have facilitated the breach of the subglacial flood to the surface in 2014. Notably, in the decade prior to the 2014 outburst event, the Greenland Ice Sheet experienced exceptionally high and sustained rates of mass loss (Shepherd et al., 2020), and both model simulations (Noël et al., 2019) and satellite altimeter observations indicate that the ice thinned by ∼13 m (or 5% of the average local ice thickness; Morlighem et al., 2017) between 1990 and 2014 (Figure 5.3d). If correct, this hypothesis suggests the emergence of highly dynamic and bidirectional hydrological connections between the surface and the bed of an ice sheet, which challenges the classical model of unidirectional ice sheet meltwater flow. Furthermore, such connections may be expected to become more common in the future, as the ice sheet thins and surface melt intensifies under a warming climate. At present, however, neither the theory nor the implications of such a phenomenon are currently understood, nor is this process included in current physical models.

Chapter 6

Synthesis

This thesis aimed to detect and monitor subglacial lakes beneath the Greenland Ice Sheet, to improve our understanding of the basal hydrological system and its influence on ice sheet behaviour. In the preceding chapters, I have met this aim by using airborne and satellite-derived data to identify and monitor new subglacial lakes on both ice sheet and regional scales. Firstly, I expanded the previous inventory of subglacial lakes in Greenland (Bowling, 2017) by reanalysing the Operation IceBridge radar depth sounding dataset over an extended temporal period (1993-2016) and detecting surface depressions in the ArcticDEM 5m Mosaic (Chapter 3). Secondly, I developed an automated technique to detect surface expressions of subglacial hydrological movement, using standard deviation of high-resolution, temporally varying ArcticDEM surface elevation data (Chapter 4). I first tested this approach on known active subglacial lakes in the literature to validate the method, and used this information to correct for artefacts in elevation data and distinguish active subglacial lake signals. I then applied the approach at an ice sheet-scale, and demonstrated the capability of this detection method by presenting 7 new potential active subglacial lakes. Finally, I explored the highly unusual behaviour of an individual active subglacial lake detected using the method outlined in Chapter 4, using a combination of optical and SAR imagery, altimetry, regional climate model simulations and ice velocity measurements (Chapter 5). In this final chapter I will summarise the key results from each chapter and how the thesis has met the aims and objectives, then synthesise the results from all the chapters, before identifying and explaining key limitations and justifying the

choices made during this thesis. Finally I suggest recommendations for future research which have emerged from the key findings and limitations.

6.1 Summary of principal findings

In the following section, I summarise the methods developed in this thesis and discuss the principal findings and conclusions across each of the chapters, and how these relate to our understanding of the Greenland Ice Sheet hydrological system.

6.1.1 A revised inventory of subglacial lakes beneath the Greenland Ice Sheet

In Chapter 3, I carried out a comprehensive, systematic survey of subglacial lakes beneath the Greenland Ice Sheet, primarily using airborne radar depth sounding data between 1993 and 2016, expanding work presented in Bowling, 2017. I also detected sinks in the static ArcticDEM 5 m Mosaic product, and compared the surface depressions to geometric characteristics of known collapse basins in Greenland, to identify 2 new active subglacial lakes in southwestern Greenland. Long-term storage of water beneath the Greenland Ice Sheet was previously thought to be limited due to the ability of the drainage system to transport meltwater to the ice margin efficiently (Livingstone et al., 2013). Furthermore, thinner ice and stronger hydraulic gradients towards the margins, compared to Antarctica, were hypothesised to lead to stable hydraulic minima (Pattyn, 2008) and reduce the potential for hydraulic minima. Our analysis provided the first systematic inventory of subglacial lakes in Greenland (Bowling et al., 2019), significantly augmenting the number of previously known subglacial lakes (Palmer et al., 2013; Howat et al., 2015; Palmer et al., 2015; Willis et al., 2015) from 4 to 60. In doing so, the study counters previous assumptions, providing evidence that subglacial lakes are more common than thought. The study also demonstrated the value and insight that could be gained from systematically analysing airborne datasets at the continental scale. These subglacial lakes could be prime targets for direct sampling and field-based geophysical surveys to constrain the mechanism of formation, extent and sediment properties (e.g., Maguire et al., 2020).

One of the most important findings of this study was that subglacial lakes in Greenland differ to Antarctic subglacial lakes, both in their size and spatial distribution. The stable subglacial lakes presented in this study are much smaller than those in Antarctica (nearly 8 times shorter in length). This reflects the different basal topography beneath the two ice sheets, with more complex bed topography beneath Antarctica (Fretwell et al., 2013) allowing large volumes of subglacial water to be stored in lakes. Stable subglacial lakes in Greenland are located above the ELA but distant from the cold-based ice sheet interior, while active lakes are located near the ELA and recharged by seasonal surface meltwater inputs. Furthermore, many airborne radar-detected stable subglacial lakes are found to be distributed in regions where the predicted basal thermal state is 'uncertain' (MacGregor et al., 2016). This finding is important because it helps constrain basal conditions and to validate numerical ice sheet models by providing a boundary condition. These conditions may allow subglacial lakes to be more efficiently identified with lakes able to pond in thawed regions. Knowledge of the location and characteristics of subglacial lakes is fundamental for developing our understanding of the basal hydrological system, which has implications for understanding the flow of ice and ultimately predictions of future ice sheet evolution.

6.1.2 A new method for mapping localised surface elevation changes

Hundreds of hydraulically active subglacial lakes have been identified and monitored in Antarctica (Wright and Siegert, 2012), primarily through satellite altimetry-based detection of localised surface elevation changes in response to subglacial lake drainage and refilling (e.g., Gray et al., 2005; Wingham et al., 2006b; Fricker et al., 2007; Smith et al., 2009). Yet few active lakes had been previously detected in Greenland (Howat et al., 2015; Palmer et al., 2015; Willis et al., 2015; Livingstone et al., 2019), and those were mostly discovered fortuitously. A systematic ice sheet-scale survey of these hydrological features was imperative for understanding their role in the wider hydrological system and their potential impact upon ice dynamics and downstream systems. In Chapter 4, I therefore developed an automated approach to classify potential active subglacial lake candidates over a $\sim$700,000 km^2 area,

using repeated acquisitions of high-resolution satellite-derived surface elevation data (ArcticDEM). I demonstrated that the approach can successfully detect larger known active subglacial lake signals and I presented evidence for several active subglacial lakes in a variety of glaciological settings. These subglacial lakes could be used as targets for future geophysical surveys (e.g., Maguire et al., 2020) and continuous monitoring to understand their potential influence on ice flow and to provide further insight into the wider hydrological system.

6.1.3 A detailed, regional study of an active subglacial lake in Northern Greenland

The results of the systematic survey reported in Chapter 4 enabled us to identify and monitor a previously unknown active subglacial lake drainage event in northern Greenland in Chapter 5. A combination of satellite-derived optical, radar and elevation data revealed a 9 $\times 10^7$ m^3 subglacial lake which drained suddenly (over a maximum of 10 days, but likely over a much shorter time period) at the ice bed, and subsequently propagated to the ice surface via englacial routeways and hydrofracturing. The degree of ice fracturing and excavation of ice blocks (up to 24 m tall), along with the drainage event coinciding with a period of sustained ice thinning, suggests that a subglacial flood wave sped towards comparatively thin ice (Roberts, 2005). Although artesian fountains or upwellings (<2 m) have been previously observed in supraglacial and proglacial settings of polythermal Arctic glaciers (Hambrey, 1984; Hodson and Ferguson, 1999; Skidmore and Sharp, 1999; Wadham et al., 2001; Pälli et al., 2003; Hodson et al., 2005; Irvine-Fynn et al., 2005; St Germain and Moorman, 2019), and the supraglacial emergence of subglacial flood water has caused ice fracturing in Iceland (Roberts et al., 2000; Roberts, 2005), my results are the first observation of this mechanism on the Greenland Ice Sheet.

Our current understanding of the ice sheet's hydrological system is that seasonal surface meltwater drains from the ice surface to the bed via moulins and crevasses (van der Veen, 2007; Das et al., 2008; Chandler et al., 2013; Andrews et al., 2014), with the variability of meltwater input exerting a critical control on seasonal ice acceleration (Bartholomaus et al., 2008; Schoof, 2010). Numerical ice sheet models assume that

meltwater is transported to the ocean without disruption (Smith et al., 2017b). My results show more varied drainage mechanisms, which so far are not accounted for in these models, by providing evidence for bidirectional water flow from the surface, to the bed, and back over transient spatial and temporal scales. Furthermore, observations of a previous drainage event with contrasting characteristics suggest that this mode of water flow is likely to become more common with sustained ice thinning under a warming climate.

6.2 Synthesis of principal findings

In the following section, I synthesise the findings and techniques developed during this thesis in order to detect and monitor subglacial lakes beneath the Greenland Ice Sheet. Together, these results improve our understanding of the subglacial hydrology, which is a fundamental component of the ice sheet system.

Ice sheet-scale mapping of airborne RES-detected lakes (Chapter 3) and satellite-derived potential active subglacial lake locations (Chapter 4), highlights the physiography of subglacial lakes in Greenland, in terms of spatial distribution, size and drainage style, which is important for understanding the processes that influence ice flow and subglacial ecosystems. Our combined results indicate that active and stable lakes are distinct hydrological features in Greenland that occur in different glaciological settings and locations. Active subglacial lakes are more likely to be found near the ELA, with the exception of some viable candidates situated beneath thin ice near land masses, in regions with high surface meltwater inputs to supply the subglacial lakes beneath. On the other hand, RES-detected lakes are typically located above the ELA, associated with regions of high geothermal heat flux, or more complex subglacial terrain.

None of the predicted active subglacial lake candidates correspond with RES-detected subglacial lakes identified in Chapter 3, despite 39% of the active lake candidates intersecting Operation IceBridge flight paths between 1993 and 2016. However, this is not entirely unexpected given that in Antarctica only a small proportion of active subglacial lakes have been confirmed by ice-penetrating radar (e.g., Fricker

and Scambos, 2009; Christianson et al., 2012; Li et al., 2020) or field-based seismic surveys (e.g., Horgan et al., 2012). Some active Antarctic subglacial lakes only meet one or two of the criteria outlined in Carter et al., 2007 for classifying subglacial lakes in radar surveys (Wright et al., 2012; Siegert et al., 2014; Wright et al., 2014), whilst others are not detectable in the radar data (e.g., Welch et al., 2009; Langley et al., 2011; Lindzey et al., 2020). It is thought that active subglacial lakes are difficult to resolve using ice-penetrating radar in regions with surface crevassing or warm ice, or due to an empty lake following drainage, or shallow water during the time of acquisition (Siegert et al., 2014). The new active lakes I have mapped in Greenland could be too small to be classified as "definite" (relatively and absolutely bright, and specular; Carter et al., 2007) subglacial lakes, or their glaciological setting could produce unclear or "fuzzy" signals (relatively and absolutely bright, but not specular reflectors, typically representing saturated sediments or swamps; Carter et al., 2007) signals. Like active lakes in Antarctica (Siegert et al., 2014), the heavily crevassed ice surface could obscure the basal reflector in the active lakes presented in this thesis. Furthermore, OIB airborne ice-penetrating radar was mostly acquired in spring; subglacial lakes that seasonally fill and drain, might be empty at this time of year and therefore be undetected in the radar data. These factors may have implications for using RES to confirm active subglacial lakes, and provide rationale for acquiring future remote sensing data throughout the season to monitor them in detail. Only 15% of higher-confidence active subglacial lake candidates identified in Chapter 4, are located within 1 km of hydraulic minima ($f = 0.9$) calculated in Chapter 3. Reasons for this low recall could be associated with errors in the bed topography data (Morlighem et al., 2017) used in the hydraulic potential analysis, or the active subglacial lake candidates could be too small or shallow to be captured as a hydraulic sink.

The techniques described in Chapter 4 and 5 are complementary; my continental-scale systematic approach is useful as an initial step to identify dynamic glaciological features. Once identified, the subsequent addition of other remote-sensing data (including optical satellite imagery, altimetry and regional climate model analysis) provides further detailed information required to fully understand – at the process level – the evolution and drivers of the detected drainage event. In conjunction, the techniques and analysis presented in Chapters 4 and 5 can be used to systematically

reveal, monitor and understand unique characteristics about the hydrological system at the ice sheet scale. In turn, this approach can be used to study the interaction between basal hydrology and the overlying ice and, ultimately, to improve our understanding of the ice sheet system as a whole.

The research described in Chapters 3, 4 and 5 cooperatively improve our understanding of the basal hydrological system beneath the Greenland Ice Sheet. The combination of airborne and spaceborne geophysical observations and techniques developed in this thesis, at both ice sheet and regional scales, have significantly advanced our view of the Greenland Ice Sheet, documenting significant water storage in both active and stable subglacial lakes, that was previously unknown. Since the presence and seasonal supply of meltwater can influence ice flow variations, biogeochemical processes, sediment fluxes and fjord circulation (Nienow et al., 2017; Davison et al., 2019), it is important to understand subglacial hydrological processes, and the transfer of meltwater throughout the system. Together, the findings in this thesis provide key information that can help assess and constrain numerical models by improving the representation of the ice sheet system and its behaviour. This, in turn, will yield better projections of the ice sheet's future evolution, and thus its contribution to sea level rise, as it responds to climatic change.

6.3 Key limitations of the research

In this section I identify and discuss the key limitations in which the research in this thesis has been constrained, and justification of some of the choices made.

In Chapter 3, I use 23 years of RES data from Operation IceBridge to detect new subglacial lakes. One of the key limitations of these data is that the flight lines only cover ∼2% of the Greenland Ice Sheet. The highest density of coverage is found at the periphery, particularly along the west coast, with large data gaps towards the centre of the ice sheet. Although subglacial lakes are unlikely to be located toward the largely frozen interior, the remaining 98% of the bed is undocumented, meaning a vast number of subglacial lakes could be left undetected. Nearer the ice margin, small subglacial lakes could be situated between radar tracks, also being missed from

the inventory. Operation IceBridge is the only Arctic-wide radar dataset available, ceasing their airborne radar campaign in 2019, therefore whilst the work carried out in Chapter 3 could be updated to this point, further analysis and flights may have to be carried out on an ad-hoc basis.

To identify subglacial lake candidates, we carried out a visual inspection for flat, smooth bed reflectors and calculated basal reflectivity relative to the mean surrounding bedrock within 10 km of a candidate. This approach was chosen to produce a high contrast in bed reflectivity between water and bedrock since the bed is not uniform across the ice sheet (MacGregor et al., 2016). However, this approach may be limited in areas such as fast-flowing ice, for example a uniformly thawed bed beneath the NEGIS will have a higher mean basal reflectivity, meaning that it may be difficult to distinguish between shallow lakes and flat areas of saturated sediment or 'fuzzy' lakes (Carter et al., 2007), and hence why no subglacial lakes were detected in the fast-flowing regions in southern and western Greenland. A further limitation of the method is that the qualitative analysis of the RES data was manual and time consuming, thus it is likely that small bodies of water remain undiscovered due to human error. The use of confidence levels to classify the identified subglacial lake candidates from low confidence (a flat reflector but low relative reflectivity) to very high confidence (a flat reflector which is three standard deviations above the mean) was utilised in order to acknowledge that some lake candidates could indeed be fuzzy lakes.

Mapping sinks in the static ArcticDEM Mosaic and comparing their geometry to known collapse basins to detect active subglacial lakes in Chapter 3 has its disadvantages. Firstly, many active subglacial lakes could have been missed due to their fill and drain cycles being averaged out in the DEM, which is an amalgamation of many time-varying DEMs. This may explain why only 2 active subglacial lakes signatures were identified in Chapter 3. As such, an improved method was developed in Chapter 4 to detect active subglacial lakes on an ice sheet scale. Secondly, comparison of the geometries of known active subglacial lakes was only based on 2 collapse basins which had previously been identified in Greenland (Howat et al., 2015; Palmer et al., 2015; Willis et al., 2015). Unidentified active subglacial lakes in Greenland could exhibit different characteristics to these known lakes (i.e. larger area or maximum

depth), indeed, several active subglacial lakes have since been identified with differing characteristics (e.g., three active lakes beneath Isunguata Sermia Livingstone et al., 2019 and those in Chapter 4 and 5).

Previous discovery of active subglacial lakes in Greenland have been random and studies have been ad-hoc (e.g., Howat et al., 2015; Palmer et al., 2015; Willis et al., 2015; Livingstone et al., 2019. In Chapter 4, I developed a new automated technique using statistical analysis of about 26,000 high-resolution digital surface models covering the entire ice sheet, to identify localised regions of elevation change which could be caused active subglacial lake filling and drainage. Our region of interest for performing the analysis was $\sim$700,000 km^2 (or within 50 km of the ice margin) due to the high level of computational processing and data storage required to maintain the high resolution of 2 m. This means, however, that potential active subglacial lakes located towards the interior (>50 km from the margin), for example in southwestern Greenland where the ELA is at higher elevations, could have been overlooked.

The ArcticDEM DSM data used to detect localised elevation changes is created from optical imagery. Artefacts and noise can be present in the DSMs due to cloud or shadow, or misalignment caused by issues such as homogeneous terrain. Despite extensively filtering the Strip DSMs for artefacts and anomalies, some artefacts persisted, creating standard deviation of elevation signals >48 m. These artefacts could conceal signals of active subglacial lake drainage and other elevation changes. The active subglacial lakes identified in Livingstone et al., 2019 near Isunguata Sermia, were not captured using our method due to noise at the ice sheet margin (mountainous terrain at the ice margins are difficult to georeference when generating the ArcticDEM products). In this region, there were few DSMs to calculate standard deviation, and thus the signals of the three marginal active subglacial lakes were difficult to distinguish from the surrounding ice changes. Some active subglacial lake candidates may be misclassified as supraglacial lakes due to similar elevation changes. We removed candidates which intersected supraglacial lakes identified in (Lea and Brough, 2019) to reduce this misclassification, however false positives still occurred.

In Chapter 5, we utilised the results from the systematic survey in Chapter 4, combined with the analysis of a variety of remotely sensed datasets to carry out a

detailed study of a particularly unique active subglaical lake in Northern Greenland. Unfortunately, no RES data are available for the collapse basin itself, and the nearest flight line is ∼9 km inland from the basin. This means that there is a lack of reliable bed topography and ice thickness data to determine the basal conditions. However, further work to model the thermal conditions at the bed (using a range of plausible ice thicknesses) will allow us to understand the drivers and dynamic impacts of the subglacial lake drainage and subsequent outburst. Furthermore, we are unable to determine precisely when the subglacial lake formed, how it changed over time and its precise geometry. This is largely due to limited satellite imagery, DEM data and field observations (cloud cover in the region creates a 10-day observational period), therefore we are unable to determine whether this drainage occurred over hours, days or weeks. We hypothesise that the subglacial lake drained in a matter of hours, however the unknown timing means that the volume of the subglacial lake is likely to be underestimated.

6.4 Recommendations for future work

In this section, I reflect upon the ways in which the methods developed in this thesis can be further improved, and employed to derive new datasets and glaciological knowledge in the future. Firstly, I explore the potential for machine learning to improve stable subglacial lake identification techniques described in Chapter 3, and how these lakes could be used as potential candidates for direct sampling. Secondly, I consider the application of the approach detailed in Chapter 4 to identify and analyse other dynamic glaciological signals, and the potential of extending the method to other datasets and locations. Lastly, I suggest how subglacial lake candidates can be further explored to evaluate their potential impact on ice sheet dynamics.

6.4.1 Automatic detection of subglacial lakes in airborne ice penetrating radar

Manual inspection of radar data for flat, bright and smooth reflectors relative to the surrounding bed, as carried out in Chapter 3, is the primary approach for identifying

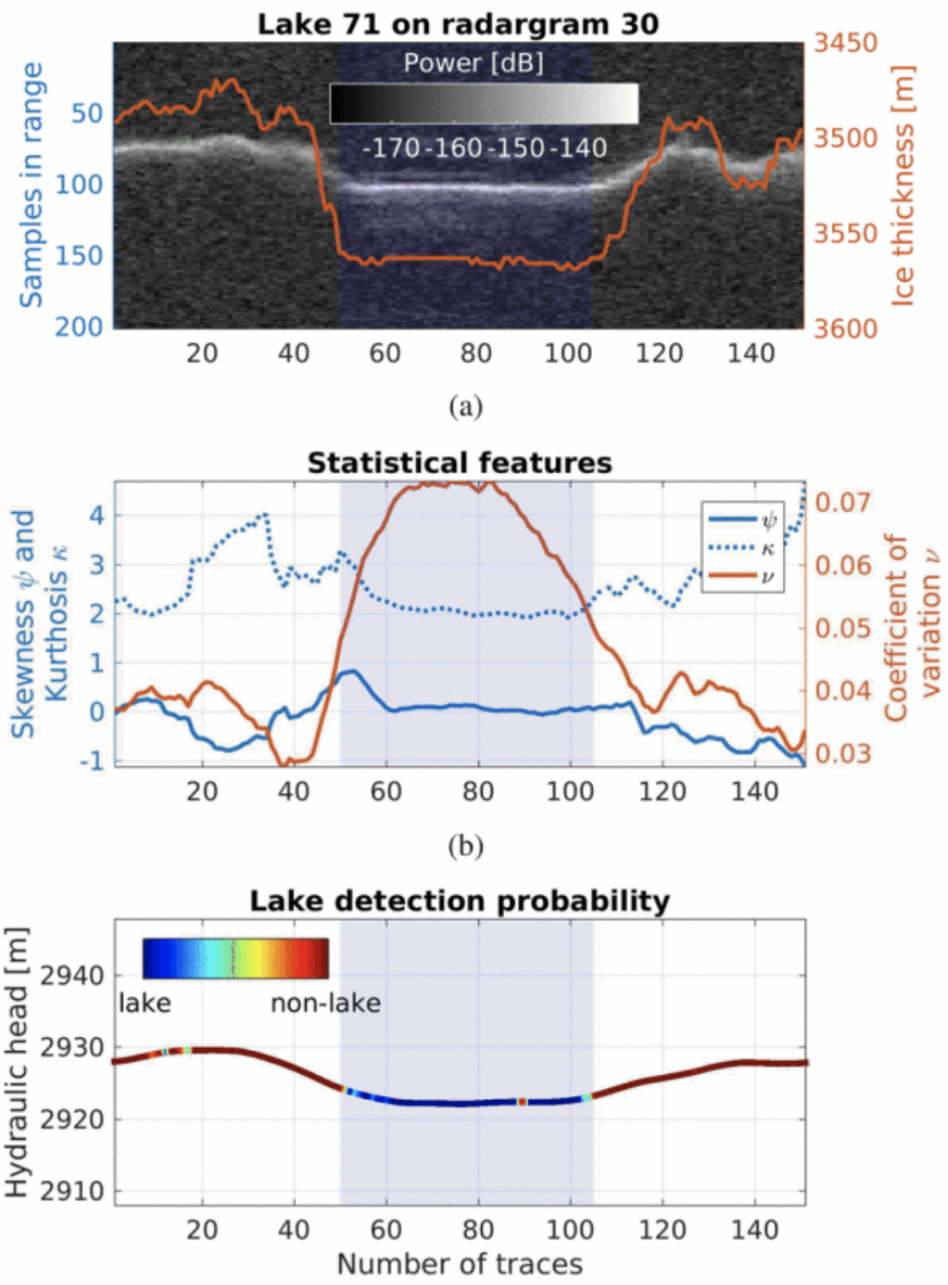

Figure 6.1: Machine learning approach to detecting subglacial lakes in Antarctica. (Source: Ilisei et al. 2018.)

subglacial lakes beneath ice masses (e.g., Popov and Masolov, 2007; Wright and Siegert, 2012). However, visual inspection is time-consuming, due to the vast quantities of radar data, highly subjective, and smaller water bodies may go undetected. Semi-automated techniques have been developed to classify Antarctic subglacial lakes based on their radar reflectivity properties on catchment scales (Carter et al., 2007), to address these limitations. In Chapter 3 I use confidence levels based on relative basal reflectivity and the presence of hydraulically flat reflectors to classify subglacial lake candidates on a case-by-case basis. Future work could seek to automate this process and extend the observation period to include more recent OIB radar data (2017-2019) which covers $\sim$5,400 km^2.

Recently, automatic delineation of subglacial lakes using a machine learning classifier to estimate the probability of the interface being a lake reflector based on variability in bed topography and reflectivity has opened new opportunities for subglacial lake detection on an ice sheet scale in Antarctica (Ilisei et al., 2018, 2019) (Figure 6.1). This approach has resulted in high accuracy and recall (>96%) (Ilisei et al., 2018, 2019). The Greenland subglacial lakes identified in Chapter 3 could be used as a training dataset to train and validate the machine learning model (since the Greenland subglacial lakes have subtly different characteristics to those in Antarctica). Previous to this study, only 2 RES-detected subglacial lakes were known, but my inventory provides 54 previously uncharted subglacial lakes, allowing future application of this machine learning technique over the Greenland Ice Sheet at scale.

6.4.2 Exploration of subglacial lakes

Stable subglacial lakes identified in this thesis could be used as candidates for direct lake sampling, to investigate lake and sediment properties and potential ecosystems, which are important for understanding how microbial life has adapted to extreme environments and stable inland subglacial lakes could provide information about ice sheet history. Ground-based surveys using seismics and ground-penetrating radar at these candidates, particularly those relatively close to settlements, for example Thule, northwestern Greenland, would improve geometric constrains of the subglacial water bodies and enable estimations of their volumes (e.g., Maguire et al., 2020).

6.4.3 Diagnosing other sources of localised surface elevation changes

In Chapter 4, I demonstrated the capability of applying a simple standard deviation of elevation calculation to multi-temporal surface elevation data to identify potential active subglacial lake candidates at an ice-sheet scale. Temporal changes in the ice surface are, however, not solely caused by subglacial lake dynamics, and as such a multitude of dynamic signals are captured in my standard deviation product. Standard altimetry methods typically have a resolution of hundreds of metres to kilometres, however mapping these changes using metre-scale resolution ArcticDEM opens up the opportunity to explore various dynamic signals, such as supraglacial lake filling and draining, terminus retreat, ice marginal lakes, and grounding line dynamics, at a minimum of two orders of magnitude finer detail.

Figure 6.2 shows a variety of supraglacial lakes in central western Greenland, which are highlighted by their moderate time-variance in elevation. My approach, outlined in Chapter 4, could be tailored to capture periodic supraglacial lake drainage events by carrying out more detailed studies of their signals and comparison to automatically detected supraglacial lake outlines (e.g., Lea and Brough, 2019). This would provide high-resolution basin geometries and supraglacial lake depths, which are typically derived indirectly using radiative transfer equations (Sneed and Hamilton, 2007). These signals could be utilised to validate radiative transfer approaches and identify suitable candidates for field surveys to improve our understanding of supraglacial lakes and their influence on ice flow. Furthermore, ice-marginal lakes are depicted with very high variance of elevation signals using our technique (Figure 4.6 and 6.4). My approach could therefore also be tailored to identify ice marginal lake drainage events and associated outburst floods, to further understand their dynamics and influence on ice sheet behaviour.

The product could also be used to monitor changes occurring at the ice sheet margin, for example, to monitor terminus retreat or advance, and grounding line dynamics. Figure 6.3a depicts several dynamic signals at near the ice margin of Storstrømmen Glacier and L. Bistrup Bræ in northeastern Greenland. High standard deviation of elevation ($>$10 m) is observed near the terminus, representing $\sim$1.5 km ice

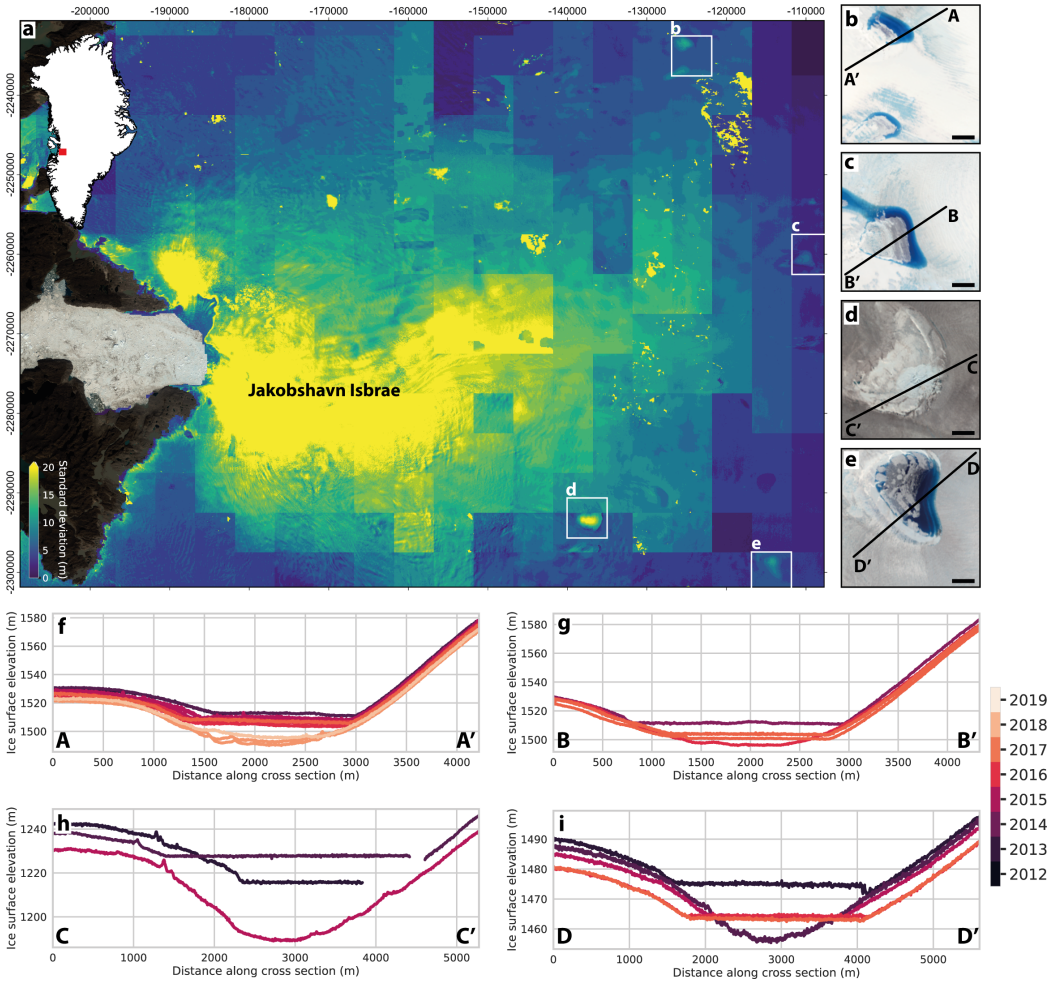

Figure 6.2: (a) Standard deviation of elevation product produced in Chapter 4 over Jakobshavn Isbrae, southwestern Greenland. (b-e) Landsat 8 RGB composite image acquired on 2nd August 2019 of several supraglacial lakes highlighted in panel (a). Black bars indicate 1 km scale bars. (f-i) Elevation profiles across supraglacial lakes showing their evolution between 2012 and 2019 (transects shown in panels b-e). Flat surfaces depict water level.

retreat between 2015 - 2017 (Figure 6.3). Typically terminus retreat is calculated by digitising the terminus extent using high-resolution optical imagery such as Landsat and Sentinel-2, and calculating area change over time. This standard method is, however, 2-dimensional, and our product could be adapted to map the calving flux, i.e. the volume of ice that has been lost, which is important for constraining ice sheet models.

Interestingly, the grounding line (the transition between the floating ice tongue and where the ice is grounded at the ice bed) is highlighted by a boundary in the standard deviation product (Figure 6.3a), and this corresponds closely with the Mouginot et al., 2018 2015 grounding line detected using Sentinel-1a/b SAR. Grounding zones are inherently difficult to locate and monitor since it is impossible to distinguish between floating and grounded ice tongues from optical imagery (Figure 6.3b). However, initial results from the variance in elevation product show promise in this field, as such it is possible that our dataset could be used to systematically detect grounding zones at a continental scale, which would benefit the ice sheet modelling community.

Small floating ice tongues which terminate in ice-marginal lakes produce high standard deviation of elevation signals when the ice-marginal lake drains, causing the ice surface to lower substantially (Figure 4.6 and 6.5). As the ice-marginal lake fills, the ice surface rises again. The dynamics at grounded and floating sections of the ice sheet are important to map and understand for numerical ice sheet models to accurately predict future ice sheet evolution.

Preliminary analysis of the variance in elevation at the grounding line of Petermann Glacier, in North-west Greenland suggests that the evolution of subglacial conduits beneath the ice may be detected in my product. Figure 6.6 shows a linear, high standard deviation feature near the grounding zone of Petermann Glacier. Cross-sections along this feature show localised lowering of the ice surface, which I posit to be due to the development of an efficient channel beneath the ice which exports subglacial meltwater to the fjord. Knowledge of the subglacial system morphology and its evolution are critical for understanding the ice sheet system.

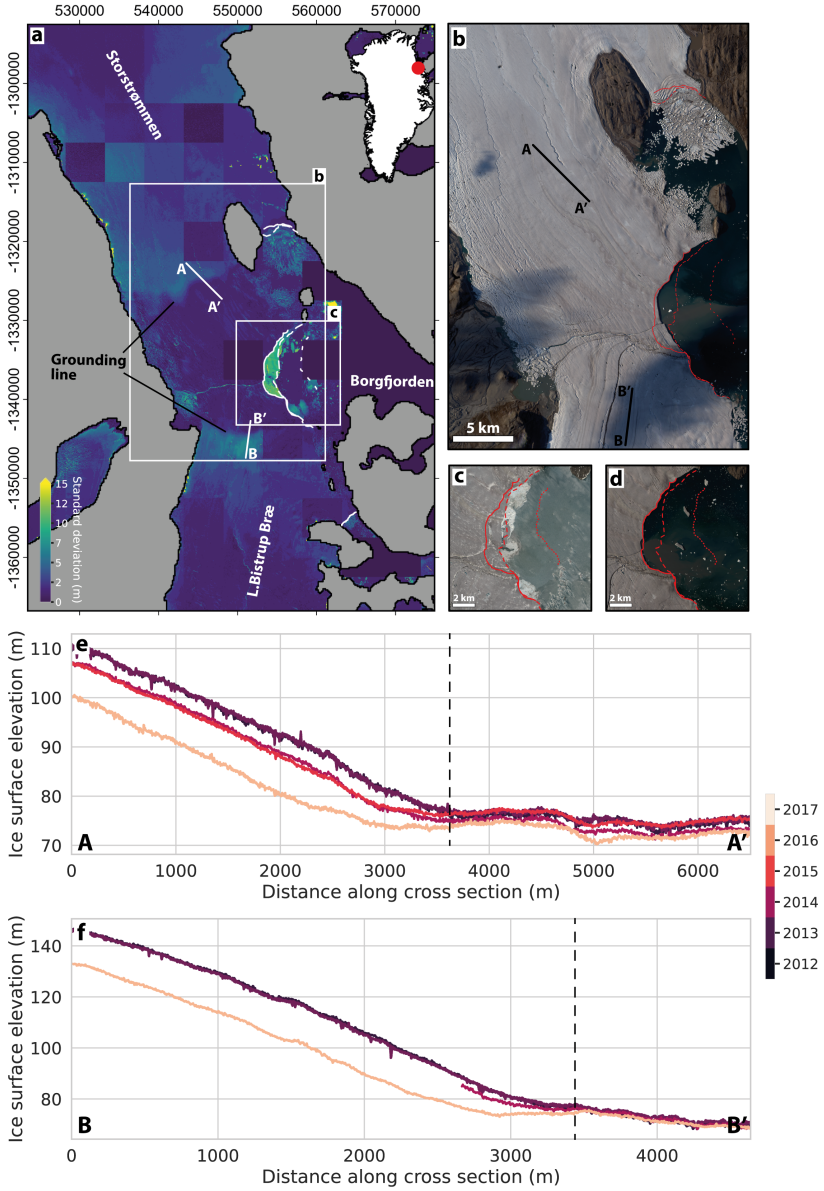

Figure 6.3: (a) Standard deviation of elevation product produced in Chapter 4 over Storstrømmen and L. Bistrup Bræ, northeastern Greenland (location shown by red point in inset map). MEaSUREs terminus positions derived from SAR are shown by solid (2016/17) and dashed white lines (2014/15 and 2000/01). Grounding lines are depicted by boundary in standard deviation product. (b) Landsat 8 RGB composite image acquired on 13th August 2016, with terminus positions in red. (c) Landsat 8 RGB composite image acquired on 14th July 2015 and (d) Landsat 8 RGB composite image acquired on 29th July 2017, showing terminus retreat of ∼1.5 km. (e) Elevation profiles across grounding line at Storstrommen Glacier (transects shown in panels a and b), with approximate location of grounding line shown by dashed black line. (f) Elevation profiles across grounding line at L. Bistrup Bræ (transects shown in panels a and b), with approximate location of grounding line shown by dashed black line.

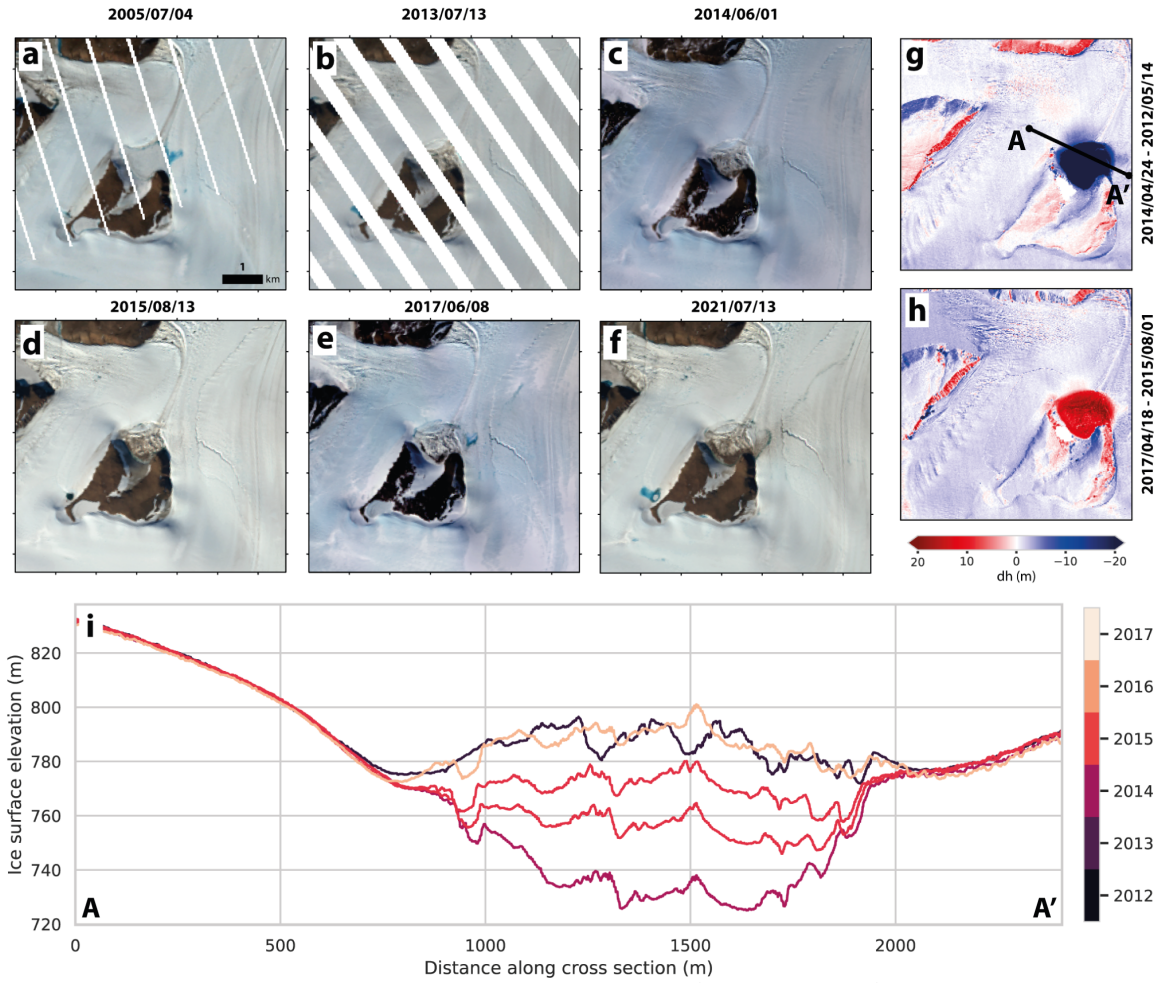

Figure 6.4: (a-f) Landsat 8 RGB composite images acquired on 4th April 2005, 13th July 2013, 1st June 2014, 13th August 2015, 8th June 2017 and 13th July 2021. (g) Elevation difference between DSMs acquired on 24th April 2014 and 14th May 2012. (h) Elevation difference between DSMs acquired on 18th April 2017 and 1st August 2015. Elevation profiles across lake showing its evolution between 2012 and 2017 (transects shown in panels g). Location map shown in Figure 4.6.

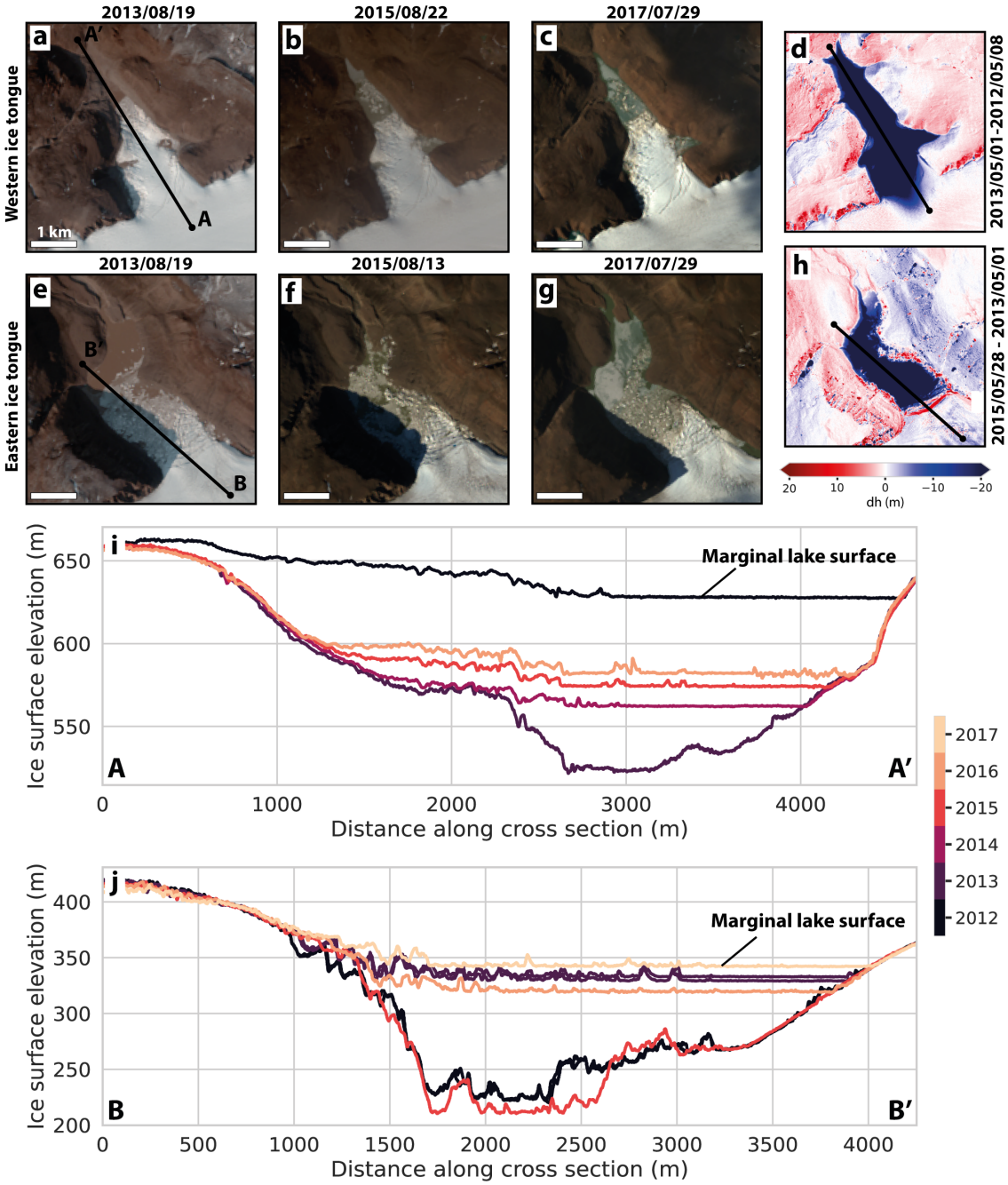

Figure 6.5: (a-c) Landsat 8 RGB composite images acquired on 19th August 2013, 22nd August 2015, 29th July 2017 over floating ice tongue. Location map shown in Figure 4.6. (d) Elevation difference between DSMs acquired on 1st May 2015 and 8th May 2012. (e-g) Landsat 8 RGB composite images acquired on 19th August 2013, 13th August 2015, 29th July 2017 over second floating ice tongue. Location map shown in Figure 4.6. (h) Elevation difference between DSMs acquired on 28th May 2015 and 1st May 2013.

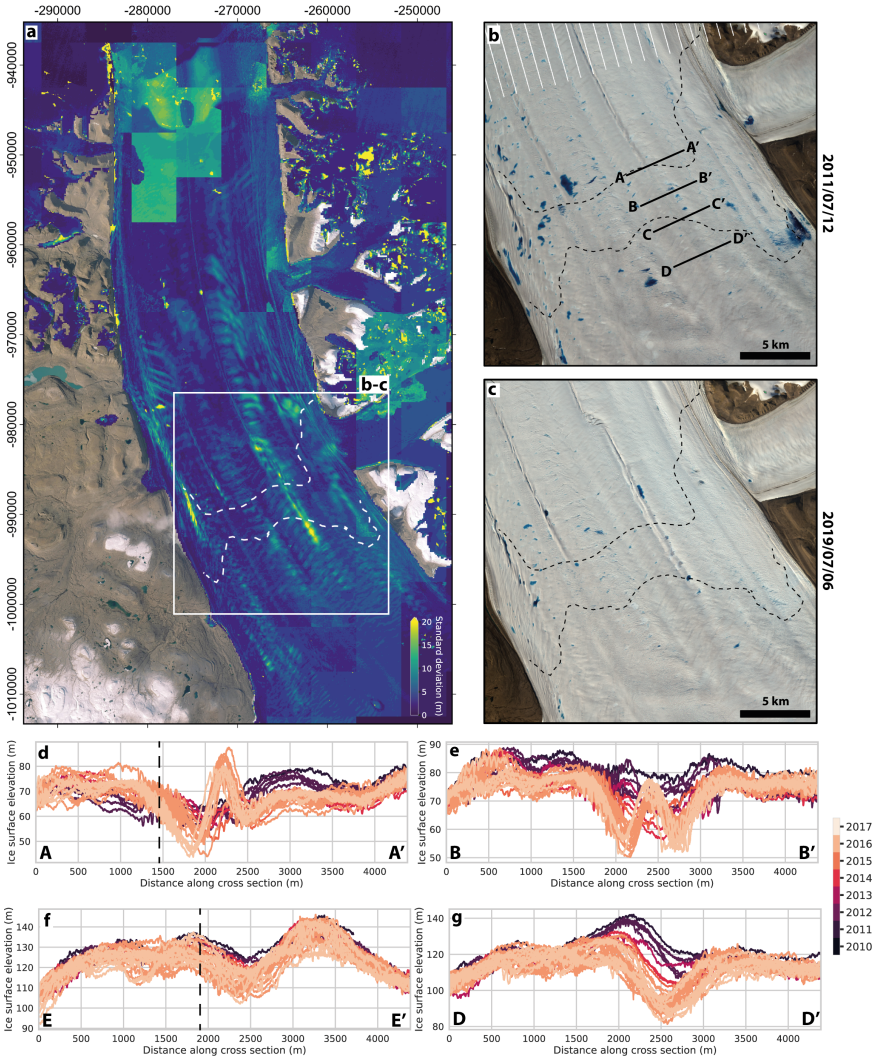

Figure 6.6: (a) Standard deviation of elevation product produced in Chapter 4 over Petermann Glacier, northern Greenland, with ESA Grounding Lines from SAR Interferometry shown by white dashed lines (9th February 2017). (b) Landsat 7 RGB composite image acquired on 12th July 2011, grounding lines are now shown by black dashed lines. (c) Landsat 8 RGB composite image acquired on 6th July 2019, with grounding lines in dashed black lines. (d-g) Elevation profiles taken across linear feature with high standard deviation near upper grounding line, showing the surface topography between 2010 and 2019 (transects shown in panel b). Grounding line is shown by dashed black line.

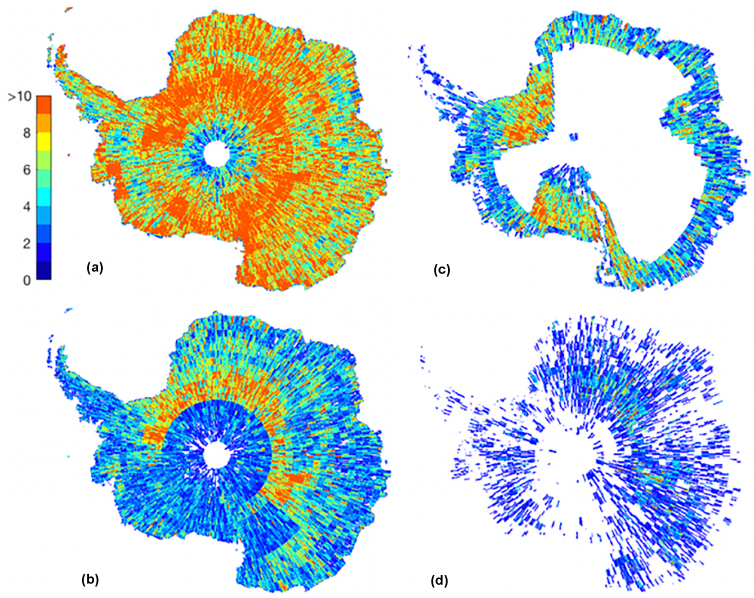

Figure 6.7: Spatial coverage of digital surface models produced for the REMA project. (a) Number of DSMs using all data. (b) Number of DSMs that passed the visual quality inspection. (c) Quality controlled DSMs within acceptable criteria from CryoSat-2 and (d) ICESat GLAS 2D campaign (Source: Howat et al., 2019).

6.4.4 Extension of method to other ice masses

In Chapter 4, I demonstrated the potential of applying standard deviation to high-resolution ArcticDEM elevation data to identify localised surface elevation changes across the Greenland Ice Sheet associated with the drainage of subglacial lakes. Future work could seek to explore the ability of my method to delineate subglacial lakes in beneath all Arctic ice caps, providing there is sufficient ArcticDEM data. My approach could also be applied to other temporally-varying DSM datasets, for example REMA in Antarctica which is available at 2 and 8 m spatial resolution (Figure 6.7), to detect and monitor new and existing active subglacial lakes beneath the Antarctic Ice Sheet and improve understanding of their distribution and dynamics. Since this Antarctica is over 6 times larger in area than Greenland, this approach might demand improvements in automation and computational power.

6.4.5 Potential impact of subglacial lake drainage activity on ice dynamics

Whilst my findings reveal the presence and spatial distribution of active and stable subglacial lakes in Greenland and that water flow from the ice surface to bed is not always unidirectional, an important next step is to understand how subglacial lake drainage influences the evolution of the subglacial system, and, in turn, the impact it might have upon the flow of ice in Greenland. Rapid drainage of subglacial lakes can have a transient impact on the flow of ice in Antarctica (Stearns et al., 2008) and many active lakes have been linked with the onset of fast-flowing ice streams (Siegert and Bamber, 2000; Bell et al., 2007b). By combining remote sensing techniques, a complete subglacial drainage history can be built for each active subglacial lake, and the associated ice velocity response can be monitored. This is important since subglacial hydrological system is a key parameter in ice sheet modelling, and therefore important for predicting the ice sheets contribution to sea level rise in response to climate change.

6.5 Concluding remarks

The research presented in this thesis has advanced our understanding of subglacial lakes beneath the Greenland Ice Sheet. It has illuminated the prevalence of long-term storage of subglacial water beneath the Greenland Ice Sheet, through the first systematic ice-sheet-wide survey of radio-echo sounding data (Chapter 3). Moreover, that small stable subglacial lakes are primarily distributed above the ELA, driven by regions of high geothermal heat flux and complex basal topography, which differs to the physiography of Antarctic subglacial lakes. The novel framework presented in this thesis was developed to process high-volume satellite-derived high-resolution data to systematically identify active subglacial lakes on an ice-sheet scale (Chapter 4). This thesis captures several new active subglacial lake candidates with complex drainage styles and characteristics that have not been previously observed in Greenland. Finally, a range of remote sensing data are combined to illustrate the dynamics of a previously unknown active subglacial lake at Brikkerne glacier, northern Greenland (Chapter 5). These results bring new insight to glaciological science by revealing the supraglacial

emergence of subglacial flood water and subsequent re-entry into the subglacial system. Such observations are important for understanding the physical processes controlling the pathways and impacts of subglacial floods.

This thesis thus presents several critical advances in our understanding of the subglacial hydrological system beneath the Greenland Ice Sheet, through ice-sheet-wide surveys and the development of novel techniques. Better understanding of the subglacial system is crucial in order to better constrain numerical ice sheet models which project the response of the Greenland Ice Sheet to future climatic warming.

Appendix A

Supplementary material for Chapter 2: Distribution and dynamics of Greenland subglacial lakes

A.1 Supplementary Information for Chapter 2

The document includes:

1. Radar evidence for identified Greenland subglacial lakes

A.2 Radar evidence for identified Greenland subglacial lakes

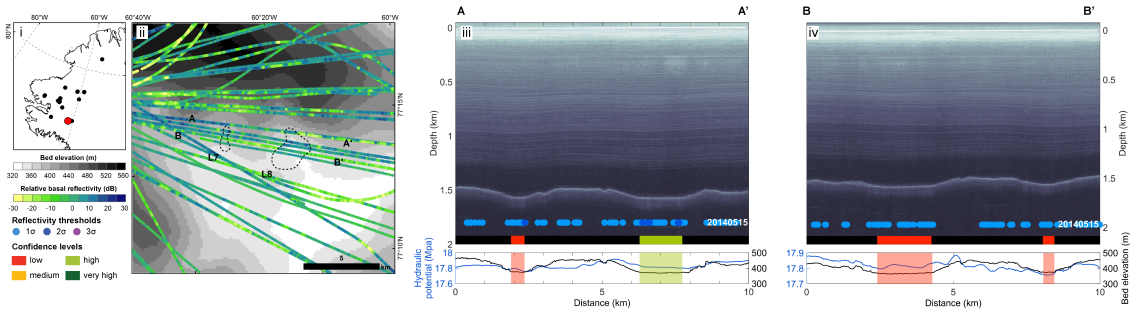

Figure A.1: Radar evidence for Greenland subglacial lakes. (i) Inset map showing location of subglacial lake L7 and L8 (red) and neighbouring lakes found in this study (black). (ii) Bed topography of the region with relative basal reflectivity along Operation IceBridge flight paths. Estimated lake extent is shown by the dashed line. Radar profile along transect (iii) A-A' (20140515_02_005) and (iv) B-B' (20145015_02_068). Subglacial lakes are depicted by a bar colour-coded according to the confidence level. Relative basal reflectivity thresholds, based on the statistics of the bed returned power within 20 km of the identified lake (1-3 σ from the mean), are indicated by the blue-purple circles. Lower graphs show bedrock elevation (black) and hydraulic potential (blue).

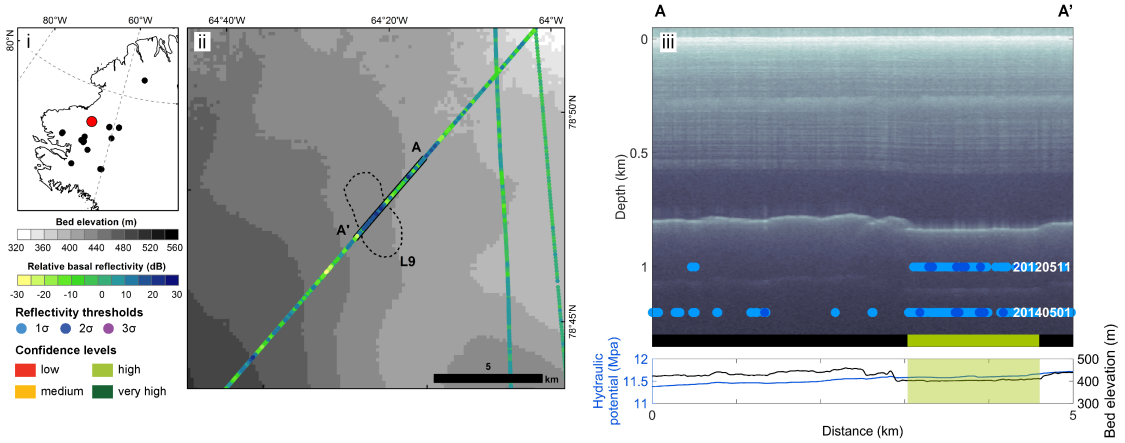

Figure A.2: Radar evidence for Greenland subglacial lakes. (i) Inset map showing location of subglacial lake L9 (red) and neighbouring lakes found in this study (black). (ii) Bed topography of the region with relative basal reflectivity along Operation IceBridge flight paths. Estimated lake extent is shown by the dashed line. Radar profile along transect (iii) A-A' (20120511_01_028/ 20140501_01_029). Subglacial lakes are depicted by a colour-coded according to the confidence level. Relative basal reflectivity thresholds, based on the statistics of the bed returned power within 20 km of the identified lake (1-3 σ from the mean), are indicated by the blue-purple circles. Lower graphs show bedrock elevation (black) and hydraulic potential (blue).

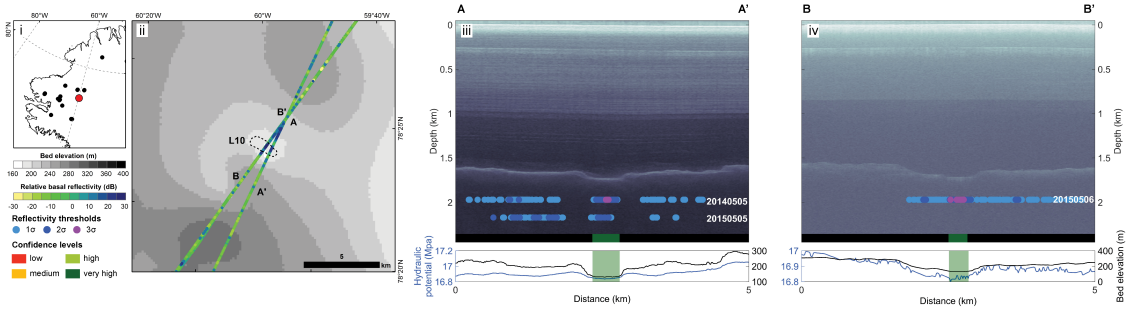

Figure A.3: Radar evidence for Greenland subglacial lakes. (i) Inset map showing location of subglacial lake L10 (red) and neighbouring lakes found in this study (black). (ii) Bed topography of the region with relative basal reflectivity along Operation IceBridge flight paths. Estimated lake extent is shown by the dashed line. Radar profile along transect (iii) A-A' (20140505_01_042/ 20150505_02_042) and (iv) B-B' (20150506_02_008). Subglacial lakes are depicted by a bar colour-coded according to the confidence level. Relative basal reflectivity thresholds, based on the statistics of the bed returned power within 20 km of the identified lake (1-3 σ from the mean), are indicated by the blue-purple circles. Lower graphs show bedrock elevation (black) and hydraulic potential (blue).

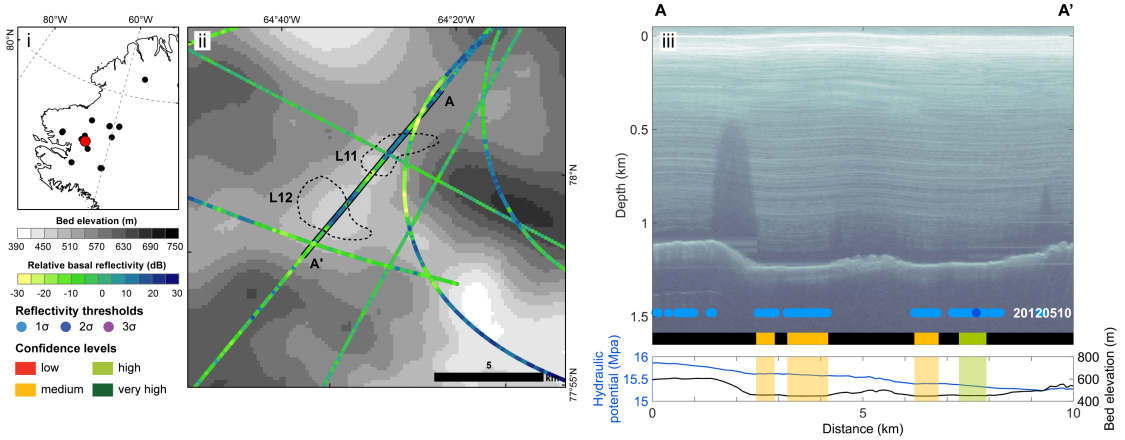

Fig 4. Radar evidence for Greenland subglacial lakes. (i) Inset map showing location of subglacial lake L11 and L12 (red) and neighbouring lakes found in this study (black). (ii) Bed topography of the region with relative basal reflectivity along Operation IceBridge flight paths. Estimated lake extent is shown by the dashed line. Radar profile along transect (iii) A-A' (20120510_01_056). Subglacial lakes are depicted by a bar colour-coded according to the confidence level. Relative basal reflectivity thresholds, based on the statistics of the bed returned power within 20 km of the identified lake (1-3 σ from the mean), are indicated by the blue-purple circles. Lower graphs show bedrock elevation (black) and hydraulic potential (blue).

Figure A.4: Radar evidence for Greenland subglacial lakes. (i) Inset map showing location of subglacial lake L11 and L12 (red) and neighbouring lakes found in this study (black). (ii) Bed topography of the region with relative basal reflectivity along Operation IceBridge flight paths. Estimated lake extent is shown by the dashed line. Radar profile along transect (iii) A-A' (20120510_01_056). Subglacial lakes are depicted by a bar colour-coded according to the confidence level. Relative basal reflectivity thresholds, based on the statistics of the bed returned power within 20 km of the identified lake (1-3 σ from the mean), are indicated by the blue-purple circles. Lower graphs show bedrock elevation (black) and hydraulic potential (blue).

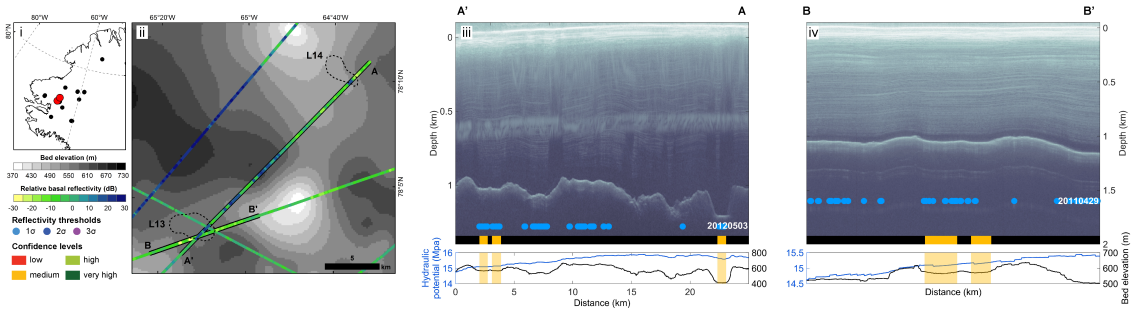

Figure A.5: Radar evidence for Greenland subglacial lakes. (i) Inset map showing location of subglacial lake L13 and L14 (red) and neighbouring lakes found in this study (black). (ii) Bed topography of the region with relative basal reflectivity along Operation IceBridge flight paths. Estimated lake extent is shown by the dashed line. Radar profile along transect (iii) A-A' (20120503_01_002) and (iv) B-B' (20110429_01_005). Subglacial lakes are depicted by a bar colour-coded according to the confidence level. Relative basal reflectivity thresholds, based on the statistics of the bed returned power within 20 km of the identified lake (1-3 σ from the mean), are indicated by the blue-purple circles. Lower graphs show bedrock elevation (black) and hydraulic potential (blue).

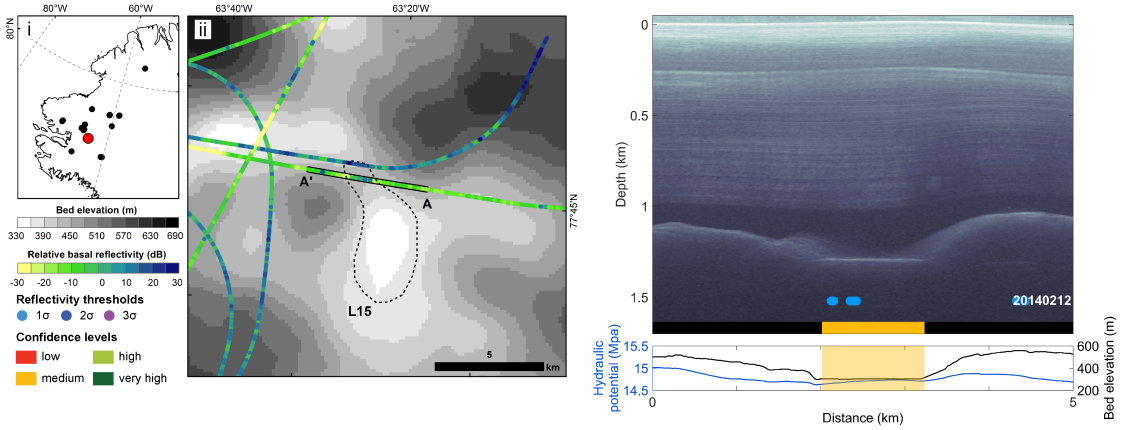

Figure A.6: Radar evidence for Greenland subglacial lakes. (i) Inset map showing location of subglacial lake L15 (red) and neighbouring lakes found in this study (black). (ii) Bed topography of the region with relative basal reflectivity along Operation IceBridge flight paths. Estimated lake extent is shown by the dashed line. Radar profile along transect (iii) A-A' (20140512_01_025). Subglacial lakes are depicted by a bar colour-coded according to the confidence level. Relative basal reflectivity thresholds, based on the statistics of the bed returned power within 20 km of the identified lake (1-3 σ from the mean), are indicated by the blue-purple circles. Lower graphs show bedrock elevation (black) and hydraulic potential (blue).

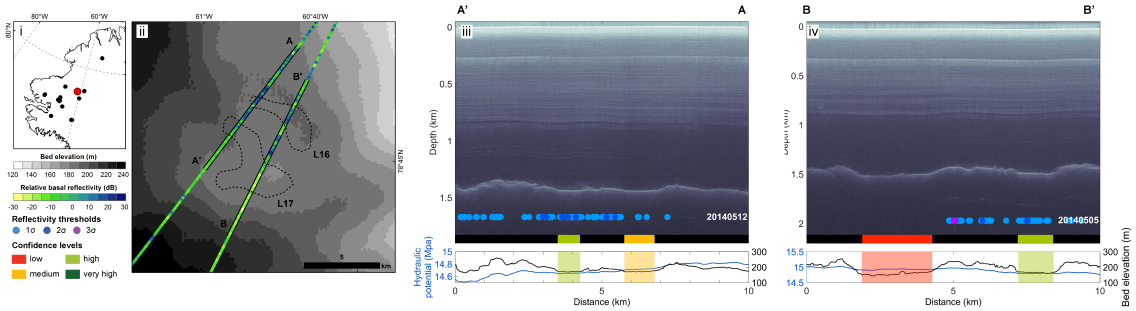

Figure A.7: Radar evidence for Greenland subglacial lakes. (i) Inset map showing location of subglacial lake L16 and L17 (red) and neighbouring lakes found in this study (black). (ii) Bed topography of the region with relative basal reflectivity along Operation IceBridge flight paths. Estimated lake extent is shown by the dashed line. Radar profile along transect (iii) A-A' (20140512_01_022) and (iv) B-B' (20140505_01_032). Subglacial lakes are depicted by a bar colour-coded according to the confidence level. Relative basal reflectivity thresholds, based on the statistics of the bed returned power within 20 km of the identified lake (1-3 σ from the mean), are indicated by the blue-purple circles. Lower graphs show bedrock elevation (black) and hydraulic potential (blue).

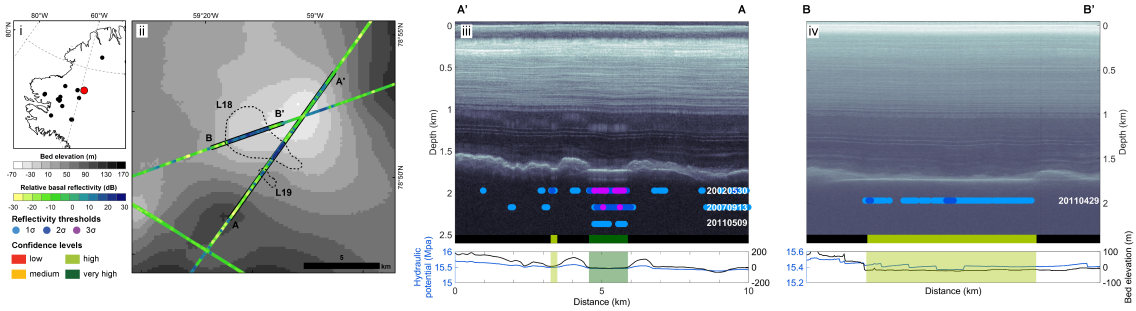

Figure A.8: Radar evidence for Greenland subglacial lakes. (i) Inset map showing location of subglacial lake L18 and L19 (red) and neighbouring lakes found in this study (black). (ii) Bed topography of the region with relative basal reflectivity along Operation IceBridge flight paths. Estimated lake extent is shown by the dashed line. Radar profile along transect (iii) A-A' (20020530_01_007/ 20070913_02_005/ 20110509_01_008) and (iv) B-B' (20110429_01_008). Subglacial lakes are depicted by a bar colour-coded according to the confidence level. Relative basal reflectivity thresholds, based on the statistics of the bed returned power within 20 km of the identified lake (1-3 σ from the mean), are indicated by the blue-purple circles. Lower graphs show bedrock elevation (black) and hydraulic potential (blue).

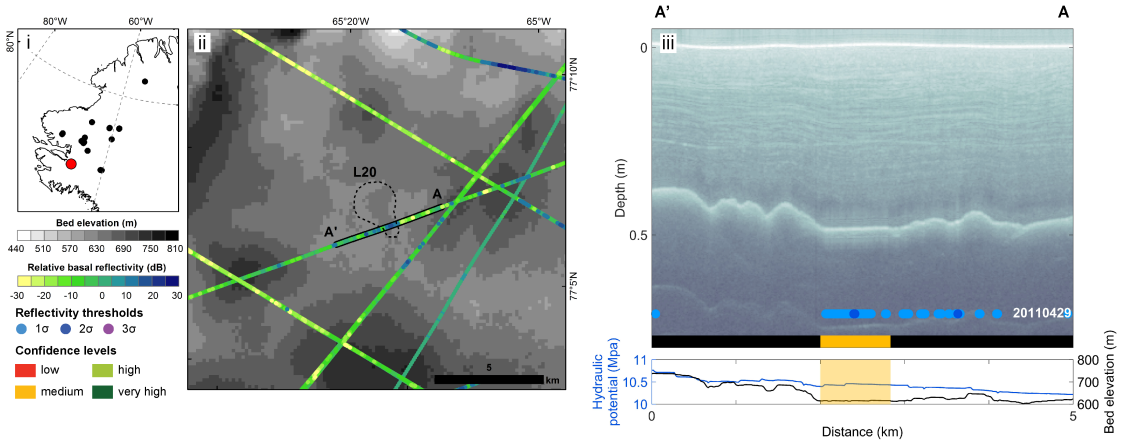

Figure A.9: Radar evidence for Greenland subglacial lakes. (i) Inset map showing location of subglacial lake L20 (red) and neighbouring lakes found in this study (black). (ii) Bed topography of the region with relative basal reflectivity along Operation IceBridge flight paths. Estimated lake extent is shown by the dashed line. Radar profile along transect (iii) A-A' (20110429_02_028). Subglacial lakes are depicted by a bar colour-coded according to the confidence level. Relative basal reflectivity thresholds, based on the statistics of the bed returned power within 20 km of the identified lake (1-3 σ from the mean), are indicated by the blue-purple circles. Lower graphs show bedrock elevation (black) and hydraulic potential (blue).

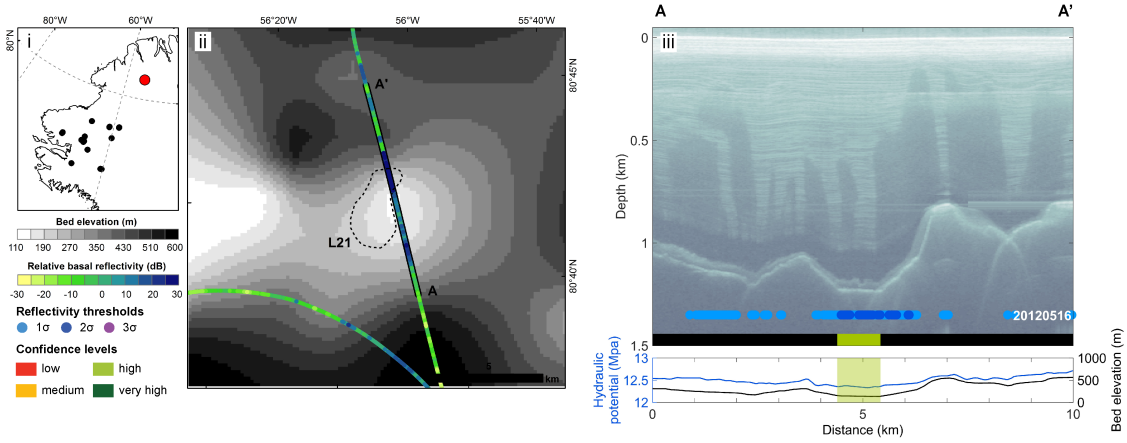

Figure A.10: Radar evidence for Greenland subglacial lakes. (i) Inset map showing location of subglacial lake L21 (red) and neighbouring lakes found in this study (black). (ii) Bed topography of the region with relative basal reflectivity along Operation IceBridge flight paths. Estimated lake extent is shown by the dashed line. Radar profile along transect (iii) A-A' (20120516_01_018). Subglacial lakes are depicted by a bar colour-coded according to the confidence level. Relative basal reflectivity thresholds, based on the statistics of the bed returned power within 20 km of the identified lake (1-3 σ from the mean), are indicated by the blue-purple circles. Lower graphs show bedrock elevation (black) and hydraulic potential (blue).

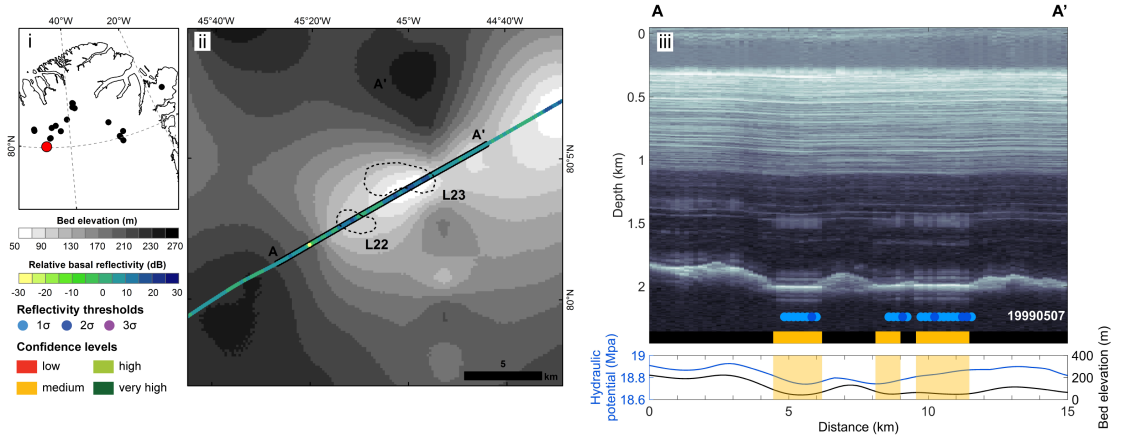

Fig 11. Radar evidence for Greenland subglacial lakes. (i) Inset map showing location of subglacial lake L22 and L23 (red) and neighbouring lakes found in this study (black). (ii) Bed topography of the region with relative basal reflectivity along Operation IceBridge flight paths. Estimated lake extent is shown by the dashed line. Radar profile along transect (iii) A-A' (19990507_01_004). Subglacial lakes are depicted by a bar colour-coded according to the confidence level. Relative basal reflectivity thresholds, based on the statistics of the bed returned power within 20 km of the identified lake (1-3 σ from the mean), are indicated by the blue-purple circles. Lower graphs show bedrock elevation (black) and hydraulic potential (blue).

Figure A.11: Radar evidence for Greenland subglacial lakes. (i) Inset map showing location of subglacial lake L22 and L23 (red) and neighbouring lakes found in this study (black). (ii) Bed topography of the region with relative basal reflectivity along Operation IceBridge flight paths. Estimated lake extent is shown by the dashed line. Radar profile along transect (iii) A-A' (19990507_01_004). Subglacial lakes are depicted by a bar colour-coded according to the confidence level. Relative basal reflectivity thresholds, based on the statistics of the bed returned power within 20 km of the identified lake (1-3 σ from the mean), are indicated by the blue-purple circles. Lower graphs show bedrock elevation (black) and hydraulic potential (blue).

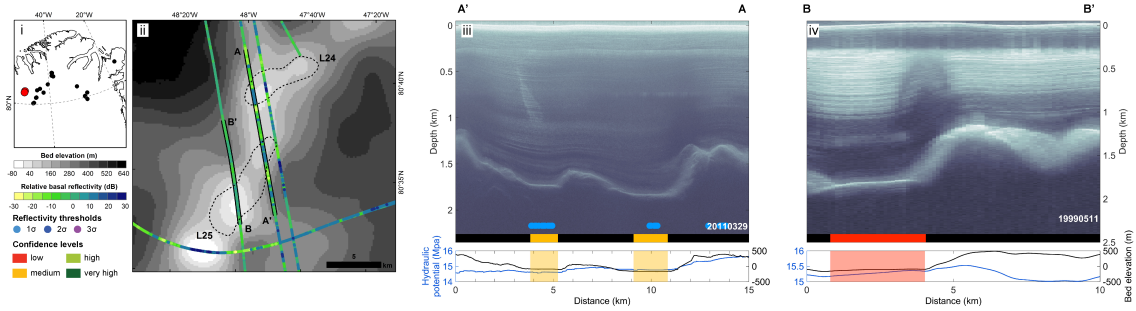

Figure A.12: Radar evidence for Greenland subglacial lakes. (i) Inset map showing location of subglacial lake L24 and L25 (red) and neighbouring lakes found in this study (black). (ii) Bed topography of the region with relative basal reflectivity along Operation IceBridge flight paths. Estimated lake extent is shown by the dashed line. Radar profile along transect (iii) A-A' (20110329_01_019) and (iv) B-B' (19990511_01_005). Subglacial lakes are depicted by a bar colour-coded according to the confidence level. Relative basal reflectivity thresholds, based on the statistics of the bed returned power within 20 km of the identified lake (1-3 σ from the mean), are indicated by the blue-purple circles. Lower graphs show bedrock elevation (black) and hydraulic potential (blue).

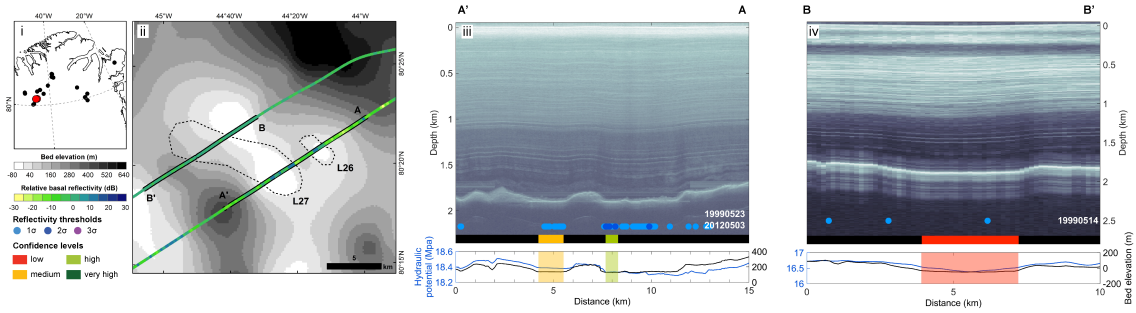

Figure A.13: Radar evidence for Greenland subglacial lakes. (i) Inset map showing location of subglacial lake L26 and L27 (red) and neighbouring lakes found in this study (black). (ii) Bed topography of the region with relative basal reflectivity along Operation IceBridge flight paths. Estimated lake extent is shown by the dashed line. Radar profile along transect (iii) A-A' (19990523_01_012/ 20120503_03_053) and (iv) B-B' (19990511_01_005). Subglacial lakes are depicted by a bar colour-coded according to the confidence level. Relative basal reflectivity thresholds, based on the statistics of the bed returned power within 20 km of the identified lake (1-3 σ from the mean), are indicated by the blue-purple circles. Lower graphs show bedrock elevation (black) and hydraulic potential (blue).

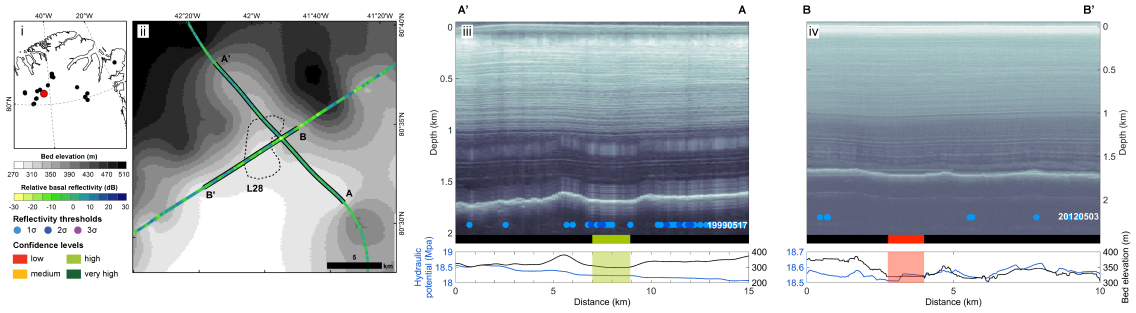

Figure A.14: Radar evidence for Greenland subglacial lakes. (i) Inset map showing location of subglacial lake L28 (red) and neighbouring lakes found in this study (black). (ii) Bed topography of the region with relative basal reflectivity along Operation IceBridge flight paths. Estimated lake extent is shown by the dashed line. Radar profile along transect (iii) A-A' (19990517_01_001) and (iv) B-B' (20120503_02_052). Subglacial lakes are depicted by a bar colour-coded according to the confidence level. Relative basal reflectivity thresholds, based on the statistics of the bed returned power within 20 km of the identified lake (1-3 σ from the mean),are indicated by the blue-purple circles. Lower graphs show bedrock elevation (black) and hydraulic potential (blue).

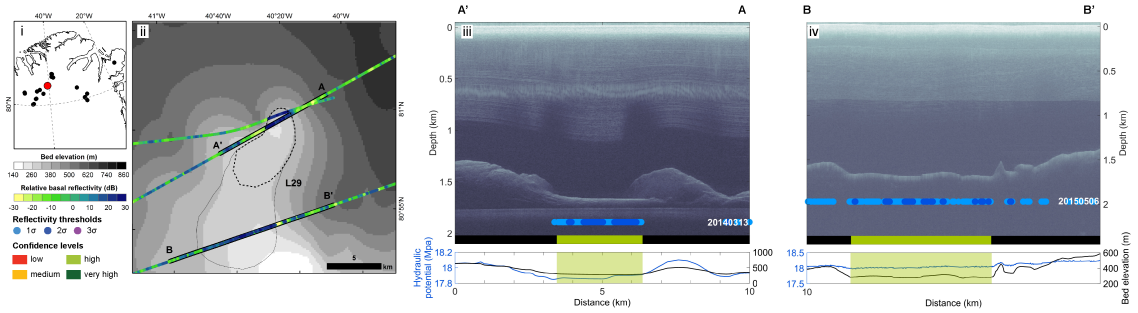

Figure A.15: Radar evidence for Greenland subglacial lakes. (i) Inset map showing location of subglacial lake L29 (red) and neighbouring lakes found in this study (black). (ii) Bed topography of the region with relative basal reflectivity along Operation IceBridge flight paths. Estimated lake extent is shown by the dashed line. Radar profile along transect (iii) A-A' (20140313_08_001) and (iv) B-B' (20150506_02_026) shows possible further extent. Subglacial lakes are depicted by a bar colour-coded according to the confidence level. Relative basal reflectivity thresholds, based on the statistics of the bed returned power within 20 km of the identified lake (1-3 σ from the mean), are indicated by the blue-purple circles. Lower graphs show bedrock elevation (black) and hydraulic potential (blue).

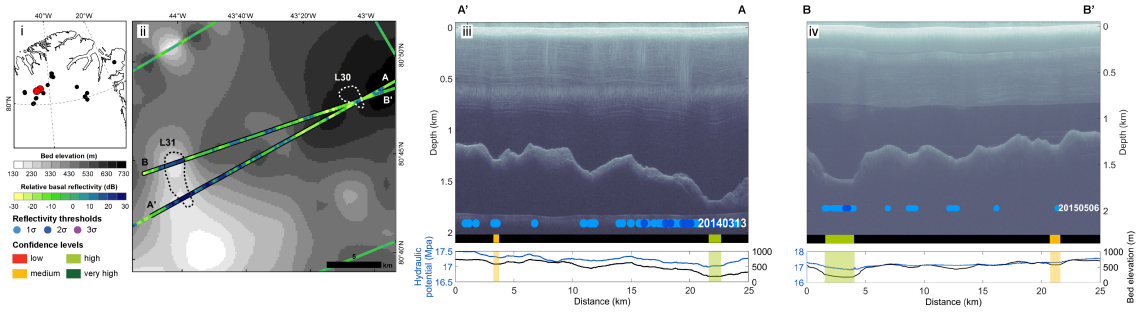

Figure A.16: Radar evidence for Greenland subglacial lakes. (i) Inset map showing location of subglacial lake L30 and L31 (red) and neighbouring lakes found in this study (black). (ii) Bed topography of the region with relative basal reflectivity along Operation IceBridge flight paths. Estimated lake extent is shown by the dashed line. Radar profile along transect (iii) A-A' (20140313_08_002) and (iv) B-B' (20120506_02_025). Subglacial lakes are depicted by a bar colour-coded according to the confidence level. Relative basal reflectivity thresholds, based on the statistics of the bed returned power within 20 km of the identified lake (1-3 σ from the mean), are indicated by the blue-purple circles. Lower graphs show bedrock elevation (black) and hydraulic potential (blue).

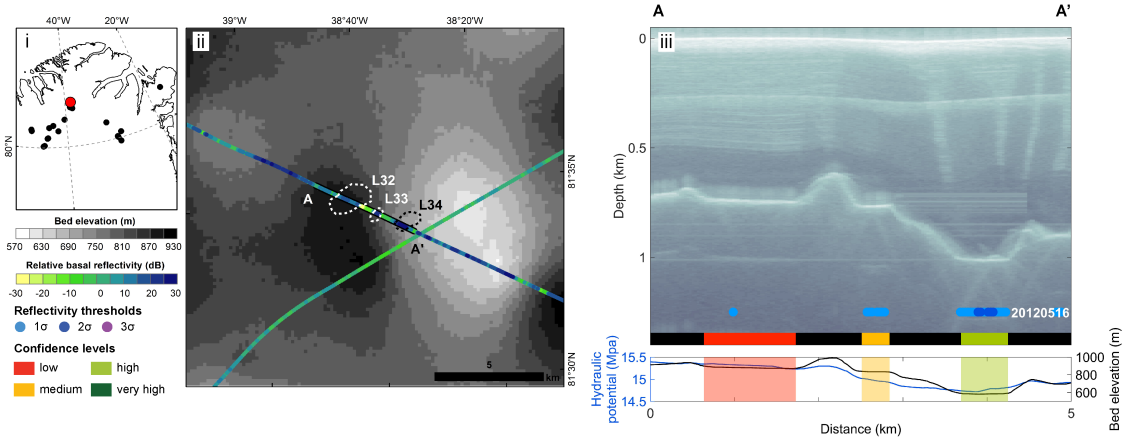

Figure A.17: Radar evidence for Greenland subglacial lakes. (i) Inset map showing location of subglacial lake L32, L33 and L34 (red) and neighbouring lakes found in this study (black). (ii) Bed topography of the region with relative basal reflectivity along Operation IceBridge flight paths. Estimated lake extent is shown by the dashed line. Radar profile along transect (iii) A-A' (20120516_01_059). Subglacial lakes are depicted by a bar colour-coded according to the confidence level. Relative basal reflectivity thresholds, based on the statistics of the bed returned power within 20 km of the identified lake (1-3 σ from the mean), are indicated by the blue-purple circles. Lower graphs show bedrock elevation (black) and hydraulic potential (blue).

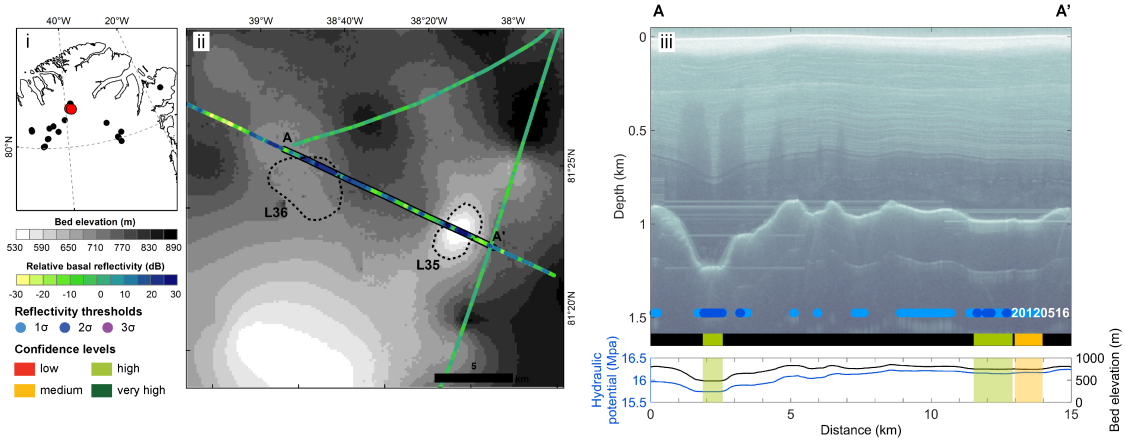

Figure A.18: Radar evidence for Greenland subglacial lakes. (i) Inset map showing location of subglacial lake L35 and L36 (red) and neighbouring lakes found in this study (black). (ii) Bed topography of the region with relative basal reflectivity along Operation IceBridge flight paths. Estimated lake extent is shown by the dashed line. Radar profile along transect (iii) A-A' (20120516_01_068). Subglacial lakes are depicted by a bar colour-coded according to the confidence level. Relative basal reflectivity thresholds, based on the statistics of the bed returned power within 20 km of the identified lake (1-3 σ from the mean), are indicated by the blue-purple circles. Lower graphs show bedrock elevation (black) and hydraulic potential (blue).

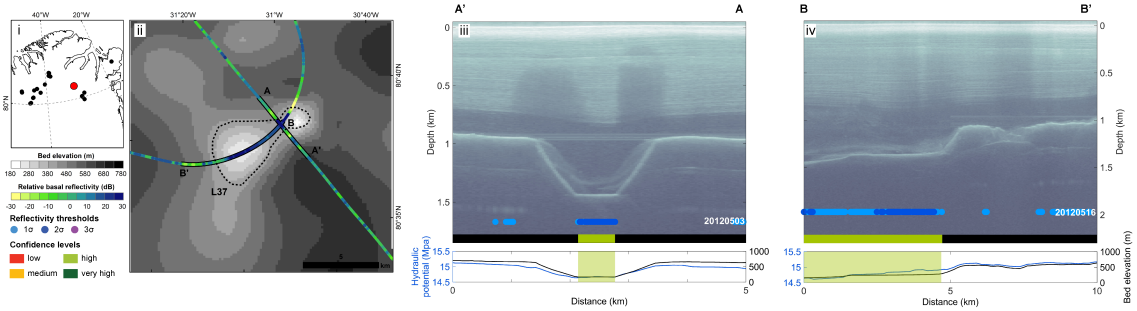

Figure A.19: Radar evidence for Greenland subglacial lakes. (i) Inset map showing location of subglacial lake L37 (red) and neighbouring lakes found in this study (black). (ii) Bed topography of the region with relative basal reflectivity along Operation IceBridge flight paths. Estimated lake extent is shown by the dashed line. Radar profile along transect (iii) A-A' (20120503_03_037) and (iv) B-B' (20120515_01_064). Subglacial lakes are depicted by a bar colour-coded according to the confidence level. Relative basal reflectivity thresholds, based on the statistics of the bed returned power within 20 km of the identified lake 1-3 σ from the mean), are indicated by the blue-purple circles. Lower graphs show bedrock elevation (black) and hydraulic potential (blue).

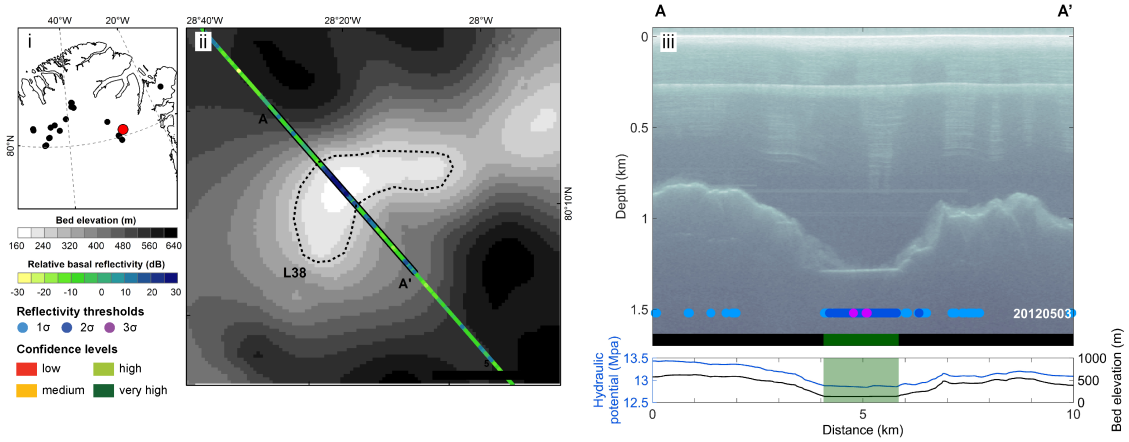

Figure A.20: Radar evidence for Greenland subglacial lakes. (i) Inset map showing location of subglacial lake L38 (red) and neighbouring lakes found in this study (black). (ii) Bed topography of the region with relative basal reflectivity along Operation IceBridge flight paths. Estimated lake extent is shown by the dashed line. Radar profile along transect (iii) A-A' (20120503_03_030). Subglacial lakes are depicted by a bar colour-coded according to the confidence level. Relative basal reflectivity thresholds, based on the statistics of the bed returned power within 20 km of the identified lake (1-3 σ from the mean), are indicated by the blue-purple circles. Lower graphs show bedrock elevation (black) and hydraulic potential (blue).

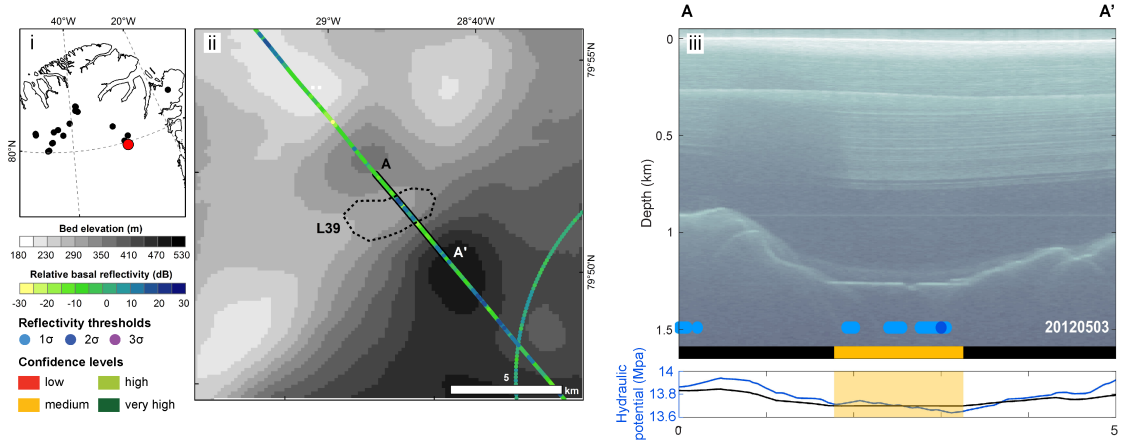

Figure A.21: Radar evidence for Greenland subglacial lakes. (i) Inset map showing location of subglacial lake L39 (red) and neighbouring lakes found in this study (black). (ii) Bed topography of the region with relative basal reflectivity along Operation IceBridge flight paths. Estimated lake extent is shown by the dashed line. Radar profile along transect (iii) A-A' (20120503_03_034). Subglacial lakes are depicted by a bar colour-coded according to the confidence level. Relative basal reflectivity thresholds, based on the statistics of the bed returned power within 20 km of the identified lake (1-3 σ from the mean), are indicated by the blue-purple circles. Lower graphs show bedrock elevation (black) and hydraulic potential (blue).

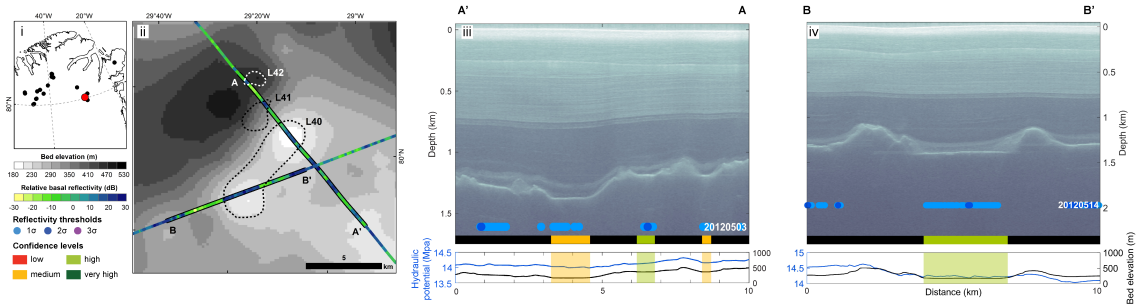

Figure A.22: Radar evidence for Greenland subglacial lakes. (i) Inset map showing location of subglacial lake L40, L41 and L42 (red) and neighbouring lakes found in this study (black). (ii) Bed topography of the region with relative basal reflectivity along Operation IceBridge flight paths. Estimated lake extent is shown by the dashed line. Radar profile along transect (iii) A-A' (20120503_03_035) and (iv) B-B' (20120514_02_003). Subglacial lakes are depicted by a bar colour-coded according to the confidence level. Relative basal reflectivity thresholds, based on the statistics of the bed returned power within 20 km of the identified lake 1-3 σ from the mean), are indicated by the blue-purple circles. Lower graphs show bedrock elevation (black) and hydraulic potential (blue).

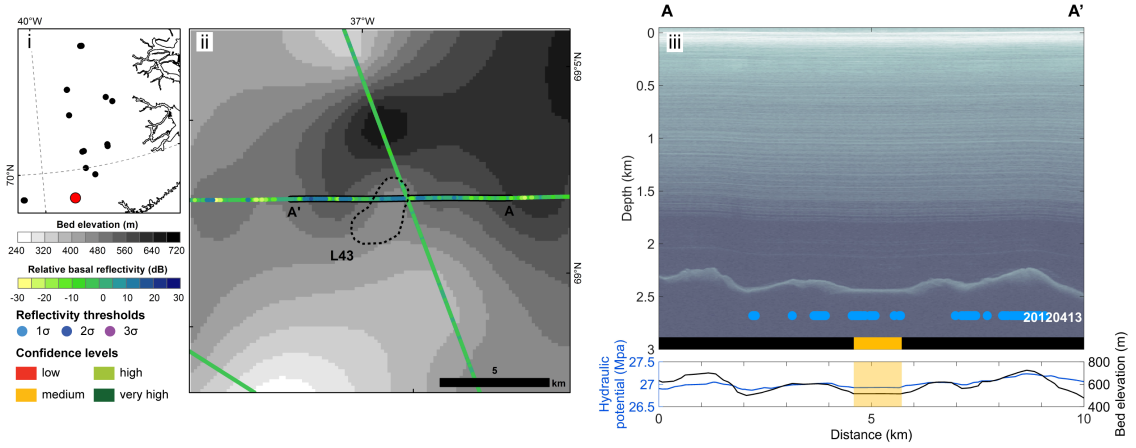

Figure A.23: Radar evidence for Greenland subglacial lakes. (i) Inset map showing location of subglacial lake L39 (red) and neighbouring lakes found in this study (black). (ii) Bed topography of the region with relative basal reflectivity along Operation IceBridge flight paths. Estimated lake extent is shown by the dashed line. Radar profile along transect (iii) A-A' (20120503_03_035). Subglacial lakes are depicted by a bar colour-coded according to the confidence level. Relative basal reflectivity thresholds, based on the statistics of the bed returned power within 20 km of the identified lake (1-3 σ from the mean), are indicated by the bl ue-purple circles. Lower graphs show bedrock elevation (black) and hydraulic potential (blue).

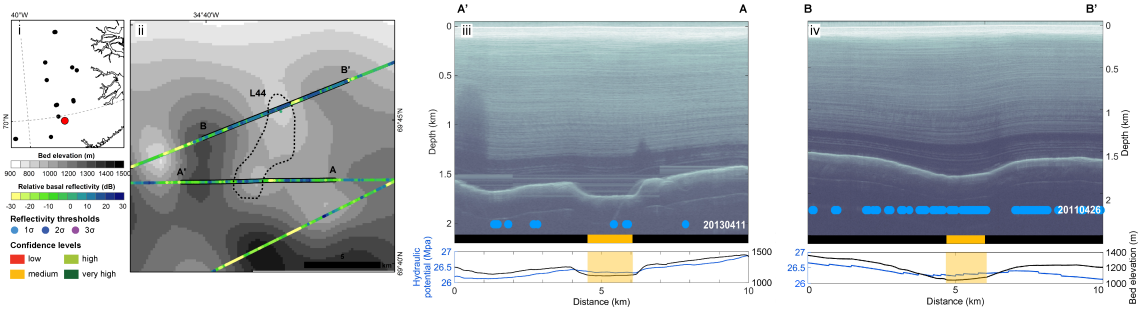

Figure A.24: Radar evidence for Greenland subglacial lakes. (i) Inset map showing location of subglacial lake L44 (red) and neighbouring lakes found in this study (black). (ii) Bed topography of the region with relative basal reflectivity along Operation IceBridge flight paths. Estimated lake extent is shown by the dashed line. Radar profile along transect (iii) A-A' (20130411_01_050) and (iv) B-B' (20140421_01_015). Subglacial lakes are depicted by a bar colour-coded according to the confidence level. Relative basal reflectivity thresholds, based on the statistics of the bed returned power within 20 km of the identified lake (1-3 σ from the mean), are indicated by the blue-purple circles. Lower graphs show bedrock elevation (black) and hydraulic potential (blue).

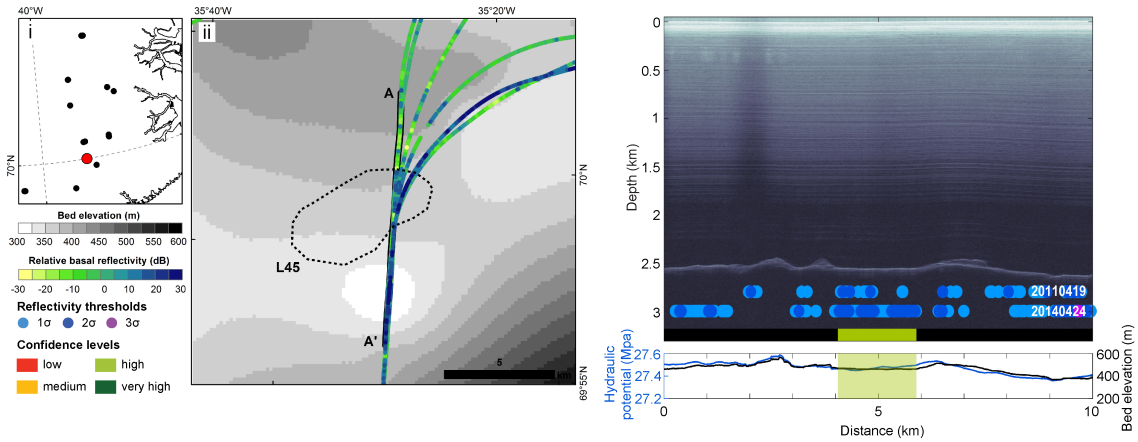

Figure A.25: Radar evidence for Greenland subglacial lakes. (i) Inset map showing location of subglacial lake L45 (red) and neighbouring lakes found in this study (black). (ii) Bed topography of the region with relative basal reflectivity along Operation IceBridge flight paths. Estimated lake extent is shown by the dashed line. Radar profile along transect (iii) A-A' (20110419_03_002/ 20140424_01_033). Subglacial lakes are depicted by a bar colour-coded according to the confidence level. Relative basal reflectivity thresholds, based on the statistics of the bed returned power within 20 km of the identified lake (1-3 σ from the mean), are indicated by the blue-purple circles. Lower graphs show bedrock elevation (black) and hydraulic potential (blue).

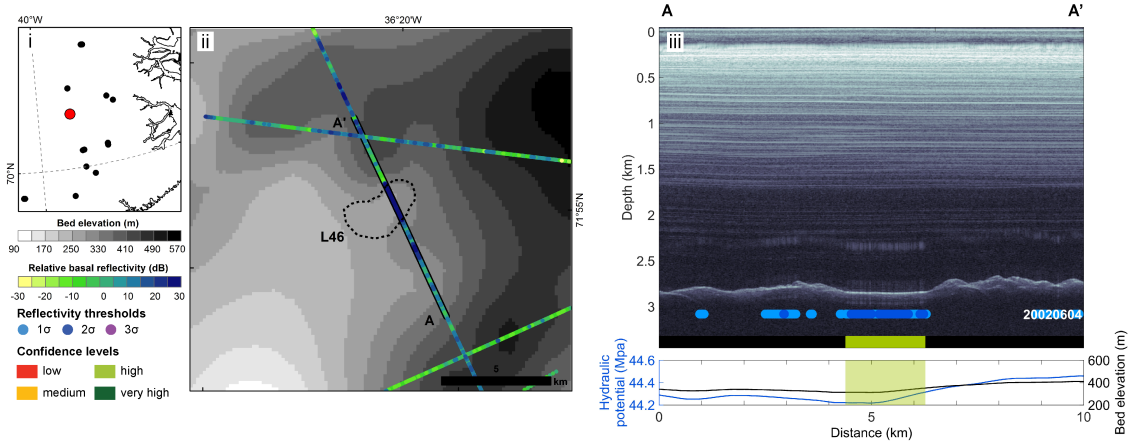

Figure A.26: Radar evidence for Greenland subglacial lakes. (i) Inset map showing location of subglacial lake L46 (red) and neighbouring lakes found in this study (black). (ii) Bed topography of the region with relative basal reflectivity along Operation IceBridge flight paths. Estimated lake extent is shown by the dashed line. Radar profile along transect (iii) A-A' (20020604_10_007). Subglacial lakes are depicted by a bar colour-coded according to the confidence level. Relative basal reflectivity thresholds, based on the statistics of the bed returned power within 20 km of the identified lake (1-3 σ from the mean), are indicated by the blue-purple circles. Lower graphs show bedrock elevation (black) and hydraulic potential (blue).

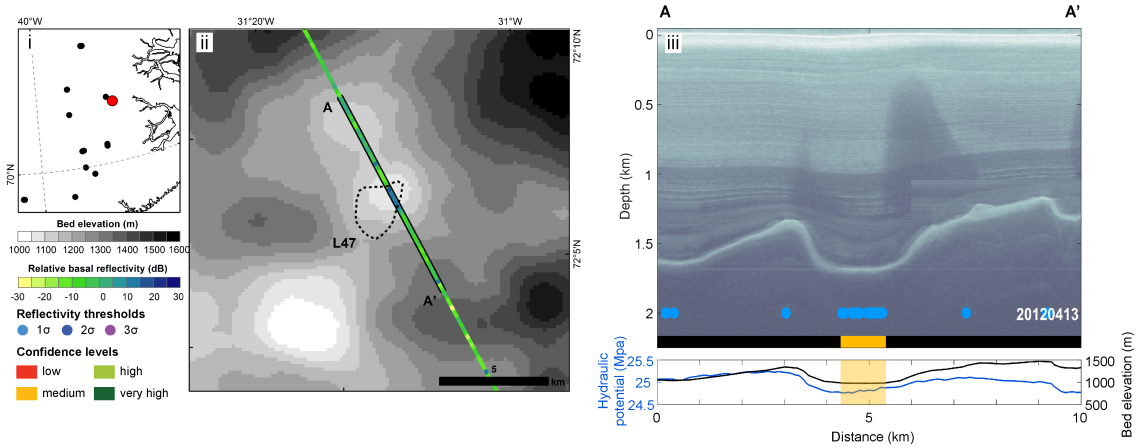

Figure A.27: Radar evidence for Greenland subglacial lakes. (i) Inset map showing location of subglacial lake L47 (red) and neighbouring lakes found in this study (black). (ii) Bed topography of the region with relative basal reflectivity along Operation IceBridge flight paths. Estimated lake extent is shown by the dashed line. Radar profile along transect (iii) A-A' (20120413_02_036). Subglacial lakes are depicted by a bar colour-coded according to the confidence level. Relative basal reflectivity thresholds, based on the statistics of the bed returned power within 20 km of the identified lake (1-3 σ from the mean), are indicated by the blue-purple circles. Lower graphs show bedrock elevation (black) and hydraulic potential (blue).

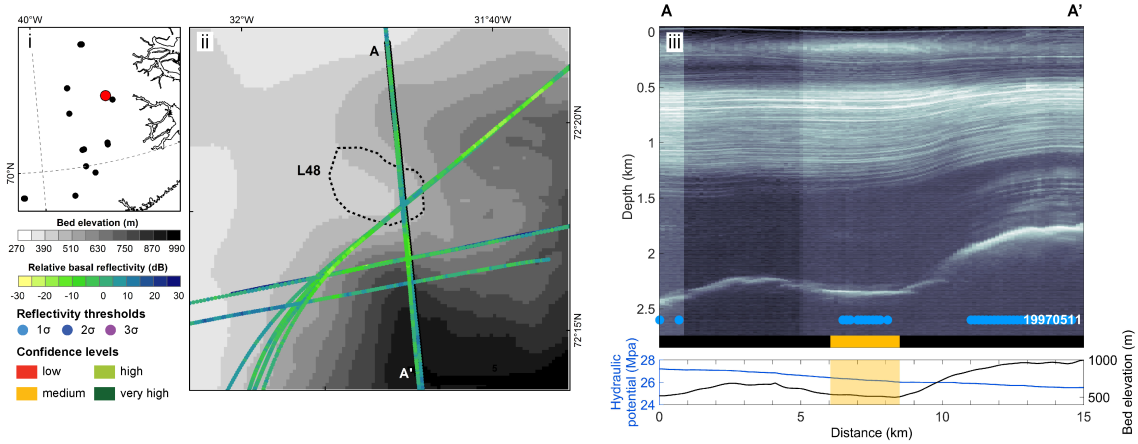

Figure A.28: Radar evidence for Greenland subglacial lakes. (i) Inset map showing location of subglacial lake L48 (red) and neighbouring lakes found in this study (black). (ii) Bed topography of the region with relative basal reflectivity along Operation IceBridge flight paths. Estimated lake extent is shown by the dashed line. Radar profile along transect (iii) A-A' (19970511_01_005). Subglacial lakes are depicted by a bar colour-coded according to the confidence level. Relative basal reflectivity thresholds, based on the statistics of the bed returned power within 20 km of the identified lake (1-3 σ from the mean), are indicated by the blue-purple circles. Lower graphs show bedrock elevation (black) and hydraulic potential (blue).

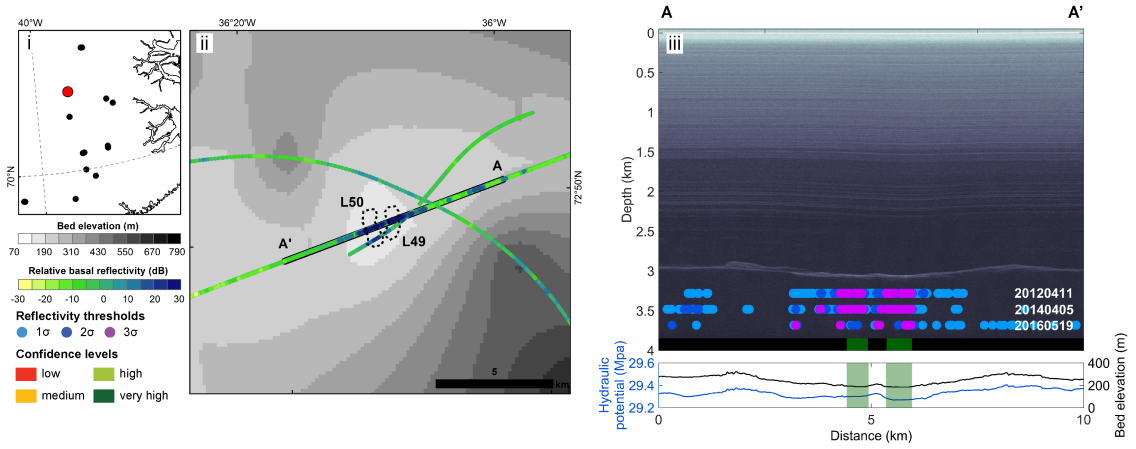

Figure A.29: Radar evidence for Greenland subglacial lakes. (i) Inset map showing location of subglacial lake L49 and L50 (red) and neighbouring lakes found in this study (black). (ii) Bed topography of the region with relative basal reflectivity along Operation IceBridge flight paths. Estimated lake extent is shown by the dashed line. Radar profile along transect (iii) A-A' (20120411_02_046/ 20140405_01_049/ 20160519_04_005). Subglacial lakes are depicted by a bar colour-coded according to the confidence level. Relative basal reflectivity thresholds, based on the statistics of the bed returned power within 20 km of the identified lake (1-3 σ from the mean), are indicated by the blue-purple circles. Lower graphs show bedrock elevation (black) and hydraulic potential (blue).

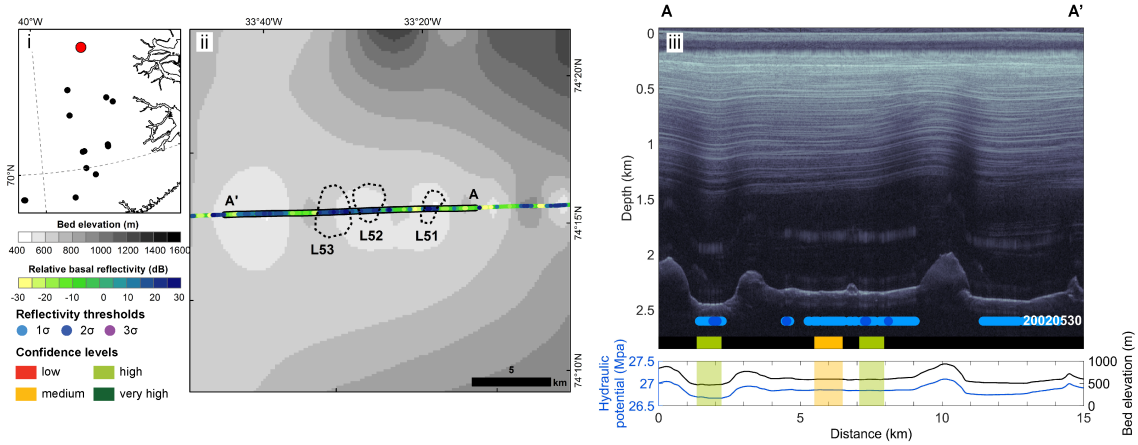

Figure A.30: Radar evidence for Greenland subglacial lakes. (i) Inset map showing location of subglacial lake L51, L52 and L52 (red) and neighbouring lakes found in this study (black). (ii) Bed topography of the region with relative basal reflectivity along Operation IceBridge flight paths. Estimated lake extent is shown by the dashed line. Radar profile along transect (iii) A-A' (20020530_05_001). Subglacial lakes are depicted by a bar colour-coded according to the confidence level. Relative basal reflectivity thresholds, based on the statistics of the bed returned power within 20 km of the identified lake (1-3 σ from the mean), are indicated by the blue-purple circles. Lower graphs show bedrock elevation (black)and hydraulic potential (blue).

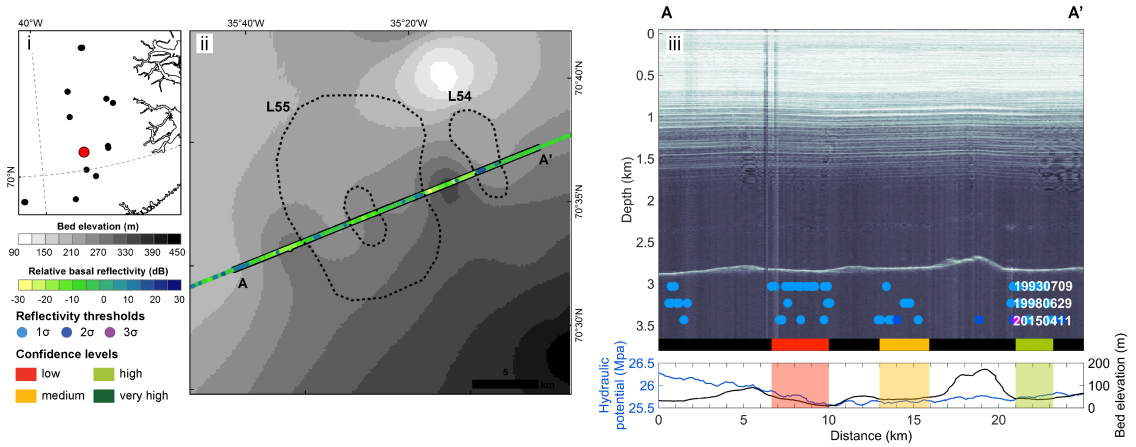

Figure A.31: Radar evidence for Greenland subglacial lakes. (i) Inset map showing location of subglacial lake L54 and L55 (red) and neighbouring lakes found in this study (black). (ii) Bed topography of the region with relative basal reflectivity along Operation IceBridge flight paths. Estimated lake extent is shown by the dashed line. Radar profile along transect (iii) A-A' (19930709_01_007/ 19980629_01_011/ 20150411_01_016). Subglacial lakes are depicted by a bar colour-coded according to the confidence level. Relative basal reflectivity thresholds, based on the statistics of the bed returned power within 20 km of the identified lake (1-3 σ from the mean), are indicated by the blue-purple circles. Lower graphs show bedrock elevation (black) and hydraulic potential (blue).

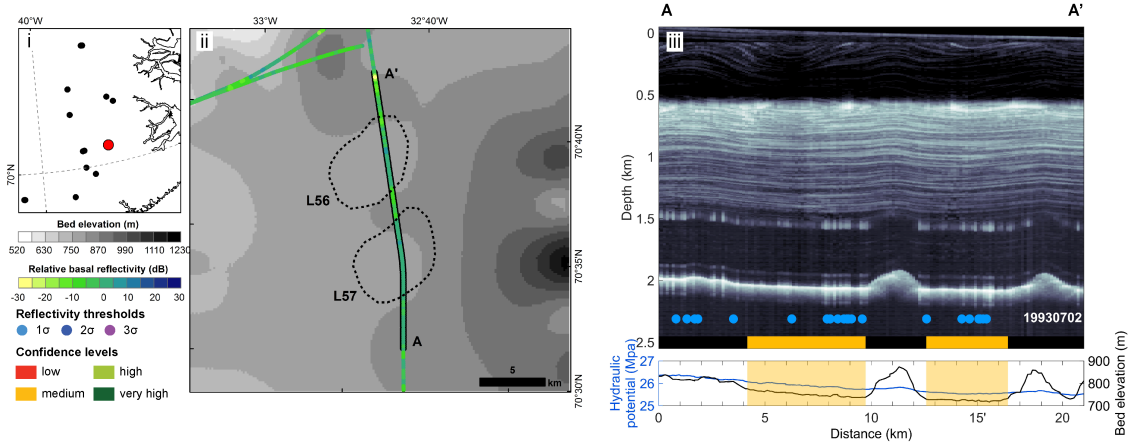

Figure A.32: Radar evidence for Greenland subglacial lakes. (i) Inset map showing location of subglacial lake L56 and L57 (red) and neighbouring lakes found in this study (black). (ii) Bed topography of the region with relative basal reflectivity along Operation IceBridge flight paths. Estimated lake extent is shown by the dashed line. Radar profile along transect (iii) A-A' (19930702_01_012). Subglacial lakes are depicted by a bar colour-coded according to the confidence level. Relative basal reflectivity thresholds, based on the statistics of the bed returned power within 20 km of the identified lake (1-3 σ from the mean), are indicated by the blue-purple circles. Lower graphs show bedrock elevation (black) and hydraulic potential (blue).

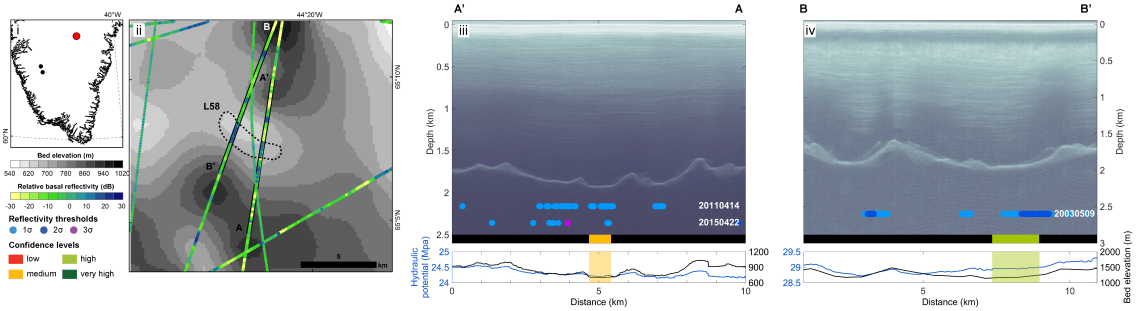

Figure A.33: Radar evidence for Greenland subglacial lakes. (i) Inset map showing location of subglacial lake L58 (red) and neighbouring lakes found in this study (black). (ii) Bed topography of the region with relative basal reflectivity along Operation IceBridge flight paths. Estimated lake extent is shown by the dashed line. Radar profile along transect (iii) A-A' (20110414_06_002/ 20150422_06_011) and (iv) B-B' (20030509_01_004). Subglacial lakes are depicted by a bar colour-coded according to the confidence level. Relative basal reflectivity thresholds, based on the statistics of the bed returned power within 20 km of the identified lake (1-3 σ from the mean), are indicated by the blue-purple circles. Lower graphs show bedrock elevation (black) and hydraulic potential (blue).

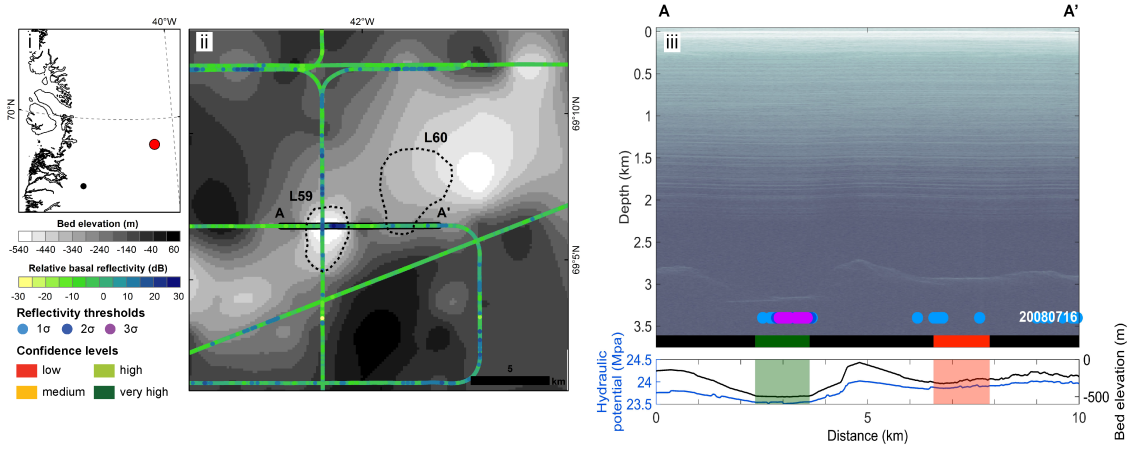

Figure A.34: Radar evidence for Greenland subglacial lakes. (i) Inset map showing location of subglacial lake L59 and L60 (red) and neighbouring lakes found in this study (black). (ii) Bed topography of the region with relative basal reflectivity along Operation IceBridge flight paths. Estimated lake extent is shown by the dashed line. Radar profile along transect (iii) A-A' (20080716_02_007). Subglacial lakes are depicted by a bar colour-coded according to the confidence level. Relative basal reflectivity thresholds, based on the statistics of the bed returned power within 20 km of the identified lake (1-3 σ from the mean), are indicated by the blue-purple circles. Lower graphs show bedrock elevation (black) and hydraulic potential (blue).

Appendix B

Supplementary material for Chapter 3: Detecting active subglacial lakes beneath the Greenland Ice Sheet using high-resolution digital elevation models

Supplementary Information for Chapter 3: Detecting active subglacial lakes beneath the Greenland Ice Sheet using high-resolution digital elevation models

The document includes:

Supplementary Methods

1. ArcticDEM processing
2. Classification framework

B.1 ArcticDEM processing

We downloaded 26,342 release 7 ArcticDEM Strip DSMs (Porter et al., 2018) at 2 m resolution from the PGC (https://www.pgc.umn.edu/data/arcticdem/), totalling >30 TB of data. Strip DSMs within the 699,448 km^2 region of interest were selected, with the earliest acquisition date of 29th March 2008 until 10th April 2019. The region of interest covers approximately 39% of the Greenland Ice Sheet, within 50 km of the ice margin, containing all outlet glaciers and ice caps. We bypass the interior of the ice sheet as this is largely frozen to the bed, where active subglacial lakes are unlikely to be situated.

To improve the vertical accuracy and spatial location of the Strip DSMs, we iteratively georeference each DSM using the dx, dy and dz offsets provided in the metadata by the PGC team. These translation values are calculated using ICESat altimetry data which have been filtered to exclude hydrographic features and regions with high relief, and where available, LiDAR or surveyed GPS points (Porter et al., 2018). The number of ICESat ground control points (GCPs) that were used to georeference the Strip DSMs, and the mean vertical residual difference between the ICESat GCPs and the ArcticDEM DSMs after adjustment, are available in the ArcticDEM metadata. We georeferenced 17,855 Strip DSMs where translation offsets were available (mean dx, dy and dz offset values of 0.02, 0.02 and -1.2 m, respectively, although these can vary between -2,000 and 2,000 m). The remaining DSMs were left uncorrected.

B.1.1 DSM filtering: Calibration

Elevation values in the Strip DSMs are subject to a number of types of error due to photogrammetric blunders, the presence of cloud, fog and shadow, systematic errors caused by the SETSM autocorrelation or poor edge matching (Porter et al., 2018). Following georeferencing, we performed an initial filtering step to remove Strip DSMs containing extreme outliers using the 100 m ArcticDEM Mosaic as a homogeneous reference DEM. All Strip DSMs were first resampled to 100 m using cubic interpolation to match the Mosaic resolution. Second, we calculated the mean

Known lake	Area (km^2)	Max depth (m)	Volume (km^3)	References
Flade Isblink ice cap	8.4	70	0.4	Willis et al. (2015)
Inugpait Quat	1.4	60	0.0048	Palmer et al. (2015); Howat et al. (2015)
Sioqaap Sermia (North)	0.18	15.4		Bowling et al. (2019)
Sioqaap Sermia (South)	0.64	18.1		Bowling et al. (2019)
Insuguata Sermia (1)	0.93	17	0.0065	Livingstone et al. (2019)
Insuguata Sermia (2)	0.88	30	0.013	Livingstone et al. (2019)
Insuguata Sermia (3)	0.67	14	0.0035	Livingstone et al. (2019)

Table B.1: Known active subglacial lakes in Greenland and their key characteristics.

and standard deviation of elevation differences dh between the reference DEM h_{MOS} and each Strip DSM h_{STR}. For example the Strip DSM acquired on 18th September 2014 at Flade Isblink active subglacial lake (Willis et al., 2015) contains elevation differences of up to -500 m relative to the reference DEM (Figure B.1a), whereas the Strip DSM acquired on 24th July 2013 contains little to no visual artefacts (Figure B.1b). The footprint of the 70 m deep, mitten-shaped collapse basin (Willis et al., 2015), is observed within the black box (Figure B.1a-b). This procedure was performed at all of the seven known active subglacial lakes in Greenland to define and test which threshold use, before applying a filter on an ice sheet scale.

A combined total of 124 Strip DSMs were available over the seven known active subglacial lakes between 2009 and 2018. The majority (93%) of these Strip DSMs have an absolute mean dh less than 10 m, however 6 Strip DSMs acquired in September 2014 and May 2017 exceed 20 m absolute mean dh (Figure B.1c-d). Elevation measurement error (σ dh) was also estimated for each Strip DSM covering the known active subglacial lakes (Figure B.1c-d). 16 Strip DSMs (13%) have high measurement error (σ dh >20 m), including 10 Strips which were not distinguished as outliers using an absolute mean dh greater than 20 m (Figure B.1e-f). Manual, visual analysis of these additional 10 DSMs confirms that they contain outliers. Large mean dh indicates a large elevation bias across a Strip, whilst large standard deviation of dh indicates localised elevation artefacts within the Strip or perhaps increases in elevation across the entire Strip. We therefore use standard deviation dh as a conservative measure to deal with these erroneous DSMs. To constrain and validate the filter we test thresholds (t) of standard deviation dh greater than $t = 10$ m, $t = 20$ m and $t = 50$ m to all seven known active subglacial lakes individually (Table B.1).

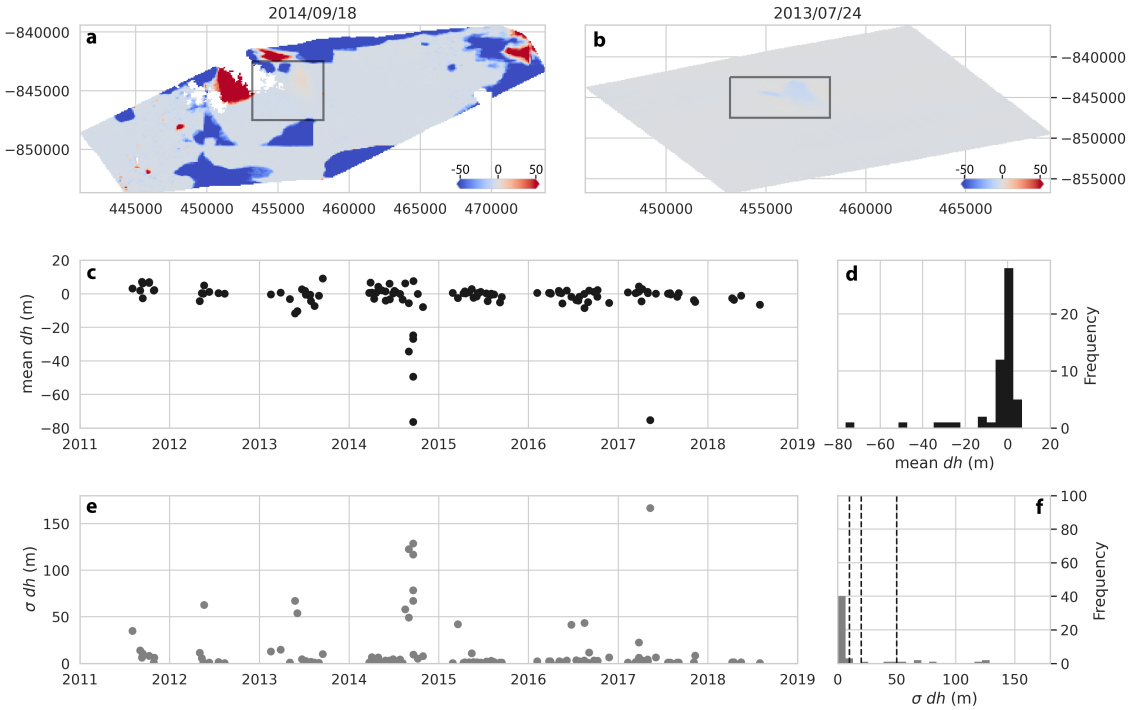

Figure B.1: Filtering of Strip DSMs with reference DEM. (a) Example of elevation difference (*dh*) between 100 m ArcticDEM Mosaic and ArcticDEM Strip DSM acquired on 19th September 2014 containing artefacts at Flade Isblink active subglacial lake detected in (Willis et al., 2015). The signature of the active subglacial lake can be seen in the black box. (b) Elevation differences (dh) between 100 m ArcticDEM Mosaic and ArcticDEM Strip DSM acquired on 24th July 2013, representing a Strip DSM at Flade Isblink active subglacial lake with few or no artefacts. The signature of the active subglacial lake can again be seen in the black box. (c) Mean *dh* between the reference DEM and all available Strip DSMs at all seven known active subglacial lakes, showing several Strips acquired in 2014 which exhibit large (>20 m) absolute differences relative to the reference DEM. (d) Histogram frequency diagram of mean *dh* between reference DEM and Strip DSMs showing most Strips have mean *dh* between -20 and 20 m. (e) Standard deviation of *dh* between reference DEM and each Strip DSM. The majority (87%) of Strips exhibit σ *dh* less than 20 m, with 16 Strips exceeding 20 m *sigma dh*. (f) Histogram of standard deviation of *dh*, showing most Strips below 10 m. Dashed line represent thresholds ($t = 10$, $t = 20$, and $t = 50$ m) used for filtering Strip DSMs.

B.1.1.1 Flade Isblink Ice Cap

The largest recorded subglacial lake in Greenland is situated at the Flade Isblink, a large ice cap in northeast Greenland (Willis et al., 2015). A ∼8 km^2, 70 m deep, mitten-shaped collapse basin was detected near the ice divide using a combination of LiDAR, DEMs derived from stereo satellite imagery, MODIS optical imagery and IceBridge airborne laser altimetry (Willis et al., 2015). The collapse basin formed over a 21-day period in late summer of 2011, due to the sudden drainage of an estimated 0.4 km^3 subglacial lake that was recharged by surface meltwater (Willis et al., 2015).

A total of 53 georeferenced Strip DSMs were available at this site between 2012 and 2017 (Figure B.2a). To assess the impact of choosing different thresholds for filtering Strip DSMs which include errors and artefacts, we tested several threshold values (t = 10 m, t = 20 m, t = 50 m) on the standard deviation of dh. Using these thresholds, a total of 7, 10 and 13 Strip DSMs were identified as outliers, respectively, and consequently removed (Figure B.2a-d).

The temporal variance of elevation was then calculated for each filtering threshold, by creating three-dimensional arrays (time t, space x and y; hereafter referred to as "stacks") of elevation h_{STR}(t, x, y) and calculating the standard deviation of elevation per pixel within the 5 km^2 grid square (Figure B.2e-h). Before filtering, several rectangular artefacts are evident within the standard deviation map, due to erroneous elevation values within individual DSMs (Figure B.2e).

Taking a transect across the collapse basin, shown by the white dashed line in Figure B.2e, we assess how this feature has evolved over time, as well as depict any artefacts or height errors in the DSMs which are removed by each filtering threshold (Figure B.2i-l). The timeseries of elevation within the basin and outside of the basin (shown by squares and triangles in Figures B.2a-d) shows rising of the floor of the basin over time, due to the slow refilling of the subglacial lake below, and extends the current record since the study of Willis et al., 2015. The red, orange and green symbols correspond to the strips removed in each threshold standard deviation dh greater than t = 10 m, t = 20 m, and t = 50 m.

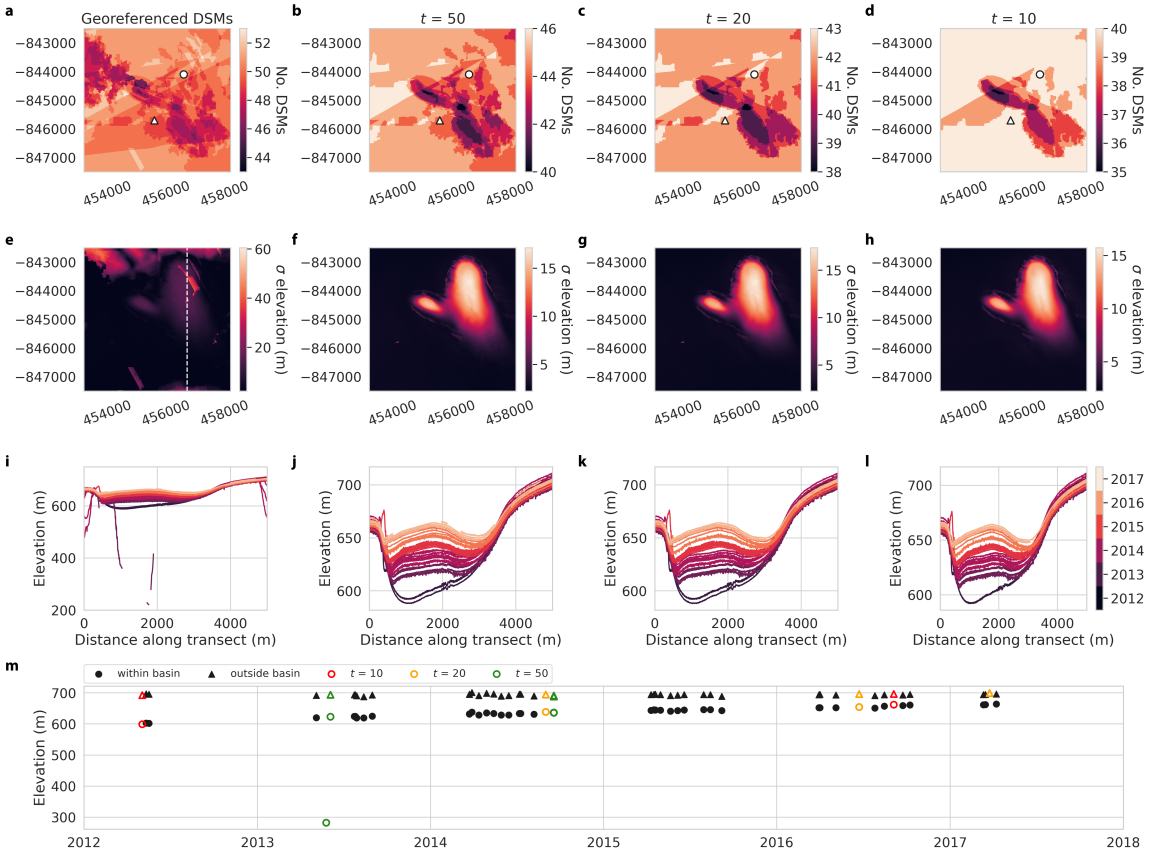

Figure B.2: Testing the impact of various filtering threshold values (standard deviation of dh greater than $t = 10$ m, $t = 20$ m, $t = 50$ m) at Flade Isblink active subglacial lake, detected by (Willis et al., 2015). (a) Number of georeferenced Strip DSMs within black outline shown in Figure B.1a-b. (b) Number of Strip DSMs after Strips with standard deviation of dh >50 m have been removed, where dh is the per-pixel difference in elevation between the DSM Strip and reference Mosaic. (c) Number of DSMs after Strips with standard deviation of dh >20 m have been removed. (d) Number of DSMs after Strips with standard deviation of dh >10 m have been removed. (e) Standard deviation of the elevation recorded by all DSM's; the dashed white line is the transect used for panels (i-l). (f) Standard deviation of elevation with <50 m dh threshold applied. (g) Standard deviation of elevation with <20 m dh threshold applied. (h) Standard deviation of elevation with <10 m dh threshold applied. The collapse basin is not visible in panel e, due to artefacts in individual DSMs, but is visible in panels f-h (i) Transect across basin with no thresholds applied, showing evolution of the ice surface through time. (j) Transect across basin using $t = 50$ m. (k) Transect across basin using $t = 20$ m. (l) Transect across basin using $t = 10$ m. (m) Timeseries of surface elevation within the basin (circles) and outside of the basin (triangles). Elevation points removed using standard deviation of dh greater than $t = 10$ m, $t = 20$ m, $t = 50$ m are displayed in red, orange and green, respectively.

B.1.1.2 Inugpait Quat

A ∼1.4 km^2, ∼60 m deep collapse basin was detected in southwestern Greenland, about 48 km inland from Inugpait Quat, in two studies (Howat et al., 2015; Palmer et al., 2015). The collapse basin formed over a 14-day period in summer 2011, due to the sudden drainage of an estimated 0.04 km^3 subglacial lake beneath the ice sheet, which was supplied by surface meltwater over several melt seasons (Palmer et al., 2015). Both studies use DEMs derived from stereo-image pairs, ICESat altimetry and optical imagery to evaluate the evolution of this feature (Howat et al., 2015; Palmer et al., 2015).

A total of 24 ArcticDEM DSMs are available at this site between 2011 and 2018. Using the same approach as for Flade Isblink (Section B.1.1.1), thresholds on the standard deviation of dh greater than $t = 10$ m, $t = 20$ m and $t = 50$ m removed a total of 1, 2 and 2 DSMs, respectively (Figure B.3a-d).

Like the previous known active subglacial lake, the temporal variance of elevation was then calculated for each filtering threshold, by creating three-dimensional arrays stacks of elevation h_{STR}(t, x, y) and calculating the standard deviation of elevation per pixel within the 5 km^2 grid square (Figure B.3e-h). The collapse basin presents a clear signal with high standard deviation of elevation, with a small artefact (<20m wide) with high (>30 m) standard deviation of elevation is apparent about 2.5 km southwest of the collapse basin (Figure B.3e). This artefact is removed when using all threshold values (Figure B.3f-h). Whilst the artefact does not coincide with the collapse basin itself, our method is developed to detect unknown active subglacial lakes, and therefore these artefacts need to be removed to reduce false positives.

Taking a transect across the basin, shown by the white dashed line in Figure B.3e, shows how the ice surface elevation above the subglacial lake has evolved over time, with no evidence outliers within the basin (Figure B.3i-l). The timeseries of elevation within the basin and outside of the basin (locations shown by circles and triangles in Figures B.3a-d) adds an additional seven years worth of interannual elevation coverage, compared with two elevation datasets in previous literature (Palmer et al., 2015). ArcticDEM data suggest that the subglacial lake is slowly refilling by 7.5 m a^{-1}

following the drainage event in 2011. The red, orange and green circles and triangles correspond to the Strips removed in each threshold standard deviation of *dh* greater than $t = 10$ m, $t = 20$ m, $t = 50$ m.

B.1.1.3 Sioqqap Sermia

Two collapse basins were identified in southwestern Greenland near Sioqqap Sermia, with areas of 0.2 and 0.6 km^2 and depths of 15 and 18 m, respectively. These were both detected in Chapter 3 through large-scale assessment of surface depressions in the time-averaged ArcticDEM Mosaic. The ice surface collapsed in summer 2012 at both basins, and had subsequently risen by 11 m at the northern basin, and 14 m at the southern basin by 2015 (Chapter 3). The subglacial lake beneath is thought to be recharged by surface meltwater from nearby supraglacial lakes and streams.

A total of 7 ArcticDEM DSMs were obtained at the northern collapse basin between 2012 and 2017, whilst 6 DSMs were acquired between 2012 and 2018 at the basin approximately 35 km further south. As before, we calculate the standard deviation of elevation per pixel within the stack of h_{STR}(t, x, y) per threshold (Figure B.4e-h). No DSMs were removed in any of the thresholds at the northern basin (Figure B.4a-d). For this reason, the standard deviation of elevation remained unchanged for each threshold (Figure B.4e-h). Taking a transect across the basin, shown by the white dashed line in Figure B.4e, again shows how this feature has evolved over time (Figure B.4i-l). The basin sits in a deepening in the ice surface, and the profile shows the main basin is about 18 m deep, with a shallower 8 m basin. The timeseries of elevation within the basin and outside of the basin (location shown by the circle and triangle in Figures B.4a-d) shows slow refilling of the subglacial lake between 2012 and 2016, compared to the relatively stable surrounding ice surface. The floor of the basin then begins to lower again in 2017 which coincide with the beginning of another drainage event. The addition of these data to extend the timeseries by two years compared to previous literature enables us to identify these types of behaviours.

At the southern collapse basin, 1 DSM acquired in 2012 is removed in all threshold values (Figure B.5a-d). The standard deviation of elevation plots identify the collapse

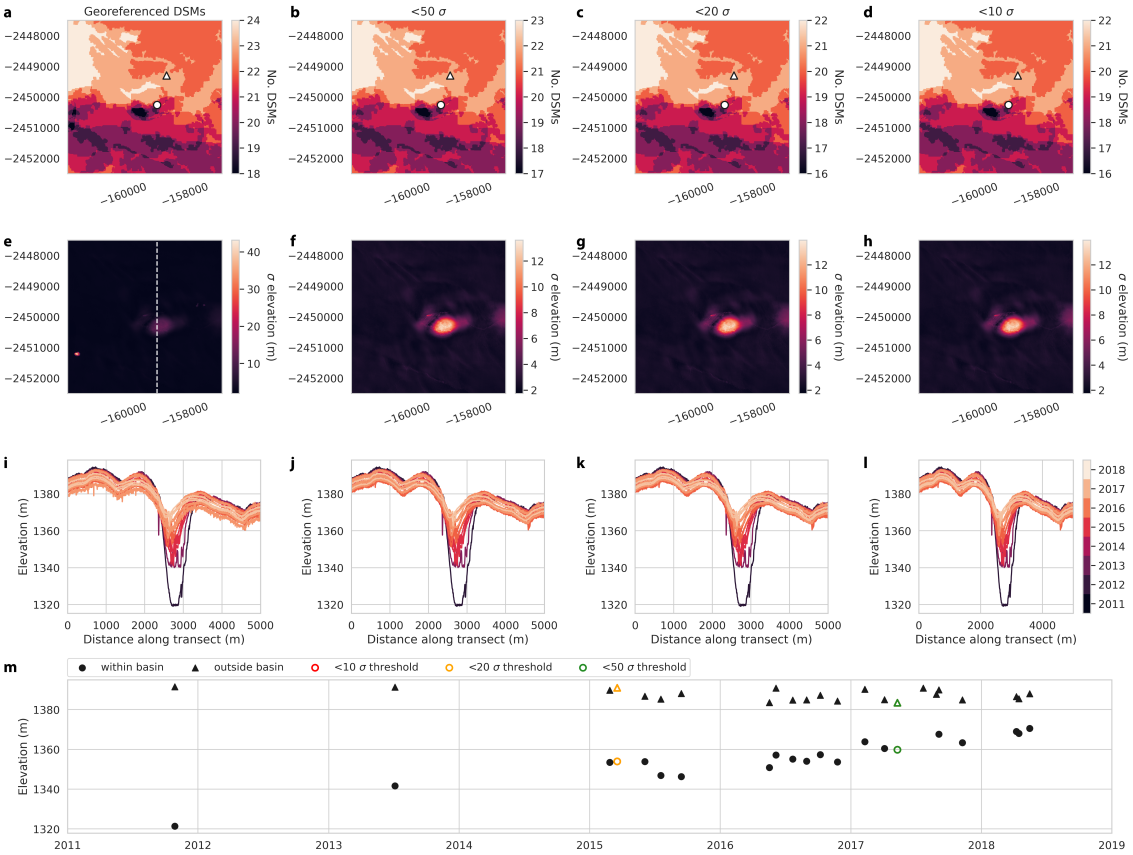

Figure B.3: Testing the impact of various filtering threshold values (standard deviation of dh greater than $t = 10$ m, $t = 20$ m, $t = 50$ m) at Inugpait Quat active subglacial lake detected by Palmer et al., 2015. (a) Number of georeferenced DSMs within 25 km^2 grid. Circles and triangles represent points within and outside the basin for the elevation timeseries in panel m (b) Number of Strip DSMs after Strips with standard deviation of dh >50 m have been removed, where dh is the per-pixel difference in elevation between the DSM Strip and reference Mosaic (c) Number of DSMs after Strips with standard deviation of dh >20 m have been removed. (d) Number of DSMs after Strips with standard deviation of dh >10 m have been removed. (e) Standard deviation of the elevation recorded by all DSM's; the dashed white line is the transect used for panels (i-l). (f) Standard deviation of elevation with <50 m dh threshold applied. (g) Standard deviation of elevation with <20 m dh threshold applied. (h) Standard deviation of elevation with <10 m dh threshold applied. The collapse basin is visible in in all panels, shown by a high standard deviation of elevation signal. A small artefact in an individual DSM is visible in panels e (i) Transect across basin with no thresholds applied, showing evolution of the ice surface between 2011 and 2018. (j) Transect across basin using $t = 50$ m. (k) Transect across basin using $t = 20$ m. (l) Transect across basin using $t = 10$ m. (m) Timeseries of surface elevation within the basin (circles) and outside of the basin (triangles). Elevation points removed using standard deviation of dh greater than $t = 10$ m, $t = 20$ m, $t = 50$ m are displayed in red, orange and green, respectively.

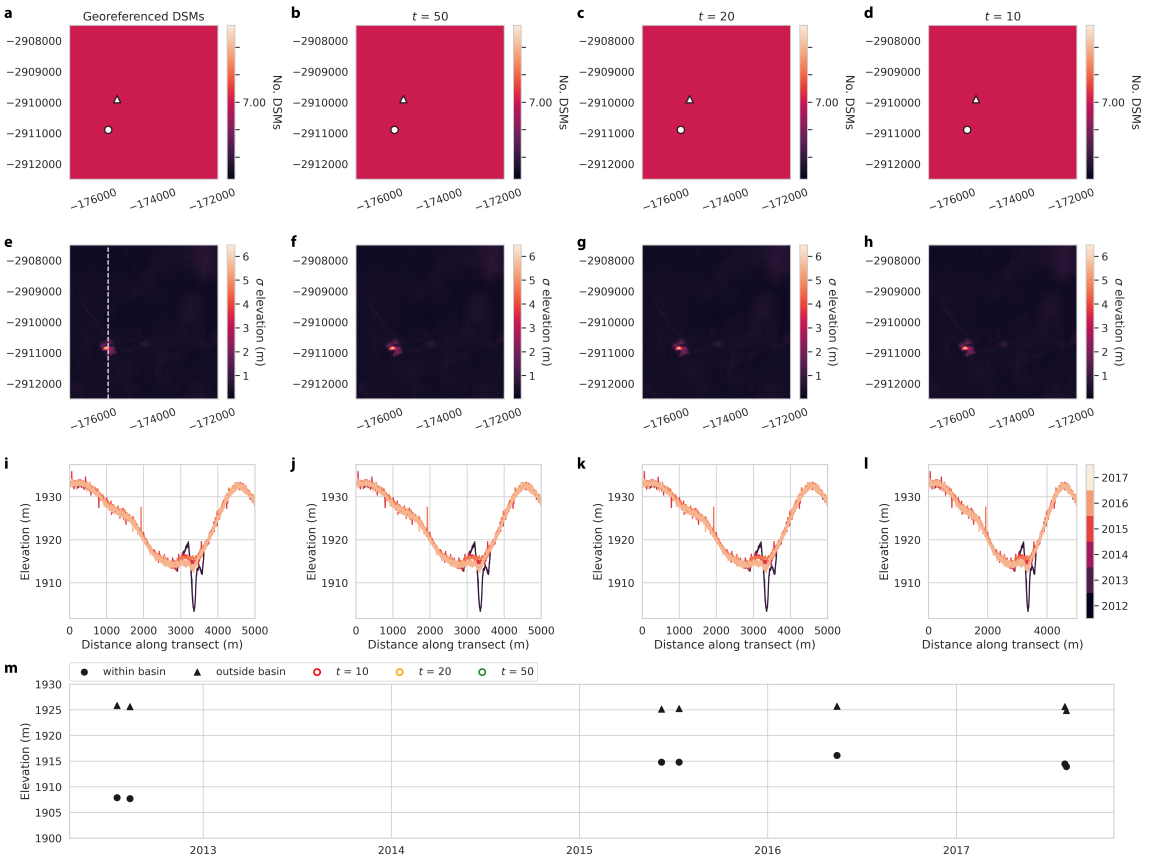

Figure B.4: Testing the impact of various filtering threshold values (standard deviation of dh greater than $t = 10$ m, $t = 20$ m, $t = 50$ m) at Sioqqap Sermia (northern) active subglacial lake detected in Chapter 2.2. (a) Number of georeferenced DSMs within 25 km^2 grid. Circles and triangles represent points within and outside the basin for the elevation timeseries in panel m (b) Number of Strip DSMs after Strips with standard deviation of dh >50 m have been removed, where dh is the per-pixel difference in elevation between the DSM Strip and reference Mosaic (c) Number of DSMs after Strips with standard deviation of dh >20 m have been removed. (d) Number of DSMs after Strips with standard deviation of dh >10 m have been removed. (e) Standard deviation of the elevation recorded by all DSM's; the dashed white line is the transect used for panels (i-l). (f) Standard deviation of elevation with <50 m dh threshold applied. (g) Standard deviation of elevation with <20 m dh threshold applied. (h) Standard deviation of elevation with <10 m dh threshold applied. The collapse basin is visible in in all panels, shown by a high standard deviation of elevation signal. No visible artefacts are apparent within the grid square. (i) Transect across basin with no thresholds applied, showing evolution of the ice surface between 2011 and 2018. (j) Transect across basin using $t = 50$ m. (k) Transect across basin using $t = 20$ m. (l) Transect across basin using $t = 10$ m. (m) Timeseries of surface elevation within the basin (circles) and outside of the basin (triangles). Elevation points removed using standard deviation of dh greater than $t = 10$ m, $t = 20$ m, $t = 50$ m are displayed in red, orange and green, respectively.

basin as having a high (>10 m), localised signal, relative to the surrounding ice (Figure B.5e-h). The removal of 1 DSM does not alter the standard deviation by much, reducing the maximum standard deviation of elevation from 12.9 to 10.8 m (Figure B.5e-h). Figure B.5i-l show the 30 m deep collapse basin which formed in 2012, compared to the relatively stable surrounding ice surface. The floor of the basin rose by approximately 24 m over the six years following the drainage event (3.8 m a^{-1}), due to refilling of the subglacial lake beneath (Bowling et al., 2019). In 2018, a supraglacial lake formed in the collapse basin, as shown by the flat surface topography which is indicative of the presence of water (Figure B.5i-l).

B.1.1.4 Isunguata Sermia

By differencing ArcticDEM strips and calculating relative elevation change, Livingstone et al., 2019 identified three active subglacial lakes in close proximity near the lateral margin of Isunguata Sermia, west Greenland (Livingstone et al., 2019). The ice surface depressions had areas of 0.9, 0.9, and 0.7 km^2, with maximum depths of 17, 13 and 14 m, respectively (Livingstone et al., 2019).

A total of 35 ArcticDEM DSMs were obtained for these lakes between 2009 and 2017 (Figure B.6a). These subglacial lakes are near the margin of the ice sheet where ArcticDEM tends to have more artefacts due to misalignment in mountainous terrain or over water bodies, therefore the land has been masked here. Lake 1 and Lake 3 have weak signals in the standard deviation of elevation, whereas Lake 2 has a clearer signal.

Applying thresholds on the standard deviation of dh $t = 50$, $t = 20$ and $t = 10$ m, a total of 1, 3 and 8 DSMs were removed, respectively (Figures B.6a-d, B.7a-d and B.8a-d). The standard deviation of elevation was then calculated for each filtering threshold (Figures B.6e-h, B.7e-h and B.8e-h), with areas of ice-free land masked out so as to only display the signals over thick ice sheet. Taking a transect across the basin, shown by the white dashed line in Figures B.6e, B.7e and B.8e), shows how these features have evolved over time. The timeseries of elevation within the basin and outside of the basin (shown by crosses in Figures B.6e-h, B.7e-h and B.8e-h) show

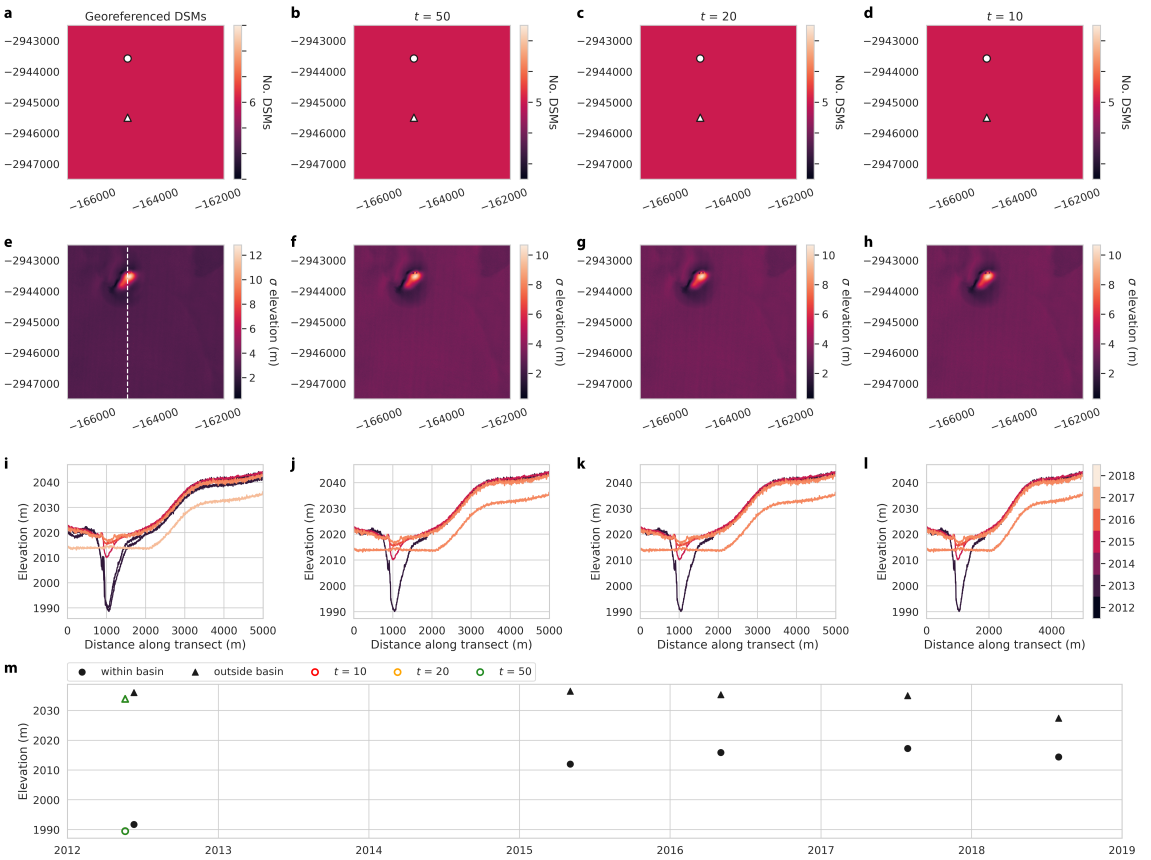

Figure B.5: Testing the impact of various filtering threshold values (standard deviation of dh greater than $t = 10$ m, $t = 20$ m, $t = 50$ m) at Sioqqap Sermia (southern) active subglacial lake detected in Chapter 2.2. (a) Number of georeferenced DSMs within 25 km^2 grid. Circles and triangles represent points within and outside the basin for the elevation timeseries in panel m (b) Number of Strip DSMs after Strips with standard deviation of dh >50 m have been removed, where dh is the per-pixel difference in elevation between the DSM Strip and reference Mosaic (c) Number of DSMs after Strips with standard deviation of dh >20 m have been removed. (d) Number of DSMs after Strips with standard deviation of dh >10 m have been removed. (e) Standard deviation of the elevation recorded by all DSM's; the dashed white line is the transect used for panels (i-l). (f) Standard deviation of elevation with <50 m dh threshold applied. (g) Standard deviation of elevation with <20 m dh threshold applied. (h) Standard deviation of elevation with <10 m dh threshold applied. The collapse basin is visible in in all panels, shown by a high standard deviation of elevation signal. No visible artefacts are apparent within the grid square. (i) Transect across basin with no thresholds applied, showing evolution of the ice surface between 2011 and 2018. (j) Transect across basin using $t = 50$ m. (k) Transect across basin using $t = 20$ m. (l) Transect across basin using $t = 10$ m. (m) Timeseries of surface elevation within the basin (circles) and outside of the basin (triangles). Elevation points removed using standard deviation of dh greater than $t = 10$ m, $t = 20$ m, $t = 50$ m are displayed in red, orange and green, respectively.

a complex evolution, with the drainage event occurring in 2011 (Livingstone et al., 2019). At Lake 2, a clearer signal is observed in the standard deviation of elevation (Figure B.7e-h), and a surface depression is apparent in the transect across the site, which corresponds to a drainage event in 2015 (Figure B.7i-l). A drainage event also occurred in 2014 at Lake 3, shown by the drop in elevation in the timeseries (Figure B.8m).

B.1.1.5 Validation

To summarise, all three different thresholds on the standard deviation of dh between the reference DEM and the Strip DSMs filtered the visible artefacts in the region and allowed all known active subglacial lakes described above to be identified. However, $t =$ 20 m provided a balance between removing "good" Strip DSMs and failing to remove Strips with artefacts or geolocation errors. A recent study suggest the Greenland Ice Sheet undergoes an average elevation change rate of around -11 cm a^{-1} (Chen et al., 2021). Using $t = 20$ m allows for large localised change rates relative to the surrounding ice, to enable detection of collapse basins. When implemented on an ice-sheet scale, a total of 4,043 (15%), 6,745 (26%) and 9,073 (34%) DSMs were removed during each threshold ($t = 50$, $t = 20$, $t = 10$ m standard deviation dh, respectively) relative to the total number of georeferenced DSMs (26,342) (Figure B.9). For the chosen threshold ($t = 20$) filtering algorithm, 74% of Strip DSMs remain unfiltered across the ice sheet scale.

B.1.2 Classification framework

To analyse and detect large, localised vertical shifts in the ice surface, following filtering steps, we calculated the temporal standard deviation of elevation iteratively at each $2m^2$ pixel within the 700,000 km^2 region of interest, divided into 139,889 tiles of 5 x 5 km to decrease computing time. The output raster was categorised using natural breaks (Jenks) classification algorithm (Jenks, 1977), which creates class breaks based on natural groupings in the data i.e. similar values, and maximises the variance between classes. We classified the standard deviation of elevation values into seven classes (1: $0 < \sigma < 4$, 2: $4 \leq \sigma < 10$, 3: $10 \leq \sigma < 19$, 4: $19 \leq \sigma < 31$, 5: $31 \leq \sigma <$

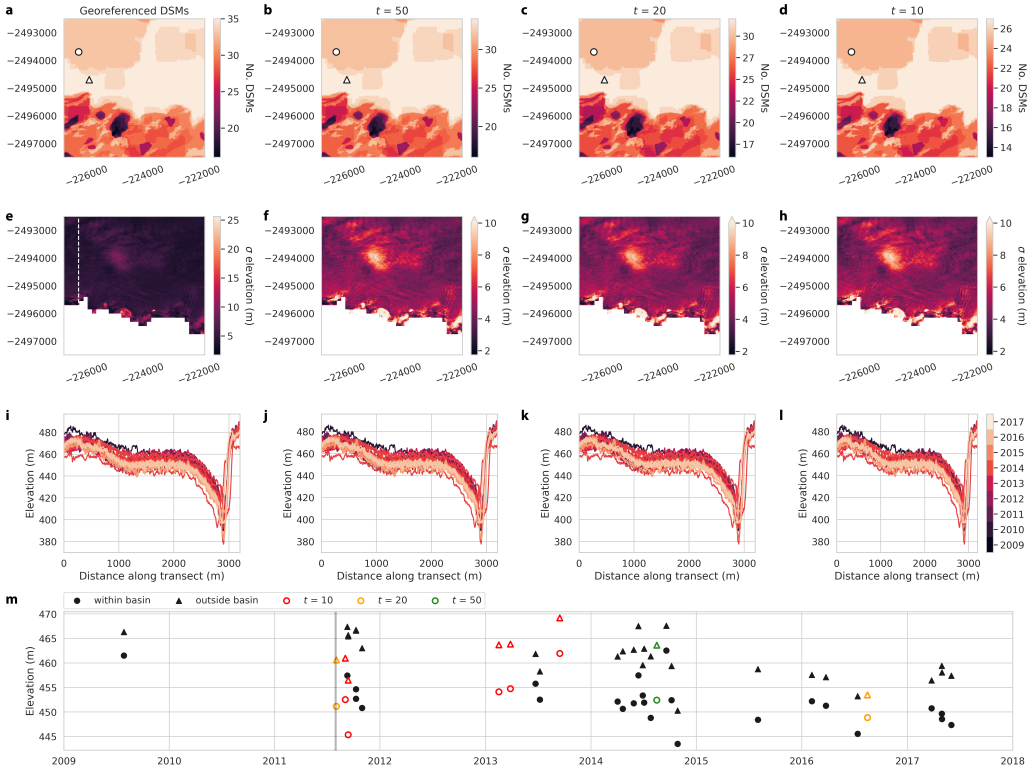

Figure B.6: Testing the impact of various filtering threshold values (standard deviation of dh greater than $t = 10$ m, $t = 20$ m, $t = 50$ m) at Isunguata Sermia active subglacial lake detected by (Livingstone et al., 2019). (a) Number of georeferenced DSMs within 25 km^2 grid. Circles and triangles represent points within and outside the basin for the elevation timeseries in panel m (b) Number of Strip DSMs after Strips with standard deviation of dh >50 m have been removed, where dh is the per-pixel difference in elevation between the DSM Strip and reference Mosaic (c) Number of DSMs after Strips with standard deviation of dh >20 m have been removed. (d) Number of DSMs after Strips with standard deviation of dh >10 m have been removed. (e) Standard deviation of the elevation recorded by all DSM's; the dashed white line is the transect used for panels (i-l). (f) Standard deviation of elevation with <50 m dh threshold applied. (g) Standard deviation of elevation with <20 m dh threshold applied. (h) Standard deviation of elevation with <10 m dh threshold applied. The collapse basin is visible in in all panels, shown by a high standard deviation of elevation signal. No visible artefacts are apparent within the grid square. (i) Transect across basin with no thresholds applied, showing evolution of the ice surface between 2011 and 2018. (j) Transect across basin using $t = 50$ m. (k) Transect across basin using $t = 20$ m. (l) Transect across basin using $t = 10$ m. (m) Timeseries of surface elevation within the basin (circles) and outside of the basin (triangles). Elevation points removed using standard deviation of dh greater than $t = 10$ m, $t = 20$ m, $t = 50$ m are displayed in red, orange and green, respectively.

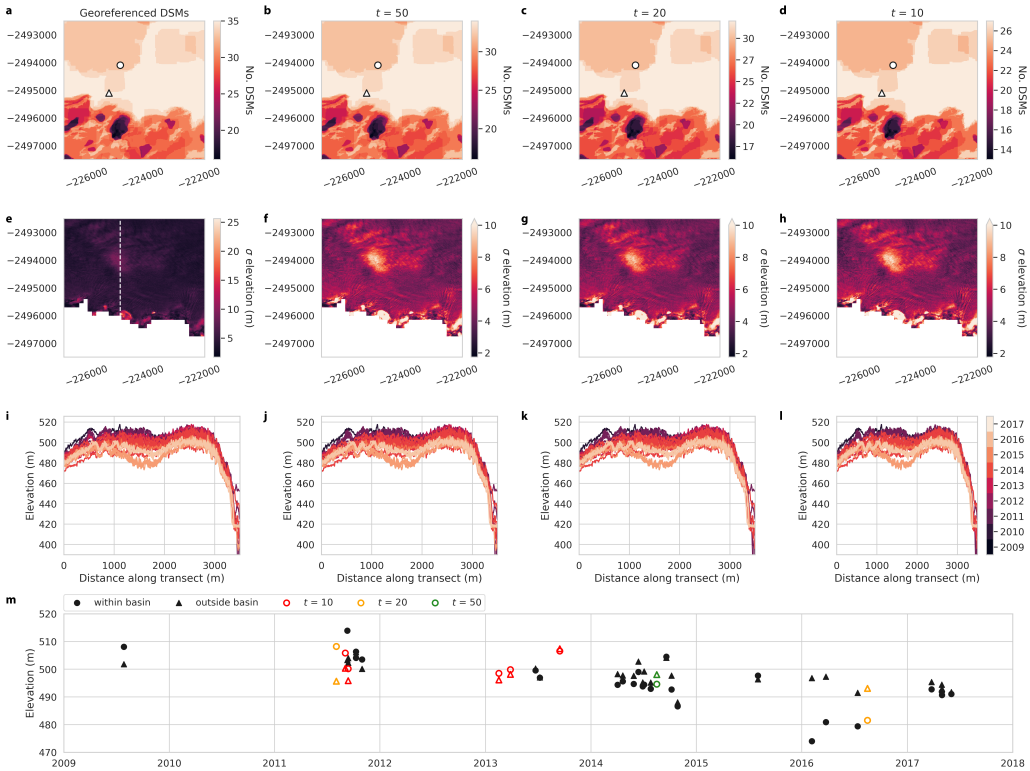

Figure B.7: Testing the impact of various filtering threshold values (standard deviation of dh greater than $t = 10$ m, $t = 20$ m, $t = 50$ m) at Isunguata Sermia active subglacial lake detected by (Livingstone et al., 2019). (a) Number of georeferenced DSMs within 25 km^2 grid. Circles and triangles represent points within and outside the basin for the elevation timeseries in panel m (b) Number of Strip DSMs after Strips with standard deviation of dh >50 m have been removed, where dh is the per-pixel difference in elevation between the DSM Strip and reference Mosaic (c) Number of DSMs after Strips with standard deviation of dh >20 m have been removed. (d) Number of DSMs after Strips with standard deviation of dh >10 m have been removed. (e) Standard deviation of the elevation recorded by all DSM's; the dashed white line is the transect used for panels (i-l). (f) Standard deviation of elevation with <50 m dh threshold applied. (g) Standard deviation of elevation with <20 m dh threshold applied. (h) Standard deviation of elevation with <10 m dh threshold applied. The collapse basin is visible in in all panels, shown by a high standard deviation of elevation signal. No visible artefacts are apparent within the grid square. (i) Transect across basin with no thresholds applied, showing evolution of the ice surface between 2011 and 2018. (j) Transect across basin using $t = 50$ m. (k) Transect across basin using $t = 20$ m. (l) Transect across basin using $t = 10$ m. (m) Timeseries of surface elevation within the basin (circles) and outside of the basin (triangles). Elevation points removed using standard deviation of dh greater than $t = 10$ m, $t = 20$ m, $t = 50$ m are displayed in red, orange and green, respectively.

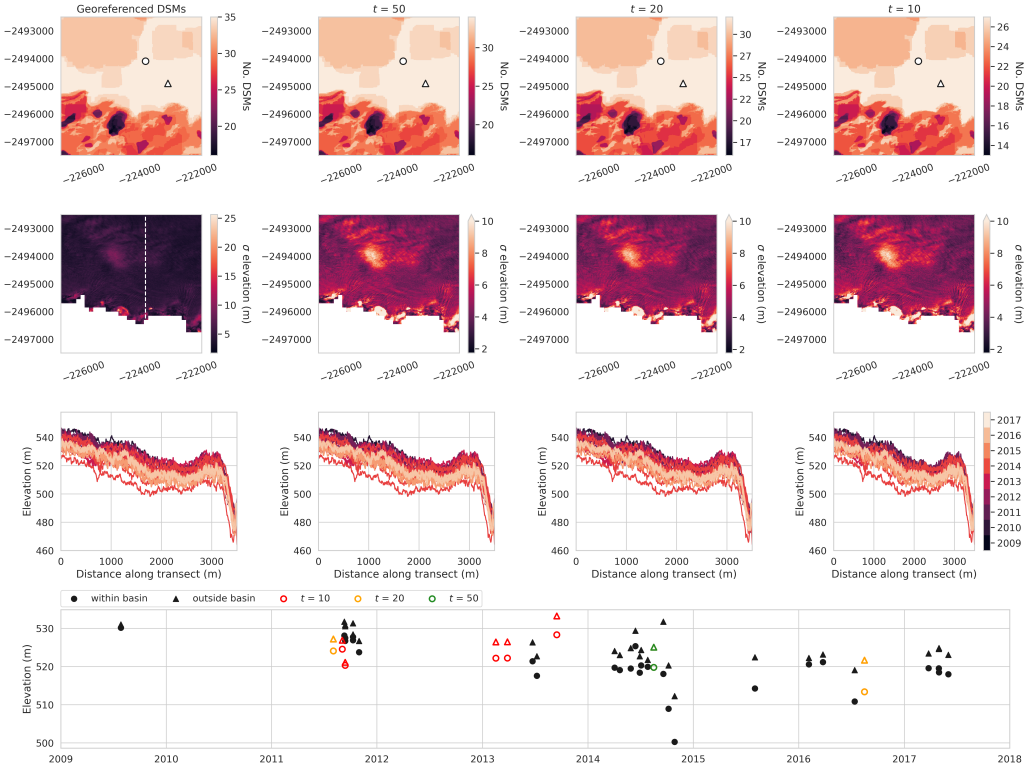

Figure B.8: Testing the impact of various filtering threshold values (standard deviation of *dh* greater than $t = 10$ m, $t = 20$ m, $t = 50$ m) at Isunguata Sermia active subglacial lake detected by (Livingstone et al., 2019). (a) Number of georeferenced DSMs within 25 km^2 grid. Circles and triangles represent points within and outside the basin for the elevation timeseries in panel m (b) Number of Strip DSMs after Strips with standard deviation of *dh* >50 m have been removed, where *dh* is the per-pixel difference in elevation between the DSM Strip and reference Mosaic (c) Number of DSMs after Strips with standard deviation of *dh* >20 m have been removed. (d) Number of DSMs after Strips with standard deviation of dh >10 m have been removed. (e) Standard deviation of the elevation recorded by all DSM's; the dashed white line is the transect used for panels (i-l). (f) Standard deviation of elevation with <50 m *dh* threshold applied. (g) Standard deviation of elevation with <20 m *dh* threshold applied. (h) Standard deviation of elevation with <10 m *dh* threshold applied. The collapse basin is visible in in all panels, shown by a high standard deviation of elevation signal. No visible artefacts are apparent within the grid square. (i) Transect across basin with no thresholds applied, showing evolution of the ice surface between 2011 and 2018. (j) Transect across basin using $t = 50$ m. (k) Transect across basin using $t = 20$ m. (l) Transect across basin using $t = 10$ m. (m) Timeseries of surface elevation within the basin (circles) and outside of the basin (triangles). Elevation points removed using standard deviation of *dh* greater than $t = 10$ m, $t = 20$ m, $t = 50$ m are displayed in red, orange and green, respectively.

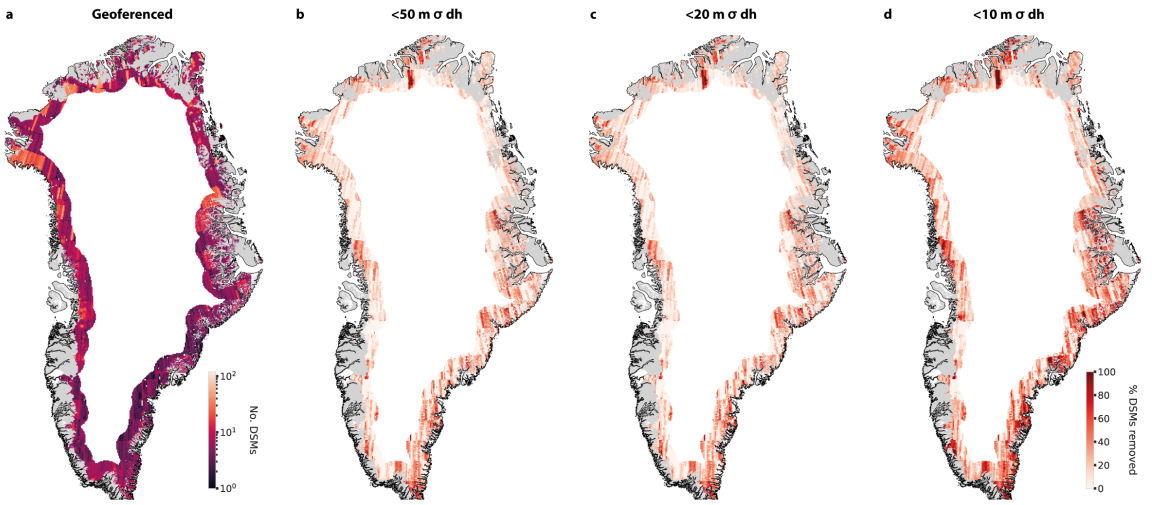

Figure B.9: (a) Number of georeferenced DSMs pre-processing within 50 km of the ice margin. (b) Percentage of DSMs removed using 50 m standard deviation of elevation difference between reference DSM (ArcticDEM mosaic) and strip DSMs. (c) Percentage of DSMs removed using 20 m standard deviation of elevation difference between reference DSM (ArcticDEM mosaic) and strip DSMs. (d) Percentage of DSMs removed using 10 m standard deviation of elevation difference between reference DSM (ArcticDEM mosaic) and strip DSMs.

48, 6: $48 \leq \sigma < 70$, 7: $70 \leq \sigma < 100$). To attribute these changes to active subglacial lake drainage events, we vetted our approach on the seven known active subglacial lakes (Table B.1).

An known active subglacial lake is successfully identified if >60% of classified pixels are within the subglacial lake boundary (manually traced outlines using Landsat optical imagery). The classification algorithm, in principal, identifies all seven of the known active subglacial lakes B.10. Combining Class 2 and 3, the most successful recall of known active subglacial lakes is the largest and deepest collapse basin at Flade Isblink ice cap (85% of pixels within boundary), with the poorest recall observed at the northern Sioqqap Sermia collapse basin (5% of pixels within boundary) . Whilst the Isunguata Sermia lakes have high successful recall (62%, 100% and 98% for L1, L2, and L3, respectively), the setting is complex being near the ice margin where the ice surface is more crevassed and the ice is faster flowing, and when converting the classified raster to features (polygons), the lakes are merged into a large (121 km^2) feature which is later removed in the processing chain.

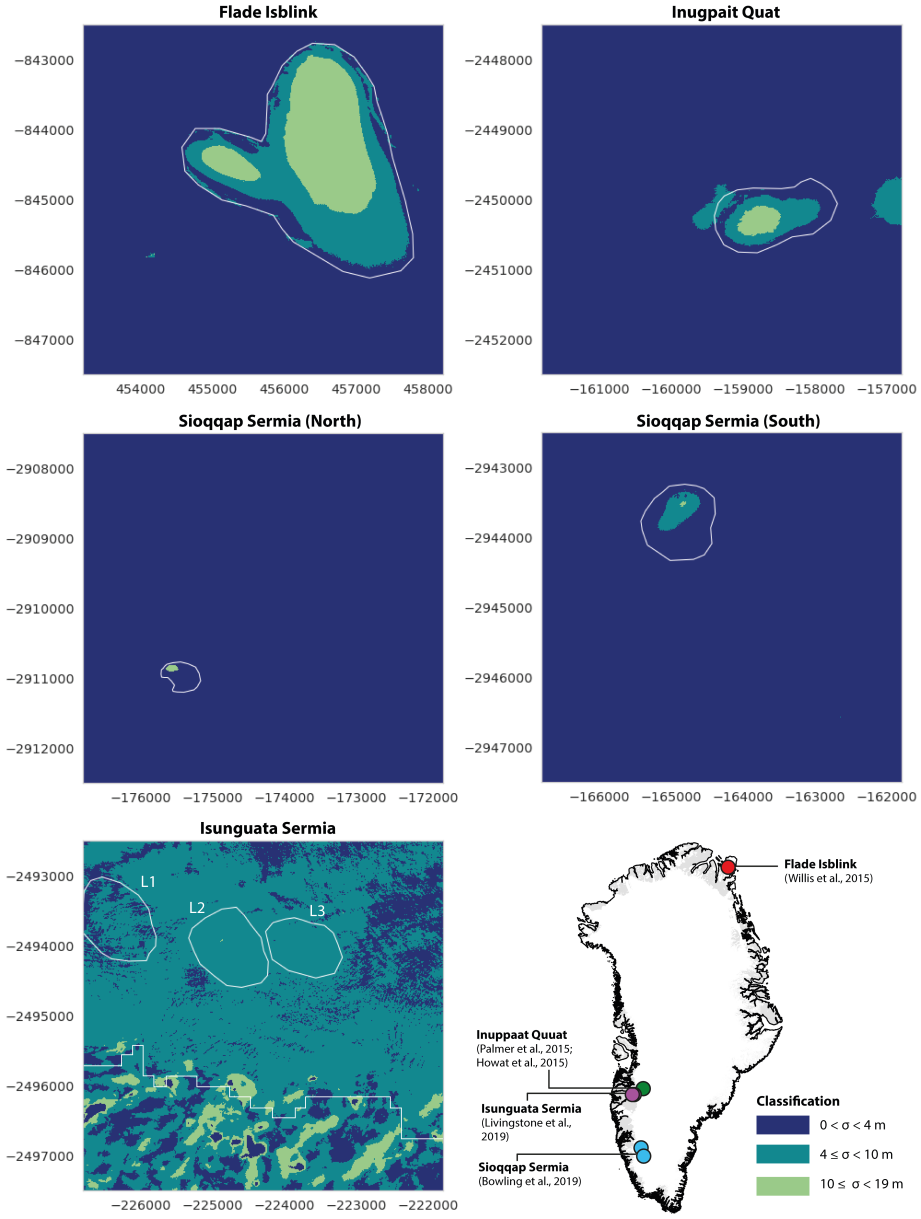

Figure B.10: Classification at each of the seven known active subglacial lakes (a) Outline of Flade Isblink subglacial lake detected by (Willis et al., 2015) show in white, and different classification of standard deviation output (Class 1-3). (b) Outline of Inugpait Quat subglacial lake detected by (Palmer et al., 2015) show in white, with the classified temporal variance output (Class 1-3). (c) Outline of Sioqqap Sermia (North) subglacial lake detected in Chapter 3 show in white, with the classified temporal variance output (Class 1-3). Outline of Sioqqap Sermia (South) subglacial lake detected in Chapter 3 show in white, with the classified temporal variance output (Class 1-3). (b) Outline of the three Isunguata Sermia subglacial lakes detected by (Livingstone et al., 2019) show in white, with the classified temporal variance output (Class 1-3). Location map of the known active subglacial lakes.

Appendix C

Appendix

The document includes:

1. Figure indicating dynamic temporal variance signal from a large supraglacial channel at the margin of Hobbs Gletscher, north east Greenland, captured using the method described in Chapter 4.

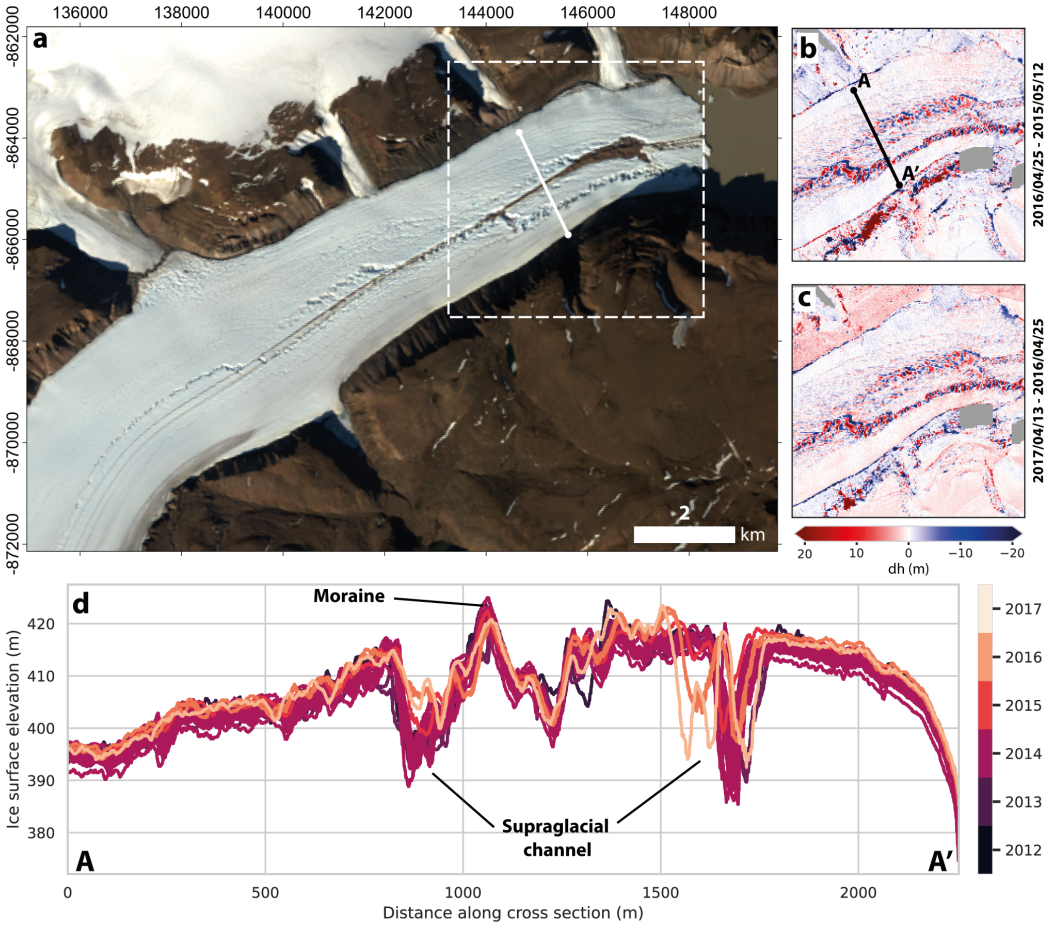

Figure C.1: Dynamic temporal variance signal from a large supraglacial channel, Hobbs Gletscher (a) Landsat satellite image acquired on 13th August 2015, region is shown in dashed box in Figure 4.6. (b) Difference in elevation between Strip DSMs acquired on 12th May 2015 and 25th April 2016, showing large supraglacial feature running parallel to ice flow. (c) Difference in elevation between Strip DSMs acquired on 25th April 2016 and 13th April 2017. (d) Transect along the profile A-A' shown in panel b, showing the temporal evolution of the supraglacial channel and position of medial moraine.

References

Abdalati, W. and K. Steffen. "The apparent effects of the Mt. Pinatubo eruption on the Greenland ice sheet melt extent". *Geophysical Research Letters* 24.14 (1997), pp. 1795–1797.

Abram, N. J., H. V. McGregor, J. E. Tierney, M. N. Evans, N. P. McKay, and D. S. Kaufman. "Early onset of industrial-era warming across the oceans and continents". *Nature* 536.7617 (2016), pp. 411–418.

Achberger, A. M., B. C. Christner, A. B. Michaud, J. C. Priscu, M. L. Skidmore, T. J. Vick-Majors, W. Adkins, S. Anandakrishnan, C. Barbante, G. Barcheck, L. Beem, A. Behar, M. Beitch, R. Bolsey, C. Branecky, S. Carter, K. Christianson, R. Edwards, A. Fisher, H. Fricker, N. Foley, B. Guthrie, T. Hodson, R. Jacobel, S. Kelley, K. Mankoff, E. McBryan, J. Mikucki, A. Mitchell, R. Powell, A. Purcell, D. Sampson, R. Scherer, J. Sherve, M. Siegfried, and S. Tulaczyk. "Microbial community structure of subglacial lake Whillans, West Antarctica". *Frontiers in microbiology* 7 (2016), p. 1457.

Albert, M. R. and F. E. Perron Jr. "Ice layer and surface crust permeability in a seasonal snow pack". *Hydrological Processes* 14.18 (2000), pp. 3207–3214.

Alley, K. E., T. A. Scambos, M. R. Siegfried, and H. A. Fricker. "Impacts of warm water on Antarctic ice shelf stability through basal channel formation". *Nature Geoscience* 9.4 (2016), pp. 290–293.

Alley, R. B. "Towards a hydrological model for computerized ice-sheet simulations". *Hydrological Processes* 10.4 (1996), pp. 649–660.

Alley, R. B., K. Cuffey, E. Evenson, J. Strasser, D. Lawson, and G. Larson. "How glaciers entrain and transport basal sediment: physical constraints". *Quaternary Science Reviews* 16.9 (1997), pp. 1017–1038.

Alley, R. B., T. Dupont, B. Parizek, S. Anandakrishnan, D. E. Lawson, G. Larson, and E. Evenson. "Outburst flooding and the initiation of ice-stream surges in response to climatic cooling: A hypothesis". *Geomorphology* 75.1-2 (2006), pp. 76–89.

Alley, R. B., T. K. Dupont, B. R. Parizek, and S. Anandakrishnan. "Access of surface meltwater to beds of sub-freezing glaciers: preliminary insights". *Annals of Glaciology* 40 (2005), pp. 8–14.

Anandakrishnan, S. and R. B. Alley. "Stagnation of ice stream C, West Antarctica by water piracy". *Geophysical Research Letters* 24.3 (1997), pp. 265–268.

Anderson, R. S. and S. P. Anderson. *Geomorphology: the mechanics and chemistry of landscapes*. Cambridge University Press, 2010.

Anderson, S. P., K. M. Fernald, R. S. Anderson, and N. F. Humphrey. "Physical and chemical characterization of a spring flood event, Bench Glacier, Alaska, USA: evidence for water storage". *Journal of Glaciology* 45.150 (1999), pp. 177–189.

Andrés, E. de, J. Otero, F. Navarro, A. Promińska, J. Lapazaran, and W. Walczowski. "A two-dimensional glacier–fjord coupled model applied to estimate submarine melt rates and front position changes of Hansbreen, Svalbard". *Journal of Glaciology* 64.247 (2018), pp. 745–758.

Andrews, L. C., G. A. Catania, M. J. Hoffman, J. D. Gulley, M. P. Lüthi, C. Ryser, R. L. Hawley, and T. A. Neumann. "Direct observations of evolving subglacial drainage beneath the Greenland Ice Sheet". *Nature* 514.7520 (2014), pp. 80–83.

Andrews, L. C., M. J. Hoffman, T. A. Neumann, G. A. Catania, M. P. Lüthi, R. L. Hawley, K. M. Schild, C. Ryser, and B. F. Morriss. "Seasonal evolution of the subglacial hydrologic system modified by supraglacial lake drainage in western Greenland". *Journal of Geophysical Research: Earth Surface* 123.6 (2018), pp. 1479–1496.

Angelen, J. H. van, M. Van den Broeke, B. Wouters, and J. T. Lenaerts. "Contemporary (1960–2012) evolution of the climate and surface mass balance of the Greenland ice sheet". *Surveys in Geophysics* 35.5 (2014), pp. 1155–1174.

Angelen, J. van, J. M. Lenaerts, M. Van den Broeke, X. Fettweis, and E. Van Meijgaard. "Rapid loss of firn pore space accelerates 21st century Greenland mass loss". *Geophysical Research Letters* 40.10 (2013), pp. 2109–2113.

Arcone, S. A., V. B. Spikes, and G. S. Hamilton. "Stratigraphic variation within polar firn caused by differential accumulation and ice flow: interpretation of a 400 MHz short-pulse radar profile from West Antarctica". *Journal of Glaciology* 51.174 (2005), pp. 407–422.

Arimitsu, M. L., J. F. Piatt, E. N. Madison, J. S. Conaway, and N. Hillgruber. "Oceanographic gradients and seabird prey community dynamics in glacial fjords". *Fisheries Oceanography* 21.2-3 (2012), pp. 148–169.

Artemieva, I. M. "Lithosphere thermal thickness and geothermal heat flux in Greenland from a new thermal isostasy method". *Earth-Science Reviews* 188 (2019), pp. 469–481.

Aschwanden, A., M. A. Fahnestock, M. Truffer, D. J. Brinkerhoff, R. Hock, C. Khroulev, R. Mottram, and S. A. Khan. "Contribution of the Greenland Ice Sheet to sea level over the next millennium". *Science advances* 5.6 (2019), eaav9396.

Bamber, J., J. Gomez-Dans, and J. Griggs. "A new 1 km digital elevation model of the Antarctic derived from combined satellite radar and laser data–Part 1: Data and methods". *The Cryosphere* 3.1 (2009), pp. 101–111.

Bamber, J., J. Griggs, R. Hurkmans, J. Dowdeswell, S. Gogineni, I. Howat, J. Mouginot, J. Paden, S. Palmer, E. Rignot, and D. Steinhage. "A new bed elevation dataset for Greenland". *The Cryosphere* 7.2 (2013), pp. 499–510.

Bamber, J., M. J. Siegert, J. A. Griggs, S. J. Marshall, and G. Spada. "Paleofluvial mega-canyon beneath the central Greenland ice sheet". *Science* 341.6149 (2013), pp. 997–999.

Bamber, J. L., S. Ekholm, and W. B. Krabill. "A new, high-resolution digital elevation model of Greenland fully validated with airborne laser altimeter data". *Journal of Geophysical Research: Solid Earth* 106.B4 (2001), pp. 6733–6745.

Banwell, A., I. Hewitt, I. Willis, and N. Arnold. "Moulin density controls drainage development beneath the Greenland ice sheet". *Journal of Geophysical Research: Earth Surface* 121.12 (2016), pp. 2248–2269.

Banwell, A. F., N. S. Arnold, I. C. Willis, M. Tedesco, and A. P. Ahlstrøm. "Modeling supraglacial water routing and lake filling on the Greenland Ice Sheet". *Journal of Geophysical Research: Earth Surface* 117.F4 (2012).

Banwell, A. F., I. C. Willis, and N. S. Arnold. "Modeling subglacial water routing at Paakitsoq, W Greenland". *Journal of Geophysical Research: Earth Surface* 118.3 (2013), pp. 1282–1295.

Barletta, V. R., L. Sandberg Sørensen, and R. Forsberg. "Scatter of mass changes estimates at basin scale for Greenland and Antarctica". *The Cryosphere* 7.5 (2013), pp. 1411–1432.

Barnes, E. A. and L. M. Polvani. "CMIP5 projections of Arctic amplification, of the North American/North Atlantic circulation, and of their relationship". *Journal of Climate* 28.13 (2015), pp. 5254–5271.

Barr, I. D., M. D. Dokukin, I. Kougkoulos, S. J. Livingstone, H. Lovell, J. Małecki, and A. Y. Muraviev. "Using ArcticDEM to analyse the dimensions and dynamics of debris-covered glaciers in Kamchatka, Russia". *Geosciences* 8.6 (2018), p. 216.

Bartholomaus, T. C., R. S. Anderson, and S. P. Anderson. "Response of glacier basal motion to transient water storage". *Nature Geoscience* 1.1 (2008), pp. 33–37.

Bartholomaus, T. C., C. F. Larsen, and S. O'Neel. "Does calving matter? Evidence for significant submarine melt". *Earth and Planetary Science Letters* 380 (2013), pp. 21–30.

Bartholomew, I., P. Nienow, D. Mair, A. Hubbard, M. A. King, and A. Sole. "Seasonal evolution of subglacial drainage and acceleration in a Greenland outlet glacier". *Nature Geoscience* 3.6 (2010), pp. 408–411.

Bartholomew, I., P. Nienow, A. Sole, D. Mair, T. Cowton, and M. A. King. "Short-term variability in Greenland Ice Sheet motion forced by time-varying meltwater drainage: Implications for the relationship between subglacial drainage system behavior and ice velocity". *Journal of Geophysical Research: Earth Surface* 117.F3 (2012).

Bartholomew, I., P. Nienow, A. Sole, D. Mair, T. Cowton, S. Palmer, and J. Wadham. "Supraglacial forcing of subglacial drainage in the ablation zone of the Greenland ice sheet". *Geophysical Research Letters* 38.8 (2011).

Beaird, N. L., F. Straneo, and W. Jenkins. "Export of strongly diluted Greenland meltwater from a major glacial fjord". *Geophysical Research Letters* 45.9 (2018), pp. 4163–4170.

Bell, R. E., M. Studinger, M. A. Fahnestock, and C. A. Shuman. "Tectonically controlled subglacial lakes on the flanks of the Gamburtsev Subglacial Mountains, East Antarctica". *Geophysical Research Letters* 33.2 (2006).

Bell, R. E., M. Studinger, C. A. Shuman, M. A. Fahnestock, and I. Joughin. "Large subglacial lakes in East Antarctica at the onset of fast-flowing ice streams". *Nature* 445.7130 (2007), pp. 904–907.

Bell, R. E., M. Studinger, C. A. Shuman, M. A. Fahnestock, and I. Joughin. "Large subglacial lakes in East Antarctica at the onset of fast-flowing ice streams". *Nature* 445.7130 (2007), pp. 904–907.

Bell, R. E., M. Studinger, A. A. Tikku, G. K. Clarke, M. M. Gutner, and C. Meertens. "Origin and fate of Lake Vostok water frozen to the base of the East Antarctic ice sheet". *Nature* 416.6878 (2002), pp. 307–310.

Bell, R. E., F. Ferraccioli, T. T. Creyts, D. Braaten, H. Corr, I. Das, D. Damaske, N. Frearson, T. Jordan, K. Rose, M. Studinger, and M. Wolovick. "Widespread persistent thickening of the East Antarctic Ice Sheet by freezing from the base". *Science* 331.6024 (2011), pp. 1592–1595.

Bennike, O. and S. Björck. "Chronology of the last recession of the Greenland Ice Sheet". *Journal of Quaternary Science* 17.3 (2002), pp. 211–219.

Benson, C. S. "Stratigraphic studies in the snow and firn of the Greenland ice sheet". PhD thesis. California Institute of Technology, 1960.

Bentley, C. R., N. Lord, and C. Liu. "Radar reflections reveal a wet bed beneath stagnant Ice Stream C and a frozen bed beneath ridge BC, West Antarctica". *Journal of Glaciology* 44.146 (1998), pp. 149–156.

Bentley, M. J., P. Christoffersen, D. A. Hodgson, A. M. Smith, S. Tulaczyk, and A. M. Le Brocq. "Subglacial Lake Sediments and Sedimentary Processes: Potential Archives of Ice Sheet Evolution, Past Environmental Change, and the Presence Of Life". In: *Antarctic Subglacial Aquatic Environments*. American Geophysical Union (AGU), 2011, pp. 83–110.

Bhatia, M. P., S. B. Das, E. B. Kujawinski, P. Henderson, A. Burke, and M. A. Charette. "Seasonal evolution of water contributions to discharge from a Greenland outlet glacier: insight from a new isotope-mixing model". *Journal of Glaciology* 57.205 (2011), pp. 929–941.

Bhatia, M. P., E. B. Kujawinski, S. B. Das, C. F. Breier, P. B. Henderson, and M. A. Charette. "Greenland meltwater as a significant and potentially bioavailable source of iron to the ocean". *Nature Geoscience* 6.4 (2013), pp. 274–278.

Bindschadler, R. "The importance of pressurized subglacial water in separation and sliding at the glacier bed". *Journal of Glaciology* 29.101 (1983), pp. 3–19.

Bingham, R. G., A. L. Hubbard, P. W. Nienow, and M. J. Sharp. "An investigation into the mechanisms controlling seasonal speedup events at a High Arctic glacier". *Journal of Geophysical Research: Earth Surface* 113.F2 (2008).

Bingham, R. G., P. W. Nienow, M. J. Sharp, and S. Boon. "Subglacial drainage processes at a High Arctic polythermal valley glacier". *Journal of Glaciology* 51.172 (2005), pp. 15–24.

Björnsson, H. "Explanations of jökulhlaups from GrıFIX ME!!!!msvötn, Vatnajökull, Iceland." *Jökull* 24 (1974), pp. 1–26.

Björnsson, H. "Jökulhlaups in Iceland: prediction, characteristics and simulation". *Annals of Glaciology* 16 (1992), pp. 95–106.

Björnsson, H. "Subglacial lakes and jökulhlaups in Iceland". *Global and Planetary Change* 35.3 (2003), pp. 255–271.

Björnsson, H. "Understanding jökulhlaups: from tale to theory". *Journal of Glaciology* 56.200 (2010), pp. 1002–1010.

Blomdin, R. and J. Harbor. "Glacial Erosional Processes and Landforms". In: *International Encyclopedia of Geography*. John Wiley & Sons, Ltd, 2017, pp. 1–12. ISBN: 9781118786352.

Bohleber, P., N. Wagner, and O. Eisen. "Permittivity of ice at radio frequencies: Part II. Artificial and natural polycrystalline ice". *Cold Regions Science and Technology* 83 (2012), pp. 13–19.

Booth, A., R. Clark, B. Kulessa, T. Murray, J. Carter, S. Doyle, and A. Hubbard. "Thin-layer effects in glaciological seismic amplitude-versus-angle (AVA) analysis: implications for characterising a subglacial till unit, Russell Glacier, West Greenland". *The Cryosphere* 6.4 (2012), pp. 909–922.

Booth, B. B., N. J. Dunstone, P. R. Halloran, T. Andrews, and N. Bellouin. "Aerosols implicated as a prime driver of twentieth-century North Atlantic climate variability". *Nature* 484.7393 (2012), pp. 228–232.

Boulton, G. and A. Jones. "Stability of temperate ice caps and ice sheets resting on beds of deformable sediment". *Journal of Glaciology* 24.90 (1979), pp. 29–43.

Bowling, J. S. "Discovery of twenty-eight subglacial lakes beneath the Greenland Ice Sheet". MRes. University of Sheffield, 2017.

Bowling, J., S. Livingstone, A. Sole, and W. Chu. "Distribution and dynamics of Greenland subglacial lakes". *Nature communications* 10.1 (2019), pp. 1–11.

Box, J. E. and K. Ski. "Remote sounding of Greenland supraglacial melt lakes: implications for subglacial hydraulics". *Journal of glaciology* 53.181 (2007), pp. 257–265.

Box, J. E., L. Yang, D. H. Bromwich, and L.-S. Bai. "Greenland ice sheet surface air temperature variability: 1840–2007". *Journal of Climate* 22.14 (2009), pp. 4029–4049.

Box, J. "Greenland ice sheet surface mass-balance variability: 1991–2003". *Annals of Glaciology* 42 (2005), pp. 90–94.

Box, J., X. Fettweis, J. Stroeve, M. Tedesco, D. Hall, and K. Steffen. "Greenland ice sheet albedo feedback: thermodynamics and atmospheric drivers". *The Cryosphere* 6.4 (2012), pp. 821–839.

Boyd, E. S., M. Skidmore, A. C. Mitchell, C. Bakermans, and J. W. Peters. "Methanogenesis in subglacial sediments". *Environmental microbiology reports* 2.5 (2010), pp. 685–692.

Braithwaite, R. J., M. Laternser, and W. T. Pfeffer. "Variations of near-surface firn density in the lower accumulation area of the Greenland ice sheet, Pâkitsoq, West Greenland". *Journal of Glaciology* 40.136 (1994), pp. 477–485.

Briner, J. P., J. K. Cuzzone, J. A. Badgeley, N. E. Young, E. J. Steig, M. Morlighem, N.-J. Schlegel, G. J. Hakim, J. M. Schaefer, J. V. Johnson, A. J. Lesnek, E. K. Thomas, E. Allan, O. Bennike, A. A. Cluett, B. Csatho, A. de Vernal, J. Downs, E. Larour, and S. Nowicki. "Rate of mass loss from the Greenland Ice Sheet will exceed Holocene values this century". *Nature* 586.7827 (2020), pp. 70–74.

Briner, J. P., N. P. McKay, Y. Axford, O. Bennike, R. S. Bradley, A. de Vernal, D. Fisher, P. Francus, B. Fréchette, K. Gajewski, A. Jennings, D. S. Kaufman, G. Miller, C. Rouston, and B. Wagner. "Holocene climate change in Arctic Canada and Greenland". *Quaternary Science Reviews* 147 (2016), pp. 340–364.

Brown, J., J. Harper, W. T. Pfeffer, N. Humphrey, and J. Bradford. "High-resolution study of layering within the percolation and soaked facies of the Greenland ice sheet". *Annals of Glaciology* 52.59 (2011), pp. 35–42.

Brunt, K., T. Neumann, and B. Smith. "Assessment of ICESat-2 ice sheet surface heights, based on comparisons over the interior of the Antarctic ice sheet". *Geophysical Research Letters* 46.22 (2019), pp. 13072–13078.

Burgers, T., L. Miller, H. Thomas, B. Else, M. Gosselin, and T. Papakyriakou. "Surface water pCO2 variations and sea-air CO2 fluxes during summer in the eastern Canadian Arctic". *Journal of Geophysical Research: Oceans* 122.12 (2017), pp. 9663–9678.

Burke, M. J., J. Woodward, A. J. Russell, P. J. Fleisher, and P. K. Bailey. "Controls on the sedimentary architecture of a single event englacial esker: Skeiðarárjökull, Iceland". *Quaternary Science Reviews* 27.19-20 (2008), pp. 1829–1847.

Campen, R., J. Kowalski, W. B. Lyons, S. Tulaczyk, B. Dachwald, E. Pettit, K. A. Welch, and J. A. Mikucki. "Microbial diversity of an Antarctic subglacial community and high-resolution replicate sampling inform hydrological connectivity in a polar desert". *Environmental Microbiology* 21.7 (2019), pp. 2290–2306.

Carroll, D., D. A. Sutherland, B. Hudson, T. Moon, G. A. Catania, E. L. Shroyer, J. D. Nash, T. C. Bartholomaus, D. Felikson, L. A. Stearns, B. P. Y. Noël, and M. R. van den Broeke. "The impact of glacier geometry on meltwater plume structure and submarine melt in Greenland fjords". *Geophysical Research Letters* 43.18 (2016), pp. 9739–9748.

Carroll, D., D. A. Sutherland, E. L. Shroyer, J. D. Nash, G. A. Catania, and L. A. Stearns. "Modeling turbulent subglacial meltwater plumes: Implications for fjord-scale buoyancy-driven circulation". *Journal of Physical Oceanography* 45.8 (2015), pp. 2169–2185.

Carter, S. P., D. D. Blankenship, M. E. Peters, D. A. Young, J. W. Holt, and D. L. Morse. "Radar-based subglacial lake classification in Antarctica". *Geochemistry, Geophysics, Geosystems* 8.3 (2007).

Carter, S. P., D. D. Blankenship, D. A. Young, M. E. Peters, J. W. Holt, and M. J. Siegert. "Dynamic distributed drainage implied by the flow evolution of

the 1996–1998 Adventure Trench subglacial lake discharge". *Earth and Planetary Science Letters* 283.1-4 (2009), pp. 24–37.

Carter, S. P., H. A. Fricker, D. D. Blankenship, J. V. Johnson, W. H. Lipscomb, S. F. Price, and D. A. Young. "Modeling 5 years of subglacial lake activity in the MacAyeal Ice Stream (Antarctica) catchment through assimilation of ICESat laser altimetry". *Journal of Glaciology* 57.206 (2011), pp. 1098–1112.

Carter, S., H. Fricker, and M. Siegfried. "Evidence of rapid subglacial water piracy under Whillans Ice Stream, West Antarctica". *Journal of Glaciology* 59.218 (2013), pp. 1147–1162.

Catania, G. A. and T. Neumann. "Persistent englacial drainage features in the Greenland Ice Sheet". *Geophysical Research Letters* 37.2 (2010).

Catania, G. A., T. A. Neumann, and S. F. Price. "Characterizing englacial drainage in the ablation zone of the Greenland ice sheet". *Journal of Glaciology* 54.187 (2008), pp. 567–578.

Chandler, D., J. Wadham, G. Lis, T. Cowton, A. Sole, I. Bartholomew, J. Telling, P. Nienow, E. Bagshaw, D. Mair, S. Vinen, and A. Hubbard. "Evolution of the subglacial drainage system beneath the Greenland Ice Sheet revealed by tracers". *Nature Geoscience* 6.3 (2013), pp. 195–198.

Charalampidis, C., D. van As, J. E. Box, M. R. van den Broeke, W. T. Colgan, S. H. Doyle, A. L. Hubbard, M. MacFerrin, H. Machguth, and C. Smeets. "Changing surface–atmosphere energy exchange and refreezing capacity of the lower accumulation area, West Greenland". *The Cryosphere* 9.6 (2015), pp. 2163–2181.

Chauche, N., A. Hubbard, J.-C. Gascard, J. Box, R. Bates, M. Koppes, A. Sole, P. Christoffersen, and H. Patton. "Ice–ocean interaction and calving front morphology at two west Greenland tidewater outlet glaciers". *The Cryosphere* 8.4 (2014), pp. 1457–1468.

Chen, G., S. Zhang, S. Liang, and J. Zhu. "Elevation and Volume Changes of Greenland Ice Sheet During 2010-2019 Derived from Altimetry Data". *Frontiers in Earth Science* 9 (2021), p. 362.

Choi, Y., M. Morlighem, E. Rignot, and M. Wood. "Ice dynamics will remain a primary driver of Greenland ice sheet mass loss over the next century". *Communications Earth & Environment* 2.1 (2021), pp. 1–9.

Christiansen, J. R., T. Röckmann, M. E. Popa, C. J. Sapart, and C. J. Jørgensen. "Carbon emissions from the edge of the Greenland Ice sheet reveal subglacial processes of methane and carbon dioxide turnover". *Journal of Geophysical Research: Biogeosciences* 126.11 (2021), e2021JG006308.

Christiansen, J. R. and C. J. Jørgensen. "First observation of direct methane emission to the atmosphere from the subglacial domain of the Greenland Ice Sheet". *Scientific reports* 8.1 (2018), pp. 1–6.

Christianson, K., R. W. Jacobel, H. J. Horgan, R. B. Alley, S. Anandakrishnan, D. M. Holland, and K. J. DallaSanta. "Basal conditions at the grounding zone of Whillans Ice Stream, West Antarctica, from ice-penetrating radar". *Journal of Geophysical Research: Earth Surface* 121.11 (2016), pp. 1954–1983.

Christianson, K., R. W. Jacobel, H. J. Horgan, S. Anandakrishnan, and R. B. Alley. "Subglacial Lake Whillans—Ice-penetrating radar and GPS observations of a shallow active reservoir beneath a West Antarctic ice stream". *Earth and Planetary Science Letters* 331 (2012), pp. 237–245.

Christner, B. C., J. C. Priscu, A. M. Achberger, C. Barbante, S. P. Carter, K. Christianson, A. B. Michaud, J. A. Mikucki, A. C. Mitchell, M. L. Skidmore, T. J. Vick-Majors, W. P. Adkins, S. Anandakrishnan, G. Barcheck, L. Beem, M. Beitch, R. Bolsey, C. Branecky, R. Edwards, A. Fisher, H. A. Fricker, N. Foley, B. Guthrie, T. Hodson, H. Horgan, R. Jacobel, S. Kelley, K. D. Mankoff, E. McBryan, R. Powell, A. Purcell, D. Sampson, R. Scherer, J. Sherve, M. Siegfried, S. Tulaczyk, and t. WISSARD Science Team. "A microbial ecosystem beneath the West Antarctic ice sheet". *Nature* 512.7514 (2014), pp. 310–313.

Christoffersen, P., M. Bougamont, A. Hubbard, S. H. Doyle, S. Grigsby, and R. Pettersson. "Cascading lake drainage on the Greenland Ice Sheet triggered by tensile shock and fracture". *Nature Communications* 9.1 (2018), pp. 1–12.

Chu, V. W. "Greenland ice sheet hydrology: A review". *Progress in Physical Geography* 38.1 (2014), pp. 19–54.

Chu, W., D. M. Schroeder, H. Seroussi, T. T. Creyts, and R. E. Bell. "Complex basal thermal transition near the onset of Petermann Glacier, Greenland". *Journal of Geophysical Research: Earth Surface* 123.5 (2018), pp. 985–995.

Chu, W., D. M. Schroeder, H. Seroussi, T. T. Creyts, S. J. Palmer, and R. E. Bell. "Extensive winter subglacial water storage beneath the Greenland Ice Sheet". *Geophysical Research Letters* 43.24 (2016), pp. 12–484.

Chudley, T. R., P. Christoffersen, S. H. Doyle, M. Bougamont, C. M. Schoonman, B. Hubbard, and M. R. James. "Supraglacial lake drainage at a fast-flowing Greenlandic outlet glacier". *Proceedings of the National Academy of Sciences* 116.51 (2019), pp. 25468–25477.

Clark, P. U., A. S. Dyke, J. D. Shakun, A. E. Carlson, J. Clark, B. Wohlfarth, J. X. Mitrovica, S. W. Hostetler, and A. M. McCabe. "The last glacial maximum". *science* 325.5941 (2009), pp. 710–714.

Clarke, G. K. "Hydraulics of subglacial outburst floods: new insights from the Spring–Hutter formulation". *Journal of Glaciology* 49.165 (2003), pp. 299–313.

Clason, C. C., D. Mair, P. Nienow, I. Bartholomew, A. Sole, S. Palmer, and W. Schwanghart. "Modelling the transfer of supraglacial meltwater to the bed of Leverett Glacier, Southwest Greenland". *The Cryosphere* 9.1 (2015), pp. 123–138.

Cohen, D., T. S. Hooyer, N. R. Iverson, J. Thomason, and M. Jackson. "Role of transient water pressure in quarrying: A subglacial experiment using acoustic emissions". *Journal of Geophysical Research: Earth Surface* 111.F3 (2006).

Colbeck, S. "A study of glacier flow for an open-pit mine: an exercise in applied glaciology". *Journal of Glaciology* 13.69 (1974), pp. 401–414.

Colgan, W., J. E. Box, M. L. Andersen, X. Fettweis, B. Csatho, R. S. Fausto, D. Van As, and J. Wahr. "Greenland high-elevation mass balance: inference and implication of reference period (1961–90) imbalance". *Annals of Glaciology* 56.70 (2015), pp. 105–117.

Colgan, W., K. D. Mankoff, K. K. Kjeldsen, A. A. Bjørk, J. E. Box, S. B. Simonsen, L. S. Sørensen, S. A. Khan, A. M. Solgaard, R. Forsberg, H. Skourup, L. Stenseng, S. S. Kristensen, S. M. Hvidegaard, M. Citterio, N. Karlsson, X. Fettweis, A. P. Ahlstrøm, S. B. Andersen, D. van As, and R. S. Fausto. "Greenland ice sheet mass balance assessed by PROMICE (1995–2015)". *GEUS Bulletin* 43 (2019).

Colgan, W., H. Rajaram, W. Abdalati, C. McCutchan, R. Mottram, M. S. Moussavi, and S. Grigsby. "Glacier crevasses: Observations, models, and mass balance implications". *Reviews of Geophysics* 54.1 (2016), pp. 119–161.

Colgan, W., H. Rajaram, R. S. Anderson, K. Steffen, H. J. Zwally, T. Phillips, and W. Abdalati. "The annual glaciohydrology cycle in the ablation zone of the Greenland ice sheet: Part 2. Observed and modeled ice flow". *Journal of Glaciology* 58.207 (2012), pp. 51–64.

Colgan, W., K. Steffen, W. S. McLamb, W. Abdalati, H. Rajaram, R. Motyka, T. Phillips, and R. Anderson. "An increase in crevasse extent, West Greenland: Hydrologic implications". *Geophysical Research Letters* 38.18 (2011).

Cook, S. J., P. Christoffersen, J. Todd, D. Slater, and N. Chauché. "Coupled modelling of subglacial hydrology and calving-front melting at Store Glacier, West Greenland". *The Cryosphere* 14.3 (2020), pp. 905–924.

Cooley, S. W. and P. Christoffersen. "Observation bias correction reveals more rapidly draining lakes on the Greenland Ice Sheet". *Journal of Geophysical Research: Earth Surface* 122.10 (2017), pp. 1867–1881.

Cooper, M., K. Michaelides, M. Siegert, and J. Bamber. "Paleofluvial landscape inheritance for Jakobshavn Isbræ catchment, Greenland". *Geophysical Research Letters* 43.12 (2016), pp. 6350–6357.

Couston, L.-A. and M. Siegert. "Dynamic flows create potentially habitable conditions in Antarctic subglacial lakes". *Science Advances* 7.8 (2021), eabc3972.

Cowton, T., P. Nienow, I. Bartholomew, A. Sole, and D. Mair. "Rapid erosion beneath the Greenland ice sheet". *Geology* 40.4 (2012), pp. 343–346.

Cowton, T., P. Nienow, A. Sole, J. Wadham, G. Lis, I. Bartholomew, D. Mair, and D. Chandler. "Evolution of drainage system morphology at a land-terminating Greenlandic outlet glacier". *Journal of Geophysical Research: Earth Surface* 118.1 (2013), pp. 29–41.

Creyts, T. T. and C. G. Schoof. "Drainage through subglacial water sheets". *Journal of Geophysical Research: Earth Surface* 114.F4 (2009).

Cuffey, K. M. and G. D. Clow. "Temperature, accumulation, and ice sheet elevation in central Greenland through the last deglacial transition". *Journal of Geophysical Research: Oceans* 102.C12 (1997), pp. 26383–26396.

Culberg, R., D. M. Schroeder, and W. Chu. "Extreme melt season ice layers reduce firn permeability across Greenland". *Nature Communications* 12.1 (2021), pp. 1–9.

Dahl-Jensen, D., K. Mosegaard, N. Gundestrup, G. D. Clow, S. J. Johnsen, A. W. Hansen, and N. Balling. "Past temperatures directly from the Greenland ice sheet". *Science* 282.5387 (1998), pp. 268–271.

Dai, A., D. Luo, M. Song, and J. Liu. "Arctic amplification is caused by sea-ice loss under increasing CO 2". *Nature communications* 10.1 (2019), pp. 1–13.

Dai, C., M. Durand, I. M. Howat, E. H. Altenau, and T. M. Pavelsky. "Estimating river surface elevation from ArcticDEM". *Geophysical Research Letters* 45.7 (2018), pp. 3107–3114.

Dai, C. and I. M. Howat. "Measuring lava flows with ArcticDEM: Application to the 2012–2013 eruption of Tolbachik, Kamchatka". *Geophysical Research Letters* 44.24 (2017), pp. 12–133.

Das, S. B., I. Joughin, M. D. Behn, I. M. Howat, M. A. King, D. Lizarralde, and M. P. Bhatia. "Fracture propagation to the base of the Greenland Ice Sheet during supraglacial lake drainage". *Science* 320.5877 (2008), pp. 778–781.

Davison, B. J., A. J. Sole, S. J. Livingstone, T. R. Cowton, and P. W. Nienow. "The influence of hydrology on the dynamics of land-terminating sectors of the Greenland ice sheet". *Frontiers in Earth Science* 7 (2019), p. 10.

Davison, B., A. J. Sole, T. Cowton, J. Lea, D. A. Slater, D. Fahrner, and P. Nienow. "Subglacial drainage evolution modulates seasonal ice flow variability of three tidewater glaciers in southwest Greenland". *Journal of Geophysical Research: Earth Surface* 125.9 (2020), e2019JF005492.

Dawes, P. R. "Explanatory notes to the geological map of Greenland, 1: 500 000, Humboldt Gletscher, Sheet 6". *Geological Survey of Denmark and Greenland Map Series* 1 (2004), pp. 1–48.

Dawes, P. R. "The bedrock geology under the Inland Ice: the next major challenge for Greenland mapping". *GEUS Bulletin* 17 (2009), pp. 57–60.

De Andrés, E., D. A. Slater, F. Straneo, J. Otero, S. Das, and F. Navarro. "Surface emergence of glacial plumes determined by fjord stratification". *The Cryosphere* 14.6 (2020), pp. 1951–1969.

de Fleurian, B., M. Morlighem, H. Seroussi, E. Rignot, M. R. van den Broeke, P. Kuipers Munneke, J. Mouginot, P. C. Smeets, and A. J. Tedstone. "A modeling study of the effect of runoff variability on the effective pressure beneath Russell

Glacier, West Greenland". *Journal of Geophysical Research: Earth Surface* 121.10 (2016), pp. 1834–1848.

de la Peña, S., I. Howat, P. Nienow, M. Van den Broeke, E. Mosley-Thompson, S. Price, D. Mair, B. Noël, and A. Sole. "Changes in the firn structure of the western Greenland Ice Sheet caused by recent warming". *The Cryosphere* 9.3 (2015), pp. 1203–1211.

Denton, G. H. and D. E. Sugden. "Meltwater features that suggest Miocene ice-sheet overriding of the Transantarctic Mountains in Victoria Land, Antarctica". *Geografiska Annaler: Series A, Physical Geography* 87.1 (2005), pp. 67–85.

Dieser, M., E. L. Broemsen, K. A. Cameron, G. M. King, A. Achberger, K. Choquette, B. Hagedorn, R. Sletten, K. Junge, and B. C. Christner. "Molecular and biogeochemical evidence for methane cycling beneath the western margin of the Greenland Ice Sheet". *The ISME Journal* 8.11 (2014), pp. 2305–2316.

Domack, E., D. Amblas, R. Gilbert, S. Brachfeld, A. Camerlenghi, M. Rebesco, M. Canals, and R. Urgeles. "Subglacial morphology and glacial evolution of the Palmer deep outlet system, Antarctic Peninsula". *Geomorphology* 75.1-2 (2006), pp. 125–142.

Dow, C., A. Hubbard, A. Booth, S. H. Doyle, A. Gusmeroli, and B. Kulessa. "Seismic evidence of mechanically weak sediments underlying Russell Glacier, West Greenland". *Annals of Glaciology* 54.64 (2013), pp. 135–141.

Dow, C., B. Kulessa, I. Rutt, S. Doyle, and A. Hubbard. "Upper bounds on subglacial channel development for interior regions of the Greenland ice sheet". *Journal of Glaciology* 60.224 (2014), pp. 1044–1052.

Dow, C. F., M. Werder, G. Babonis, S. Nowicki, R. T. Walker, B. Csathó, and M. Morlighem. "Dynamics of active subglacial lakes in Recovery Ice Stream". *Journal of Geophysical Research: Earth Surface* 123.4 (2018), pp. 837–850.

Dow, C. F., M. A. Werder, S. Nowicki, and R. T. Walker. "Modeling Antarctic subglacial lake filling and drainage cycles". *The Cryosphere* 10.4 (2016), pp. 1381–1393.

Dowdeswell, J. A. and M. J. Siegert. "The dimensions and topographic setting of Antarctic subglacial lakes and implications for large-scale water storage beneath continental ice sheets". *Geological Society of America Bulletin* 111.2 (1999), pp. 254–263.

Dowdeswell, J. A. and M. J. Siegert. "The physiography of modern Antarctic subglacial lakes". *Global and Planetary Change* 35.3-4 (2003), pp. 221–236.

Doyle, S. H., A. Hubbard, A. A. Fitzpatrick, D. Van As, A. B. Mikkelsen, R. Pettersson, and B. Hubbard. "Persistent flow acceleration within the interior of the Greenland ice sheet". *Geophysical Research Letters* 41.3 (2014), pp. 899–905.

Doyle, S. H., A. Hubbard, R. S. Van de Wal, J. E. Box, D. Van As, K. Scharrer, T. W. Meierbachtol, P. C. Smeets, J. T. Harper, E. Johansson, R. H. Mottram, A. B. Mikkelsen, F. Wilhelms, H. Patton, P. Christoffersen, and B. Hubbard. "Amplified melt and flow of the Greenland ice sheet driven by late-summer cyclonic rainfall". *Nature Geoscience* 8.8 (2015), pp. 647–653.

Doyle, S. H., A. L. Hubbard, C. F. Dow, G. A. Jones, A. Fitzpatrick, A. Gusmeroli, B. Kulessa, K. Lindback, R. Pettersson, and J. E. Box. "Ice tectonic deformation during the rapid in situ drainage of a supraglacial lake on the Greenland Ice Sheet". *The Cryosphere* 7.1 (2013), pp. 129–140.

Drewry, D. J. "Sedimentary basins of the East Antarctic craton from geophysical evidence". *Tectonophysics* 36.1-3 (1976), pp. 301–314.

Driedger, C. L. and A. G. Fountain. "Glacier outburst floods at Mount Rainier, Washington state, USA". *Annals of Glaciology* 13 (1989), pp. 51–55.

Dumont, M., E. Brun, G. Picard, M. Michou, Q. Libois, J. Petit, M. Geyer, S. Morin, and B. Josse. "Contribution of light-absorbing impurities in snow to Greenland's darkening since 2009". *Nature Geoscience* 7.7 (2014), pp. 509–512.

Duxbury, N., I. Zotikov, K. Nealson, V. Romanovsky, and F. Carsey. "A numerical model for an alternative origin of Lake Vostok and its exobiological implications for Mars". *Journal of Geophysical Research: Planets* 106.E1 (2001), pp. 1453–1462.

Echelmeyer, K., T. Clarke, and W. D. Harrison. "Surficial glaciology of Jakobshavns Isbræ, West Greenland: Part I. Surface morphology". *Journal of Glaciology* 37.127 (1991), pp. 368–382.

Einarsson, B., T. Jóhannesson, T. Thorsteinsson, E. Gaidos, and T. Zwinger. "Subglacial flood path development during a rapidly rising jökulhlaup from the western Skaftá cauldron, Vatnajökull, Iceland". *Journal of Glaciology* 63.240 (2017), pp. 670–682.

Ellis-Evans, J. C. and D. Wynn-Williams. "A great lake under the ice". *Nature* 381.6584 (1996), pp. 644–645.

Enderlin, E. M., G. S. Hamilton, F. Straneo, and D. A. Sutherland. "Iceberg meltwater fluxes dominate the freshwater budget in Greenland's iceberg-congested glacial fjords". *Geophysical Research Letters* 43.21 (2016), pp. 11–287.

Enderlin, E. M., I. M. Howat, S. Jeong, M.-J. Noh, J. H. van Angelen, and M. R. van den Broeke. "An improved mass budget for the Greenland ice sheet". *Geophysical Research Letters* 41.3 (2014), pp. 866–872.

Engelhardt, H., W. Harrison, and B. Kamb. "Basal sliding and conditions at the glacier bed as revealed by bore-hole photography". *Journal of Glaciology* 20.84 (1978), pp. 469–508.

Escher, A. and W. S. Watt. *Geology of Greenland*. Vol. 603. Geological Survey of Greenland Copenhagen, 1976.

Evan, A. T., D. J. Vimont, A. K. Heidinger, J. P. Kossin, and R. Bennartz. "The role of aerosols in the evolution of tropical North Atlantic Ocean temperature anomalies". *Science* 324.5928 (2009), pp. 778–781.

Evans, S. "Radio techniques for the measurement of ice thickness". *Polar Record* 11.73 (1963), pp. 406–410.

Evatt, G., A. Fowler, C. Clark, and N. Hulton. "Subglacial floods beneath ice sheets". *Philosophical Transactions of the Royal Society A: Mathematical, Physical and Engineering Sciences* 364.1844 (2006), pp. 1769–1794.

Fahnestock, M., W. Abdalati, I. Joughin, J. Brozena, and P. Gogineni. "High geothermal heat flow, basal melt, and the origin of rapid ice flow in central Greenland". *Science* 294.5550 (2001), pp. 2338–2342.

Felikson, D., T. C. Bartholomaus, G. A. Catania, N. J. Korsgaard, K. H. Kjær, M. Morlighem, B. Noël, M. van den Broeke, L. A. Stearns, E. L. Shroyer, D. A. Sutherland, and J. D. Nash. "Inland thinning on the Greenland ice sheet controlled by outlet glacier geometry". *Nature Geoscience* 10.5 (2017), pp. 366–369.

Ferguson, R. "Sinuosity of supraglacial streams". *Geological Society of America Bulletin* 84.1 (1973), pp. 251–256.

Ferraccioli, F., C. A. Finn, T. A. Jordan, R. E. Bell, L. M. Anderson, and D. Damaske. "East Antarctic rifting triggers uplift of the Gamburtsev Mountains". *Nature* 479.7373 (2011), pp. 388–392.

Fettweis, X., B. Franco, M. Tedesco, J. van Angelen, J. Lenaerts, M. van den Broeke, and H. Gallée. "Estimating the Greenland ice sheet surface mass balance contribution to future sea level rise using the regional atmospheric climate model MAR". *The Cryosphere* 7.2 (2013), pp. 469–489.

Fettweis, X., E. Hanna, C. Lang, A. Belleflamme, M. Erpicum, and H. Gallée. "Brief communication: Important role of the mid-tropospheric atmospheric circulation in the recent surface melt increase over the Greenland ice sheet". *The Cryosphere* 7.1 (2013), pp. 241–248.

Fettweis, X., J. E. Box, C. Agosta, C. Amory, C. Kittel, C. Lang, D. van As, H. Machguth, and H. Gallée. "Reconstructions of the 1900–2015 Greenland ice sheet surface mass balance using the regional climate MAR model". *The Cryosphere* 11.2 (2017), pp. 1015–1033.

Filina, I., V. Lukin, V. Masolov, and D. Blankenship. "Unconsolidated sediments at the bottom of Lake Vostok from seismic data". *US Geological Survey and The National Academies Short Research Paper* 31 (2007).

Filina, I. Y., D. D. Blankenship, M. Thoma, V. V. Lukin, V. N. Masolov, and M. K. Sen. "New 3D bathymetry and sediment distribution in Lake Vostok: Implication for pre-glacial origin and numerical modeling of the internal processes within the lake". *Earth and Planetary Science Letters* 276.1-2 (2008), pp. 106–114.

Fisher, A. T., K. D. Mankoff, S. M. Tulaczyk, S. W. Tyler, N. Foley, and the WISSARD Science Team. "High geothermal heat flux measured below the West Antarctic Ice Sheet". *Science advances* 1.6 (2015), e1500093.

Fitzpatrick, A. A. W., A. L. Hubbard, J. Box, D. J. Quincey, D. Van As, A. Mikkelsen, S. H. Doyle, C. Dow, B. Hasholt, and G. A. Jones. "A decade (2002–2012) of supraglacial lake volume estimates across Russell Glacier, West Greenland". *The Cryosphere* 8.1 (2014), pp. 107–121.

Fitzpatrick, A. A., A. Hubbard, I. Joughin, D. J. Quincey, D. Van As, A. P. Mikkelsen, S. H. Doyle, B. Hasholt, and G. A. Jones. "Ice flow dynamics and surface meltwater

flux at a land-terminating sector of the Greenland ice sheet". *Journal of Glaciology* 59.216 (2013), pp. 687–696.

Flament, T., E. Berthier, and F. Rémy. "Cascading water underneath Wilkes Land, East Antarctic ice sheet, observed using altimetry and digital elevation models". *The cryosphere.* 8 (2014), pp. 673–687.

Flowers, G. E., H. Björnsson, F. Pálsson, and G. K. Clarke. "A coupled sheet-conduit mechanism for jökulhlaup propagation". *Geophysical research letters* 31.5 (2004).

Forster, R. R., J. E. Box, M. R. Van Den Broeke, C. Miége, E. W. Burgess, J. H. Van Angelen, J. T. Lenaerts, L. S. Koenig, J. Paden, C. Lewis, S. P. Gogineni, C. Leuschen, and J. R. McConnell. "Extensive liquid meltwater storage in firn within the Greenland ice sheet". *Nature Geoscience* 7.2 (2014), pp. 95–98.

Fountain, A. G. and J. S. Walder. "Water flow through temperate glaciers". *Reviews of Geophysics* 36.3 (1998), pp. 299–328.

Fowler, A. "Sliding with cavity formation". *Journal of Glaciology* 33.115 (1987), pp. 255–267.

Fowler, A. "Breaking the seal at GrıFIX ME!!!!msvötn, Iceland". *Journal of Glaciology* 45.151 (1999), pp. 506–516.

Fox Maule, C., M. Purucker, and N. Olsen. "Inferring magnetic crustal thickness and geothermal heat flux from crustal magnetic field models". *Danish Climate Centre Report* 9.09 (2009).

Fretwell, P., H. D. Pritchard, D. G. Vaughan, J. L. Bamber, N. E. Barrand, R. Bell, C. Bianchi, R. G. Bingham, D. D. Blankenship, G. Casassa, G. Catania, D. Callens, H. Conway, A. J. Cook, H. F. J. Corr, D. Damaske, V. Damm, F. Ferraccioli, R. Forsberg, S. Fujita, Y. Gim, P. Gogineni, J. A. Griggs, R. C. A. Hindmarsh, P. Holmlund, J. W. Holt, R. W. Jacobel, A. Jenkins, W. Jokat, T. Jordan, E. C. King, J. Kohler, W. Krabill, M. Riger-Kusk, K. A. Langley, G. Leitchenkov, C. Leuschen, B. P. Luyendyk, K. Matsuoka, J. Mouginot, F. O. Nitsche, Y. Nogi, O. A. Nost, S. V. Popov, E. Rignot, D. M. Rippin, A. Rivera, J. Roberts, N. Ross, M. J. Siegert, A. M. Smith, D. Steinhage, M. Studinger, B. Sun, B. K. Tinto, B. C. Welch, D. Wilson, D. A. Young, C. Xiangbin, and A. Zirizzotti. "Bedmap2: improved ice bed, surface and thickness datasets for Antarctica". *The Cryosphere* 7.1 (2013), pp. 375–393.

Fricker, H. A., M. R. Siegfried, S. P. Carter, and T. A. Scambos. "A decade of progress in observing and modelling Antarctic subglacial water systems". *Philosophical Transactions of the Royal Society A: Mathematical, Physical and Engineering Sciences* 374.2059 (2016), p. 20140294.

Fricker, H. A., S. P. Carter, R. E. Bell, and T. Scambos. "Active lakes of Recovery Ice Stream, East Antarctica: a bedrock-controlled subglacial hydrological system". *Journal of Glaciology* 60.223 (2014), pp. 1015–1030.

Fricker, H. A. and T. Scambos. "Connected subglacial lake activity on lower Mercer and Whillans ice streams, West Antarctica, 2003–2008". *Journal of Glaciology* 55.190 (2009), pp. 303–315.

Fricker, H. A., T. Scambos, R. Bindschadler, and L. Padman. "An active subglacial water system in West Antarctica mapped from space". *Science* 315.5818 (2007), pp. 1544–1548.

Fricker, H. A., T. Scambos, S. Carter, C. Davis, T. Haran, and I. Joughin. "Synthesizing multiple remote-sensing techniques for subglacial hydrologic mapping: application to a lake system beneath MacAyeal Ice Stream, West Antarctica". *Journal of Glaciology* 56.196 (2010), pp. 187–199.

Fujita, S., P. Holmlund, K. Matsuoka, H. Enomoto, K. Fukui, F. Nakazawa, S. Sugiyama, and S. Surdyk. "Radar diagnosis of the subglacial conditions in Dronning Maud Land, East Antarctica". *The Cryosphere* 6.5 (2012), pp. 1203–1219.

Fujita, S., H. Maeno, and K. Matsuoka. "Radio-wave depolarization and scattering within ice sheets: a matrix-based model to link radar and ice-core measurements and its application". *Journal of Glaciology* 52.178 (2006), pp. 407–424.

Funder, S. and L. Hansen. "The Greenland ice sheet—a model for its culmination and decay during and after the last glacial maximum". *Bulletin of the Geological Society of Denmark* 42.2 (1996), pp. 137–152.

Funder, S., K. K. Kjeldsen, K. H. Kjær, and C. Ó. Cofaigh. "The Greenland Ice Sheet during the past 300,000 years: A review". *Developments in Quaternary Sciences* 15 (2011), pp. 699–713.

Gabrielli, P., D. Hardy, N. Kehrwald, M. Davis, G. Cozzi, C. Turetta, C. Barbante, and L. Thompson. "Deglaciated areas of Kilimanjaro as a source of volcanic trace

elements deposited on the ice cap during the late Holocene". *Quaternary Science Reviews* 93 (2014), pp. 1–10.

Gaidos, E., T. Jóhannesson, B. Einarsson, T. Thorsteinsson, J. Amend, and M. Skidmore. "Aprés Nous, le Déluge: A Human-Triggered Jökulhlaup From a Subglacial Lake". *Geophysical Research Letters* 47.22 (2020), e2020GL089876.

Glen, J. and J. Paren. "The electrical properties of snow and ice". *Journal of Glaciology* 15.73 (1975), pp. 15–38.

Glennie, C. "Arctic high-resolution elevation models: Accuracy in sloped and vegetated terrain". *Journal of Surveying Engineering* 144.1 (2018), p. 06017003.

Goeller, S., D. Steinhage, M. Thoma, and K. Grosfeld. "Assessing the subglacial lake coverage of Antarctica". *Annals of Glaciology* 57.72 (2016), pp. 109–117.

Goelzer, H., S. Nowicki, A. Payne, E. Larour, H. Seroussi, W. H. Lipscomb, J. Gregory, A. Abe-Ouchi, A. Shepherd, E. Simon, C. Agosta, P. Alexander, A. Aschwanden, A. Barthel, R. Calov, C. Chambers, Y. Choi, J. Cuzzone, C. Dumas, T. Edwards, D. Felikson, X. Fettweis, N. R. Golledge, R. Greve, A. Humbert, P. Huybrechts, S. Le clec'h, V. Lee, G. Leguy, C. Little, D. P. Lowry, M. Morlighem, I. Nias, A. Quiquet, M. Rückamp, N.-J. Schlegel, D. A. Slater, R. S. Smith, F. Straneo, L. Tarasov, R. van de Wal, and M. van den Broeke. "The future sea-level contribution of the Greenland ice sheet: a multi-model ensemble study of ISMIP6". *The Cryosphere* 14.9 (2020), pp. 3071–3096.

Gogineni, S., D. Tammana, D. Braaten, C. Leuschen, T. Akins, J. Legarsky, P. Kanagaratnam, J. Stiles, C. Allen, and K. Jezek. "Coherent radar ice thickness measurements over the Greenland ice sheet". *Journal of Geophysical Research: Atmospheres* 106.D24 (2001), pp. 33761–33772.

Golledge, N. R., E. D. Keller, N. Gomez, K. A. Naughten, J. Bernales, L. D. Trusel, and T. L. Edwards. "Global environmental consequences of twenty-first-century ice-sheet melt". *Nature* 566.7742 (2019), pp. 65–72.

Gooch, B. T., D. A. Young, and D. D. Blankenship. "Potential groundwater and heterogeneous heat source contributions to ice sheet dynamics in critical submarine basins of East Antarctica". *Geochemistry, Geophysics, Geosystems* 17.2 (2016), pp. 395–409.

Gray, L., I. Joughin, S. Tulaczyk, V. B. Spikes, R. Bindschadler, and K. Jezek. "Evidence for subglacial water transport in the West Antarctic Ice Sheet through three-dimensional satellite radar interferometry". *Geophysical Research Letters* 32.3 (2005).

Greenwood, S. L., C. C. Clason, C. Helanow, and M. Margold. "Theoretical, contemporary observational and palaeo-perspectives on ice sheet hydrology: processes and products". *Earth-Science Reviews* 155 (2016), pp. 1–27.

Grima, C., D. M. Schroeder, D. D. Blankenship, and D. A. Young. "Planetary landing-zone reconnaissance using ice-penetrating radar data: Concept validation in Antarctica". *Planetary and Space Science* 103 (2014), pp. 191–204.

Groh, A., M. Horwath, A. Horvath, R. Meister, L. Sandberg Sørensen, V. R. Barletta, R. Forsberg, B. Wouters, P. Ditmar, J. Ran, R. Klees, X. Su, K. Shang, J. Guo, C. K. Shum, E. Schrama, and A. Shepherd. "Evaluating GRACE mass change time series for the Antarctic and Greenland Ice Sheet—Methods and results". *Geosciences* 9.10 (2019), p. 415.

Gudmundsson, M. and T. Högnadóttir. "Volcanic systems and calderas in the Vatnajökull region, central Iceland: Constraints on crustal structure from gravity data". *Journal of Geodynamics* 43.1 (2007), pp. 153–169.

Haeberli, W. "Frequency and characteristics of glacier floods in the Swiss Alps". *Annals of Glaciology* 4 (1983), pp. 85–90.

Hagen, J., O. Korsen, and G. Vatne. "Drainage pattern in a subpolar glacier: Brøggerbreen, Svalbard". *Arctic Hydrology, Present and Future Tasks* (1991), pp. 121–131.

Halbach, L., M. Vihtakari, P. Duarte, A. Everett, M. A. Granskog, H. Hop, H. M. Kauko, S. Kristiansen, P. I. Myhre, A. K. Pavlov, A. Pramanik, A. Tatarek, T. Torsvik, J. M. Wiktor, A. Wold, A. Wulff, H. Steen, and P. Assmy. "Tidewater glaciers and bedrock characteristics control the phytoplankton growth environment in a fjord in the arctic". *Frontiers in Marine Science* 6 (2019), p. 254.

Hall, R., R. Erdélyi, E. Hanna, J. M. Jones, and A. A. Scaife. "Drivers of North Atlantic polar front jet stream variability". *International Journal of Climatology* 35.8 (2015), pp. 1697–1720.

Hallet, B., L. Hunter, and J. Bogen. "Rates of erosion and sediment evacuation by glaciers: A review of field data and their implications". *Global and Planetary Change* 12.1-4 (1996), pp. 213–235.

Hambrey, M. "Sedimentary processes and buried ice phenomena in the pro-glacial areas of Spitsbergen glaciers". *Journal of Glaciology* 30.104 (1984), pp. 116–119.

Hanna, E., T. E. Cropper, R. J. Hall, and J. Cappelen. "Greenland Blocking Index 1851–2015: a regional climate change signal". *International Journal of Climatology* 36.15 (2016), pp. 4847–4861.

Hanna, E., P. Huybrechts, K. Steffen, J. Cappelen, R. Huff, C. Shuman, T. Irvine-Fynn, S. Wise, and M. Griffiths. "Increased runoff from melt from the Greenland Ice Sheet: a response to global warming". *Journal of Climate* 21.2 (2008), pp. 331–341.

Hanna, E., J. McConnell, S. Das, J. Cappelen, and A. Stephens. "Observed and modeled Greenland ice sheet snow accumulation, 1958–2003, and links with regional climate forcing". *Journal of Climate* 19.3 (2006), pp. 344–358.

Hanna, E., F. J. Navarro, F. Pattyn, C. M. Domingues, X. Fettweis, E. R. Ivins, R. J. Nicholls, C. Ritz, B. Smith, S. Tulaczyk, P. L. Whitehouse, and H. J. Zwally. "Ice-sheet mass balance and climate change". *Nature* 498.7452 (2013), pp. 51–59.

Harper, J., N. Humphrey, W. T. Pfeffer, J. Brown, and X. Fettweis. "Greenland ice-sheet contribution to sea-level rise buffered by meltwater storage in firn". *Nature* 491.7423 (2012), pp. 240–243.

Harper, J. T., N. F. Humphrey, T. W. Meierbachtol, J. A. Graly, and U. H. Fischer. "Borehole measurements indicate hard bed conditions, Kangerlussuaq sector, western Greenland Ice Sheet". *Journal of Geophysical Research: Earth Surface* 122.9 (2017), pp. 1605–1618.

Hasholt, B., A. B. Mikkelsen, M. H. Nielsen, and M. A. D. Larsen. "Observations of runoff and sediment and dissolved loads from the Greenland ice sheet at Kangerlussuaq, West Greenland, 2007 to 2010". *Zeitschrift für Geomorphologie* 57.2 (2013), pp. 3–27.

Haubner, K., J. E. Box, N. J. Schlegel, E. Y. Larour, M. Morlighem, A. M. Solgaard, K. K. Kjeldsen, S. H. Larsen, E. Rignot, T. K. Dupont, and K. H. Kjær. "Simulating ice thickness and velocity evolution of Upernavik Isstrøm 1849–2012 by forcing prescribed terminus positions in ISSM". *The Cryosphere* 12.4 (2018), pp. 1511–1522.

Hawkings, J., J. Wadham, M. Tranter, E. Lawson, A. Sole, T. Cowton, A. Tedstone, I. Bartholomew, P. Nienow, D. Chandler, and J. Telling. "The effect of warming climate on nutrient and solute export from the Greenland Ice Sheet". *Geochemical Perspectives Letters* 1 (2015), pp. 94–104.

Hawley, R. L., T. A. Neumann, C. M. Stevens, K. M. Brunt, and T. C. Sutterley. "Greenland Ice Sheet Elevation Change: Direct Observation of Process and Attribution at Summit". *Geophysical Research Letters* 47.22 (2020), e2020GL088864.

Herron, M. M. and C. C. Langway. "Firn densification: an empirical model". *Journal of Glaciology* 25.93 (1980), pp. 373–385.

Higgins, A. K. "North Greenland glacier velocities and calf ice production". *Polarforschung* 60.1 (1991), pp. 1–23.

Hill, E. A., J. R. Carr, and C. R. Stokes. "A review of recent changes in major marine-terminating outlet glaciers in Northern Greenland". *Frontiers in Earth Science* 4 (2017), p. 111.

Hill, E. A., J. R. Carr, C. R. Stokes, and G. H. Gudmundsson. "Dynamic changes in outlet glaciers in northern Greenland from 1948 to 2015". *The cryosphere.* 12.10 (2018), pp. 3243–3263.

Hindmarsh, R. C., J.-M. Gwendolyn, and F. Parrenin. "A large-scale numerical model for computing isochrone geometry". *Annals of Glaciology* 50.51 (2009), pp. 130–140.

Hirano, A., R. Welch, and H. Lang. "Mapping from ASTER stereo image data: DEM validation and accuracy assessment". *ISPRS Journal of Photogrammetry and remote sensing* 57.5-6 (2003), pp. 356–370.

Hock, R. and R. L. Hooke. "Evolution of the internal drainage system in the lower part of the ablation area of Storglaciären, Sweden". *Geological Society of America Bulletin* 105.4 (1993), pp. 537–546.

Hodge, S. M. "Direct Measurement of Basal Water Pressures: Progress and Problemss". *Journal of Glaciology* 23.89 (1979), pp. 309–319.

Hodgson, D. A., M. J. Bentley, J. A. Smith, J. Klepacki, K. Makinson, A. M. Smith, K. Saw, R. Scherer, R. Powell, S. Tulaczyk, M. Rose, D. Pearce, M. Mowlem, P. Keen, and M. J. Siegert. "Technologies for retrieving sediment cores in Antarctic subglacial settings". *Philosophical Transactions of the Royal Society A: Mathematical, Physical and Engineering Sciences* 374.2059 (2016), p. 20150056.

Hodson, A. and R. I. Ferguson. "Fluvial suspended sediment transport from cold and warm-based glaciers in Svalbard". *Earth Surface Processes and Landforms* 24.11 (1999), pp. 957–974.

Hodson, A., J. Kohler, M. Brinkhaus, and P. Wynn. "Multi-year water and surface energy budget of a high-latitude polythermal glacier: evidence for overwinter water storage in a dynamic subglacial reservoir". *Annals of Glaciology* 42 (2005), pp. 42–46.

Hodson, T., R. Powell, S. A. Brachfeld, S. Tulaczyk, R. Scherer, and W. S. Team. "Physical processes in Subglacial Lake Whillans, West Antarctica: inferences from sediment cores". *Earth and Planetary Science Letters* 444 (2016), pp. 56–63.

Hofer, S., C. Lang, C. Amory, C. Kittel, A. Delhasse, A. Tedstone, and X. Fettweis. "Greater Greenland Ice Sheet contribution to global sea level rise in CMIP6". *Nature Communications* 11.1 (2020), pp. 1–11.

Hofer, S., A. J. Tedstone, X. Fettweis, and J. L. Bamber. "Decreasing cloud cover drives the recent mass loss on the Greenland Ice Sheet". *Science Advances* 3.6 (2017), e1700584.

Hoffman, A. O., K. Christianson, D. Shapero, B. E. Smith, and I. Joughin. "Brief communication: Heterogenous thinning and subglacial lake activity on Thwaites Glacier, West Antarctica". *The Cryosphere* 14.12 (2020), pp. 4603–4609.

Hoffman, M. J., M. Perego, L. C. Andrews, S. F. Price, T. A. Neumann, J. V. Johnson, G. Catania, and M. P. Lüthi. "Widespread moulin formation during supraglacial lake drainages in Greenland". *Geophysical Research Letters* 45.2 (2018), pp. 778–788.

Hoffman, M., G. Catania, T. Neumann, L. Andrews, and J. Rumrill. "Links between acceleration, melting, and supraglacial lake drainage of the western Greenland Ice Sheet". *Journal of Geophysical Research: Earth Surface* 116.F4 (2011).

Holdsworth, G. "Primary transverse crevasses". *Journal of Glaciology* 8.52 (1969), pp. 107–129.

Holinde, L. and O. Zielinski. "Bio-optical characterization and light availability parameterization in Uummannaq Fjord and Vaigat–Disko Bay (West Greenland)". *Ocean Science* 12.1 (2016), pp. 117–128.

Holmlund, P. "Internal geometry and evolution of moulins, Storglaciären, Sweden". *Journal of Glaciology* 34.117 (1988), pp. 242–248.

Hooke, R. L. *Principles of glacier mechanics*. Cambridge university press, 2005.

Hooke, R. L. "On the role of mechanical energy in maintaining subglacial water conduits at atmospheric pressure". *Journal of Glaciology* 30.105 (1984), pp. 180–187.

Hooke, R. L., T. Laumann, and J. Kohler. "Subglacial water pressures and the shape of subglacial conduits". *Journal of Glaciology* 36.122 (1990), pp. 67–71.

Hopwood, M. J., D. Carroll, T. Browning, L. Meire, J. Mortensen, S. Krisch, and E. P. Achterberg. "Non-linear response of summertime marine productivity to increased meltwater discharge around Greenland". *Nature Communications* 9.1 (2018), pp. 1–9.

Horgan, H. J., S. Anandakrishnan, R. W. Jacobel, K. Christianson, R. B. Alley, D. S. Heeszel, S. Picotti, and J. I. Walter. "Subglacial Lake Whillans—Seismic observations of a shallow active reservoir beneath a West Antarctic ice stream". *Earth and Planetary Science Letters* 331 (2012), pp. 201–209.

How, P., K. M. Schild, D. I. Benn, R. Noormets, N. Kirchner, A. Luckman, D. Vallot, N. R. Hulton, and C. Borstad. "Calving controlled by melt-under-cutting: detailed calving styles revealed through time-lapse observations". *Annals of Glaciology* 60.78 (2019), pp. 20–31.

Howat, I. M., J. E. Box, Y. Ahn, A. Herrington, and E. M. McFadden. "Seasonal variability in the dynamics of marine-terminating outlet glaciers in Greenland". *Journal of Glaciology* 56.198 (2010), pp. 601–613.

Howat, I. M., A. Negrete, and B. E. Smith. "The Greenland Ice Mapping Project (GIMP) land classification and surface elevation data sets". *The Cryosphere* 8.4 (2014), pp. 1509–1518.

Howat, I. M., S. Pena, J. van Angelen, J. Lenaerts, and M. van den Broeke. "Brief Communication: Expansion of meltwater lakes on the Greenland ice sheet". *The Cryosphere* 7.1 (2013), pp. 201–204.

Howat, I. M., C. Porter, M.-J. Noh, B. Smith, and S. Jeong. "Brief Communication: Sudden drainage of a subglacial lake beneath the Greenland Ice Sheet". *The Cryosphere* 9.1 (2015), pp. 103–108.

Howat, I. M., C. Porter, B. E. Smith, M.-J. Noh, and P. Morin. "The reference elevation model of Antarctica". *The Cryosphere* 13.2 (2019), pp. 665–674.

Howat, I. M., B. E. Smith, I. Joughin, and T. A. Scambos. "Rates of southeast Greenland ice volume loss from combined ICESat and ASTER observations". *Geophysical Research Letters* 35.17 (2008).

Hubbard, A., W. Lawson, B. Anderson, B. Hubbard, and H. Blatter. "Evidence for subglacial ponding across Taylor Glacier, Dry Valleys, Antarctica". *Annals of Glaciology* 39 (2004), pp. 79–84.

Hubbard, B., M. Sharp, I. Willis, M. Nielsen, and C. Smart. "Borehole water-level variations and the structure of the subglacial hydrological system of Haut Glacier d'Arolla, Valais, Switzerland". *Journal of Glaciology* 41.139 (1995), pp. 572–583.

Hubbard, B. and N. F. Glasser. *Field techniques in glaciology and glacial geomorphology.* John Wiley & Sons, 2005.

Hubbard, B. and M. Sharp. "Weertman regelation, multiple refreezing events and the isotopic evolution of the basal ice layer". *Journal of Glaciology* 39.132 (1993), pp. 275–291.

Hudson, B., I. Overeem, D. McGrath, J. Syvitski, A. Mikkelsen, and B. Hasholt. "MODIS observed increase in duration and spatial extent of sediment plumes in Greenland fjords". *The Cryosphere* 8.4 (2014), pp. 1161–1176.

Humphrey, N. F., J. T. Harper, and W. T. Pfeffer. "Thermal tracking of meltwater retention in Greenland's accumulation area". *Journal of Geophysical Research: Earth Surface* 117.F1 (2012).

Iken, A. "The effect of the subglacial water pressure on the sliding velocity of a glacier in an idealized numerical model". *Journal of Glaciology* 27.97 (1981), pp. 407–421.

Iken, A. and R. A. Bindschadler. "Combined measurements of subglacial water pressure and surface velocity of Findelengletscher, Switzerland: conclusions about drainage system and sliding mechanism". *Journal of Glaciology* 32.110 (1986), pp. 101–119.

Ilisei, A.-M., M. Khodadadzadeh, and L. Bruzzone. "Extraction of Statistical Features for Improved Automatic Detection of Subglacial Lakes in Radar Sounder Data". *IGARSS 2018 - 2018 IEEE International Geoscience and Remote Sensing Symposium* (2018), pp. 6792–6795.

Ilisei, A.-M., M. Khodadadzadeh, A. Ferro, and L. Bruzzone. "An Automatic Method for Subglacial Lake Detection in Ice Sheet Radar Sounder Data". *IEEE Transactions on Geoscience and Remote Sensing* 57.6 (2019), pp. 3252–3270.

Inall, M. E., T. Murray, F. R. Cottier, K. Scharrer, T. J. Boyd, K. J. Heywood, and S. L. Bevan. "Oceanic heat delivery via Kangerdlugssuaq Fjord to the south-east Greenland ice sheet". *Journal of Geophysical Research: Oceans* 119.2 (2014), pp. 631–645.

Irvine-Fynn, T., B. Moorman, I. Willis, D. Sjogren, A. Hodson, P. Mumford, F. Walter, and J. Williams. "Geocryological processes linked to High Arctic proglacial stream suspended sediment dynamics: examples from Bylot Island, Nunavut, and Spitsbergen, Svalbard". *Hydrological Processes: An International Journal* 19.1 (2005), pp. 115–135.

Iverson, N. R. "A theory of glacial quarrying for landscape evolution models". *Geology* 40.8 (2012), pp. 679–682.

Iverson, N. R., R. W. Baker, R. L. Hooke, B. Hanson, and P. Jansson. "Coupling between a glacier and a soft bed: I. A relation between effective pressure and local shear stress determined from till elasticity". *Journal of Glaciology* 45.149 (1999), pp. 31–40.

Jackson, R. H., E. L. Shroyer, J. D. Nash, D. A. Sutherland, D. Carroll, M. J. Fried, G. A. Catania, T. C. Bartholomaus, and L. A. Stearns. "Near-glacier surveying of a subglacial discharge plume: Implications for plume parameterizations". *Geophysical Research Letters* 44.13 (2017), pp. 6886–6894.

Jacobel, R. W., B. C. Welch, D. Osterhouse, R. Pettersson, and J. A. MacGregor. "Spatial variation of radar-derived basal conditions on Kamb Ice Stream, West Antarctica". *Annals of Glaciology* 50.51 (2009), pp. 10–16.

Jamieson, S. S., N. Ross, J. S. Greenbaum, D. A. Young, A. R. Aitken, J. L. Roberts, D. D. Blankenship, S. Bo, and M. J. Siegert. "An extensive subglacial lake and canyon system in Princess Elizabeth Land, East Antarctica". *Geology* 44.2 (2016), pp. 87–90.

Jansson, P., R. Hock, and T. Schneider. "The concept of glacier storage: a review". *Journal of Hydrology* 282.1-4 (2003), pp. 116–129.

Jenks, G. F. *Optimal data classification for choropleth maps*. Department of Geographiy, University of Kansas Occasional Paper, 1977.

Johannesson, T. "Propagation of a subglacial flood wave during the initiation of a jökulhlaup". *Hydrological Sciences Journal* 47.3 (2002), pp. 417–434.

Johansson, A. M., P. Jansson, and I. A. Brown. "Spatial and temporal variations in lakes on the Greenland Ice Sheet". *Journal of hydrology* 476 (2013), pp. 314–320.

Johari, G. P. and P. Charette. "The permittivity and attenuation in polycrystalline and single-crystal ice Ih at 35 and 60 MHz". *Journal of Glaciology* 14.71 (1975), pp. 293–303.

Jordan, T., F. Ferraccioli, H. Corr, A. Graham, E. Armadillo, and E. Bozzo. "Hypothesis for mega-outburst flooding from a palaeo-subglacial lake beneath the East Antarctic Ice Sheet". *Terra Nova* 22.4 (2010), pp. 283–289.

Jordan, T. M., J. Bamber, C. Williams, J. Paden, M. J. Siegert, P. Huybrechts, O. Gagliardini, and F. Gillet-Chaulet. "An ice-sheet-wide framework for englacial attenuation from ice-penetrating radar data". *The Cryosphere* 10.4 (2016), pp. 1547–1570.

Jordan, T. M., M. A. Cooper, D. M. Schroeder, C. N. Williams, J. D. Paden, M. J. Siegert, and J. L. Bamber. "Self-affine subglacial roughness: consequences for radar scattering and basal water discrimination in northern Greenland". *The Cryosphere* 11.3 (2017), pp. 1247–1264.

Jordan, T. M., C. N. Williams, D. M. Schroeder, Y. M. Martos, M. A. Cooper, M. J. Siegert, J. D. Paden, P. Huybrechts, and J. L. Bamber. "A constraint upon the basal water distribution and thermal state of the Greenland Ice Sheet from radar bed echoes". *The Cryosphere* 12.9 (2018), pp. 2831–2854.

Joughin, I., B. Smith, I. Howat, T. Scambos, and T. Moon. *MEaSUREs Greenland ice sheet velocity map from InSAR data, last accessed: 1 December 2021)*. Version 2. National Snow and Ice Data Center, 2017. URL: https://nsidc.org/the-drift/data-update/measures-greenland-ice-sheet-velocity-map-from-insar-data-version-2-released/.

Joughin, I., S. B. Das, M. A. King, B. E. Smith, I. M. Howat, and T. Moon. "Seasonal speedup along the western flank of the Greenland Ice Sheet". *Science* 320.5877 (2008), pp. 781–783.

Joughin, I., M. Fahnestock, D. MacAyeal, J. L. Bamber, and P. Gogineni. "Observation and analysis of ice flow in the largest Greenland ice stream". *Journal of Geophysical Research: Atmospheres* 106.D24 (2001), pp. 34021–34034.

Joughin, I., B. E. Smith, and I. M. Howat. "A complete map of Greenland ice velocity derived from satellite data collected over 20 years". *Journal of Glaciology* 64.243 (2018), pp. 1–11.

Joughin, I., B. E. Smith, I. M. Howat, T. Scambos, and T. Moon. "Greenland flow variability from ice-sheet-wide velocity mapping". *Journal of Glaciology* 56.197 (2010), pp. 415–430.

Joughin, I., S. Tulaczyk, D. R. MacAyeal, and H. Engelhardt. "Melting and freezing beneath the Ross ice streams, Antarctica". *Journal of Glaciology* 50.168 (2004), pp. 96–108.

Jouzel, J., J.-R. Petit, R. Souchez, N. Barkov, V. Y. Lipenkov, D. Raynaud, M. Stievenard, N. Vassiliev, V. Verbeke, and F. Vimeux. "More than 200 meters of lake ice above subglacial Lake Vostok, Antarctica". *Science* 286.5447 (1999), pp. 2138–2141.

Kamb, B. "Glacier surge mechanism based on linked cavity configuration of the basal water conduit system". *Journal of Geophysical Research: Solid Earth* 92.B9 (1987), pp. 9083–9100.

Kanna, N., S. Sugiyama, Y. Ohashi, D. Sakakibara, Y. Fukamachi, and D. Nomura. "Upwelling of macronutrients and dissolved inorganic carbon by a subglacial freshwater driven plume in Bowdoin Fjord, northwestern Greenland". *Journal of Geophysical Research: Biogeosciences* 123.5 (2018), pp. 1666–1682.

Kapitsa, A. "Novye dannye o moshchnosti lednikovogo pokrova tsentral'nyh rayonov Antarktidy [New data about ice thickness of the Central parts of Antarctica]". *SAE Rep* 19 (1960), pp. 10–15.

Kapitsa, A. "Podlenyy rel'ef Antarktidy [Subglacial topography of Antarctica]". *Results of researches on International Geophysical Projects* (1968).

Kapitsa, A., J. Ridley, G. d. Q. Robin, M. Siegert, and I. Zotikov. "A large deep freshwater lake beneath the ice of central East Antarctica". *Nature* 381.6584 (1996), pp. 684–686.

Karl, D., D. Bird, K. Björkman, T. Houlihan, R. Shackelford, and L. Tupas. "Microorganisms in the accreted ice of Lake Vostok, Antarctica". *Science* 286.5447 (1999), pp. 2144–2147.

Karlsson, N. B. and D. Dahl-Jensen. "Response of the large-scale subglacial drainage system of Northeast Greenland to surface elevation changes". *The Cryosphere* 9.4 (2015), pp. 1465–1479.

Karlsson, N. B., A. M. Solgaard, K. D. Mankoff, F. Gillet-Chaulet, J. A. MacGregor, J. E. Box, M. Citterio, W. T. Colgan, S. H. Larsen, K. K. Kjeldsen, N. J. Korsgaard, D. I. Benn, I. J. Hewitt, and R. S. Fausto. "A first constraint on basal melt-water production of the Greenland ice sheet". *Nature Communications* 12.1 (2021), pp. 1–10.

Kavanaugh, J. L. and G. K. Clarke. "Evidence for extreme pressure pulses in the subglacial water system". *Journal of Glaciology* 46.153 (2000), pp. 206–212.

Keegan, K. M., M. R. Albert, J. R. McConnell, and I. Baker. "Climate change and forest fires synergistically drive widespread melt events of the Greenland Ice Sheet". *Proceedings of the National Academy of Sciences* 111.22 (2014), pp. 7964–7967.

Kern, M., R. Cullen, B. Berruti, J. Bouffard, T. Casal, M. R. Drinkwater, A. Gabriele, A. Lecuyot, M. Ludwig, R. Midthassel, I. Navas Traver, T. Parrinello, G. Ressler, E. Andersson, C. Martin-Puig, O. Andersen, A. Bartsch, S. Farrell, S. Fleury, S. Gascoin, A. Guillot, A. Humbert, E. Rinne, A. Shepherd, M. R. van den Broeke, and J. Yackel. "The Copernicus Polar Ice and Snow Topography Altimeter (CRISTAL) high-priority candidate mission". *The Cryosphere* 14.7 (2020), pp. 2235–2251.

Khan, S. A., A. Aschwanden, A. A. Bjørk, J. Wahr, K. K. Kjeldsen, and K. H. Kjaer. "Greenland ice sheet mass balance: a review". *Reports on progress in physics* 78.4 (2015), p. 046801.

Kim, B.-H., C.-K. Lee, K.-W. Seo, W. S. Lee, and T. Scambos. "Active subglacial lakes and channelized water flow beneath the Kamb Ice Stream". *The Cryosphere* 10.6 (2016), pp. 2971–2980.

Kimura, S., P. R. Holland, A. Jenkins, and M. Piggott. "The effect of meltwater plumes on the melting of a vertical glacier face". *Journal of Physical Oceanography* 44.12 (2014), pp. 3099–3117.

Kirkham, J. D., K. A. Hogan, R. D. Larter, N. S. Arnold, F. O. Nitsche, N. R. Golledge, and J. A. Dowdeswell. "Past water flow beneath pine Island and Thwaites glaciers, west Antarctica". *The Cryosphere* 13.7 (2019), pp. 1959–1981.

Kjeldsen, K. K., J. Mortensen, J. Bendtsen, D. Petersen, K. Lennert, and S. Rysgaard. "Ice-dammed lake drainage cools and raises surface salinities in a tidewater outlet glacier fjord, west Greenland". *Journal of Geophysical Research: Earth Surface* 119.6 (2014), pp. 1310–1321.

Koenig, L. S., D. J. Lampkin, L. N. Montgomery, S. L. Hamilton, J. B. Turrin, C. A. Joseph, S. E. Moutsafa, B. Panzer, K. A. Casey, J. D. Paden, C. Leuschen, and P. Gogineni. "Wintertime storage of water in buried supraglacial lakes across the Greenland Ice Sheet". *The Cryosphere* 9.4 (2015), pp. 1333–1342.

Koenig, S., R. DeConto, and D. Pollard. "Impact of reduced Arctic sea ice on Greenland ice sheet variability in a warmer than present climate". *Geophysical Research Letters* 41.11 (2014), pp. 3933–3942.

Korsun, S. and M. Hald. "Seasonal dynamics of benthic foraminifera in a glacially fed fjord of Svalbard, European Arctic". *The Journal of Foraminiferal Research* 30.4 (2000), pp. 251–271.

Koziol, C., N. Arnold, A. Pope, and W. Colgan. "Quantifying supraglacial meltwater pathways in the Paakitsoq region, West Greenland". *Journal of Glaciology* 63.239 (2017), pp. 464–476.

Koziol, C. P. and N. Arnold. "Modelling seasonal meltwater forcing of the velocity of land-terminating margins of the Greenland Ice Sheet". *The Cryosphere* 12.3 (2018), pp. 971–991.

Krawczynski, M., M. Behn, S. Das, and I. Joughin. "Constraints on the lake volume required for hydro-fracture through ice sheets". *Geophysical Research Letters* 36.10 (2009).

Kremser, S., L. W. Thomason, M. von Hobe, M. Hermann, T. Deshler, C. Timmreck, M. Toohey, A. Stenke, J. P. Schwarz, R. Weigel, S. Fueglistaler, F. J. Prata, J.-P. Vernier, H. Schlager, J. E. Barnes, J.-C. Antuña-Marrero, D. Fairlie, M. Palm, E. Mahieu, J. Notholt, M. Rex, C. Bingen, F. Vanhellemont, A. Bourassa, J. M. C. Plane, D. Klocke, S. A. Carn, L. Clarisse, T. Trickl, R. Neely, A. D. James, L. Rieger, J. C. Wilson, and M. Brian. "Stratospheric aerosol—Observations, processes, and impact on climate". *Reviews of Geophysics* 54.2 (2016), pp. 278–335.

Krieger, G., A. Moreira, H. Fiedler, I. Hajnsek, M. Werner, M. Younis, and M. Zink. "TanDEM-X: A satellite formation for high-resolution SAR interferometry". *IEEE Transactions on Geoscience and Remote Sensing* 45.11 (2007), pp. 3317–3341.

Kuhn, G., C.-D. Hillenbrand, S. Kasten, J. A. Smith, F. O. Nitsche, T. Frederichs, S. Wiers, W. Ehrmann, J. P. Klages, and J. M. Mogollón. "Evidence for a palaeo-subglacial lake on the Antarctic continental shelf'. *Nature Communications* 8.1 (2017), pp. 1–10.

Kulessa, B., A. L. Hubbard, A. D. Booth, M. Bougamont, C. F. Dow, S. H. Doyle, P. Christoffersen, K. Lindbäck, R. Pettersson, A. A. W. Fitzpatrick, and G. A. Jones. "Seismic evidence for complex sedimentary control of Greenland Ice Sheet flow". *Science Advances* 3.8 (2017), e1603071.

Lamarche-Gagnon, G., J. L. Wadham, B. S. Lollar, S. Arndt, P. Fietzek, A. D. Beaton, A. J. Tedstone, J. Telling, E. A. Bagshaw, J. R. Hawkings, T. J. Kohler, J. D. Zarsky, M. C. Mowlem, A. M. Anesio, and M. Stibal. "Greenland melt drives continuous export of methane from the ice-sheet bed". *Nature* 565.7737 (2019), pp. 73–77.

Lampkin, D. J., L. Koenig, C. Joseph, and J. E. Box. "Investigating controls on the formation and distribution of wintertime storage of water in supraglacial lakes". *Frontiers in Earth Science* 8 (2020), p. 370.

Lampkin, D. and J. van der Berg. "A preliminary investigation of the influence of basal and surface topography on supraglacial lake distribution near Jakobshavn Isbrae, western Greenland". *Hydrological Processes* 25.21 (2011), pp. 3347–3355.

Lampkin, D. and J. van der Berg. "Supraglacial melt channel networks in the Jakobshavn Isbræ region during the 2007 melt season". *Hydrological Processes* 28.25 (2014), pp. 6038–6053.

Langley, K., J. Kohler, K. Matsuoka, A. Sinisalo, T. Scambos, T. Neumann, A. Muto, J.-G. Winther, and M. Albert. "Recovery Lakes, East Antarctica: Radar assessment of sub-glacial water extent". *Geophysical Research Letters* 38.5 (2011).

Larsen, S. H., S. A. Khan, A. P. Ahlstrøm, C. S. Hvidberg, M. J. Willis, and S. B. Andersen. "Increased mass loss and asynchronous behavior of marine-terminating outlet glaciers at Upernavik Isstrøm, NW Greenland". *Journal of Geophysical Research: Earth Surface* 121.2 (2016), pp. 241–256.

Larter, R. D., K. A. Hogan, C.-D. Hillenbrand, J. A. Smith, C. L. Batchelor, M. Cartigny, A. J. Tate, J. D. Kirkham, Z. A. Roseby, G. Kuhn, A. G. C. Graham, and J. A. Dowdeswell. "Subglacial hydrological control on flow of an Antarctic Peninsula palaeo-ice stream". *The Cryosphere* 13.6 (2019), pp. 1583–1596.

Law, R., N. Arnold, C. Benedek, M. Tedesco, A. Banwell, and I. Willis. "Over-winter persistence of supraglacial lakes on the Greenland Ice Sheet: Results and insights from a new model". *Journal of Glaciology* 66.257 (2020), pp. 362–372.

Le Brocq, A. M., N. Ross, J. A. Griggs, R. G. Bingham, H. F. Corr, F. Ferraccioli, A. Jenkins, T. A. Jordan, A. J. Payne, D. M. Rippin, and M. J. Siegert. "Evidence from ice shelves for channelized meltwater flow beneath the Antarctic Ice Sheet". *Nature Geoscience* 6.11 (2013), pp. 945–948.

Lea, J. and S. Brough. "Supraglacial lake mapping of the entire Greenland Ice Sheet using Google Earth Engine". In: *AGU Fall Meeting Abstracts*. Vol. 2019. 2019, C31A–1483.

Lecavalier, B. S., D. A. Fisher, G. A. Milne, B. M. Vinther, L. Tarasov, P. Huybrechts, D. Lacelle, B. Main, J. Zheng, J. Bourgeois, and A. S. Dyke. "High Arctic Holocene temperature record from the Agassiz ice cap and Greenland ice sheet evolution". *Proceedings of the National Academy of Sciences* 114.23 (2017), pp. 5952–5957.

Leeson, A., A. Shepherd, K. Briggs, I. Howat, X. Fettweis, M. Morlighem, and E. Rignot. "Supraglacial lakes on the Greenland ice sheet advance inland under warming climate". *Nature Climate Change* 5.1 (2015), pp. 51–55.

Lewis, A. R., D. R. Marchant, D. E. Kowalewski, S. L. Baldwin, and L. E. Webb. "The age and origin of the Labyrinth, western Dry Valleys, Antarctica: Evidence for extensive middle Miocene subglacial floods and freshwater discharge to the Southern Ocean". *Geology* 34.7 (2006), pp. 513–516.

Li, Y., Y. Lu, and M. J. Siegert. "Radar sounding confirms a hydrologically active deep-water subglacial lake in East Antarctica" (2020).

Li, Y., H. Shi, Y. Lu, Z. Zhang, and H. Xi. "Subglacial discharge weakens the stability of the Ross Ice Shelf around the grounding line". *Polar Research* 40 (2021).

Liang, Y.-L., W. Colgan, Q. Lv, K. Steffen, W. Abdalati, J. Stroeve, D. Gallaher, and N. Bayou. "A decadal investigation of supraglacial lakes in West Greenland using a

fully automatic detection and tracking algorithm". *Remote Sensing of Environment* 123 (2012), pp. 127–138.

Liljedahl, L. C., T. Meierbachtol, J. Harper, D. van As, J.-O. Näslund, J.-O. Selroos, J. Saito, S. Follin, T. Ruskeeniemi, A. Kontula, and N. Humphrey. "Rapid and sensitive response of Greenland's groundwater system to ice sheet change". *Nature Geoscience* 14.10 (2021), pp. 751–755.

Lim, Y.-K., S. D. Schubert, S. M. Nowicki, J. N. Lee, A. M. Molod, R. I. Cullather, B. Zhao, and I. Velicogna. "Atmospheric summer teleconnections and Greenland Ice Sheet surface mass variations: Insights from MERRA-2". *Environmental Research Letters* 11.2 (2016), p. 024002.

Lindbäck, K., R. Pettersson, A. L. Hubbard, S. H. Doyle, D. van As, A. B. Mikkelsen, and A. A. Fitzpatrick. "Subglacial water drainage, storage, and piracy beneath the Greenland ice sheet". *Geophysical Research Letters* 42.18 (2015), pp. 7606–7614.

Lindzey, L. E., L. H. Beem, D. A. Young, E. Quartini, D. D. Blankenship, C.-K. Lee, W. S. Lee, J. I. Lee, and J. Lee. "Aerogeophysical characterization of an active subglacial lake system in the David Glacier catchment, Antarctica". *The Cryosphere* 14.7 (2020), pp. 2217–2233.

Livingstone, S., C. Clark, J. Woodward, and J. Kingslake. "Potential subglacial lake locations and meltwater drainage pathways beneath the Antarctic and Greenland ice sheets". *The Cryosphere* 7.6 (2013), pp. 1721–1740.

Livingstone, S. J., W. Chu, J. C. Ely, and J. Kingslake. "Paleofluvial and subglacial channel networks beneath Humboldt Glacier, Greenland". *Geology* 45.6 (2017), pp. 551–554.

Livingstone, S. J., C. D. Clark, J. A. Piotrowski, M. Tranter, M. J. Bentley, A. Hodson, D. A. Swift, and J. Woodward. "Theoretical framework and diagnostic criteria for the identification of palaeo-subglacial lakes". *Quaternary Science Reviews* 53 (2012), pp. 88–110.

Livingstone, S. J., Y. Li, A. Rutishauser, R. J. Sanderson, K. Winter, J. A. Mikucki, H. Björnsson, J. S. Bowling, W. Chu, C. F. Dow, H. A. Fricker, M. McMillan, F. S. L. Ng, N. Ross, M. J. Siegert, M. Siegfried, and A. J. Sole. "Subglacial lakes and their changing role in a warming climate". *Nature Reviews Earth & Environment* (2022), pp. 1–19.

Livingstone, S. J., A. J. Sole, R. D. Storrar, D. Harrison, N. Ross, and J. Bowling. "Brief communication: Subglacial lake drainage beneath Isunguata Sermia, West Greenland: Geomorphic and ice dynamic effects". *The Cryosphere* 13.10 (2019), pp. 2789–2796.

Lliboutry, L. "Local friction laws for glaciers: a critical review and new openings". *Journal of Glaciology* 23.89 (1979), pp. 67–95.

Lliboutry, L. "General theory of subglacial cavitation and sliding of temperate glaciers". *Journal of Glaciology* 7.49 (1968), pp. 21–58.

Lliboutry, L. "Modifications to the theory of intraglacial waterways for the case of subglacial ones". *Journal of Glaciology* 29.102 (1983), pp. 216–226.

Luckman, A., D. I. Benn, F. Cottier, S. Bevan, F. Nilsen, and M. Inall. "Calving rates at tidewater glaciers vary strongly with ocean temperature". *Nature communications* 6.1 (2015), pp. 1–7.

Luthcke, S., D. Rowlands, T. Williams, and M. Sirota. "Reduction of ICESat systematic geolocation errors and the impact on ice sheet elevation change detection". *Geophysical Research Letters* 32.21 (2005).

Lüthje, M., L. Pedersen, N. Reeh, and W. Greuell. "Modelling the evolution of supraglacial lakes on the West Greenland ice-sheet margin". *Journal of Glaciology* 52.179 (2006), pp. 608–618.

Lyons, W. B., J. A. Mikucki, L. A. German, K. A. Welch, S. A. Welch, C. B. Gardner, S. M. Tulaczyk, E. C. Pettit, J. Kowalski, and B. Dachwald. "The geochemistry of englacial brine from Taylor Glacier, Antarctica". *Journal of Geophysical Research: Biogeosciences* 124.3 (2019), pp. 633–648.

Lyons, W. B., K. A. Welch, G. Snyder, J. Olesik, E. Y. Graham, G. M. Marion, and R. J. Poreda. "Halogen geochemistry of the McMurdo Dry Valleys lakes, Antarctica: clues to the origin of solutes and lake evolution". *Geochimica et Cosmochimica Acta* 69.2 (2005), pp. 305–323.

MacFerrin, M., H. Machguth, D. van As, C. Charalampidis, C. M. Stevens, A. Heilig, B. Vandecrux, P. L. Langen, R. Mottram, X. Fettweis, M. R. van den Broeke, W. T. Pfeffer, M. S. Moussavi, and W. Abdalati. "Rapid expansion of Greenland's low-permeability ice slabs". *Nature* 573.7774 (2019), pp. 403–407.

MacGregor, J. A., G. A. Catania, H. Conway, D. M. Schroeder, I. Joughin, D. A. Young, S. D. Kempf, and D. D. Blankenship. "Weak bed control of the eastern shear margin of Thwaites Glacier, West Antarctica". *Journal of Glaciology* 59.217 (2013), pp. 900–912.

MacGregor, J. A., M. A. Fahnestock, G. A. Catania, A. Aschwanden, G. D. Clow, W. T. Colgan, S. P. Gogineni, M. Morlighem, S. M. Nowicki, J. D. Paden, S. F. Price, and H. Seroussi. "A synthesis of the basal thermal state of the Greenland Ice Sheet". *Journal of Geophysical Research: Earth Surface* 121.7 (2016), pp. 1328–1350.

MacGregor, J. A., D. P. Winebrenner, H. Conway, K. Matsuoka, P. A. Mayewski, and G. D. Clow. "Modeling englacial radar attenuation at Siple Dome, West Antarctica, using ice chemistry and temperature data". *Journal of Geophysical Research: Earth Surface* 112.F3 (2007).

MacGregor, J. A., L. N. Boisvert, B. Medley, A. A. Petty, J. P. Harbeck, R. E. Bell, J. B. Blair, E. Blanchard-Wrigglesworth, E. M. Buckley, M. S. Christoffersen, J. R. Cochran, B. M. Csathó, E. L. De Marco, R. T. Dominguez, M. A. Fahnestock, S. L. Farrell, S. P. Gogineni, J. S. Greenbaum, C. M. Hansen, M. A. Hofton, J. W. Holt, K. C. Jezek, L. S. Koenig, N. T. Kurtz, R. Kwok, C. F. Larsen, C. J. Leuschen, C. D. Locke, S. S. Manizade, S. Martin, T. A. Neumann, S. M. Nowicki, J. D. Paden, J. A. Richter-Menge, E. J. Rignot, F. Rodríguez-Morales, M. R. Siegfried, B. E. Smith, J. G. Sonntag, M. Studinger, K. J. Tinto, M. Truffer, T. P. Wagner, J. E. Woods, D. A. Young, and J. K. Yungel. "The scientific legacy of NASA's Operation IceBridge". *Reviews of Geophysics* 59.2 (2021).

Machguth, H., M. MacFerrin, D. van As, J. E. Box, C. Charalampidis, W. Colgan, R. S. Fausto, H. A. Meijer, E. Mosley-Thompson, and R. S. van de Wal. "Greenland meltwater storage in firn limited by near-surface ice formation". *Nature Climate Change* 6.4 (2016), pp. 390–393.

MacKie, E., D. Schroeder, J. Caers, M. Siegfried, and C. Scheidt. "Antarctic topographic realizations and geostatistical modeling used to map subglacial lakes". *Journal of Geophysical Research: Earth Surface* 125.3 (2020), e2019JF005420.

Magnússon, E., F. Pálsson, M. Gudmundsson, T. Högnadóttir, C. Rossi, T. Thorsteinsson, B. Ófeigsson, E. Sturkell, and T. Jóhannesson. "Development of a subglacial lake monitored with radio-echo sounding: Case study from the Eastern Skaftá

Cauldron in the Vatnajökull ice cap, Iceland". *The Cryosphere Discussions* (2021), pp. 1–30.

Maguire, R., N. Schmerr, E. Pettit, K. Riverman, C. Gardner, D. N. DellaGiustina, B. Avenson, N. Wagner, A. G. Marusiak, N. Habib, J. I. Broadbeck, V. J. Bray, and S. H. Bailey. "Geophysical constraints on the properties of a subglacial lake in northwest Greenland". *The Cryosphere Discussions* (2020), pp. 1–19.

Maizels, J. "Jökulhlaup deposits in proglacial areas". *Quaternary Science Reviews* 16.7 (1997), pp. 793–819.

Malczyk, G., N. Gourmelen, D. Goldberg, J. Wuite, and T. Nagler. "Repeat Subglacial Lake Drainage and Filling Beneath Thwaites Glacier". *Geophysical Research Letters* 47.23 (2020), e2020GL089658.

Mallalieu, J., J. L. Carrivick, D. J. Quincey, and M. W. Smith. "Calving seasonality associated with melt-undercutting and lake ice cover". *Geophysical Research Letters* 47.8 (2020), e2019GL086561.

Mankoff, K. D., F. Straneo, C. Cenedese, S. B. Das, C. G. Richards, and H. Singh. "Structure and dynamics of a subglacial discharge plume in a Greenlandic fjord". *Journal of Geophysical Research: Oceans* 121.12 (2016), pp. 8670–8688.

Markus, T., T. Neumann, A. Martino, W. Abdalati, K. Brunt, B. Csatho, S. Farrell, H. Fricker, A. Gardner, D. Harding, M. Jasinski, R. Kwok, L. Magruder, D. Lubin, S. Luthcke, J. Morison, R. Nelson, A. Neuenschwander, S. Palm, S. Popescu, C. Shum, B. E. Schutz, B. Smith, Y. Yang, and J. Zwally. "The Ice, Cloud, and land Elevation Satellite-2 (ICESat-2): science requirements, concept, and implementation". *Remote sensing of environment* 190 (2017), pp. 260–273.

Marsh, O. J., H. A. Fricker, M. R. Siegfried, K. Christianson, K. W. Nicholls, H. F. Corr, and G. Catania. "High basal melting forming a channel at the grounding line of Ross Ice Shelf, Antarctica". *Geophysical Research Letters* 43.1 (2016), pp. 250–255.

Marsh, P. and M.-K. Woo. "Wetting front advance and freezing of meltwater within a snow cover: 1. Observations in the Canadian Arctic". *Water Resources Research* 20.12 (1984), pp. 1853–1864.

Marston, R. A. "Supraglacial stream dynamics on the Juneau Icefield". *Annals of the Association of American Geographers* 73.4 (1983), pp. 597–608.

Martos, Y. M., T. A. Jordan, M. Catalán, T. M. Jordan, J. L. Bamber, and D. G. Vaughan. "Geothermal heat flux reveals the Iceland hotspot track underneath Greenland". *Geophysical Research Letters* 45.16 (2018), pp. 8214–8222.

Matsuno, K., N. Kanna, S. Sugiyama, A. Yamaguchi, and E. J. Yang. "Impacts of meltwater discharge from marine terminating glaciers on the protist community in Inglefield Bredning, northwestern Greenland". *Marine ecology progress series* 642 (2020), pp. 55–65.

Matsuoka, K. "Pitfalls in radar diagnosis of ice-sheet bed conditions: Lessons from englacial attenuation models". *Geophysical Research Letters* 38.5 (2011).

Matsuoka, K., J. A. MacGregor, and F. Pattyn. "Using englacial radar attenuation to better diagnose the subglacial environment: A review". In: *Proceedings of the XIII Internarional Conference on Ground Penetrating Radar*. IEEE. 2010, pp. 1–5.

Matsuoka, K., F. Pattyn, D. Callens, and H. Conway. "Radar characterization of the basal interface across the grounding zone of an ice-rise promontory in East Antarctica". *Annals of Glaciology* 53.60 (2012), pp. 29–34.

Matsuoka, K., L. Wilen, S. P. Hurley, and C. F. Raymond. "Effects of birefringence within ice sheets on obliquely propagating radio waves". *IEEE Transactions on Geoscience and Remote Sensing* 47.5 (2009), pp. 1429–1443.

McGrath, D., W. Colgan, K. Steffen, P. Lauffenburger, and J. Balog. "Assessing the summer water budget of a moulin basin in the Sermeq Avannarleq ablation region, Greenland ice sheet". *Journal of Glaciology* 57.205 (2011), pp. 954–964.

McKay, C. P., C. C. Porco, T. Altheide, W. L. Davis, and T. A. Kral. "The possible origin and persistence of life on Enceladus and detection of biomarkers in the plume". *Astrobiology* 8.5 (2008), pp. 909–919.

McKay, N. P., D. S. Kaufman, C. C. Routson, M. P. Erb, and P. D. Zander. "The onset and rate of Holocene Neoglacial cooling in the Arctic". *Geophysical Research Letters* 45.22 (2018), pp. 12–487.

McMillan, M., A. Muir, A. Shepherd, R. Escolá, M. Roca, J. Aublanc, P. Thibaut, M. Restano, A. Ambrozio, and J. Benveniste. "Sentinel-3 Delay-Doppler altimetry over Antarctica". *The Cryosphere* 13.2 (2019), pp. 709–722.

McMillan, M., H. Corr, A. Shepherd, A. Ridout, S. Laxon, and R. Cullen. "Three-dimensional mapping by CryoSat-2 of subglacial lake volume changes". *Geophysical Research Letters* 40.16 (2013), pp. 4321–4327.

McMillan, M., A. Leeson, A. Shepherd, K. Briggs, T. W. K. Armitage, A. Hogg, P. Kuipers Munneke, M. van den Broeke, B. Noël, W. J. van de Berg, S. Ligtenberg, M. Horwath, A. Groh, A. Muir, and L. Gilbert. "A high-resolution record of Greenland mass balance". *Geophysical Research Letters* 43.13 (2016), pp. 7002–7010.

McMillan, M., P. Nienow, A. Shepherd, T. Benham, and A. Sole. "Seasonal evolution of supra-glacial lakes on the Greenland Ice Sheet". *Earth and Planetary Science Letters* 262.3-4 (2007), pp. 484–492.

Meierbachtol, T., J. Harper, and N. Humphrey. "Basal drainage system response to increasing surface melt on the Greenland ice sheet". *Science* 341.6147 (2013), pp. 777–779.

Meire, L., P. Meire, E. Struyf, D. Krawczyk, K. Arendt, J. Yde, T. Juul Pedersen, M. J. Hopwood, S. Rysgaard, and F. Meysman. "High export of dissolved silica from the Greenland Ice Sheet". *Geophysical Research Letters* 43.17 (2016), pp. 9173–9182.

Meire, L., J. Mortensen, P. Meire, T. Juul-Pedersen, M. K. Sejr, S. Rysgaard, R. Nygaard, P. Huybrechts, and F. J. Meysman. "Marine-terminating glaciers sustain high productivity in Greenland fjords". *Global Change Biology* 23.12 (2017), pp. 5344–5357.

Meire, L., J. Mortensen, S. Rysgaard, J. Bendtsen, W. Boone, P. Meire, and F. J. Meysman. "Spring bloom dynamics in a subarctic fjord influenced by tidewater outlet glaciers (Godthåbsfjord, SW Greenland)". *Journal of Geophysical Research: Biogeosciences* 121.6 (2016), pp. 1581–1592.

Meire, L., D. Søgaard, J. Mortensen, F. Meysman, K. Soetaert, K. Arendt, T. Juul-Pedersen, M. Blicher, and S. Rysgaard. "Glacial meltwater and primary production are drivers of strong CO2 uptake in fjord and coastal waters adjacent to the Greenland Ice Sheet". *Biogeosciences* 12.8 (2015), pp. 2347–2363.

Meybeck, M. "Global distribution of lakes". In: *Physics and chemistry of lakes*. Springer, 1995, pp. 1–35.

Michaud, A. B., J. E. Dore, A. M. Achberger, B. C. Christner, A. C. Mitchell, M. L. Skidmore, T. J. Vick-Majors, and J. C. Priscu. "Microbial oxidation as

a methane sink beneath the West Antarctic Ice Sheet". *Nature Geoscience* 10.8 (2017), pp. 582–586.

Miége, C., R. R. Forster, L. Brucker, L. S. Koenig, D. K. Solomon, J. D. Paden, J. E. Box, E. W. Burgess, J. Z. Miller, L. McNerney, N. Brautigam, R. S. Fausto, and S. Gogineni. "Spatial extent and temporal variability of Greenland firn aquifers detected by ground and airborne radars". *Journal of Geophysical Research: Earth Surface* 121.12 (2016), pp. 2381–2398.

Mignot, J., M. Khodri, C. Frankignoul, and J. Servonnat. "Volcanic impact on the Atlantic Ocean over the last millennium". *Climate of the Past* 7.4 (2011), pp. 1439–1455.

Mikkelsen, A. B., A. Hubbard, M. MacFerrin, J. E. Box, S. H. Doyle, A. Fitzpatrick, B. Hasholt, H. L. Bailey, K. Lindbäck, and R. Pettersson. "Extraordinary runoff from the Greenland ice sheet in 2012 amplified by hypsometry and depleted firn retention". *The Cryosphere* 10.3 (2016), pp. 1147–1159.

Mikucki, J. A., P. A. Lee, D. Ghosh, A. M. Purcell, A. C. Mitchell, K. D. Mankoff, A. T. Fisher, S. Tulaczyk, S. Carter, M. R. Siegfried, H. A. Fricker, T. Hodson, J. Coenen, R. Powell, R. Scherer, T. Vick-Majors, A. A. Achberger, B. C. Christner, M. Tranter, and t. WISSARD Science Team. "Subglacial Lake Whillans microbial biogeochemistry: a synthesis of current knowledge". *Philosophical Transactions of the Royal Society A: Mathematical, Physical and Engineering Sciences* 374.2059 (2016), p. 20140290.

Mikucki, J. A., A. Pearson, D. T. Johnston, A. V. Turchyn, J. Farquhar, D. P. Schrag, A. D. Anbar, J. C. Priscu, and P. A. Lee. "A contemporary microbially maintained subglacial ferrous" ocean"". *Science* 324.5925 (2009), pp. 397–400.

Miles, K. E., I. C. Willis, C. L. Benedek, A. G. Williamson, and M. Tedesco. "Toward monitoring surface and subsurface lakes on the Greenland ice sheet using Sentinel-1 SAR and Landsat-8 OLI imagery". *Frontiers in Earth Science* 5 (2017), p. 58.

Minchew, B. M., C. R. Meyer, S. S. Pegler, B. P. Lipovsky, A. W. Rempel, G. H. Gudmundsson, and N. R. Iverson. "Comment on "Friction at the bed does not control fast glacier flow"". *Science* 363.6427 (2019), eaau6055.

Möller, R., M. Möller, H. Björnsson, S. Gudmundsson, F. Pálsson, B. Oddsson, P. A. Kukla, and C. Schneider. "MODIS-derived albedo changes of Vatnajökull

(Iceland) due to tephra deposition from the 2004 Grímsvötn eruption". *International journal of applied earth observation and geoinformation* 26 (2014), pp. 256–269.

Moon, T., D. Sutherland, D. Carroll, D. Felikson, L. Kehrl, and F. Straneo. "Subsurface iceberg melt key to Greenland fjord freshwater budget". *Nature Geoscience* 11.1 (2018), pp. 49–54.

Moon, T. and I. Joughin. "Changes in ice front position on Greenland's outlet glaciers from 1992 to 2007". *Journal of Geophysical Research: Earth Surface* 113.F2 (2008).

Moon, T., I. Joughin, B. Smith, M. R. Van Den Broeke, W. J. Van De Berg, B. Noël, and M. Usher. "Distinct patterns of seasonal Greenland glacier velocity". *Geophysical research letters* 41.20 (2014), pp. 7209–7216.

Moore, J. C. and S. Fujita. "Dielectric properties of ice containing acid and salt impurity at microwave and low frequencies". *Journal of Geophysical Research: Solid Earth* 98.B6 (1993), pp. 9769–9780.

Moreira, A., G. Krieger, I. Hajnsek, D. Hounam, M. Werner, S. Riegger, and E. Settelmeyer. "TanDEM-X: a TerraSAR-X add-on satellite for single-pass SAR interferometry". In: *IGARSS 2004. 2004 IEEE International Geoscience and Remote Sensing Symposium*. Vol. 2. IEEE. 2004, pp. 1000–1003.

Morlighem, M., E. Rignot, T. Binder, D. Blankenship, R. Drews, G. Eagles, O. Eisen, F. Ferraccioli, R. Forsberg, P. Fretwell, V. Goel, J. S. Greenbaum, H. Gudmundsson, J. Guo, V. Helm, C. Hofstede, I. Howat, A. Humbert, W. Jokat, N. B. Karlsson, W. S. Lee, K. Matsuoka, R. Millan, J. Mouginot, J. Paden, F. Pattyn, J. Roberts, S. Rosier, A. Ruppel, H. Seroussi, E. C. Smith, D. Steinhage, B. Sun, M. R. van den Broeke, T. D. van Ommen, M. van Wessem, and D. A. Young. "Deep glacial troughs and stabilizing ridges unveiled beneath the margins of the Antarctic ice sheet". *Nature Geoscience* 13.2 (2020), pp. 132–137.

Morlighem, M., C. N. Williams, E. Rignot, L. An, J. E. Arndt, J. L. Bamber, G. Catania, N. Chauché, J. A. Dowdeswell, B. Dorschel, I. Fenty, K. Hogan, I. Howat, A. Hubbard, M. Jakobsson, T. M. Jordan, K. K. Kjeldsen, R. Millan, L. Mayer, J. Mouginot, B. P. Y. Noël, C. O'Cofaigh, S. Palmer, S. Rysgaard, H. Seroussi, M. J. Siegert, P. Slabon, F. Straneo, M. R. van den Broeke, W. Weinrebe, M. Wood, and K. B. Zinglersen. "BedMachine v3: Complete Bed Topography and Ocean Bathymetry Mapping of Greenland From Multibeam Echo Sounding Combined

With Mass Conservation". *Geophysical Research Letters* 44.21 (2017), pp. 11, 051–11, 061.

Mortensen, J., J. Bendtsen, R. Motyka, K. Lennert, M. Truffer, M. Fahnestock, and S. Rysgaard. "On the seasonal freshwater stratification in the proximity of fast-flowing tidewater outlet glaciers in a sub-Arctic sill fjord". *Journal of Geophysical Research: Oceans* 118.3 (2013), pp. 1382–1395.

Motyka, R. J., W. P. Dryer, J. Amundson, M. Truffer, and M. Fahnestock. "Rapid submarine melting driven by subglacial discharge, LeConte Glacier, Alaska". *Geophysical Research Letters* 40.19 (2013), pp. 5153–5158.

Motyka, R. J., M. Fahnestock, and M. Truffer. "Volume change of Jakobshavn Isbræ, West Greenland: 1985–1997–2007". *Journal of Glaciology* 56.198 (2010), pp. 635–646.

Mouginot, J., A. A. Bjørk, R. Millan, B. Scheuchl, and E. Rignot. "Insights on the surge behavior of Storstrømmen and L. Bistrup Brae, Northeast Greenland, over the last century". *Geophysical Research Letters* 45.20 (2018), pp. 11–197.

Mouginot, J., E. Rignot, B. Scheuchl, and R. Millan. "Comprehensive annual ice sheet velocity mapping using Landsat-8, Sentinel-1, and RADARSAT-2 data". *Remote Sensing* 9.4 (2017), p. 364.

Mouginot, J., E. Rignot, A. A. Bjørk, M. Van Den Broeke, R. Millan, M. Morlighem, B. Noël, B. Scheuchl, and M. Wood. "Forty-six years of Greenland Ice Sheet mass balance from 1972 to 2018". *Proceedings of the National Academy of Sciences* 116.19 (2019), pp. 9239–9244.

Munneke, P. K., S. M. Ligtenberg, M. Van den Broeke, J. Van Angelen, and R. Forster. "Explaining the presence of perennial liquid water bodies in the firn of the Greenland Ice Sheet". *Geophysical Research Letters* 41.2 (2014), pp. 476–483.

Murray, C., S. Markager, C. A. Stedmon, T. Juul-Pedersen, M. K. Sejr, and A. Bruhn. "The influence of glacial melt water on bio-optical properties in two contrasting Greenlandic fjords". *Estuarine, Coastal and Shelf Science* 163 (2015), pp. 72–83.

Naito, A., Y. Abe, K. Matsuno, B. Nishizawa, N. Kanna, S. Sugiyama, and A. Yamaguchi. "Surface zooplankton size and taxonomic composition in Bowdoin Fjord, north-western Greenland: a comparison of ZooScan, OPC and microscopic analyses". *Polar Science* 19 (2019), pp. 120–129.

Napoleoni, F., S. S. R. Jamieson, N. Ross, M. J. Bentley, A. Rivera, A. M. Smith, M. J. Siegert, G. J. G. Paxman, G. Gacitúa, J. A. Uribe, R. Zamora, A. M. Brisbourne, and D. G. Vaughan. "Subglacial lakes and hydrology across the Ellsworth Subglacial Highlands, West Antarctica". *The Cryosphere* 14.12 (2020), pp. 4507–4524.

Nath, P. and D. Vaughan. "Subsurface crevasse formation in glaciers and ice sheets". *Journal of Geophysical Research: Solid Earth* 108.B1 (2003), ECV–7.

Ng, F. S. "Canals under sediment-based ice sheets". *Annals of Glaciology* 30 (2000), pp. 146–152.

Nghiem, S., D. Hall, T. Mote, M. Tedesco, M. Albert, K. Keegan, C. Shuman, N. DiGirolamo, and G. Neumann. "The extreme melt across the Greenland ice sheet in 2012". *Geophysical Research Letters* 39.20 (2012).

Nienow, P., M. Sharp, and I. Willis. "Seasonal changes in the morphology of the subglacial drainage system, Haut Glacier d'Arolla, Switzerland". *Earth Surface Processes and Landforms: The Journal of the British Geomorphological Group* 23.9 (1998), pp. 825–843.

Nienow, P., A. Sole, D. A. Slater, and T. Cowton. "Recent advances in our understanding of the role of meltwater in the Greenland Ice Sheet system". *Current Climate Change Reports* 3.4 (2017), pp. 330–344.

Noël, B., L. van Kampenhout, J. Lenaerts, W. van de Berg, and M. Van Den Broeke. "A 21st Century Warming Threshold for Sustained Greenland Ice Sheet Mass Loss". *Geophysical Research Letters* 48.5 (2021), e2020GL090471.

Noël, B., W. Van De Berg, E. Van Meijgaard, P. Kuipers Munneke, R. Van De Wal, and M. Van Den Broeke. "Evaluation of the updated regional climate model RACMO2. 3: summer snowfall impact on the Greenland Ice Sheet". *The Cryosphere* 9.5 (2015), pp. 1831–1844.

Noël, B., W. J. van de Berg, S. Lhermitte, and M. R. van den Broeke. "Rapid ablation zone expansion amplifies north Greenland mass loss". *Science advances* 5.9 (2019), eaaw0123.

Noël, B., X. Fettweis, W. Van de Berg, M. Van den Broeke, and M. Erpicum. "Sensitivity of Greenland Ice Sheet surface mass balance to perturbations in sea surface temperature and sea ice cover: a study with the regional climate model MAR". *The Cryosphere* 8.5 (2014), pp. 1871–1883.

Noël, B., W. Van de Berg, S. Lhermitte, B. Wouters, H. Machguth, I. Howat, M. Citterio, G. Moholdt, J. T. Lenaerts, and M. R. van den Broeke. "A tipping point in refreezing accelerates mass loss of Greenland's glaciers and ice caps". *Nature Communications* 8.1 (2017), pp. 1–8.

Noh, M.-J. and I. M. Howat. "Automated stereo-photogrammetric DEM generation at high latitudes: Surface Extraction with TIN-based Search-space Minimization (SETSM) validation and demonstration over glaciated regions". *GIScience & Remote Sensing* 52.2 (2015), pp. 198–217.

Nolin, A. W. and M. C. Payne. "Classification of glacier zones in western Greenland using albedo and surface roughness from the Multi-angle Imaging SpectroRadiometer (MISR)". *Remote Sensing of Environment* 107.1-2 (2007), pp. 264–275.

Nyberg, R. "Observations of slushflows and their geomorphological effects in the Swedish mountain area". *Geografiska Annaler: Series A, Physical Geography* 71.3-4 (1989), pp. 185–198.

Nye, J. F. "Water flow in glaciers: jökulhlaups, tunnels and veins". *Journal of Glaciology* 17.76 (1976), pp. 181–207.

O'Leary, M. and P. Christoffersen. "Calving on tidewater glaciers amplified by submarine frontal melting". *The Cryosphere* 7.1 (2013), pp. 119–128.

Ohashi, Y., S. Aoki, Y. Matsumura, S. Sugiyama, N. Kanna, and D. Sakakibara. "Vertical distribution of water mass properties under the influence of subglacial discharge in Bowdoin Fjord, northwestern Greenland". *Ocean Science* 16.3 (2020), pp. 545–564.

Onesti, L. J. and E. Hestnes. "Slush-flow questionnaire". *Annals of glaciology* 13 (1989), pp. 226–230.

Oswald, G. and S. Gogineni. "Recovery of subglacial water extent from Greenland radar survey data". *Journal of Glaciology* 54.184 (2008), pp. 94–106.

Oswald, G. and G. d. Q. Robin. "Lakes beneath the Antarctic ice sheet". *Nature* 245.5423 (1973), pp. 251–254.

Oswald, G. K., S. Rezvanbehbahani, and L. A. Stearns. "Radar evidence of ponded subglacial water in Greenland". *Journal of Glaciology* 64.247 (2018), pp. 711–729.

Otterå, O. H., M. Bentsen, H. Drange, and L. Suo. "External forcing as a metronome for Atlantic multidecadal variability". *Nature Geoscience* 3.10 (2010), pp. 688–694.

Pain, A. J., J. B. Martin, E. E. Martin, Å. K. Rennermalm, and S. Rahman. "Heterogeneous CO 2 and CH 4 content of glacial meltwater from the Greenland Ice Sheet and implications for subglacial carbon processes". *The Cryosphere* 15.3 (2021), pp. 1627–1644.

Pälli, A., J. C. Moore, J. Jania, L. Kolondra, and P. Glowacki. "The drainage pattern of Hansbreen and Werenskioldbreen, two polythermal glaciers in Svalbard". *Polar Research* 22.2 (2003), pp. 355–371.

Palmer, S., M. McMillan, and M. Morlighem. "Subglacial lake drainage detected beneath the Greenland ice sheet". *Nature communications* 6.1 (2015), pp. 1–7.

Palmer, S. J., J. A. Dowdeswell, P. Christoffersen, D. A. Young, D. D. Blankenship, J. S. Greenbaum, T. Benham, J. Bamber, and M. J. Siegert. "Greenland subglacial lakes detected by radar". *Geophysical Research Letters* 40.23 (2013), pp. 6154–6159.

Pappalardo, R., S. Vance, F. Bagenal, B. Bills, D. Blaney, D. Blankenship, W. Brinckerhoff, J. Connerney, K. Hand, T. Hoehler, J. Leisner, W. Kurth, M. McGrath, M. Mellon, J. Moore, G. Patterson, L. Prockter, D. Senske, B. Schmidt, E. Shock, D. Smith, and K. Soderlund. "Science potential from a Europa lander". *Astrobiology* 13.8 (2013), pp. 740–773.

Pattyn, F. "Investigating the stability of subglacial lakes with a full Stokes ice-sheet model". *Journal of Glaciology* 54.185 (2008), pp. 353–361.

Pattyn, F. "Antarctic subglacial conditions inferred from a hybrid ice sheet/ice stream model". *Earth and Planetary Science Letters* 295.3-4 (2010), pp. 451–461.

Pattyn, F., S. P. Carter, and M. Thoma. "Advances in modelling subglacial lakes and their interaction with the Antarctic ice sheet". *Philosophical Transactions of the Royal Society A: Mathematical, Physical and Engineering Sciences* 374.2059 (2016), p. 20140296.

Pattyn, F., C. Ritz, E. Hanna, X. Asay-Davis, R. DeConto, G. Durand, L. Favier, X. Fettweis, H. Goelzer, N. R. Golledge, P. Kuipers Munneke, J. T. M. Lenaerts, S. Nowicki, A. J. Payne, A. Robinson, H. Seroussi, L. D. Trusel, and M. van den Broeke. "The Greenland and Antarctic ice sheets under 1.5 C global warming". *Nature Climate Change* 8.12 (2018), pp. 1053–1061.

Payne, T., S. Nowicki, and H. Goelzer. "Contrasting contributions to future sea level under CMIP5 and CMIP6 scenarios from the Greenland and Antarctic ice sheets". In: *EGU General Assembly Conference Abstracts*. 2020, p. 11667.

Pendleton, S., G. Miller, N. Lifton, and N. Young. "Cryosphere response resolves conflicting evidence for the timing of peak Holocene warmth on Baffin Island, Arctic Canada". *Quaternary Science Reviews* 216 (2019), pp. 107–115.

Peters, L., S. Anandakrishnan, C. Holland, H. Horgan, D. Blankenship, and D. Voigt. "Seismic detection of a subglacial lake near the South Pole, Antarctica". *Geophysical Research Letters* 35.23 (2008).

Peters, L. E., S. Anandakrishnan, R. B. Alley, and A. M. Smith. "Extensive storage of basal meltwater in the onset region of a major West Antarctic ice stream". *Geology* 35.3 (2007), pp. 251–254.

Peters, M. E., D. D. Blankenship, and D. L. Morse. "Analysis techniques for coherent airborne radar sounding: Application to West Antarctic ice streams". *Journal of Geophysical Research: Solid Earth* 110.B6 (2005).

Pettinelli, E., B. Cosciotti, F. Di Paolo, S. E. Lauro, E. Mattei, R. Orosei, and G. Vannaroni. "Dielectric properties of Jovian satellite ice analogs for subsurface radar exploration: A review". *Reviews of Geophysics* 53.3 (2015), pp. 593–641.

Pfeffer, W. T., M. F. Meier, and T. H. Illangasekare. "Retention of Greenland runoff by refreezing: implications for projected future sea level change". *Journal of Geophysical Research: Oceans* 96.C12 (1991), pp. 22117–22124.

Pfeffer, W. and N. Humphrey. "Formation of ice layers by infiltration and refreezing of meltwater". *Annals of Glaciology* 26 (1998), pp. 83–91.

Phillips, T., H. Rajaram, W. Colgan, K. Steffen, and W. Abdalati. "Evaluation of cryo-hydrologic warming as an explanation for increased ice velocities in the wet snow zone, Sermeq Avannarleq, West Greenland". *Journal of Geophysical Research: Earth Surface* 118.3 (2013), pp. 1241–1256.

Phillips, T., H. Rajaram, and K. Steffen. "Cryo-hydrologic warming: A potential mechanism for rapid thermal response of ice sheets". *Geophysical Research Letters* 37.20 (2010).

Pitcher, L. H. and L. C. Smith. "Supraglacial streams and rivers". *Annual Review of Earth and Planetary Sciences* 47 (2019), pp. 421–452.

Poinar, K., I. Joughin, S. B. Das, M. D. Behn, J. T. Lenaerts, and M. R. Van Den Broeke. "Limits to future expansion of surface-melt-enhanced ice flow into the interior of western Greenland". *Geophysical Research Letters* 42.6 (2015), pp. 1800–1807.

Poinar, K., I. Joughin, D. Lilien, L. Brucker, L. Kehrl, and S. Nowicki. "Drainage of Southeast Greenland firn aquifer water through crevasses to the bed". *Frontiers in Earth Science* 5 (2017), p. 5.

Pope, E. L., A. Normandeau, C. Ó. Cofaigh, C. R. Stokes, and P. J. Talling. "Controls on the formation of turbidity current channels associated with marine-terminating glaciers and ice sheets". *Marine Geology* 415 (2019), p. 105951.

Popov, S. V. and V. N. Masolov. "Forty-seven new subglacial lakes in the 0–110 E sector of East Antarctica". *Journal of Glaciology* 53.181 (2007), pp. 289–297.

Popov, S. and Y. Chernoglazov. "Vostok Subglacial Lake, East Antarctica: lake shoreline and subglacial water caves". *Ice and Snow* 1.113 (2011), pp. 12–24.

Popov, S., V. Masolov, V. Lukin, and A. Popkov. "Russian seismic, radio and seismological investigations of subglacial Lake Vostok". *Ice and Snow* 4.120 (2012), pp. 31–38.

Porter, C., P. Morin, I. Howat, M.-J. Noh, B. Bates, K. Peterman, S. Keesey, M. Schlenk, J. Gardiner, K. Tomko, M. Willis, C. Kelleher, M. Cloutier, E. Husby, S. Foga, H. Nakamura, M. Platson, J. Wethington Michael, C. Williamson, G. Bauer, J. Enos, G. Arnold, W. Kramer, P. Becker, A. Doshi, C. D'Souza, P. Cummens, F. Laurier, and M. Bojesen. *ArcticDEM, last accessed: 1 December 2021*. Version 1. Polar Geospatial Center, 2018. URL: https://www.pgc.umn.edu/data/arcticdem/.

Post, A., B. Galton-Fenzi, M. Riddle, L. Herraiz-Borreguero, P. O'Brien, M. Hemer, A. McMinn, D. Rasch, and M. Craven. "Modern sedimentation, circulation and life beneath the Amery Ice Shelf, East Antarctica". *Continental Shelf Research* 74 (2014), pp. 77–87.

Powell, R. D. "Glacimarine processes at grounding-line fans and their growth to ice-contact deltas". In: *Glacimarine Environments: Processes and Sediments*. Ed. by J. Dowdeswell and J. Scourse. London: Geological Society, 1990. Chap. 53, pp. 53–73.

Priscu, J. C., J. Kalin, J. Winans, T. Campbell, M. R. Siegfried, M. Skidmore, J. E. Dore, A. Leventer, D. M. Harwood, D. Duling, R. Zook, J. Burnett, D. Gibson, E. Krula, A. Mironov, J. McManis, G. Roberts, B. E. Rosenheim, B. C. Christner,

K. Kasic, H. A. Fricker, W. B. Lyons, J. Barker, M. Bowling, B. Collins, C. Davis, A. Gagnon, C. Gardner, C. Gustafson, O.-S. Kim, W. Li, A. Michaud, M. O. Patterson, M. Tranter, R. Venturelli, T. Vick-Majors, C. Elsworth, and T. SALSA Science Team. "Scientific access into Mercer Subglacial Lake: scientific objectives, drilling operations and initial observations". *Annals of Glaciology* (2020), pp. 1–13.

Pritchard, H. D., R. J. Arthern, D. G. Vaughan, and L. A. Edwards. "Extensive dynamic thinning on the margins of the Greenland and Antarctic ice sheets". *Nature* 461.7266 (2009), pp. 971–975.

Purcell, A. M., J. A. Mikucki, A. M. Achberger, I. A. Alekhina, C. Barbante, B. C. Christner, D. Ghosh, A. B. Michaud, A. C. Mitchell, J. C. Priscu, R. Scherer, M. L. Skidmore, T. J. Vick-Majors, and the WISSARD Science Team. "Microbial sulfur transformations in sediments from Subglacial Lake Whillans". *Frontiers in Microbiology* 5 (2014), p. 594.

Rennermalm, A. K., S. E. Moustafa, J. Mioduszewski, V. Chu, R. Forster, B. Hagedorn, J. T. Harper, T. Mote, D. A. Robinson, C. Shuman, L. Smith, and M. Tedesco. "Understanding Greenland ice sheet hydrology using an integrated multi-scale approach". *Environmental Research Letters* 8.1 (2013), p. 015017.

Rex, D. "Blocking action in the middle troposphere and its effects on regional climate, I: an aerological study of blocking". *Tellus* 2 (1950), pp. 196–211.

Ridley, J. K., W. Cudlip, and S. W. Laxon. "Identification of subglacial lakes using ERS-1 radar altimeter". *Journal of Glaciology* 39.133 (1993), pp. 625–634.

Rignot, E., J. Box, E. Burgess, and E. Hanna. "Mass balance of the Greenland ice sheet from 1958 to 2007". *Geophysical Research Letters* 35.20 (2008).

Rignot, E., I. Fenty, Y. Xu, C. Cai, and C. Kemp. "Undercutting of marine-terminating glaciers in West Greenland". *Geophysical Research Letters* 42.14 (2015), pp. 5909–5917.

Rignot, E. and P. Kanagaratnam. "Changes in the velocity structure of the Greenland Ice Sheet". *Science* 311.5763 (2006), pp. 986–990.

Rignot, E. and J. Mouginot. "Ice flow in Greenland for the international polar year 2008–2009". *Geophysical Research Letters* 39.11 (2012).

Rippin, D. M. "Bed roughness beneath the Greenland ice sheet". *Journal of Glaciology* 59.216 (2013), pp. 724–732.

Rivera, A., J. Uribe, R. Zamora, and J. Oberreuter. "Subglacial Lake CECs: Discovery and in situ survey of a privileged research site in West Antarctica". *Geophysical Research Letters* 42.10 (2015), pp. 3944–3953.

Roberts, M. J. "Jökulhlaups: a reassessment of floodwater flow through glaciers". *Reviews of Geophysics* 43.1 (2005).

Roberts, M. J., A. J. Russell, F. S. Tweed, and Ó. Knudsen. "Ice fracturing during jökulhlaups: implications for englacial floodwater routing and outlet development". *Earth surface processes and landforms* 25.13 (2000), pp. 1429–1446.

Robin, G. d. Q., D. Drewry, and D. Meldrum. "International studies of ice sheet and bedrock". *Philosophical Transactions of the Royal Society of London. B, Biological Sciences* 279.963 (1977), pp. 185–196.

Robin, G. d. Q., S. Evans, and J. T. Bailey. "Interpretation of radio echo sounding in polar ice sheets". *Philosophical Transactions of the Royal Society of London. Series A, Mathematical and Physical Sciences* 265.1166 (1969), pp. 437–505.

Robin, G. d. Q., C. Swithinbank, and B. Smith. "Radio echo exploration of the Antarctic ice sheet". *International Association of Scientific Hydrology Publication* 86 (1970), pp. 97–115.

Robinson, A., R. Calov, and A. Ganopolski. "Multistability and critical thresholds of the Greenland ice sheet". *Nature Climate Change* 2.6 (2012), pp. 429–432.

Robinson, R. "Experiment in visual orientation during flights in the Antarctic". *Soviet Antarctic Expedition Information Bulletin* 18 (1961), pp. 28–29.

Robock, A. "Volcanic eruptions and climate". *Reviews of geophysics* 38.2 (2000), pp. 191–219.

Rogozhina, I., A. G. Petrunin, A. P. Vaughan, B. Steinberger, J. V. Johnson, M. K. Kaban, R. Calov, F. Rickers, M. Thomas, and I. Koulakov. "Melting at the base of the Greenland ice sheet explained by Iceland hotspot history". *Nature Geoscience* 9.5 (2016), pp. 366–369.

Röthlisberger, H. "Water pressure in intra-and subglacial channels". *Journal of Glaciology* 11.62 (1972), pp. 177–203.

Russell, A. J. and Ó. Knudsen. "An ice-contact rhythmite (turbidite) succession deposited during the November 1996 catastrophic outburst flood (jökulhlaup), Skeiðarárjökull, Iceland". *Sedimentary Geology* 127.1-2 (1999), pp. 1–10.

Russell, A. J., M. J. Roberts, H. Fay, P. M. Marren, N. J. Cassidy, F. S. Tweed, and T. Harris. "Icelandic jökulhlaup impacts: implications for ice-sheet hydrology, sediment transfer and geomorphology". *Geomorphology* 75.1-2 (2006), pp. 33–64.

Rutishauser, A., D. D. Blankenship, M. Sharp, M. L. Skidmore, J. S. Greenbaum, C. Grima, D. M. Schroeder, J. A. Dowdeswell, and D. A. Young. "Discovery of a hypersaline subglacial lake complex beneath Devon Ice Cap, Canadian Arctic". *Science advances* 4.4 (2018), eaar4353.

Ryan, J., L. Smith, D. Van As, S. Cooley, M. Cooper, L. Pitcher, and A. Hubbard. "Greenland Ice Sheet surface melt amplified by snowline migration and bare ice exposure". *Science Advances* 5.3 (2019), eaav3738.

Sandberg Sørensen, L., S. B. Simonsen, K. Nielsen, P. Lucas-Picher, G. Spada, G. Adalgeirsdottir, R. Forsberg, and C. S. Hvidberg. "Mass balance of the Greenland ice sheet (2003–2008) from ICESat data–the impact of interpolation, sampling and firn density". *The Cryosphere* 5.1 (2011), pp. 173–186.

Sandberg Sørensen, L., S. B. Simonsen, R. Forsberg, K. Khvorostovsky, R. Meister, and M. E. Engdahl. "25 years of elevation changes of the Greenland Ice Sheet from ERS, Envisat, and CryoSat-2 radar altimetry". *Earth and Planetary Science Letters* 495 (2018), pp. 234–241.

Sanders, R., S. A. Henson, M. Koski, L. Christina, S. C. Painter, A. J. Poulton, J. Riley, B. Salihoglu, A. Visser, A. Yool, R. Bellerby, and A. P. Martin. "The biological carbon pump in the North Atlantic". *Progress in Oceanography* 129 (2014), pp. 200–218.

Sasgen, I., B. Wouters, A. S. Gardner, M. D. King, M. Tedesco, F. W. Landerer, C. Dahle, H. Save, and X. Fettweis. "Return to rapid ice loss in Greenland and record loss in 2019 detected by the GRACE-FO satellites". *Communications Earth & Environment* 1.1 (2020), pp. 1–8.

Scambos, T. A., E. Berthier, and C. A. Shuman. "The triggering of subglacial lake drainage during rapid glacier drawdown: Crane Glacier, Antarctic Peninsula". *Annals of Glaciology* 52.59 (2011), pp. 74–82.

Schild, K., C. Renshaw, D. I. Benn, A. Luckman, R. Hawley, P. How, L. Trusel, F. Cottier, A. Pramanik, and N. Hulton. "Glacier calving rates due to subglacial

discharge, fjord circulation, and free convection". *Journal of Geophysical Research: Earth Surface* 123.9 (2018), pp. 2189–2204.

Schoof, C. "Ice sheet grounding line dynamics: Steady states, stability, and hysteresis". *Journal of Geophysical Research: Earth Surface* 112.F3 (2007).

Schoof, C. "Ice-sheet acceleration driven by melt supply variability". *Nature* 468.7325 (2010), pp. 803–806.

Schröder, L., M. Horwath, R. Dietrich, V. Helm, M. R. Van Den Broeke, and S. R. Ligtenberg. "Four decades of Antarctic surface elevation changes from multi-mission satellite altimetry". *The Cryosphere* 13.2 (2019), pp. 427–449.

Schroeder, D. M., C. Grima, and D. D. Blankenship. "Evidence for variable grounding-zone and shear-margin basal conditions across Thwaites Glacier, West AntarcticaThwaites grounding zone and shear margin". *Geophysics* 81.1 (2016), WA35–WA43.

Schroeder, D. M., H. Seroussi, W. Chu, and D. A. Young. "Adaptively constraining radar attenuation and temperature across the Thwaites Glacier catchment using bed echoes". *Journal of Glaciology* 62.236 (2016), pp. 1075–1082.

Schutz, B. E., H. J. Zwally, C. A. Shuman, D. Hancock, and J. P. DiMarzio. "Overview of the ICESat mission". *Geophysical Research Letters* 32.21 (2005).

Schwanghart, W. and D. Scherler. "TopoToolbox 2–MATLAB-based software for topographic analysis and modeling in Earth surface sciences". *Earth Surface Dynamics* 2.1 (2014), pp. 1–7.

Sciascia, R., F. Straneo, C. Cenedese, and P. Heimbach. "Seasonal variability of submarine melt rate and circulation in an East Greenland fjord". *Journal of Geophysical Research: Oceans* 118.5 (2013), pp. 2492–2506.

Selmes, N., T. Murray, and T. James. "Fast draining lakes on the Greenland Ice Sheet". *Geophysical Research Letters* 38.15 (2011).

Seo, K.-W., D. E. Waliser, C.-K. Lee, B. Tian, T. Scambos, B.-M. Kim, J. H. van Angelen, and M. R. van den Broeke. "Accelerated mass loss from Greenland ice sheet: Links to atmospheric circulation in the North Atlantic". *Global and Planetary Change* 128 (2015), pp. 61–71.

Sergienko, O. V. "Glaciological twins: basally controlled subglacial and supraglacial lakes". *Journal of Glaciology* 59.213 (2013), pp. 3–8.

Shannon, S. R., A. J. Payne, I. D. Bartholomew, M. R. van den Broeke, T. L. Edwards, X. Fettweis, O. Gagliardini, F. Gillet-Chaulet, H. Goelzer, M. J. Hoffman, P. Huybrechts, D. W. F. Mair, P. W. Nienow, M. Perego, S. F. Price, C. P. Smeets, J. Sole Andrew, R. S. van de Wal, and T. Zwinger. "Enhanced basal lubrication and the contribution of the Greenland ice sheet to future sea-level rise". *Proceedings of the National Academy of Sciences* 110.35 (2013), pp. 14156–14161.

Shapiro, N. M. and M. H. Ritzwoller. "Inferring surface heat flux distributions guided by a global seismic model: particular application to Antarctica". *Earth and Planetary Science Letters* 223.1-2 (2004), pp. 213–224.

Shaw, J. "Drumlins, subglacial meltwater floods, and ocean responses". *Geology* 17.9 (1989), pp. 853–856.

Shepherd, A., L. Gilbert, A. S. Muir, H. Konrad, M. McMillan, T. Slater, K. H. Briggs, A. V. Sundal, A. E. Hogg, and M. E. Engdahl. "Trends in Antarctic Ice Sheet elevation and mass". *Geophysical Research Letters* 46.14 (2019), pp. 8174–8183.

Shepherd, A., A. Hubbard, P. Nienow, M. King, M. McMillan, and I. Joughin. "Greenland ice sheet motion coupled with daily melting in late summer". *Geophysical Research Letters* 36.1 (2009).

Shepherd, A., E. Ivins, E. Rignot, B. Smith, M. van Den Broeke, I. Velicogna, P. Whitehouse, K. Briggs, I. Joughin, G. Krinner, S. Nowicki, T. Payne, T. Scambos, N. Schlegel, G. A, C. Agosta, A. Ahlstrøm, G. Babonis, V. R. Barletta, A. A. Bjørk, et al. "Mass balance of the Greenland Ice Sheet from 1992 to 2018". *Nature* 579.7798 (2020), pp. 233–239.

Shreve, R. "Movement of water in glaciers". *Journal of Glaciology* 11.62 (1972), pp. 205–214.

Siegert, M. J. "Antarctic subglacial lakes". *Earth-Science Reviews* 50.1-2 (2000), pp. 29–50.

Siegert, M. J. "Radar evidence of water-saturated sediments beneath the East Antarctic Ice Sheet". *Geological Society, London, Special Publications* 176.1 (2000), pp. 217–229.

Siegert, M. J. and J. L. Bamber. "Subglacial water at the heads of Antarctic ice-stream tributaries". *Journal of Glaciology* 46.155 (2000), pp. 702–703.

Siegert, M. J., S. Carter, I. Tabacco, S. Popov, and D. D. Blankenship. "A revised inventory of Antarctic subglacial lakes". *Antarctic Science* 17.3 (2005), pp. 453–460.

Siegert, M. J., J. C. Ellis-Evans, M. Tranter, C. Mayer, J.-R. Petit, A. Salamatin, and J. C. Priscu. "Physical, chemical and biological processes in Lake Vostok and other Antarctic subglacial lakes". *Nature* 414.6864 (2001), pp. 603–609.

Siegert, M. J., B. Kulessa, M. Bougamont, P. Christoffersen, K. Key, K. R. Andersen, A. D. Booth, and A. M. Smith. "Antarctic subglacial groundwater: a concept paper on its measurement and potential influence on ice flow". *Geological Society, London, Special Publications* 461.1 (2018), pp. 197–213.

Siegert, M. J., A. Le Brocq, and A. J. Payne. "Hydrological connections between Antarctic subglacial lakes, the flow of water beneath the East Antarctic Ice Sheet and implications for sedimentary processes". *Glacial Sedimentary Processes and Products* 39 (2007), pp. 3–10.

Siegert, M. J. and J. K. Ridley. "Determining basal ice-sheet conditions in the Dome C region of East Antarctica using satellite radar altimetry and airborne radio-echo sounding". *Journal of Glaciology* 44.146 (1998), pp. 1–8.

Siegert, M. J., N. Ross, H. Corr, B. Smith, T. Jordan, R. Bingham, F. Ferraccioli, D. Rippin, and A. Le Brocq. "Boundary conditions of an active West Antarctic subglacial lake: implications for storage of water beneath the ice sheet". *The Cryosphere* 8.1 (2014), pp. 15–24.

Siegert, M. J., N. Ross, and A. M. Le Brocq. "Recent advances in understanding Antarctic subglacial lakes and hydrology". *Philosophical Transactions of the Royal Society A: Mathematical, Physical and Engineering Sciences* 374.2059 (2016), p. 20140306.

Siegert, M. J., N. Ross, J. Li, D. M. Schroeder, D. Rippin, D. Ashmore, R. Bingham, and P. Gogineni. "Subglacial controls on the flow of Institute Ice Stream, West Antarctica". *Annals of Glaciology* 57.73 (2016), pp. 19–24.

Siegert, M. J., M. Tranter, J. C. Ellis-Evans, J. C. Priscu, and W. Berry Lyons. "The hydrochemistry of Lake Vostok and the potential for life in Antarctic subglacial lakes". *Hydrological processes* 17.4 (2003), pp. 795–814.

Siegert, M., J. Dowdeswell, M. Gorman, and N. McIntyre. "An inventory of Antarctic sub-glacial lakes". *Antarctic science. Oxford etc.* 8.3 (1996), pp. 281–286.

Siegfried, M. R. and H. A. Fricker. "Thirteen years of subglacial lake activity in Antarctica from multi-mission satellite altimetry". *Annals of Glaciology* 59.76pt1 (2018), pp. 42–55.

Siegfried, M. R., H. A. Fricker, S. P. Carter, and S. Tulaczyk. "Episodic ice velocity fluctuations triggered by a subglacial flood in West Antarctica". *Geophysical Research Letters* 43.6 (2016), pp. 2640–2648.

Siegfried, M. R., H. A. Fricker, M. Roberts, T. A. Scambos, and S. Tulaczyk. "A decade of West Antarctic subglacial lake interactions from combined ICESat and CryoSat-2 altimetry". *Geophysical Research Letters* 41.3 (2014), pp. 891–898.

Siegfried, M. and H. Fricker. "Illuminating active subglacial lake processes with ICESat-2 laser altimetry". *Geophysical Research Letters* (2021), e2020GL091089.

Sigman, D. M. and E. A. Boyle. "Glacial/interglacial variations in atmospheric carbon dioxide". *Nature* 407.6806 (2000), pp. 859–869.

Simonsen, S. B., V. R. Barletta, W. T. Colgan, and L. Sandberg Sørensen. "Greenland Ice Sheet mass balance (1992–2020) from calibrated radar altimetry". *Geophysical Research Letters* 48.3 (2021), e2020GL091216.

Skidmore, M. L. and M. J. Sharp. "Drainage system behaviour of a High-Arctic polythermal glacier". *Annals of Glaciology* 28 (1999), pp. 209–215.

Slater, D., P. Nienow, T. Cowton, D. Goldberg, and A. Sole. "Effect of near-terminus subglacial hydrology on tidewater glacier submarine melt rates". *Geophysical Research Letters* 42.8 (2015), pp. 2861–2868.

Slater, D., F. Straneo, S. Das, C. Richards, T. Wagner, and P. Nienow. "Localized plumes drive front-wide ocean melting of a Greenlandic tidewater glacier". *Geophysical Research Letters* 45.22 (2018), pp. 12–350.

Slater, T., A. Shepherd, M. McMillan, A. Muir, L. Gilbert, A. E. Hogg, H. Konrad, and T. Parrinello. "A new digital elevation model of Antarctica derived from CryoSat-2 altimetry". *The Cryosphere* 12.4 (2018), pp. 1551–1562.

Smeets, C., W. Boot, A. Hubbard, R. Pettersson, F. Wilhelms, M. R. Van Den Broeke, and R. S. Van De Wal. "A wireless subglacial probe for deep ice applications". *Journal of glaciology* 58.211 (2012), pp. 841–848.

Smith, A. M., J. Woodward, N. Ross, M. J. Bentley, D. A. Hodgson, M. J. Siegert, and E. C. King. "Evidence for the long-term sedimentary environment in an Antarctic subglacial lake". *Earth and Planetary Science Letters* 504 (2018), pp. 139–151.

Smith, B. E., H. A. Fricker, A. Gardner, M. R. Siegfried, S. Adusumilli, B. M. Csathó, N. Holschuh, J. Nilsson, F. S. Paolo, and the ICESat-2 team. "ATLAS/ICESat-2 L3A Land Ice Height, Version 3. [AL06]" (2020). DOI: 10.5067/ATLAS/ATL06.003.

Smith, B. E., H. A. Fricker, A. S. Gardner, B. Medley, J. Nilsson, F. S. Paolo, N. Holschuh, S. Adusumilli, K. Brunt, B. Csatho, K. Harbeck, T. Markus, T. Neumann, M. R. Siegfried, and H. J. Zwally. "Pervasive ice sheet mass loss reflects competing ocean and atmosphere processes". *Science* 368.6496 (2020), pp. 1239–1242.

Smith, B. E., H. A. Fricker, I. R. Joughin, and S. Tulaczyk. "An inventory of active subglacial lakes in Antarctica detected by ICESat (2003–2008)". *Journal of Glaciology* 55.192 (2009), pp. 573–595.

Smith, B. E., N. Gourmelen, A. Huth, and I. Joughin. "Connected subglacial lake drainage beneath Thwaites Glacier, West Antarctica". *The Cryosphere* 11.1 (2017), pp. 451–467.

Smith, L. C., V. W. Chu, K. Yang, C. J. Gleason, L. H. Pitcher, A. K. Rennermalm, C. J. Legleiter, A. E. Behar, B. T. Overstreet, S. E. Moustafa, M. Tedesco, R. R. Forster, A. L. LeWinter, D. C. Finnegan, Y. Sheng, and J. Balog. "Efficient meltwater drainage through supraglacial streams and rivers on the southwest Greenland ice sheet". *Proceedings of the National Academy of Sciences* 112.4 (2015), pp. 1001–1006.

Smith, L. C., K. Yang, L. H. Pitcher, B. T. Overstreet, V. W. Chu, Å. K. Rennermalm, J. C. Ryan, M. G. Cooper, C. J. Gleason, M. Tedesco, et al. "Direct measurements of meltwater runoff on the Greenland ice sheet surface". *Proceedings of the National Academy of Sciences* 114.50 (2017), E10622–E10631.

Sneed, W. and G. S. Hamilton. "Evolution of melt pond volume on the surface of the Greenland Ice Sheet". *Geophysical research letters* 34.3 (2007).

Snorrason, Á., P. Jónsson, O. Sigurðsson, S. Pálsson, S. Árnason, S. ViFIX ME!!!!kingsson, and I. Kaldal. "November 1996 jökulhlaup on Skeiðarársandur outwash plain, Iceland". *Flood and megaflood processes and deposits: recent and ancient examples* (2002), pp. 53–65.

Sole, A., P. Nienow, I. Bartholomew, D. Mair, T. Cowton, A. Tedstone, and M. A. King. "Winter motion mediates dynamic response of the Greenland Ice Sheet to warmer summers". *Geophysical Research Letters* 40.15 (2013), pp. 3940–3944.

Spring, U. and K. Hutter. "Numerical studies of jökulhlaups". *Cold Regions Science and Technology* 4.3 (1981), pp. 227–244.

St Germain, S. L. and B. J. Moorman. "Long-term observations of supraglacial streams on an Arctic glacier". *Journal of Glaciology* 65.254 (2019), pp. 900–911.

Stearns, L. and C. Van der Veen. "Friction at the bed does not control fast glacier flow". *Science* 361.6399 (2018), pp. 273–277.

Stearns, L. A., B. E. Smith, and G. S. Hamilton. "Increased flow speed on a large East Antarctic outlet glacier caused by subglacial floods". *Nature Geoscience* 1.12 (2008), pp. 827–831.

Steger, C. R., C. H. Reijmer, M. R. van den Broeke, N. Wever, R. R. Forster, L. S. Koenig, P. Kuipers Munneke, M. Lehning, S. Lhermitte, S. R. M. Ligtenberg, C. Miège, and B. P. Y. Noël. "Firn meltwater retention on the Greenland ice sheet: A model comparison". *Frontiers in Earth Science* 5 (2017), p. 3.

Stenchikov, G., T. L. Delworth, V. Ramaswamy, R. J. Stouffer, A. Wittenberg, and F. Zeng. "Volcanic signals in oceans". *Journal of Geophysical Research: Atmospheres* 114.D16 (2009).

Stevens, L. A., M. D. Behn, J. J. McGuire, S. B. Das, I. Joughin, T. Herring, D. E. Shean, and M. A. King. "Greenland supraglacial lake drainages triggered by hydrologically induced basal slip". *Nature* 522.7554 (2015), pp. 73–76.

Stevens, L. A., F. Straneo, S. B. Das, A. J. Plueddemann, A. L. Kukulya, and M. Morlighem. "Linking glacially modified waters to catchment-scale subglacial discharge using autonomous underwater vehicle observations". *The Cryosphere* 10.1 (2016), pp. 417–432.

Stillman, D. E., J. A. MacGregor, and R. E. Grimm. "The role of acids in electrical conduction through ice". *Journal of Geophysical Research: Earth Surface* 118.1 (2013), pp. 1–16.

Straneo, F. and C. Cenedese. "The dynamics of Greenland's glacial fjords and their role in climate". *Annual review of marine science* 7 (2015), pp. 89–112.

Straneo, F., R. G. Curry, D. A. Sutherland, G. S. Hamilton, C. Cenedese, K. Våge, and L. A. Stearns. "Impact of fjord dynamics and glacial runoff on the circulation near Helheim Glacier". *Nature Geoscience* 4.5 (2011), pp. 322–327.

Straneo, F. and P. Heimbach. "North Atlantic warming and the retreat of Greenland's outlet glaciers". *Nature* 504.7478 (2013), pp. 36–43.

Straneo, F., D. A. Sutherland, D. Holland, C. Gladish, G. S. Hamilton, H. L. Johnson, E. Rignot, Y. Xu, and M. Koppes. "Characteristics of ocean waters reaching Greenland's glaciers". *Annals of Glaciology* 53.60 (2012), pp. 202–210.

Studinger, M., R. E. Bell, D. D. Blankenship, C. A. Finn, R. A. Arko, D. L. Morse, and I. Joughin. "Subglacial sediments: A regional geological template for ice flow in West Antarctica". *Geophysical Research Letters* 28.18 (2001), pp. 3493–3496.

Studinger, M., R. E. Bell, G. D. Karner, A. A. Tikku, J. W. Holt, D. L. Morse, T. G. Richter, S. D. Kempf, M. E. Peters, D. D. Blankenship, R. E. Sweeney, and V. L. Rystrom. "Ice cover, landscape setting, and geological framework of Lake Vostok, East Antarctica". *Earth and Planetary Science Letters* 205.3-4 (2003), pp. 195–210.

Sundal, A. V., A. Shepherd, P. Nienow, E. Hanna, S. Palmer, and P. Huybrechts. "Melt-induced speed-up of Greenland ice sheet offset by efficient subglacial drainage". *Nature* 469.7331 (2011), pp. 521–524.

Sundal, A., A. Shepherd, P. Nienow, E. Hanna, S. Palmer, and P. Huybrechts. "Evolution of supra-glacial lakes across the Greenland Ice Sheet". *Remote Sensing of Environment* 113.10 (2009), pp. 2164–2171.

Sutherland, D., R. H. Jackson, C. Kienholz, J. M. Amundson, W. Dryer, D. Duncan, E. Eidam, R. Motyka, and J. Nash. "Direct observations of submarine melt and subsurface geometry at a tidewater glacier". *Science* 365.6451 (2019), pp. 369–374.

Swift, D. A., P. W. Nienow, N. Spedding, and T. B. Hoey. "Geomorphic implications of subglacial drainage configuration: rates of basal sediment evacuation controlled by seasonal drainage system evolution". *Sedimentary Geology* 149.1-3 (2002), pp. 5–19.

Swingedouw, D., P. Ortega, J. Mignot, E. Guilyardi, V. Masson-Delmotte, P. G. Butler, M. Khodri, and R. Séférian. "Bidecadal North Atlantic ocean circulation variability controlled by timing of volcanic eruptions". *Nature communications* 6.1 (2015), pp. 1–12.

Tabacco, I., P. Cianfarra, A. Forieri, F. Salvini, and A. Zirizotti. "Physiography and tectonic setting of the subglacial lake district between Vostok and Belgica subglacial highlands (Antarctica)". *Geophysical Journal International* 165.3 (2006), pp. 1029–1040.

Tabacco, I., A. Forieri, A. Della Vedova, A. Zirizzotti, C. Bianchi, P. De Michelis, and A. Passerini. "Evidence of 14 new subglacial lakes in the Dome C-Vostok area". In: *4th Meeting on Italian Antarctic Glaciology*. Terra Antartica Publication. 2003.

Tachikawa, T., M. Hato, M. Kaku, and A. Iwasaki. "Characteristics of ASTER GDEM version 2". In: *2011 IEEE international geoscience and remote sensing symposium*. IEEE. 2011, pp. 3657–3660.

Tedesco, M., S. Doherty, X. Fettweis, P. Alexander, J. Jeyaratnam, and J. Stroeve. "The darkening of the Greenland ice sheet: trends, drivers, and projections (1981–2100)". *The Cryosphere* 10.2 (2016), pp. 477–496.

Tedesco, M., X. Fettweis, T. Mote, J. Wahr, P. Alexander, J. Box, and B. Wouters. "Evidence and analysis of 2012 Greenland records from spaceborne observations, a regional climate model and reanalysis data". *The Cryosphere* 7.2 (2013), pp. 615–630.

Tedesco, M., M. Lüthje, K. Steffen, N. Steiner, X. Fettweis, I. Willis, N. Bayou, and A. Banwell. "Measurement and modeling of ablation of the bottom of supraglacial lakes in western Greenland". *Geophysical Research Letters* 39.2 (2012).

Tedesco, M., M. Serreze, and X. Fettweis. "Diagnosing the extreme surface melt event over southwestern Greenland in 2007". *The Cryosphere* 2.2 (2008), pp. 159–166.

Tedesco, M. and N. Steiner. "In-situ multispectral and bathymetric measurements over a supraglacial lake in western Greenland using a remotely controlled watercraft". *The Cryosphere* 5.2 (2011), pp. 445–452.

Tedstone, A., P. Nienow, N. Gourmelen, and A. Sole. "Greenland ice sheet annual motion insensitive to spatial variations in subglacial hydraulic structure". *Geophysical Research Letters* 41.24 (2014), pp. 8910–8917.

Tedstone, A. J. "Hydrological controls on Greenland ice sheet motion". PhD thesis. University of Edinburgh, 2015.

Thoma, M., K. Grosfeld, I. Filina, and C. Mayer. "Modelling flow and accreted ice in subglacial Lake Concordia, Antarctica". *Earth and Planetary Science Letters* 286.1-2 (2009), pp. 278–284.

Thoma, M., K. Grosfeld, and C. Mayer. "Modelling mixing and circulation in subglacial Lake Vostok, Antarctica". *Ocean Dynamics* 57.6 (2007), pp. 531–540.

Thoma, M., K. Grosfeld, C. Mayer, and F. Pattyn. "Ice-flow sensitivity to boundary processes: a coupled model study in the Vostok Subglacial Lake area, Antarctica". *Annals of glaciology* 53.60 (2012), pp. 173–180.

Thoma, M., K. Grosfeld, C. Mayer, A. M. Smith, J. Woodward, and N. Ross. "The "tipping" temperature within Subglacial Lake Ellsworth, West Antarctica and its implications for lake access". *The Cryosphere* 5.3 (2011), pp. 561–567.

Tikku, A. A., R. E. Bell, M. Studinger, G. K. Clarke, I. Tabacco, and F. Ferraccioli. "Influx of meltwater to subglacial Lake Concordia, east Antarctica". *Journal of Glaciology* 51.172 (2005), pp. 96–104.

Tómasson, H. "The jökulhlaup from Katla in 1918". *Annals of Glaciology* 22 (1996), pp. 249–254.

Tranter, M., G. Brown, R. Raiswell, M. Sharp, and A. Gurnell. "A conceptual model of solute acquisition by Alpine glacial meltwaters". *Journal of Glaciology* 39.133 (1993), pp. 573–581.

Tranter, M., M. Skidmore, and J. Wadham. "Hydrological controls on microbial communities in subglacial environments". *Hydrological Processes: An International Journal* 19.4 (2005), pp. 995–998.

Tulaczyk, S., J. A. Mikucki, M. R. Siegfried, J. C. Priscu, C. G. Barcheck, L. H. Beem, A. Behar, J. Burnett, B. C. Christner, A. T. Fisher, H. A. Fricker, K. D. Mankoff, R. D. Powell, F. Rack, D. Sampson, R. P. Scherer, S. Y. Schwartz, and T. Wissard Science Team. "WISSARD at Subglacial Lake Whillans, West Antarctica: scientific operations and initial observations". *Annals of Glaciology* 55.65 (2014), pp. 51–58.

Vallot, D., J. Åström, T. Zwinger, R. Pettersson, A. Everett, D. I. Benn, A. Luckman, W. J. van Pelt, F. Nick, and J. Kohler. "Effects of undercutting and sliding on calving: a global approach applied to Kronebreen, Svalbard". *The Cryosphere* 12.2 (2018), pp. 609–625.

van de Wal, R. S. W., C. J. P. P. Smeets, W. Boot, M. Stoffelen, R. van Kampen, S. H. Doyle, F. Wilhelms, M. R. van den Broeke, C. H. Reijmer, J. Oerlemans, and A. Hubbard. "Self-regulation of ice flow varies across the ablation area in south-west Greenland". *Cryosphere* 9.2 (2015), pp. 603–611.

van de Wal, R. S., W. Boot, M. Van den Broeke, C. Smeets, C. Reijmer, J. Donker, and J. Oerlemans. "Large and rapid melt-induced velocity changes in the ablation zone of the Greenland Ice Sheet". *Science* 321.5885 (2008), pp. 111–113.

van den Broeke, M., J. Bamber, J. Ettema, E. Rignot, E. Schrama, W. J. van de Berg, E. van Meijgaard, I. Velicogna, and B. Wouters. "Partitioning recent Greenland mass loss". *science* 326.5955 (2009), pp. 984–986.

van der Veen, C. "Fracture mechanics approach to penetration of surface crevasses on glaciers". *Cold Regions Science and Technology* 27.1 (1998), pp. 31–47.

van der Veen, C. "Crevasses on glaciers". *Polar Geography* 23.3 (1999), pp. 213–245.

van der Veen, C. J. "Fracture propagation as means of rapidly transferring surface meltwater to the base of glaciers". *Geophysical Research Letters* 34.1 (2007).

Vandecrux, B., R. Mottram, P. L. Langen, R. S. Fausto, M. Olesen, C. M. Stevens, V. Verjans, A. Leeson, S. Ligtenberg, P. Kuipers Munneke, S. Marchenko, W. van Pelt, C. R. Meyer, S. B. Simonsen, A. Heilig, S. Samimi, S. Marshall, H. Machguth, M. MacFerrin, M. Niwano, O. Miller, C. I. Voss, and J. E. Box. "The firn meltwater Retention Model Intercomparison Project (RetMIP): evaluation of nine firn models at four weather station sites on the Greenland ice sheet". *The Cryosphere* 14.11 (2020), pp. 3785–3810.

Vaughan, D. G., H. F. Corr, A. M. Smith, H. D. Pritchard, and A. Shepherd. "Flow-switching and water piracy between Rutford ice stream and Carlson inlet, West Antarctica". *Journal of Glaciology* 54.184 (2008), pp. 41–48.

Velicogna, I., Y. Mohajerani, F. Landerer, J. Mouginot, B. Noel, E. Rignot, T. Sutterley, M. van den Broeke, M. van Wessem, and D. Wiese. "Continuity of ice sheet mass loss in Greenland and Antarctica from the GRACE and GRACE Follow-On missions". *Geophysical Research Letters* 47.8 (2020), e2020GL087291.

Velicogna, I., T. C. Sutterley, and M. R. Van Den Broeke. "Regional acceleration in ice mass loss from Greenland and Antarctica using GRACE time-variable gravity data". *Geophysical Research Letters* 41.22 (2014), pp. 8130–8137.

Verjans, V., A. A. Leeson, C. M. Stevens, M. MacFerrin, B. Noël, and M. R. Broeke. "Development of physically based liquid water schemes for Greenland firn-densification models". *The Cryosphere* 13.7 (2019), pp. 1819–1842.

Vick-Majors, T. J., A. C. Mitchell, A. M. Achberger, B. C. Christner, J. E. Dore, A. B. Michaud, J. A. Mikucki, A. M. Purcell, M. L. Skidmore, J. C. Priscu, and. "Physiological ecology of microorganisms in subglacial Lake Whillans". *Frontiers in microbiology* 7 (2016), p. 1705.

Vijay, S., S. A. Khan, A. Kusk, A. M. Solgaard, T. Moon, and A. A. Bjørk. "Resolving seasonal ice velocity of 45 Greenlandic glaciers with very high temporal details". *Geophysical Research Letters* 46.3 (2019), pp. 1485–1495.

Wadham, J. L., S. Arndt, S. Tulaczyk, M. Stibal, M. Tranter, J. Telling, G. Lis, E. Lawson, A. Ridgwell, A. Dubnick, M. J. Sharp, A. M. Anesio, and C. E. H. Butler. "Potential methane reservoirs beneath Antarctica". *Nature* 488.7413 (2012), pp. 633–637.

Wadham, J. L., R. De'Ath, F. Monteiro, M. Tranter, A. Ridgwell, R. Raiswell, and S. Tulaczyk. "The potential role of the Antarctic Ice Sheet in global biogeochemical cycles". *Earth and Environmental Science Transactions of the Royal Society of Edinburgh* 104.1 (2013), pp. 55–67.

Wadham, J. L., J. Hawkings, L. Tarasov, L. Gregoire, R. Spencer, M. Gutjahr, A. Ridgwell, and K. Kohfeld. "Ice sheets matter for the global carbon cycle". *Nature communications* 10.1 (2019), pp. 1–17.

Wadham, J. L., M. Tranter, S. Tulaczyk, and M. Sharp. "Subglacial methanogenesis: a potential climatic amplifier?" *Global Biogeochemical Cycles* 22.2 (2008).

Wadham, J. L., J. Hawkings, J. Telling, D. Chandler, J. Alcock, E. O'Donnell, P. Kaur, E. Bagshaw, M. Tranter, A. Tedstone, and P. Nienow. "Sources, cycling and export of nitrogen on the Greenland Ice Sheet". *Biogeosciences* 13.22 (2016), pp. 6339–6352.

Wadham, J., R. Hodgkins, R. Cooper, and M. Tranter. "Evidence for seasonal subglacial outburst events at a polythermal glacier, Finsterwalderbreen, Svalbard". *Hydrological Processes* 15.12 (2001), pp. 2259–2280.

Walder, J. and B. Hallet. "Geometry of former subglacial water channels and cavities". *Journal of Glaciology* 23.89 (1979), pp. 335–346.

Walder, J. S. "Stability of sheet flow of water beneath temperate glaciers and implications for glacier surging". *Journal of Glaciology* 28.99 (1982), pp. 273–293.

Walder, J. S. "Hydraulics of subglacial cavities". *Journal of Glaciology* 32.112 (1986), pp. 439–445.

Walder, J. S. and J. E. Costa. "Outburst floods from glacier-dammed lakes: The effect of mode of lake drainage on flood magnitude". *Earth Surface Processes and Landforms* 21.8 (1996), pp. 701–723.

Walder, J. S. and A. Fowler. "Channelized subglacial drainage over a deformable bed". *Journal of glaciology* 40.134 (1994), pp. 3–15.

Walter, F., J. Chaput, and M. P. Lüthi. "Thick sediments beneath Greenland's ablation zone and their potential role in future ice sheet dynamics". *Geology* 42.6 (2014), pp. 487–490.

Weertman, J. and G. Birchfield. "Stability of sheet water flow under a glacier". *Journal of Glaciology* 29.103 (1983), pp. 374–382.

Weertman, J. "Catastrophic glacier advances" (1962).

Weertman, J. "General theory of water flow at the base of a glacier or ice sheet". *Reviews of Geophysics* 10.1 (1972), pp. 287–333.

Weidick, A., M. Kelly, and O. Bennike. "Late Quaternary development of the southern sector of the Greenland Ice Sheet, with particular reference to the Qassimiut lobe". *Boreas* 33.4 (2004), pp. 284–299.

Welch, B. C., R. W. Jacobel, and S. A. Arcone. "First results from radar profiles collected along the US-ITASE traverse from Taylor Dome to South Pole (2006–2008)". *Annals of Glaciology* 50.51 (2009), pp. 35–41.

Werder, M. A., I. J. Hewitt, C. G. Schoof, and G. E. Flowers. "Modeling channelized and distributed subglacial drainage in two dimensions". *Journal of Geophysical Research: Earth Surface* 118.4 (2013), pp. 2140–2158.

Williams, M. W., T. A. Erickson, and J. L. Petrzelka. "Visualizing meltwater flow through snow at the centimetre-to-metre scale using a snow guillotine". *Hydrological Processes* 24.15 (2010), pp. 2098–2110.

Williams, M. J. "Application of a three-dimensional numerical model to Lake Vostok: An Antarctic subglacial lake". *Geophysical research letters* 28.3 (2001), pp. 531–534.

Williamson, A. G., A. F. Banwell, I. C. Willis, and N. S. Arnold. "Dual-satellite (Sentinel-2 and Landsat 8) remote sensing of supraglacial lakes in Greenland". *The Cryosphere* 12.9 (2018), pp. 3045–3065.

Willis, I. C., C. D. Fitzsimmons, K. Melvold, L. M. Andreassen, and R. H. Giesen. "Structure, morphology and water flux of a subglacial drainage system, Midtdalsbreen, Norway". *Hydrological Processes* 26.25 (2012), pp. 3810–3829.

Willis, M. J., B. G. Herried, M. G. Bevis, and R. E. Bell. "Recharge of a subglacial lake by surface meltwater in northeast Greenland". *Nature* 518.7538 (2015), pp. 223–227.

Wingham, D. J., C. Francis, S. Baker, C. Bouzinac, D. Brockley, R. Cullen, P. de Chateau-Thierry, S. Laxon, U. Mallow, C. Mavrocordatos, L. Phalippou, G. Ratier, L. Rey, F. Rostan, P. Viau, and D. Wallis. "CryoSat: A mission to determine the fluctuations in Earth's land and marine ice fields". *Advances in Space Research* 37.4 (2006), pp. 841–871.

Wingham, D. J., A. J. Ridout, R. Scharroo, R. J. Arthern, and C. Shum. "Antarctic elevation change from 1992 to 1996". *Science* 282.5388 (1998), pp. 456–458.

Wingham, D. J., M. J. Siegert, A. Shepherd, and A. S. Muir. "Rapid discharge connects Antarctic subglacial lakes". *Nature* 440.7087 (2006), pp. 1033–1036.

Wolovick, M. J., R. E. Bell, T. T. Creyts, and N. Frearson. "Identification and control of subglacial water networks under Dome A, Antarctica". *Journal of Geophysical Research: Earth Surface* 118.1 (2013), pp. 140–154.

Woodward, J., A. M. Smith, N. Ross, M. Thoma, H. Corr, E. C. King, M. King, K. Grosfeld, M. Tranter, and M. Siegert. "Location for direct access to subglacial Lake Ellsworth: An assessment of geophysical data and modeling". *Geophysical Research Letters* 37.11 (2010).

Wright, A. and M. Siegert. "A fourth inventory of Antarctic subglacial lakes". *Antarctic Science* 24.6 (2012), p. 659.

Wright, A. and M. J. Siegert. "The identification and physiographical setting of Antarctic subglacial lakes: An update based on recent discoveries". *Geophysical Monograph Series* 192 (2011), pp. 9–26.

Wright, A., D. Young, J. Bamber, J. Dowdeswell, A. Payne, D. Blankenship, and M. Siegert. "Subglacial hydrological connectivity within the Byrd Glacier catchment, East Antarctica". *Journal of Glaciology* 60.220 (2014), pp. 345–352.

Wright, A., D. Young, J. Roberts, D. Schroeder, J. Bamber, J. Dowdeswell, N. Young, A. Le Brocq, R. Warner, A. Payne, D. Blankenship, T. van Ommen, and M. Siegert. "Evidence of a hydrological connection between the ice divide and ice sheet margin in the Aurora Subglacial Basin, East Antarctica". *Journal of Geophysical Research: Earth Surface* 117.F1 (2012).

Wright, A., M. Siegert, A. Le Brocq, and D. Gore. "High sensitivity of subglacial hydrological pathways in Antarctica to small ice-sheet changes". *Geophysical Research Letters* 35.17 (2008).

Wright, P. J., J. T. Harper, N. F. Humphrey, and T. W. Meierbachtol. "Measured basal water pressure variability of the western Greenland Ice Sheet: Implications for hydraulic potential". *Journal of Geophysical Research: Earth Surface* 121.6 (2016), pp. 1134–1147.

Wüest, A. and E. Carmack. "A priori estimates of mixing and circulation in the hard-to-reach water body of Lake Vostok". *Ocean Modelling* 2.1-2 (2000), pp. 29–43.

Xu, Y., E. Rignot, I. Fenty, D. Menemenlis, and M. M. Flexas. "Subaqueous melting of Store Glacier, west Greenland from three-dimensional, high-resolution numerical modeling and ocean observations". *Geophysical Research Letters* 40.17 (2013), pp. 4648–4653.

Xu, Y., E. Rignot, D. Menemenlis, and M. Koppes. "Numerical experiments on subaqueous melting of Greenland tidewater glaciers in response to ocean warming and enhanced subglacial discharge". *Annals of Glaciology* 53.60 (2012), pp. 229–234.

Yamazaki, D., D. Ikeshima, R. Tawatari, T. Yamaguchi, F. O'Loughlin, J. C. Neal, C. C. Sampson, S. Kanae, and P. D. Bates. "A high-accuracy map of global terrain elevations". *Geophysical Research Letters* 44.11 (2017), pp. 5844–5853.

Yang, K. and L. C. Smith. "Internally drained catchments dominate supraglacial hydrology of the southwest Greenland Ice Sheet". *Journal of Geophysical Research: Earth Surface* 121.10 (2016), pp. 1891–1910.

Young, C. L., I. N. Sokolik, M. G. Flanner, and J. Dufek. "Surface radiative impacts of ash deposits from the 2009 eruption of Redoubt volcano". *Journal of Geophysical Research: Atmospheres* 119.19 (2014), pp. 11–387.

Young, D. A., J. L. Roberts, C. Ritz, M. Frezzotti, E. Quartini, M. G. P. Cavitte, C. R. Tozer, D. Steinhage, S. Urbini, H. F. J. Corr, T. van Ommen, and D. D.

Blankenship. "High-resolution boundary conditions of an old ice target near Dome C, Antarctica". *The Cryosphere* 11.4 (2017), pp. 1897–1911.

Zanchettin, D., O. Bothe, H. F. Graf, S. J. Lorenz, J. Luterbacher, C. Timmreck, and J. H. Jungclaus. "Background conditions influence the decadal climate response to strong volcanic eruptions". *Journal of Geophysical Research: Atmospheres* 118.10 (2013), pp. 4090–4106.

Zwally, H. J., W. Abdalati, T. Herring, K. Larson, J. Saba, and K. Steffen. "Surface Melt-Induced Acceleration of Greenland Ice-Sheet Flow". *Science* 297.5579 (2002), pp. 218–222.

Zwally, H. J., B. Schutz, W. Abdalati, J. Abshire, C. Bentley, A. Brenner, J. Bufton, J. Dezio, D. Hancock, D. Harding, T. Herring, B. Minster, K. Quinn, S. Palm, J. Spinhirne, and R. Thomas. "ICESat's laser measurements of polar ice, atmosphere, ocean, and land". *Journal of Geodynamics* 34.3-4 (2002), pp. 405–445.